

学位論文

**Schwinger Mechanism in QCD**

**and**

**its Applications to**

**Ultra-relativistic Heavy Ion Collisions**

( QCDにおけるSchwinger機構と,  
その超相対論的重イオン衝突事象への応用 )

平成28年12月博士(理学)申請

東京大学大学院理学系研究科

物理学専攻

田屋 英俊



# Abstract

In the presence of strong classical gauge fields, one encounters essentially new phenomena that are not observed in the vacuum. Such phenomena are collectively called “strong-field physics”, which has been attracting attention of many researchers in various fields in physics. One of the most intriguing examples of the strong-field physics is spontaneous particle production from strong classical gauge fields, i.e., the *Schwinger mechanism*. The Schwinger mechanism has a long history especially in the context of the Quantum ElectroDynamics (QED), however, there still remains a number of unsolved problems. Formulation of the Schwinger mechanism in Quantum ChromoDynamics (QCD) and its application to the pre-equilibrium stage dynamics of ultra-relativistic heavy ion collisions are examples of the problems.

In the first half of this thesis, we formulate the Schwinger mechanism in QCD based on quantum field theory, including backreaction effects from quark, gluon, and ghost fluctuations. To be more specific, we consider quantum fluctuations of quarks, gluons, and ghosts on top of a classical color gauge field. By adopting mean field approximation for the quantum fluctuations appearing in the QCD Lagrangian, we derive a set of linear differential equations for the fluctuations, which accounts for particle production, backreaction, and (partial effects of) scatterings. Within the mean field approximation, we extensively study the Schwinger mechanism in QCD both analytically and numerically. For instance, we discuss finite pulse effects for particle production; the plasma oscillation induced by the backreaction; quantum interferences among created quarks and gluons; chemical composition of produced matter; and an evolution towards isotropization of the system.

In the last half of thesis, we apply the formalism to the pre-equilibrium stage dynamics of ultra-relativistic heavy ion collisions by modeling initial color flux tubes existing just after a collision with a boost-invariantly expanding, and spatially uniform classical electric field. By numerically tracing the time-evolution of the classical field strength, quark and gluon distribution functions, and thermodynamic quantities such as pressure and energy density, we reveal how the system evolves towards a formation of quark-gluon plasma in ultra-relativistic heavy ion collisions. In particular, we show (i) the classical electric field decays quite fast  $\sim 3 \text{ fm}/c$  because of the decoherence of the classical field into quantum quark and gluon particles and the longitudinal expansion of the system; (ii) huge number of quarks  $\sim 1000$  per unit rapidity are produced very quickly  $\sim 1 \text{ fm}/c$ ; and (iii) because of the decoherence and the longitudinal expansion, the system becomes less anisotropic as  $\langle : \hat{P}_z : \rangle / \langle : \hat{P}_\perp : \rangle \sim 0.5$  within a few  $\text{fm}/c$ .



# Table of Contents

<b>1</b>	<b>Introduction</b>	<b>1</b>
1.1	Schwinger mechanism . . . . .	1
1.1.1	basics . . . . .	1
1.1.2	time-dependent electromagnetic fields . . . . .	6
1.1.3	backreaction . . . . .	7
1.1.4	application to quantum chromodynamics . . . . .	10
1.2	Ultra-relativistic heavy ion collisions . . . . .	12
1.2.1	overview . . . . .	12
1.2.2	pre-equilibrium dynamics . . . . .	16
1.3	Objectives and outline of thesis . . . . .	22
<b>2</b>	<b>Schwinger Mechanism in Quantum Electrodynamics</b>	<b>25</b>
2.1	Formalism . . . . .	25
2.1.1	QED under a classical gauge field . . . . .	25
2.1.2	assumptions on the system . . . . .	28
2.1.3	mean field approximation . . . . .	29
2.1.4	canonical quantization and particle production . . . . .	31
2.1.5	regularization . . . . .	37
2.2	$e^+e^-$ pair production from a constant electric field . . . . .	39
2.2.1	particle spectrum at $t \rightarrow \infty$ . . . . .	40
2.2.2	vacuum persistence probability at $t \rightarrow \infty$ . . . . .	41
2.3	Finite pulse effects . . . . .	41
2.3.1	perturbative formula . . . . .	42
2.3.2	comparison of perturbative and non-perturbative evaluation . . . . .	43
2.4	Dynamical evolution without backreaction . . . . .	51
2.4.1	electron distribution . . . . .	53
2.4.2	total number of electrons . . . . .	55
2.5	Dynamical evolution with backreaction . . . . .	56
2.5.1	setup . . . . .	56
2.5.2	electron distribution . . . . .	56
2.5.3	decay of electric field . . . . .	59

2.5.4	total number of electrons . . . . .	60
2.5.5	energy density . . . . .	61
2.5.6	pressure . . . . .	62
2.6	Brief summary . . . . .	63
<b>3</b>	<b>Schwinger Mechanism in <math>SU_c(N_c = 2)</math> Yang-Mills theory</b>	<b>67</b>
3.1	Formalism . . . . .	67
3.1.1	$SU_c(N_c = 2)$ Yang-Mills theory under a classical gauge field . . . . .	67
3.1.2	assumptions on the system . . . . .	73
3.1.3	mean field approximation . . . . .	73
3.1.4	canonical quantization and particle production . . . . .	77
3.1.5	massless approximation . . . . .	84
3.2	Gluon production from a constant color electric field . . . . .	85
3.2.1	gluon distribution . . . . .	85
3.2.2	total number of gluons . . . . .	88
3.3	Dynamical evolution with backreaction . . . . .	89
3.3.1	setup . . . . .	90
3.3.2	gluon distribution . . . . .	90
3.3.3	decay of color electric field . . . . .	91
3.3.4	total number of gluons . . . . .	92
3.3.5	energy density . . . . .	93
3.3.6	pressure . . . . .	93
3.4	Brief summary . . . . .	94
<b>4</b>	<b>Schwinger Mechanism in Quantum Chromodynamics</b>	<b>97</b>
4.1	Formalism . . . . .	97
4.1.1	QCD under a classical gauge field . . . . .	97
4.1.2	assumptions on the system . . . . .	101
4.1.3	mean field and massless approximation . . . . .	101
4.1.4	canonical quantization and particle production . . . . .	105
4.2	Quark and gluon production from a constant color electric field . . . . .	111
4.2.1	quark and gluon distribution . . . . .	111
4.2.2	total number of quarks and gluons . . . . .	116
4.3	Dynamical evolution with backreaction . . . . .	120
4.3.1	setup . . . . .	121
4.3.2	quark and gluon distribution . . . . .	121
4.3.3	decay of color electric field . . . . .	124
4.3.4	total number of quarks and gluons . . . . .	124
4.3.5	energy density . . . . .	125

4.3.6	pressure	126
4.4	Brief summary	128
<b>5</b>	<b>Particle Production in Ultra-relativistic Heavy Ion Collisions</b>	<b>133</b>
5.1	Schwinger mechanism in $\tau$ - $\eta$ coordinates	133
5.1.1	$\tau$ - $\eta$ coordinates	134
5.1.2	assumptions on the system	139
5.1.3	canonical quantization	140
5.1.4	particle production	150
5.2	Dynamical evolution without backreaction	153
5.2.1	$p_\eta$ -spectrum of quarks and gluons	154
5.2.2	momentum rapidity $y_P$ -spectrum of quarks and gluons	157
5.2.3	total number of quarks and gluons	158
5.3	Dynamical evolution with backreaction	160
5.3.1	setup	160
5.3.2	$p_\eta$ -spectrum of quarks and gluons	161
5.3.3	momentum rapidity $y_P$ -spectrum of quarks and gluons	165
5.3.4	total number of quarks and gluons	166
5.3.5	decay of color electric field	168
5.3.6	energy density	169
5.3.7	pressure	172
5.4	Brief summary	174
<b>6</b>	<b>Summary and Outlook</b>	<b>177</b>
<b>A</b>	<b>Analytic Mode Functions for Fermions in a Box</b>	<b>183</b>
A.1	Plane wave solutions	184
A.2	Under a constant electric field	184
A.3	Under a Sauter-type electric field	186
<b>B</b>	<b>Analytic Mode Functions for Bosons in a Box</b>	<b>189</b>
B.1	Plane wave solutions	189
B.2	Under a constant electric field	189
<b>C</b>	<b>Analytic Mode Functions under an Expanding Electric Field</b>	<b>191</b>
C.1	fermion	191
C.2	boson	194



# Chapter 1

## Introduction

In the presence of strong classical gauge fields, one encounters essentially new phenomena that are not observed in the vacuum. Such phenomena are collectively called “strong-field physics”, which has been attracting attention of many researchers in various fields in physics.

A typical example of strong-field physics is spontaneous particle production from strong classical gauge fields, which is often referred to as the *Schwinger mechanism*. The Schwinger mechanism has a long history especially in the context of the Quantum ElectroDynamics (QED), however, there still remain a number of unsolved problems. Formulation of the Schwinger mechanism in Quantum ChromoDynamics (QCD) and its application to the pre-equilibrium stage dynamics of ultra-relativistic heavy ion collisions, which we discuss in this thesis, are examples of such problems.

This chapter is devoted to an introduction which provides the physics background of this thesis: In Section 1.1, basics of the Schwinger mechanism, including its early and recent developments, are explained. In Section 1.2, we give a brief overview of ultra-relativistic heavy ion collisions, focusing on their pre-equilibrium stage dynamics and relevance to the Schwinger mechanism. In Section 1.3, objectives and an outline of this thesis is explained.

### 1.1 Schwinger mechanism

#### 1.1.1 basics

Study of the Schwinger mechanism has a long history. The first recognition of the Schwinger mechanism dates back to the dawn of QED: It was Dirac who first discovered a relativistic wave equation for an electron, which is known as the Dirac equation today [1]. The Dirac equation admits infinitely negative energy states. This looks problematic because any state would fall into lower and lower energy states by emitting photons and hence there seem no stable states. This problem was resolved by Dirac by re-interpreting that negative energy states are all occupied (and hence any state cannot fall into negative energy states because of the Pauli principle) in a physical vacuum (Dirac sea picture) [2]. Soon after the discovery of the Dirac

equation, Klein applied the Dirac equation to a problem of an electron scattering off a potential barrier, and found a paradox that for a sufficiently strong potential the number of reflected electrons is larger than that of injected electrons (Klein paradox) [3]. This paradox was resolved by Sauter [4]. Sauter claimed that a level crossing occurs for a sufficiently strong potential and that electrons filling the negative energy states (Dirac sea) can tunnel into the positive energy states as in Fig. 1.1. Therefore, a pair of an electron and a positron is produced, with which Sauter explained the anomalous excess of the reflected electrons in the Klein paradox.

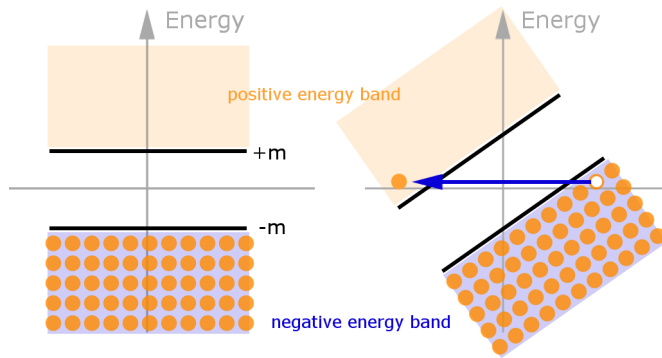


Figure 1.1: The level crossing of QED vacuum under a strong potential.

Sauter's idea indicates that a vacuum under a strong potential is no longer a vacant space but behaves like a charged medium because of the pair creation. If this is true, then one can expect that a non-zero source term appears in the Maxwell equation even in a vacuum when it is exposed to a strong potential. This expectation was first theoretically confirmed by Heisenberg and Euler within relativistic quantum mechanics [5]. They considered a *constant strong classical electromagnetic background field* as a strong potential, and derived the so-called Euler-Heisenberg effective Lagrangian  $\mathcal{L}_{\text{EH}}$ :

$$\mathcal{L}_{\text{EH}} = -\frac{1}{4}F^{\mu\nu}F_{\mu\nu} + \frac{(e^2/4\pi)^2}{360m_e^4} \left[ 4(F^{\mu\nu}F_{\mu\nu})^2 + 7(F^{\mu\nu}\tilde{F}_{\mu\nu})^2 \right], \quad (1.1)$$

where terms higher than  $\mathcal{O}((F/m_e^2)^6)$  are neglected.  $e > 0$  is the coupling constant of QED and  $m_e$  is the electron mass.  $F^{\mu\nu} \equiv \partial^\mu A^\nu - \partial^\nu A^\mu$  is the classical electromagnetic field strength and  $\tilde{F}^{\mu\nu} \equiv \epsilon^{\mu\nu\rho\sigma}F_{\rho\sigma}$  ( $\epsilon^{\mu\nu\rho\sigma}$  is a completely anti-symmetric tensor normalized by  $\epsilon^{0123} = 1$ ) is its dual. The first term in Eq. (1.1) is nothing but the usual Maxwell Lagrangian. The second term describes the source term, which is the manifestation of the pair production from a strong classical electromagnetic field. We note that here the strong field is not dynamical but is treated as a background, i.e., backreaction effects from the produced particles to the strong field is neglected and the field strength is kept fixed. This approximation is justified only when the number of produced electrons is small enough. It was not until 1980s that the backreaction problem was seriously discussed; we will come back to this issue in Section 1.1.3.

Sauter's pair production claims that the particle number is no longer conserved. This suggests that one has to use quantum field theory rather than single-particle quantum mechanics to fully formulate Sauter's idea. Schwinger was the first one to formulate Sauter's idea within quantum field theory [6]. Schwinger re-derived the Euler-Heisenberg effective Lagrangian (1.1) as a one-loop effective Lagrangian described by the following diagram,

$$\text{Thick circle} = \text{Thin circle} + \text{Thin circle with 2 blobs} + \text{Thin circle with 4 blobs} + \dots, \quad (1.2)$$

where the wavy line with a blob represents an insertion of a classical field. The thin line is a bare propagator of an electron, and the thick line is a full one dressed by infinite number of insertions of classical fields. Only even numbers of insertions are non-vanishing because of the Furry theorem (charge symmetry in QED) [7]. Furthermore, Schwinger found that an imaginary part appears in the Euler-Heisenberg effective Lagrangian (1.1). This means that a vacuum under a strong classical electromagnetic field is unstable, i.e, transition probability from an in-vacuum to an out-vacuum is less than unity as

$$|\langle \text{vac}; \text{out} | \text{vac}; \text{in} \rangle|^2 = \exp \left[ -2 \text{Im} \int d^4x \mathcal{L}_{\text{EH}} \right] < 1. \quad (1.3)$$

The physical meaning of the imaginary part,  $w \equiv \text{Im} \mathcal{L}_{\text{EH}}$ , is the vacuum decay rate. One can explicitly compute the vacuum decay rate  $w$  for a constant and homogeneous electric field  $\mathbf{E}$  as

$$w = \frac{|e\mathbf{E}|}{(2\pi)^3} \sum_{\text{spin}} \int d^2\mathbf{p}_\perp \sum_{n=1}^{\infty} \frac{1}{n} \exp \left[ -n\pi \frac{m_e^2 + \mathbf{p}_\perp^2}{|e\mathbf{E}|} \right] = \frac{|e\mathbf{E}|^2}{4\pi^3} \sum_{n=1}^{\infty} \frac{1}{n^2} \exp \left[ -n\pi \frac{m_e^2}{|e\mathbf{E}|} \right], \quad (1.4)$$

where  $\mathbf{p}_\perp$  labels the transverse momentum (perpendicular to the direction of the electric field  $\mathbf{E}$ ). The summation,  $\sum_{\text{spin}} = 2$ , accounts for the summation over the electron spin degrees of freedom  $s = 1/2$ . The non-vanishing vacuum decay rate  $w$  is a consequence of Sauter's pair production. In this way, Sauter's idea was fully formulated by Schwinger, and this is the reason why particle production from a strong classical electromagnetic field is called the (Sauter-)Schwinger mechanism. We should remark here that the vacuum decay rate  $w$  is not the same as the pair production rate  $\Gamma \equiv dN_{e^+e^-}/d\mathbf{x}^3 dt$  although confused in some literatures. This is intuitively because the former is the rate for at least one pair of particles to be produced, while the latter is the rate for pairs to be produced. This aspect was first made clear by Nikishov [8] and recently revisited in Ref. [9]. Indeed, Nikishov directly computed the pair production rate  $\Gamma$ , and found that

$$\Gamma = \frac{|e\mathbf{E}|}{(2\pi)^3} \sum_{\text{spin}} \int d^2\mathbf{p}_\perp \exp \left[ -\pi \frac{m_e^2 + \mathbf{p}_\perp^2}{|e\mathbf{E}|} \right] = \frac{|e\mathbf{E}|^2}{4\pi^3} \exp \left[ -\pi \frac{m_e^2}{|e\mathbf{E}|} \right]. \quad (1.5)$$

Thus, the pair production rate  $\Gamma$  is identical to the first term in the series of the vacuum decay rate  $w$ . These two quantities coincide with each other only for  $|e\mathbf{E}| \ll m_e^2$ .

Until now, we have restricted our attention only to the Schwinger mechanism for *electrons*. However, the Schwinger mechanism is not limited to electrons. It can be generalized to charged particles with arbitrary spin. In fact, the Euler-Heisenberg Lagrangian was extended for scalar particles in Ref. [10] and for vector particles in Ref. [11]. These results were further generalized by Marinov and Popov to the case of particles with arbitrary spin [12]. They found the following expressions for the vacuum decay rate  $w$  and the pair production rate  $\Gamma$  for a constant and homogeneous electric field  $\mathbf{E}$ :

$$w = \frac{|e\mathbf{E}|}{(2\pi)^3} \sum_{\text{spin}} \int d^2\mathbf{p}_\perp \sum_{n=1}^{\infty} \frac{\beta_n}{n} \exp \left[ -n\pi \frac{m^2 + \mathbf{p}_\perp^2}{|e\mathbf{E}|} \right] = (2s + 1) \frac{|e\mathbf{E}|^2}{(2\pi)^3} \sum_{n=1}^{\infty} \frac{\beta_n}{n^2} \exp \left[ -n\pi \frac{m^2}{|e\mathbf{E}|} \right], \quad (1.6)$$

$$\Gamma = \frac{|e\mathbf{E}|}{(2\pi)^3} \sum_{\text{spin}} \int d^2\mathbf{p}_\perp \exp \left[ -\pi \frac{m^2 + \mathbf{p}_\perp^2}{|e\mathbf{E}|} \right] = (2s + 1) \frac{|e\mathbf{E}|^2}{(2\pi)^3} \exp \left[ -\pi \frac{m^2}{|e\mathbf{E}|} \right], \quad (1.7)$$

where  $\beta_n$  is a statistical factor given by

$$\beta_n \equiv \begin{cases} (-1)^{n-1} & \text{for bosons} \\ 1 & \text{for fermions} \end{cases}. \quad (1.8)$$

$m$  is the mass of the charged particle. The summation,  $\sum_{\text{spin}} = 2s + 1$ , accounts for the degeneracy of the spin degrees of freedom with  $s = 0, 1/2, 1, \dots$ . The vacuum decay rate  $w$  and the pair production rate  $\Gamma$  for a single spin degree of freedom are independent of the value of the spin  $s$ . This is because electric fields do not couple to the spin degrees of freedom. This situation changes when one considers a magnetic field in addition to the electric field. Consider a constant and homogeneous magnetic field in parallel to the electric field as an example (one can easily extend the following discussion by a Lorentz-boost to general cases, where the angle between the electric and the magnetic field is non-zero). In this case, one can analytically compute the vacuum decay rate  $w$  and the pair production rate  $\Gamma$  for arbitrary spin particles [12]. The essence of the results is that magnetic fields do couple to the spin degrees of freedom, and discretize the transverse motion as  $\sqrt{m^2 + \mathbf{p}_\perp^2} \rightarrow \sqrt{m^2 + (2n - gs_z + 1)|e\mathbf{B}|}$  (Landau quantization), where  $n = 0, 1, 2, \dots$  labels the Landau level,  $g$  denotes the gyromagnetic ratio, and  $s_z$  is the longitudinal component of the spin  $s_z = -s, -s + 1, \dots, s$ . As a consequence, the lowest Landau level (low transverse momentum particles with  $n = 0$ ) dominates the pair production. More interestingly, the pair production is dramatically suppressed and/or enhanced depending on the spin  $s$  of particles. Indeed, one finds an exponential suppression for scalar particle production, while vector particle production is exponentially enhanced for  $s_\parallel = 1$  with  $g = 2$ . The latter is related to the Nielsen-Olesen instability [13, 14] inherent in charged vector particles such as  $W$ -bosons and gluons [15].

Since the Dirac sea picture is invalid for bosons, the original Sauter's explanation for the Schwinger mechanism should be modified now. The point is that Sauter's explanation is based on single-particle quantum mechanics, although the Schwinger mechanism, by its nature, must be explained with the language of quantum field theory. This is related to how we reconcile the negative energy states problem within quantum field theory, where the Dirac sea picture is replaced by virtual pair fluctuations in a vacuum. The modern interpretation for the Schwinger mechanism is as follows: In quantum field theory, a vacuum is not a vacant space but is full of virtual pair fluctuations. The virtual pairs are ceaselessly created and annihilated in a vacuum with a typical time scale  $\Delta t \sim 1/m$  because of the uncertainty principle. The presence of an electromagnetic field, then, accelerates the virtual pairs and supply energy. If the work done by the electromagnetic field  $\sim |e\mathbf{E}| \times \Delta t = |e\mathbf{E}|/m$  (notice that magnetic fields do no work on an orbital motion<sup>1</sup>) exceeds the mass gap  $m$ , i.e.,  $|e\mathbf{E}| \gtrsim m^2/e \equiv E_{\text{cr}}$ , the virtual pairs become on-shell resulting in production of real pair particles. We note that, in this explanation, we have implicitly assumed that the typical work done by the electromagnetic field is determined by the field strength only. This assumption is valid for fields slowly varying in time, where the typical frequency of the field is sufficiently smaller than the field strength so that the typical energy scale of the electromagnetic field is solely determined by the field strength. We will clarify this statement and review effects of time-dependent electromagnetic fields in Section 1.1.2.

One of the outstanding properties of the Schwinger mechanism is the exponential factor in the vacuum decay rate  $w$  and/or in the pair production rate  $\Gamma$ , which depend on  $|e\mathbf{E}|/m^2$  inversely in the exponential. From this factor, it is evident that the Schwinger mechanism for a constant electric field is genuinely a non-perturbative phenomenon. This is in contrast to usual perturbative phenomena, whose dependence on  $|e\mathbf{E}|/m^2$  always appears with positive powers. On the other hand, one can also understand that an extraordinary strong electromagnetic field of the order of  $E_{\text{cr}} = m^2/e \sim 10^{-2} \text{ MeV}^2 \sim \sqrt{10^{28} \text{ W/cm}^2}$  (for an electron-positron pair production  $m = m_e = 0.511 \text{ MeV}$ ) is required to make the Schwinger mechanism manifest. This is the reason why the Schwinger mechanism has not been confirmed in laboratory experiments until today. The strongest electromagnetic field that the human beings have now at hand is the HERCULES laser in the United States of America, whose strength is about  $2 \times 10^{22} \text{ W/cm}^2$  [16] although the attainable laser intensity is rapidly growing in these days [17] thanks to advents of new technologies (e.g. the chirped pulse amplification (CPA) [18]) and there are many intense laser facilities planned around the world (e.g. ELI [19], HiPER [20]).

In finishing this subsection, let us mention that the Schwinger mechanism has a wide range of applications in various fields in physics. In particular, it plays an important role in the area of QCD, which is reviewed in Section 1.1.4. Here, let us discuss other examples: As is mentioned, intense laser facilities give us an unique opportunity to study the Schwinger mechanism in

---

<sup>1</sup>Effects of magnetic fields appear in the modification of the effective mass through the Landau quantization as is explained in the last paragraph.

laboratory experiments, although its strength is still below the critical one  $E_{\text{cr}} \equiv m^2/e$ . In addition, extraordinary strong classical electromagnetic fields, which may exceed the critical strength are expected to appear in various physical systems (although it is not controllable) such as super-heavy nuclei [21, 22, 23], ultra-relativistic heavy ion collisions [24, 25], charged black holes [26], the early Universe [27, 28] and so on. Furthermore, it is recently argued in the condensed matter community that the Schwinger mechanism can be tested experimentally via quasi-particle excitations in graphene [29] and/or in cold atoms on a optical lattice [30, 31, 32]. It should also be noted that many interesting phenomena such as the Landau-Zener transition in Mott insulators, the Unruh effect, the Hawking radiation, particle production during the inflation era can be discussed in an analogue of the Schwinger mechanism because the underlying physics is the same, i.e., particle production mechanism from strong fields. Finally, let us comment that the theoretical formulation of the Schwinger mechanism was first given by Schwinger [6] by the proper-time regularization of the one-loop digram (proper-time method). Since then, many other formulations have been developed such as canonical method [33, 34], quantum kinetic method [35, 36], worldline instanton method [37], stochastic method [38], and so on.

### 1.1.2 time-dependent electromagnetic fields

So far, we have considered an idealized situation, where the strong classical electromagnetic field is *constant* in time. In actual physical situations, however, one frequently has to deal with *time-dependent* strong fields. For example, strong electromagnetic fields produced in ultra-relativistic heavy ion collisions decay quite fast. Those in intense lasers are also time-dependent. Under such situations, particle production mechanism from strong fields is significantly modified by the time-dependence. Indeed, the non-perturbative nature of the Schwinger mechanism for a constant electromagnetic field can be understood as a scattering process of a vacuum virtual pair with an *infinite* number photons with zero frequency. This is not the case for a time-depending field, where photons have *non-zero* frequency  $\omega$ : A *finite* number of photons  $\sim m/\omega$  is enough to excite a particle from a vacuum. Hence, the particle production may no longer be non-perturbative, but *perturbative* particle production may occur.

The interplay between the perturbative and the non-perturbative particle production from a strong classical electromagnetic field was first discussed by Brèzin and Izykson [39] and by Popov [40]. They considered electron-positron pair production from a sinusoidal electric field with frequency  $\omega$ :  $\mathbf{E} = \mathbf{E}_0 \sin \omega t$ . In a weak field limit  $|e\mathbf{E}_0|/m^2 \ll 1$ , they found that the pair production rate  $\Gamma$  varies with  $\omega$  as

$$\Gamma = \begin{cases} \frac{|e\mathbf{E}|^2}{4\pi^2} \exp\left[-\pi \frac{m_e^2}{|e\mathbf{E}|}\right] & (\gamma_K \ll 1) \\ \frac{|e\mathbf{E}|^2}{16\pi} \left|\frac{e\mathbf{E}}{2m_e\omega}\right|^{4m_e/\omega} & (\gamma_K \gg 1) \end{cases}. \quad (1.9)$$

Here,  $\gamma_K \equiv m_e \omega / |e\mathbf{E}_0|$  is the so-called Keldysh parameter, which was previously introduced in theory of ionizations of atoms [41]. For  $\gamma_K \ll 1$  or  $\omega \rightarrow 0$  (constant field limit), one naturally reproduces the well-known non-perturbative formula for the Schwinger mechanism for a constant electric field. On the other hand, for  $\gamma_K \gg 1$ , the frequency becomes so large that the particle production becomes purely a perturbative phenomenon. The pair production rate  $\Gamma$  is now free from the non-perturbative exponential factor, and the exponent  $\propto m_e/\omega \sim$  (number of photons scattered for the particle production) in  $\Gamma$  reflects the fact that the multi-photon scattering dominates the particle production mechanism.

One can also discuss effects of time-dependence via a pulsed electric field. This is done by the author [42], and is discussed in detail in Section 2.3

One of the most interesting theoretical developments involving the time-dependent effects is the dynamically assisted Schwinger mechanism [43]. It predicts that the pair production rate  $\Gamma$  is dramatically enhanced compared to the naive Schwinger pair production rate for a slowly varying  $\gamma_K^{(1)} \ll 1$  electric field  $\mathbf{E}^{(1)}$ , if one superimposes fast  $\gamma_K^{(2)} \gg 1$  and weak  $|\mathbf{E}^{(2)}| \ll |\mathbf{E}^{(1)}|$  fluctuations  $\mathbf{E}^{(2)}$  on top of  $\mathbf{E}^{(1)}$ . In this configuration, the fast electric field  $\mathbf{E}^{(2)}$  “assists” the Schwinger pair production by supplying sizable energy via multi-photon scattering, which results in lowering the pair production threshold. The dynamically assisted Schwinger mechanism attracts much attention of experimentalists because it presents an efficient way to observe the Schwinger mechanism in laboratory experiments. Optimization of the field profile is also studied vigorously, for example, in Refs. [44, 45, 46].

### 1.1.3 backreaction

In the previous two subsections, we have treated the strong classical electromagnetic field as a background and neglected the backreaction effects. Unfortunately, this treatment *is* unphysical because it apparently violates the energy conservation law [47]. In reality, particles are accelerated by the electromagnetic field after they are created, and electromagnetic current flows. The current generates an additional electromagnetic field according to Ampère’s law, which in turn screens the original field. The backreaction effects were first phenomenologically addressed within a transport model, which is often referred to as the flux tube model [48, 49]. In this model, the classical Boltzman-Vlasov equation coupled to the classical Maxwell equation,

$$p^\mu \frac{\partial f(x, p)}{\partial x^\mu} - ep^\mu F_{\mu\nu} \frac{\partial f(x, p)}{\partial p^\nu} = \mathcal{C}(x, p) + \mathcal{S}(x, p), \quad (1.10)$$

$$\frac{\partial F^{\mu\nu}}{\partial x^\mu} = j^\nu, \quad (1.11)$$

is considered. Here,  $f$  is a one-particle distribution function.  $\mathcal{C}$  is a collision integral.  $\mathcal{S}$  is a source term, which accounts for the particle production from the Schwinger mechanism.  $j$  is the current of the produced particles, which screen the original field via the Maxwell equation (1.11). The flux tube model is intuitively clear and thus appealing, however, it is highly non-trivial from a theoretical point of view. For instance,

- What is a correct expression for the source term?

In the original works [48, 49], the source term is assumed to have the same form as what the Schwinger mechanism for a constant electric field has (Eq. (1.5)). This assumption is apparently incorrect because now the field strength depends on spacetime in general, and hence Eq. (1.5) is not applicable. Note that no formula exists so far for the pair production rate for arbitrary spacetime-dependent electromagnetic fields.

- What is a correct expression for the current?

In the original works [48, 49], a spatially uniform electric field pointing to the  $z$ -direction is considered. They *assumed* that the current  $j_\mu \equiv j\delta_{\mu z}$  is expressed as

$$j = j_{\text{cond}}^\mu + j_{\text{pol}}^\mu, \quad (1.12)$$

$$j_{\text{cond}} = e \int \frac{d^3\mathbf{p}}{(2\pi)^3} \frac{p_z}{p^0} f, \quad (1.13)$$

$$j_{\text{pol}} = \frac{1}{|\mathbf{E}|} \int \frac{d^3\mathbf{p}}{(2\pi)^3} \mathcal{S} \quad (1.14)$$

so as to satisfy the energy conservation law. Here,  $j_{\text{cond}}$  and  $j_{\text{pol}}$  may represent the conduction and the polarization current, respectively. The justification of this expression from a microscopic point of view is quite unobvious. Indeed, in the framework of quantum field theory, a classical current is obtained by taking an expectation value of a current operator  $j^\mu \equiv \langle \hat{j}^\mu \rangle$  ( $\hat{j}^\mu = e\hat{\psi}\gamma^\mu\hat{\psi}$  for fermions for example) with a certain regularization scheme. The expression depends on the regularization scheme one chooses (or, physical conditions one imposes) in general, however, no unique scheme exists for our problem because one has to consider a spacetime-depending regularization when there is a spacetime-depending electromagnetic field<sup>2</sup>.

- How can one justify the *classical* transport equation?

In the presence of strong fields, propagation of a particle should significantly differ from that of the bare (i.e., classical) one because it receives large *quantum* corrections from the strong field.

- Is the one-particle distribution function well-defined?

Theoretically speaking, a one-particle distribution function is well-defined *only* when interactions are switched off. This is in contrast to our situation, where particles are strongly interacting with the field.

---

<sup>2</sup>This situation is essentially the same as what we encounter in cosmological problems, where the spacetime is curved [50].

A more transparent way is the quantum-field-theoretical approach, which was developed in Refs. [34, 51, 52, 53] (for a review, see [54]). In this approach, field equations

$$0 = [i\hat{\not{\partial}} - e\hat{A} - m]\hat{\psi}, \quad (1.15)$$

$$j^\nu = \partial_\mu F^{\mu\nu} \quad (1.16)$$

are directly solved. (For scalar particles, the Klein-Gordon equation,  $0 = [(i\partial - eA)^2 - m^2]\hat{\phi}$ , is considered instead of the Dirac equation. ) Here, quantum operators are distinguished from classical numbers by a hat ( $\hat{\bullet}$ ) as usual. In this approach, mean field approximation is adopted so that only an expectation value of the gauge field operator,  $A_\mu \equiv \langle \hat{A}_\mu \rangle$ , and of the current operator,  $j^\mu \equiv \langle \hat{j}^\mu \rangle$ , are considered. This approximation is valid when quantum fluctuations,  $(\hat{A}_\mu - A_\mu)/A_\mu$  and  $(\hat{j}^\mu - j^\mu)/j^\mu$ , are negligible, i.e., the classical contributions,  $A_\mu$  and  $j^\mu$ , are large enough. In the first equation, the Dirac (or the Klein-Gordon) equation is solved non-pertubatively with respect to the strong classical electromagnetic field  $A_\mu$ . This is equivalent to evaluating the one-loop quantum correction illustrated in Eq. (1.2), which accounts for the pair creation. The backreaction effects are embedded in the classical Maxwell equation, described by the second equation, as in the phenomenological flux tube model. The theoretical formulation of this approach is presented in detail in Section 2.1. We note for completeness that a quantum kinetic method is also developed in Ref. [55], which is essentially the same as the quantum-field-theoretical approach explained above. In this approach, quantum Vlasov equation with a source term, instead of the Dirac (or the Klein-Gordon) equation, coupled to the classical Maxwell equation is considered. It is, however, much simpler to solve the field equation directly, rather than solving a quantum kinetic equation with a complicated non-Markovian source term [35, 56]. Another equivalent approach is recent real-time lattice simulations [57, 58, 59] based on the classical statistical approximation [60]. In this approach, classical equations of motion are numerically solved on a lattice and quantum effects are (partly) taken into account by an ensemble average of initial field fluctuations. It is an advantage of this approach that numerical costs are smaller than the previous two approaches for 3-dimensional problems; especially for problems, where strong fields are inhomogeneous in space. However, it is speculated that the classical statistical approximation may destroy the renormalizability of an underlying theory [61].

The backreaction problem attracts much attention even today. In particular, it is recently argued that avalanche-like particle production (QED cascade) occurs if one considers backreaction effects beyond the mean field level [62, 63, 64]: Let us suppose that a charged particle is present in a strong field (seeded by the Schwinger mechanism, for example). Then, since the field is so strong that the particle would be quickly accelerated by the field to emit hard photons, which in turn decay into an electron-positron pair. Repeating these steps to increase the number of particles so rapidly that the original field would decay much faster than expected in the mean field studies. Although the theoretical foundation for the QED cascade is still far from complete, numerical simulations based on a simple phenomenological kinetic description

support the QED cascade scenario [65, 66]. In addition, it is interesting to point out that such an avalanche-like particle production was experimentally observed in an electron-hole plasma created by a strong THz laser [67].

### 1.1.4 application to quantum chromodynamics

The Schwinger mechanism plays an important role in the area of QCD, especially in the physics of multi-particle production: It is the strong classical *color* electromagnetic flux tubes that bind quarks and gluons inside hadrons (color confinement) [68]. The typical strength of the flux tubes is as strong as  $gE \sim 1 \text{ GeV}^2$ , which can be determined by the Reggae slope in hadron spectroscopy and/or by lattice QCD (for a review, see Ref. [69] for instance). Notice that the strength is much larger than the critical field strength of the Schwinger mechanism for both quarks and gluons. In high energy processes (e.g. lepton-hadron, hadron-hadron scatterings), partons (quarks and gluons) inside a hadron are shot out and flux tubes span between the partons expand (Low-Nussinov model [70, 71])<sup>3</sup>. The flux tubes do not expand macroscopically, but decay through production of quark–anti-quark and/or gluon pairs via (a colored version of) the Schwinger mechanism; otherwise the energy of a flux tube would increase ultimately with increasing its length. These particles are eventually observed as (color neutral) hadrons in detectors. This is the so-called string breaking picture of hadron production in high energy processes [72, 73]. The string breaking picture is implemented in some phenomenological models such as the Lund model [74], which has been very successful in reproducing hadron spectra observed in actual high energy processes.

*Static* properties of the string breaking mechanism can be studied well within lattice QCD: The emergence of color flux tubes in QCD was studied for mesonic (quark and anti-quark) system in Refs. [75, 76, 77], baryonic (three quark) system in Refs. [77, 78], tetra-quark system in Ref. [79], and penta-quark system in Ref. [80]. The breaking of color flux tubes was confirmed in Refs. [81, 82] by analyzing a static quark and anti-quark potential separated with each other by fixed distance  $l$ . They found that  $l \sim 1.25 \text{ fm}$ , which coincides with the typical size of hadrons, sets critical distance for the string breaking to occur.

*Dynamical* aspects of the string breaking mechanism are, however, less understood. Indeed, lattice QCD tells us nothing about dynamics because real-time information is lost in a Euclidean formulation, with which lattice QCD stands. In order to understand dynamical aspects of the string breaking mechanism, one has to follow real-time dynamics of the Schwinger mechanism in QCD including backreaction effects. For this purpose, one has to extend the Schwinger mechanism developed in QED to the case of QCD.

Study of this direction was initiated by Refs. [83, 84, 85, 86], in which the quark and gluon pair production rates,  $\Gamma_{q\bar{q}}$  and  $\Gamma_{g\bar{g}}$ , for a constant and homogeneous classical strong color

<sup>3</sup>The flux tube picture is also applicable to lepton-lepton scatterings. For this case,  $\bar{l}l \rightarrow \gamma \rightarrow q\bar{q}$  dominates the cross section, and the flux tubes should span between the produced quark and anti-quark pair.

electric background field was computed. They considered a covariant constant background field satisfying  $0 = D_\mu F^{\mu\nu} \equiv \partial_\mu F^{\mu\nu} + ig[A_\mu, F^{\mu\nu}]$ . For covariant constant fields, there exists a global color rotation such that it diagonalizes, i.e., Abelianizes the background field strength as  $F^{\mu\nu} = \bar{F}^{\mu\nu} \sum_{\alpha=1}^{N_c-1} w^\alpha H^\alpha$  with  $H^\alpha$  being diagonal matrices which belong to the Cartan subalgebra of  $SU(N_c)$ . Now that the problem is essentially reduced to the Abelian one, one finds a pair production rate  $\Gamma$  similar to that for QED (Eq. (1.7)) as

$$\Gamma_{q\bar{q}} = \sum_{i=1}^{N_c} \sum_{\text{flavor}} \sum_{\text{spin}} \frac{|q_i^{(\text{fund.})} \bar{\mathbf{E}}|}{(2\pi)^3} \int d^2 \mathbf{p}_\perp \exp \left[ -\pi \frac{m_f^2 + \mathbf{p}_\perp^2}{|q_i^{(\text{fund.})} \bar{\mathbf{E}}|} \right] = \sum_{i=1}^{N_c} \frac{|q_i^{(\text{fund.})} \bar{\mathbf{E}}|^2}{4\pi^3} \exp \left[ -\pi \frac{m_f^2}{|q_i^{(\text{fund.})} \bar{\mathbf{E}}|} \right], \quad (1.17)$$

$$\Gamma_{\text{gg}} = \sum_{A=1}^{N_c(N_c-1)/2} \sum_{\text{pol.}} \frac{|q_A^{(\text{ad.})} \bar{\mathbf{E}}|}{(2\pi)^3} \int d^2 \mathbf{p}_\perp \exp \left[ -\pi \frac{\mathbf{p}_\perp^2}{|q_A^{(\text{ad.})} \bar{\mathbf{E}}|} \right] = \sum_{A=1}^{N_c(N_c-1)/2} \frac{|q_A^{(\text{ad.})} \bar{\mathbf{E}}|^2}{4\pi^3}. \quad (1.18)$$

In deriving Eq. (1.18), we have used the fact that gluons are massless.  $m_f$  is the mass of a quark of flavor  $f$ . The indices  $i$  and  $A$  are the color indices of fundamental and adjoint representations, respectively, and  $\sum_i$  and  $\sum_A$  account for the summation over the color degrees of freedom.  $\sum_{\text{pol.}} = 2$  counts the number of physical polarization of gluons; unphysical particles, i.e., ghosts and scalar and longitudinal gluons are never produced. The effective color charges,  $q_i^{(\text{fund.})}$  for quarks and  $q_A^{(\text{ad.})}$  for gluons, are defined by

$$q_i^{(\text{fund.})} \equiv g \sum_{\alpha=1}^{N_c-1} w^\alpha (H^\alpha)_{ii}, \quad (1.19)$$

$$q_A^{(\text{ad.})} \equiv g \sum_{\alpha=1}^{N_c-1} w^\alpha (v^\alpha)^A, \quad (1.20)$$

where  $g$  is the coupling constant of QCD, and  $(v^\alpha)^A$  is the root vector of  $SU(N_c)$ .

Backreaction effects in QCD have been studied within the QCD version of the flux tube model explained in Section 1.1.3 in Ref. [87]. Ref. [87] considered the Boltzman-Vlasov equation [88, 89, 90] coupled to the classical Yang-Mills equation:

$$p^\mu \frac{\partial f_i^{(q)}(x, p)}{\partial x^\mu} - q_i^{(\text{fund.})} p^\mu \bar{F}_{\mu\nu} \frac{\partial f_i^{(q)}(x, p)}{\partial p^\nu} = \mathcal{C}_i^{(q)}(x, p) + \mathcal{S}_i^{(q)}(x, p), \quad (1.21)$$

$$p^\mu \frac{\partial f_A^{(g)}(x, p)}{\partial x^\mu} - q_A^{(\text{ad.})} p^\mu \bar{F}_{\mu\nu} \frac{\partial f_A^{(g)}(x, p)}{\partial p^\nu} = \mathcal{C}_A^{(g)}(x, p) + \mathcal{S}_A^{(g)}(x, p), \quad (1.22)$$

$$\frac{\partial \bar{F}^{\mu\nu}}{\partial x^\mu} = j^\nu, \quad (1.23)$$

where the source term  $\mathcal{S}$  is assumed to be expressed by the particle production rate  $\Gamma$  in QCD (Eqs. (1.17) and (1.18)). As the classical field is Abelianized, the non-Abelian part of the Yang-Mills equation,  $ig[A_\mu, F^{\mu\nu}]$ , vanishes in Eq. (1.23) so that it reduces to the Abelian Maxwell equation.

The phenomenological flux tube model is, unfortunately, far from self-evident as was explained in detail in Section 1.1.3. Quantum field theory should give us a rigorous formulation from the first principle, however, study along this direction is insufficient. The quantum-field-theoretical approach was applied in [91], where only backreaction effects from quarks are considered and those from gluons are neglected. In reality, the backreaction effects from quarks and gluons must give the same order contributions. Hence, inclusion of the gluon backreaction effects is important, although it has not been completed so far. We resolve this problem in this thesis.

## 1.2 Ultra-relativistic heavy ion collisions

Pre-equilibrium stage dynamics in ultra-relativistic heavy ion collisions is a big missing piece in our current understanding of the event evolution. The physics is, on the other hand, very similar to the string breaking dynamics reviewed in the last section as we will see, and hence it is crucial to deepen our understanding of the Schwinger mechanism to fill in the missing piece. In this Section, we explain what the problem is, and review recent theoretical attempts for this problem.

### 1.2.1 overview

In our current Universe, i.e., with almost zero temperature and density, quarks and gluons are confined in hadrons so that one can never observe them individually. The theory of quarks and gluons, i.e., QCD predicts that the situation dramatically changes when we go to high temperature and/or density. There, a phase transition occurs, and quarks and gluons are liberated from hadrons to form a plasma state [92, 93]. This is the so-called *Quark-Gluon Plasma state* (QGP) [94]. Lattice QCD predicts that the phase transition takes place at temperature around  $T_{\text{QCD}} \sim 170$  MeV [95, 96]. According to the Big Bang theory [97, 98], such a high temperature state may be realized just after the birth of our Universe, and thus all the matter existing in our current Universe can be thought of as remnants of QGP. Hence, understanding QGP is important not only to unveil rich QCD physics, but also to elucidate the origin of the matter.

Ultra-relativistic heavy ion collisions are the only way that the human beings have now at hand to create QGP in laboratory experiments. Heavy nuclei such as copper ( $^{63}\text{Cu}$ ), gold ( $^{197}\text{Au}$ ), and lead ( $^{208}\text{Pb}$ ) with ultra-relativistic energies are collided, and a fraction of the collision energy is converted into the thermal energy to achieve extremely high temperature with macroscopic dimensions  $\sim (10 \text{ fm})^3$ . So far, these collisions are operated at the Relativistic Heavy Ion Collider (RHIC) with typical collision energy  $\sqrt{s_{\text{NN}}} = 200$  GeV/nucleon since 2000, and at the Large Hadron Collider (LHC) with  $\sqrt{s_{\text{NN}}} = 5.5$  TeV/nucleon since 2010. Many experimental observables (e.g. elliptic flow  $v_2$ , jet quenching, quarkonium suppression, thermal photon, Hanbury-Brown-Twiss (HBT) interferometry, chemical equilibration) strongly indicate

that QGP is actually created in ultra-relativistic heavy ion collisions.

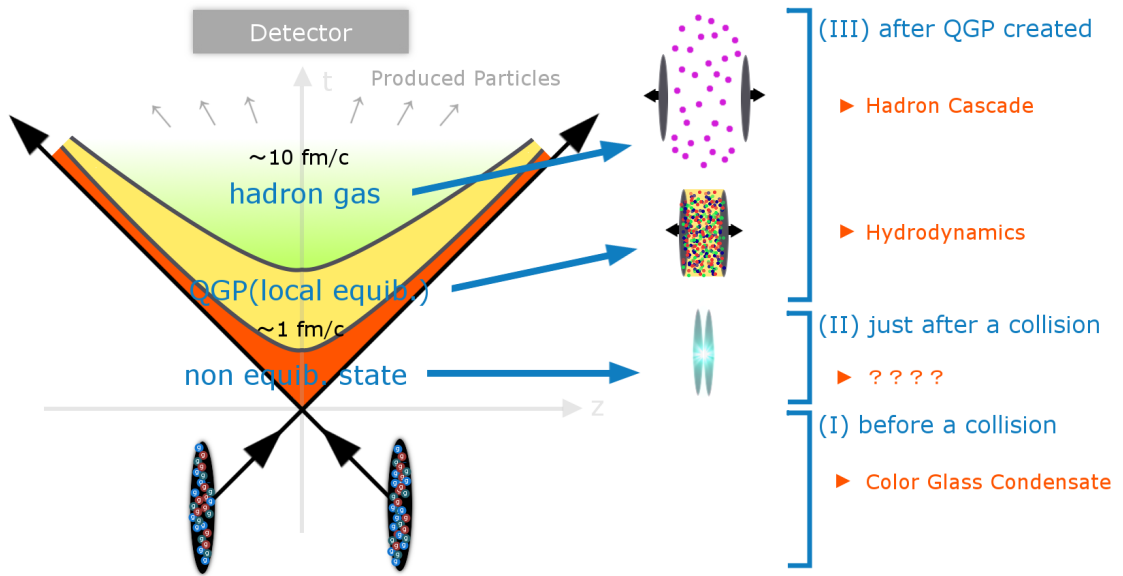


Figure 1.2: Spacetime evolution of ultra-relativistic heavy ion collisions.

The spacetime evolution of ultra-relativistic heavy ion collisions can be roughly divided into three stages (see Fig. 1.2); (I) before a collision ( $\tau < 0$ ), (II) pre-equilibrium stage just after a collision ( $0 < \tau < \tau_{\text{QGP}}$ ), and (III) locally equilibrated stage after QGP is created ( $\tau_{\text{QGP}} < \tau$ ). Thanks to vigorous theoretical and experimental studies of the past decades, there has been significant progress in understanding the stages (I) and (III):

### (I) Before a collision ( $\tau < 0$ )

Before a collision, two incident nuclei at very high energies are saturated with a huge number of gluons with typical phase space densities  $\sim 1/g^2$  (see the left panel of Fig. 1.3). Such a very dense gluon state is well approximated by coherent classical gluon fields sourced by  $\vec{\rho}$ , rather than incoherent particles (Color Glass Condensate picture; CGC [99, 100, 101, 102]). This is a non-Abelian analogue of the Weizsäcker-Williams fields in QED. In this picture, quark contributions are negligible because they are sub-leading effects compared to that from abundant gluons.

The non-linear interaction among gluons  $g \leftrightarrow gg$  plays an essential role in CGC: A gluon with large momentum inside a nucleus emits gluons one after another through successive  $g \rightarrow gg$  processes, and the number of gluons dramatically increases with increasing the energy of the nucleus, or equivalently with decreasing Bjorken's  $x \sim Q^2/s$  ( $Q^2$  is the virtuality and  $s$  is the center of mass squared). This cascade eventually ceases at sufficiently small  $x$ . There, gluons start to overlap with each other, and the inverse process  $gg \rightarrow g$  becomes significant to balance the gluon emitting process so that gluon production saturates (see the right panel of Fig. 1.3).

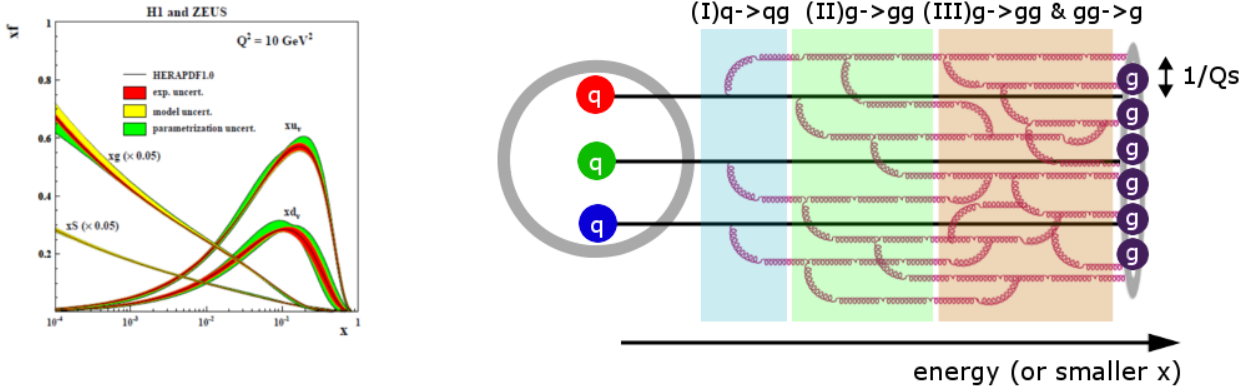


Figure 1.3: [Left] Particle Distribution Function (PDF) measured at HERA [103]. [Right] Intuitive picture of gluon saturation.

As a result of this saturation mechanism, gluons are randomly distributed in the transverse plane of the nucleus with typical correlation length  $\sim 1/Q_s$ . The only scale  $Q_s$  is the so-called saturation scale, which evolves with  $x$  as

$$Q_s^2 \sim A^{1/3} \left( \frac{x_0}{x} \right)^\lambda \text{ GeV}^2, \quad (1.24)$$

where  $A^{1/3}$  represents thickness of a nucleus with  $A$  being the atomic mass number. The unknown parameters  $x_0, \lambda$  are determined from experiments as  $x_0 = 3 \times 10^{-4}, \lambda = 0.288$  for  $x < 10^{-2}$  (Golec-Biernat–Wüsthoff (GBW) parametrization [104, 105]). Typical values of  $Q_s$  read  $Q_s \sim 1 \text{ GeV}$  for RHIC energy scale, and  $Q_s \sim 3 \text{ GeV}$  for the LHC energy scale. The randomness of the transverse gluon distribution can be described by a probability function  $W[\rho]$  with  $\rho$  being the gluon density. Now that the number of color constituents, i.e., gluons are sufficiently large, the central limit theorem tells us that it is good to model  $W[\rho]$  by the following Gaussian ansatz (McLerran-Venugopalan (MV) model [99, 100, 101]) as

$$W[\rho] = \exp \left[ -\frac{1}{2} \text{tr}_c \int d^2 \mathbf{x}_\perp \frac{\rho^2}{g^2 \mu^2} \right], \quad (1.25)$$

where the model parameter  $\mu$  is related to the saturation scale  $Q_s$  as  $g^2 \mu \sim Q_s$  [106]. In the CGC framework, any observable  $\langle O \rangle_{\text{CGC}}$  is computed as an ensemble average of the probability function  $W[\rho]$  as

$$\langle O \rangle_{\text{CGC}} = \int [d\rho] W[\rho] O[\rho]. \quad (1.26)$$

An important consequence of CGC is that high energy hadrons are *universally* characterized only by a single energy scale, i.e., the saturation scale  $Q_s$ . This CGC prediction is actually confirmed in scaling behaviors in deep inelastic scattering cross sections (geometric scaling) [107, 108, 109].

**(II) pre-equilibrium stage just after a collision ( $0 < \tau < \tau_{\text{QGP}}$ )**

The colliding nuclei pass through each other (Bjorken picture [110]) leaving a fraction of the collision energy into the cylindrical shaped region between the two nuclei. The energy would be converted into the thermal energy to create QGP through non-equilibrium processes, which we review in Section 1.2.2.

**(III) equilibrated stage after QGP is created ( $\tau_{\text{QGP}} < \tau$ )**

QGP is created shortly after a collision  $\tau > \tau_{\text{QGP}}$ . The spacetime evolution of the system is, then, well described within relativistic hydrodynamics. In particular, (a relativistic version of) the Euler equation together with an equation of state, for instance, extracted from lattice QCD is very successful in reproducing experimentally observed large elliptic flow  $v_2$ . This success strongly indicates that QGP behaves like a perfect liquid with tiny viscosity, which means that

- QGP is a strongly interacting matter rather than a weakly interacting gas as the asymptotic freedom of QCD [111, 112] naively implies; and
- the entropy (almost) conserves during the stage (III), so that the huge entropy observed in the experiment (about 1000 charged hadrons per unit rapidity [113, 114]) must be produced during the pre-equilibrium stage (II).

Hydrodynamics also implies that the formation time of QGP may be very short  $\tau_{\text{QGP}} \lesssim 1 \text{ fm}/c$  because the large elliptic flow  $v_2$  requires that the hydrodynamical evolution starts at early times, when the anisotropy in the pressure gradients is large enough. The short formation time  $\tau_{\text{QGP}}$  is also suggested by hydrodynamical analysis of direct photons. Numerical codes including higher order effects such as shear/bulk viscosity and initial state fluctuations are also developing in these days, which are indispensable tools to extract bulk properties of QGP in detail.

The cylindrical shaped region, where QGP is created, expands in the beam direction in accordance with the motion of the colliding nuclei (Bjorken expansion [110]). QGP cools down with this expansion, and the temperature eventually gets lower than the critical temperature of the QCD phase transition  $T_{\text{QCD}} \sim 170 \text{ MeV}$ . Then, quarks and gluons are confined to form a gas of hadrons, which are finally caught by detectors after hadronic cascading evolution. This stage of dynamics is described by hadron transport models (e.g. UrQMD [115], JAM [116]). The hadron transport models have been successful in reproducing a number of observables in low-energy heavy ion collisions up to SPS (Super Proton Synchrotron at CERN) energy scale  $\sqrt{s} \sim 17 \text{ GeV/nucleon}$ , where more relevant degrees of freedom in the process are given by hadrons rather than quarks and gluons.

### 1.2.2 pre-equilibrium dynamics

There is a big missing link between the stages (I) and (III), i.e., a bridge between CGC and hydrodynamics. Namely, the questions are

- (a) How can one theorize the non-equilibrium QCD dynamics during the stage (II)?
- (b) How are the huge number of quark and gluon *particles* produced from the purely classical gluon *fields* characterized by CGC?
- (c) How does the system evolve to form QGP? In particular, the applicability of hydrodynamics to QGP *naively* implies that QGP is (at least) close to isotropic  $P_z/P_\perp \sim 1$  because the foundation of hydrodynamics relies on a derivative expansion around an equilibrium, and hence a complete isotropization or a state very close to it is assumed for the expansion to make sense. Is isotropization and/or hydrodynamization possible within an extremely short formation time  $\tau_{\text{QGP}} \lesssim 1 \text{ fm}/c$ ?

Unfortunately, no complete answer exists for these questions starting from QCD, despite of numerous and incessant (see Ref. [117] for example) theoretical attempts. What makes it difficult is that there is no experimental probe so far for the pre-equilibrium dynamics during the stage (II) because the strongly interacting matter in the stage (III) smears out the pre-equilibrium information.

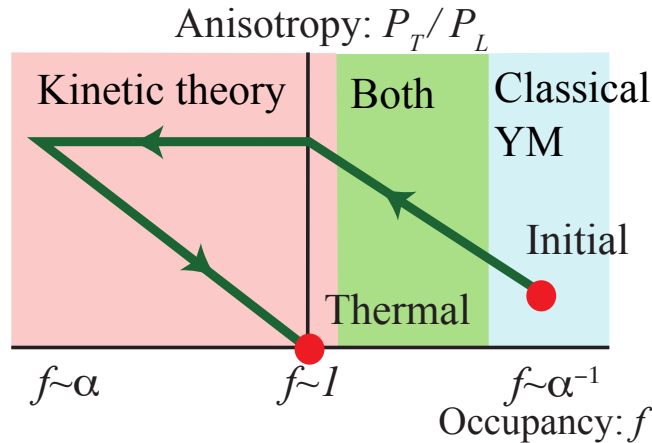


Figure 1.4: A cartoon of the field and particle regime in the pre-equilibrium stage dynamics of ultra-relativistic heavy ion collisions. The figure is taken from Ref. [118].

Here, we review recent theoretical developments for this problem. The pre-equilibrium stage (II) might further be divided into two regimes, namely, classical ( $0 < \tau \lesssim \tau_{\text{part}}$ ) and particle ( $\tau_{\text{part}} \lesssim \tau \lesssim \tau_{\text{QGP}}$ ) regime (see Fig. 1.4). Different degrees of freedom dominate for each regime (classical fields for the field regime, and particles for the particle regime), so that different theoretical approaches are applied depending on the regime.

## field regime

As was explained in the last subsection, CGC tells us that incident nuclei are a highly dense system of gluons with typical phase space density  $f \sim 1/g^2 \gg 1$ , whose behavior is well approximated by classical gluon fields sourced by  $\rho$ . Hence, the system can solely be described by classical dynamics and one may use the classical Yang-Mills theory to describe the subsequent spacetime evolution after a collision because quantum scattering processes are suppressed by an inverse of the phase space density  $1/f \ll 1$ . In the following, we shall neglect quarks for the first approximation, because it would give only subleading contributions compared to that from dense gluons. Inclusion of quark degrees of freedom is an open issue in this research area.

The classical Yang-Mills theory tells us that a collision of these classical gluon fields results in a formation of longitudinal color electromagnetic flux tubes between the two nuclei receding from each other [119, 120, 121] (often referred to as *glasma* named after that it is a transient state between color-GLAss-condensate and quark-gluon plaSMA). These flux tubes can be understood as an analogue of the Low-Nussinov model in the string breaking dynamics.

Let us explain how these flux tubes emerge. Intuitively speaking, this is a colored version of a capacitor, where each nucleus plays a role of a capacitor plate with large color charges due to the gluon saturation. Theoretically, our task is to solve the classical Yang-Mills equation with sources  $\rho^{(n)}$  ( $n = 1, 2$  differentiate the colliding nucleus 1 and 2 moving at the speed of light to the positive and negative beam direction, respectively). This program is analytically doable at the instant of a collision  $\tau = 0^+$ . Now, let us assume a perfect boost-invariance, i.e., the resulting color electromagnetic fields do not depend on a spacetime rapidity coordinate. This is because boost-invariance is a good approximation at the classical level since the incident nuclei are highly Lorentz contracted to be pancake-shaped and move almost at the speed of light. Then, one can analytically solve the classical Yang-Mills equation at the instant of a collision  $\tau = 0^+$  to obtain (before color averaging by Eq. (1.26))

$$E_x = E_y = 0, \quad E_z = -ig \left( [\alpha_x^{(1)}, \alpha_x^{(2)}] + [\alpha_y^{(1)}, \alpha_y^{(2)}] \right), \quad (1.27)$$

$$B_x = B_y = 0, \quad B_z = -ig \left( -[\alpha_x^{(1)}, \alpha_y^{(2)}] + [\alpha_y^{(1)}, \alpha_x^{(2)}] \right). \quad (1.28)$$

Here, we define the  $z$ -axis as the beam direction. The quantity  $\alpha_i^{(n)}$  are the gauge potentials associated to the incident nuclei, respectively, and characterize the longitudinal component of the field strength. They are given by

$$\alpha_{x,y}^{(n)} = \frac{i}{g} U^{(n)\dagger} \partial_{x,y} U^{(n)} \quad \text{with} \quad U^{(n)} = \mathcal{P} \exp \left[ ig \int d\xi \nabla_{\perp}^{-2} \rho^{(n)} \right], \quad (1.29)$$

where  $\mathcal{P}$  denotes the path-ordering, and  $\xi = (t - z)/\sqrt{2}$  for  $n = 1$  and  $\xi = (t + z)/\sqrt{2}$  for  $n = 2$ . From Eqs. (1.27) and (1.28), we understand that:

- At the instant of a collision  $\tau = 0^+$ , the system is characterized by the above boost-invariant strong classical color electromagnetic flux tubes as depicted in Fig. 1.5. This

means that understanding the pre-equilibrium stage dynamics is to reveal how the initial flux tubes at  $\tau = 0^+$  decohere into a huge number of particles, which eventually form QGP.

- The system is highly anisotropic with negative longitudinal pressure,

$$P_z = \frac{1}{2} \text{tr}_c [(E_x^2 + E_y^2 - E_z^2) + (B_x^2 + B_y^2 - B_z^2)] < 0, \quad (1.30)$$

$$P_\perp = \frac{1}{2} \text{tr}_c [E_z^2 + B_z^2] > 0. \quad (1.31)$$

- Non-vanishing topological charge density exists because  $\mathbf{E} \cdot \mathbf{B} \neq 0$ .

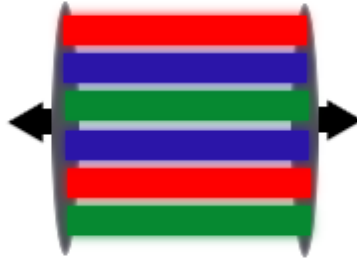


Figure 1.5: Boost-invariant strong classical color electromagnetic flux tubes created at the instant of a collision  $\tau = 0^+$ .

Let us again stress that the “initial” condition at  $\tau = 0^+$  for the pre-equilibrium stage dynamics is given by the above boost-invariant *strong classical color electromagnetic flux tubes* just like in the strong breaking dynamics. This is a very natural situation where the Schwinger mechanism is at play. From this fact, one understands that it is crucial to deepen our understanding of the Schwinger mechanism to elucidate the pre-equilibrium stage dynamics of ultra-relativistic heavy ion collisions.

One has to employ numerical methods to follow the subsequent evolution  $\tau > 0$ . This is done in Ref. [121] for a perfectly boost-invariant system. In reality, however, there always exist quantum fluctuations around classical quantities that can break the boost-invariance. Interestingly, it was first demonstrated by Refs. [122, 123] that initial quantum fluctuations seeded at  $\tau = 0^+$  bring unstable behaviors in the subsequent evolution (their time scale is, however, rather long  $\sim 100/Q_s$ ), although the fluctuations considered in Refs. [122, 123] are somewhat artificial ones. These unstable behaviors, which are often referred to as *glasma instability*, are related to the Weibel instability, which is well-known in the context of plasma physics, and/or the Nievesen-Olesen instability inherent in QCD [13, 14]. A more realistic initial quantum fluctuations based on CGC are considered within classical statistical approximation in Ref. [124]. Effects of initial quantum fluctuations are investigated in more detail in Refs. [125,

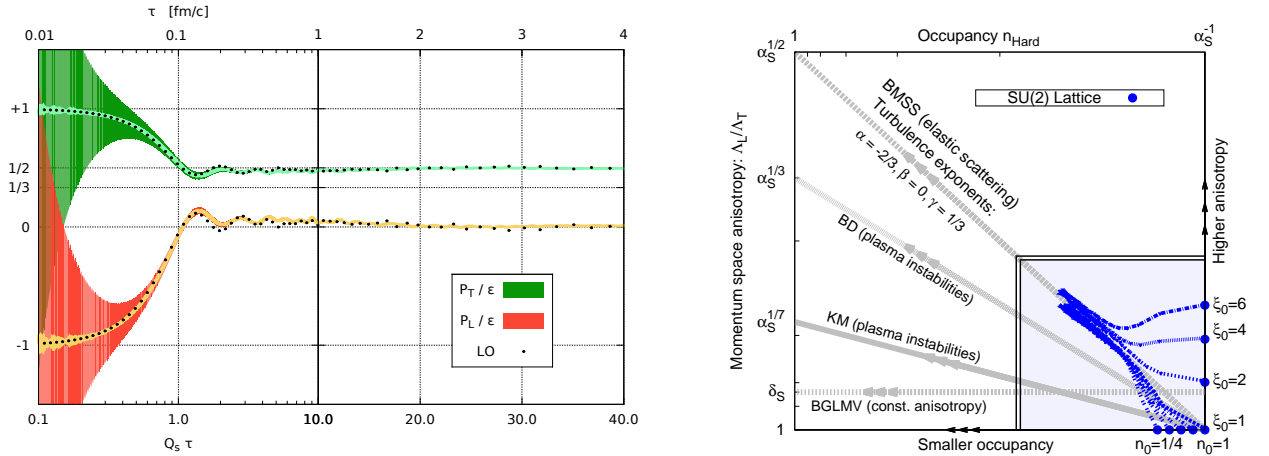


Figure 1.6: Classical evolution of the system. [Left] Time-evolution of the longitudinal and transverse pressure of the system with CGC initial quantum fluctuations. The figure is taken from Ref. [124]. [Right] Time-evolution of the anisotropy and the phase space density with different initial quantum fluctuations. The figure is taken from Refs. [125, 126].

126]. These results are displayed in Fig. 1.6, which claim that the system stays anisotropic during the whole spacetime evolution because  $P_z$  approaches zero (free streaming) regardless of initial quantum fluctuations one considers. This is truly a bad news for the question (c): The classical evolution never isotropitizes or hydrodynamizes the system. This discrepancy may be resolved in the subsequent particle regime. Indeed, it is argued within scalar  $\phi^4$  theory in Ref. [127] that the quantum scattering processes, although they are subdominant by a factor of  $1/f \ll 1$  and are neglected in the field regime, are essential to isotropitize and/or thermalize the system.

### particle regime

As time proceeds, the system becomes more and more dilute because of the expansion, so that particle degrees of freedom become more and more important than those of classical fields. This transition from the field regime to, say, the particle regime smoothly occurs at around  $1 \ll f \ll 1/g^2$ , where both field and particle picture give faithful description [60]. For  $f \ll 1$ , particle degrees of freedom dominate the system. In this particle regime, quantum scattering processes, which are suppressed by a factor of  $1/f$  in the field regime, become significant. It is impossible to describe quantum scattering processes within the classical Yang-Mills theory, and hence one has to use another theoretical approach to follow the spacetime evolution.

As such an approach, kinetic theory is a powerful theoretical framework to describe non-equilibrium dynamics in dilute systems. An effective kinetic theory for QCD was developed in Ref. [128], which is based on the Boltzman transport equation for the gluon distribution function

with an elastic  $2 \leftrightarrow 2$  and an inelastic  $1 \leftrightarrow 2$  collision integrals. As the collision integrals, especially that for the  $1 \leftrightarrow 2$  process, are complicated functionals, it is a hard task to evaluate the kinetic equation. The state-of-art numerical simulation was done in Ref. [129], where a boost-invariantly expanding  $2 + 1$  dimensional system was treated for simplicity. Figure 1.7 summarizes the main results of Ref. [129].

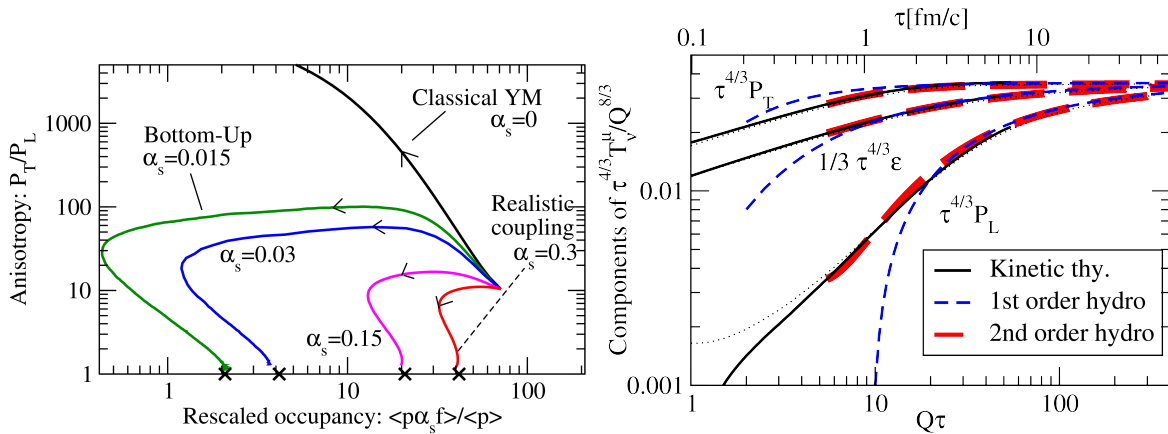


Figure 1.7: [Left] Time-evolution of the anisotropy and the phase space density within the effective kinetic theory with various coupling constant. The arrow indicates the flow of the time-evolution. The black line corresponds to the limit of the classical evolution. The figure is taken from [118]. [Right] Onset of hydrodynamical evolution from the effective kinetic theory. The figure is taken from [129].

One of the important lessons from [129] is that the isotropization  $P_z/P_\perp \sim 1$  actually occurs in the particle regime (left panel of Fig. 1.7) verifying the importance of quantum scattering processes in the isotropization.

On the other hand, however, the time scale is very long to achieve a complete isotropization  $\gtrsim 100/Q_s$  for a realistic coupling constant  $\alpha_s \equiv g^2/4\pi \sim 0.3$ . This is a bad news for the question (c): It does not seem to explain the *fast* hydrodynamization of the system  $\tau_{\text{QGP}} \sim 1 \text{ fm}/c$ . There is no satisfactory answer for this problem so far. One of the promising scenarios is based on the assumption that one may apply hydrodynamics even before the system is isotropitized. Based on this assumption, Ref. [129] analyzed the time-evolution of thermodynamic quantities (energy density  $\epsilon$  and pressure  $P_z, P_\perp$ ) within the effective kinetic theory and the first and second order viscous hydrodynamics. As depicted in the right panel of Fig. 1.7, Ref. [129] found that the effective kinetic theory agrees with hydrodynamics within a short time scale  $\tau \sim 10/Q_s$ , which is consistent with the fast hydrodynamization. Notice that the anisotropy is still quite large  $P_z/P_\perp \sim 0.2$  at this time scale. The theoretical justification of the assumption is quite unobvious, and deserves to be investigated further. One of the interesting trials to this problem is the so-called aHydro framework [130, 131], which tries to extend the ordinary hydrodynamics to such a highly anisotropic regime.

Let us go back to the original questions (a)-(c), and briefly summarize what is answered and what is not:

- (a) The current understanding is that one may use the classical Yang-Mills equation for the field regime and the effective kinetic theory for the particle regime (see Fig. 1.4).

It is, however, totally unclear what is a unified theory which can deal with both regions. This is a very tough task because one has to directly follow non-equilibrium dynamics of a certain quantum field theory. One of the promising approaches is the two particle irreducible approximation for the Kadanoff-Baym equation (2PI formalism; for a review [132]), although numerical simulations of this formalism in QCD are so difficult. Another interesting approach is based on the gauge/gravity duality, which is a conjecture that relates a certain class of gauge theories to the classical gravitational theory. This is done in Refs. [133, 134] for the  $\mathcal{N} = 4$  supersymmetric Yang-Mills theory in the large  $N_c$ -limit. They observed for the first time, preceded to QCD studies, the onset of hydrodynamics occurring before a complete isotropization  $P_z/P_\perp \neq 1$ . The formalism presented in this thesis may give us a first step to resolve this problem.

- (b) Not answered yet. The main focus was gluon production only, and much less attention has been paid to quark production.

Quark production is essential in understanding the chemical equilibration of the system. It is also important in understanding photon and dilepton production mechanism in the pre-equilibrium stage, which may serve as non-vanishing probes for the pre-equilibrium stage because they are free from strong interactions. Furthermore, it is argued that the non-vanishing topological charge density in the glasma results in novel anomaly-induced transport phenomena of quarks such as the chiral magnetic effect [135].

In spite of the importance and the applications listed above, there are only a few studies about quark production in the pre-equilibrium stage dynamics of heavy ion collisions. It was done by Gelis *et al.* [136] and by the author [137] under an assumption that backreaction effects from quarks are negligible. We will overcome this limitation in this thesis.

- (c) Up to now, there is no consensus on this question in the heavy-ion community. One of the promising scenarios is that isotropization and hydrodynamization may take place in the particle regime. In particular, a fast hydrodynamization occurs if we assume that hydrodynamics is still valid to highly anisotropic systems.

As was pointed out, the validity of anisotropic hydrodynamics is quite unclear, and should be investigated further to justify this scenario. We note that there are other scenarios based on bottom-up thermalization [138], transient Bose-Einstein condensate [139], glasma instability [140], chaosity in classical Yang-Mills theory [141], and so on.

### 1.3 Objectives and outline of thesis

The purpose of this thesis is to formulate the backreaction problem of the Schwinger mechanism in QCD starting from quantum field theory. We also apply the formalism (within mean field and massless approximations) to investigate the time-evolution of the field strength, particle distribution functions, and thermodynamic quantities such as pressure and energy density of the system. We furthermore apply the formalism to describe the pre-equilibrium stage dynamics of ultra-relativistic heavy ion collisions by modeling the initial flux tubes by a boost-invariantly expanding, and spatially uniform classical electric field.

To be more specific, we consider quantum fluctuations of quarks, gluons, and ghosts on top of a classical color gauge field. By adopting mean field approximation for the quantum fluctuations on top of a classical gauge field appearing in the QCD Lagrangian, we derive a set of linear differential equations, which accounts for particle production, backreaction, and (partial effects of) scatterings. Our formalism has some advantages and can resolve some problems explained in this Introduction. Namely, our formalism

- includes backreaction and scattering effects of the Schwinger mechanism from both the quark and the gluon (and also the ghost) sectors for the first time based on quantum field theory;
- describes both quark and gluon production, which are missing especially in previous studies of the pre-equilibrium stage dynamics of ultra-relativistic heavy ion collisions;
- naturally explains a transition from the field regime to the particle regime, which may give us a first step for the unified theoretical description of the pre-equilibrium stage dynamics of ultra-relativistic heavy ion collisions; and
- is numerically feasible because it does not suffer from complicated functionals and/or memory integrals as in 2PI formalism.

This thesis is organized as follows: In Chapter 2, the Schwinger mechanism in QED is further reviewed. In Section 2.1, we explain how we formulate the Schwinger mechanism in QED based on quantum field theory within mean field approximation. In Section 2.2, we apply the formalism to a constant and spatially uniform electric field. By neglecting backreaction, we re-derive the Schwinger formula for the vacuum decay rate  $w$  and the pair creation rate  $\Gamma$ . In Section 2.3, we consider a pulsed electric field (Sauter-type electric field [142]) to examine effects of time-dependence; backreaction is still neglected in this section. The results presented in this section is based on my published work [42]. In Section 2.4, dynamical aspects of pair creation is discussed for a constant electric field without backreaction. In Section 2.5, we finally consider backreaction, and see how they affects the time-evolution of the system by numerically evaluating particle distribution functions and thermodynamic quantities such as energy density and pressure. Chapters 3, 4, and 5 are main parts of this thesis. In Chapter 3, we extend the QED

study to  $SU(N_c = 2)$  Yang-Mills theory without quarks. In Section 3.1, starting from quantum field theory, we formulate for the first time the Schwinger mechanism in the Yang-Mills theory including backreaction by adopting mean field approximation. In Section 3.2, we apply the formalism for a constant and spatially uniform color electric field, and analytically follow the time-evolution of the gluon particle distribution function by neglecting higher order quantum effects such as backreaction and scatterings. In Section 3.3, we investigate backreaction effects by numerically tracing particle distribution functions and thermodynamic quantities such as energy density and pressure within massless approximation, and clarify similarities/differences between the gluon production and the previous electron production. In Chapter 4, we further extend our study to the case of  $SU(N_c = 3) \otimes SU(N_f)$  QCD. The formulation will be explained in detail in Section 4.1. In Section 4.2, we first apply the formalism for a constant color electric background field. By neglecting the backreaction, we analytically follow the time-evolution of the quark and gluon distribution functions. Various effects, such as the color angle  $\theta$ -, the number of flavor  $N_f$ -, the quark mass  $m_f$ -effects are examined in detail. In Section 4.3, backreaction is considered, and we shall see that the different quantum statistics of gluons and quarks results in a significant difference in the particle production. In Chapter 5, we apply the formalism presented in Chapter 4 to the pre-equilibrium stage dynamics of ultra-relativistic heavy ion collisions by modeling the initial color flux tubes by a boost-invariantly expanding, spatially uniform classical color electric field. In Section 5.1, we first explain how we extend the Schwinger mechanism, which was originally formulated in a non-expanding geometry, in such a boost-invariantly expanding one. In Section 5.2, particle production without backreaction is discussed based on my unpublished work [137]. In Section 5.3, we take into account backreaction. By numerically tracing the time-evolution of particle distribution functions and thermodynamic quantities such as energy density and pressure within massless approximation, we discuss some phenomenological consequences of our formalism in the pre-equilibrium stage dynamics of ultra-relativistic heavy ion collisions. Chapter 6 is devoted to a summary and an outlook of this thesis.

This thesis contains three appendices: Analytic solutions of the Dirac equation and the Klein-Gordon equation in a non-expanding geometry are presented in Appendix A and B, respectively. Analytic solutions of the Dirac equation and the Klein-Gordon equation for an expanding electric field are derived in Appendix C.

Throughout this thesis, we work in the Heisenberg picture. We implicitly take summation over the repeated indices  $\mu, \nu, \dots$  for *spacetime* only, and not for other repeated indices, for instance, color labels  $A, B, \dots$ , spin labels  $s, s', \dots$ , and so on.



## Chapter 2

# Schwinger Mechanism in Quantum Electrodynamics

The purpose of this chapter is to provide the modern understanding of the nature of the pair production from a strong classical electric field in QED, prior to the extension to the QCD study. In Section 2.1, we formulate the pair production from a strong classical electric field in QED starting from quantum field theory, and explain how one can formulate the backreaction problem within mean field approximation. In Section 2.2, we apply the formalism to a constant electric field. By neglecting backreaction, we re-derive the Schwinger formula for the vacuum decay rate  $w$  and the pair creation rate  $\Gamma$ . In Section 2.3, we consider a pulsed electric field (Sauter-type electric field [142]) to examine effects of time-dependence of the applied field; backreaction is still neglected in this section. In Section 2.4, dynamical aspects of the pair production are discussed for a constant electric field without backreaction. In Section 2.5, we finally discuss backreaction effects by numerically evaluating particle distribution functions and thermodynamic quantities such as energy density and pressure.

Some parts of this chapter are based on works by other authors; in particular, by Tanji [34, 91], and by Kluger *et al.* [51, 52, 53, 54]. The results presented in Section 2.3 are based on my own published work [42].

## 2.1 Formalism

### 2.1.1 QED under a classical gauge field

#### Lagrangian

Throughout this chapter, we consider QED, whose Lagrangian  $\hat{\mathcal{L}}_{\text{QED}}$  is given by

$$\hat{\mathcal{L}}_{\text{QED}} = \underbrace{\hat{\psi}[i\hat{\not{\partial}} - e\hat{\not{A}} - m_e]\hat{\psi} - \frac{1}{4}\hat{F}^{\mu\nu}\hat{F}_{\mu\nu} - \frac{1}{2}(\partial_\mu\hat{A}^\mu)^2}_{\equiv\hat{\mathcal{L}}} - \underbrace{J^\mu\hat{A}_\mu}_{\equiv\hat{\mathcal{L}}_{\text{ext}}}. \quad (2.1)$$

Here,  $\hat{\psi}$  and  $\hat{A}$  are an electron and a photon field operator, respectively.  $J^\mu$  is a classical external source.  $e > 0$  is the coupling constant of QED.  $m_e$  is the electron mass. The field strength tensor is defined by  $\hat{F}_{\mu\nu} \equiv \partial_\mu \hat{A}_\nu - \partial_\nu \hat{A}_\mu$  as usual.  $\not{\hat{\phi}} \equiv \hat{\phi}_\mu \gamma^\mu$  is the Feynman slash notation with  $\gamma^\mu$  being the gamma matrices. We fix the gauge by the Feynman gauge condition by introducing the gauge fixing term as  $-(1/2)(\partial_\mu \hat{A}^\mu)^2$ .

### expansion around a classical field

Generally, there exists a classical gauge field  $\langle \hat{A}_\mu \rangle \neq 0$  because of the presence of the classical source  $J^\mu$ . Now, we wish to understand how the classical field affects the quantum mechanical evolution of a system. To make this situation manifest, we split the total gauge field  $\hat{A}_\mu$  into an incoherent quantum fluctuation (particle)  $\hat{a}_\mu$  and a coherent gauge field (classical field)  $A_\mu$  as

$$\hat{A}_\mu \equiv A_\mu + \hat{a}_\mu, \quad (2.2)$$

where

$$A_\mu \equiv \langle \hat{A}_\mu \rangle, \quad \hat{a}_\mu \equiv \hat{A}_\mu - A_\mu. \quad (2.3)$$

Here,  $\langle \hat{\bullet} \rangle$  is an expectation value of a given initial state  $\langle \hat{\bullet} \rangle \equiv \langle \text{state}; \text{in} | \hat{\bullet} | \text{state}; \text{in} \rangle$ .

We furthermore expand the total Lagrangian  $\hat{\mathcal{L}}_{\text{QED}}$  in terms of the quantum fluctuation  $\hat{a}_\mu$  to obtain

$$\begin{aligned} \hat{\mathcal{L}}_{\text{QED}} = & \hat{\bar{\psi}} [i\not{\partial} - e\not{A} - m_e] \hat{\psi} \\ & - \frac{1}{4} F^{\mu\nu} F_{\mu\nu} - J^\mu A_\mu - \frac{1}{2} (\partial_\mu A^\mu)^2 \\ & - \frac{1}{2} F_{\mu\nu} \hat{f}^{\mu\nu} - (\partial_\mu A^\mu) (\partial_\nu \hat{a}^\nu) - J^\mu \hat{a}_\mu - e \hat{\bar{\psi}} \not{\hat{\phi}} \hat{\psi} \\ & - \frac{1}{4} \hat{f}^{\mu\nu} \hat{f}_{\mu\nu} - \frac{1}{2} (\partial_\mu \hat{a}^\mu)^2. \end{aligned} \quad (2.4)$$

Here,  $F_{\mu\nu} \equiv \partial_\mu A_\nu - \partial_\nu A_\mu$  and  $\hat{f}_{\mu\nu} \equiv \partial_\mu \hat{a}_\nu - \partial_\nu \hat{a}_\mu$  are the classical and the quantum part of the field strength tensor  $\hat{F}_{\mu\nu}$ , respectively.

### conserved quantities

The QED Lagrangian  $\hat{\mathcal{L}}_{\text{QED}}$  (Eq. (2.4)) possesses some symmetries, and there exist some conserved quantities associated with the symmetries. Among them, the electromagnetic current  $\hat{j}^\mu$  and the symmetric energy-momentum tensor  $\hat{T}^{\mu\nu}$  are important.

#### electromagnetic current $\hat{j}^\mu$

The electromagnetic current  $\hat{j}^\mu$  is a conserved quantity associated with a global  $U(1)$  gauge symmetry:

$$\hat{\psi} \rightarrow e^{-ie\theta} \hat{\psi}. \quad (2.5)$$

The conserved quantity associated with this symmetry, i.e., the electromagnetic current  $\hat{j}^\mu$  can be obtained via the Noether theorem [143] as

$$\hat{j}^\mu = e\hat{\psi}\gamma^\mu\hat{\psi}, \quad (2.6)$$

which is conserved as

$$0 = \partial_\mu \hat{j}^\mu. \quad (2.7)$$

Notice that the conservation law Eq. (2.7) is an operator relation, which strictly holds anytime as long as equations of motion of  $\hat{\mathcal{L}}_{\text{QED}}$  are satisfied.

symmetric energy-momentum tensor  $\hat{T}^{\mu\nu}$

Another important quantity is the symmetric energy-momentum tensor  $\hat{T}^{\mu\nu}$  associated with a translational invariance of the system. The symmetric energy-momentum tensor  $\hat{T}^{\mu\nu}$  is defined as a metric variant of the Lagrangian  $\hat{\mathcal{L}}$  as<sup>1</sup>

$$\hat{T}^{\mu\nu} = \frac{-2}{\sqrt{|\mathbf{g}|}} \frac{\delta(|\mathbf{g}|\hat{\mathcal{L}})}{\delta g_{\mu\nu}} = -g^{\mu\nu}\hat{\mathcal{L}} - 2 \left[ \frac{\partial \hat{\mathcal{L}}}{\partial g_{\mu\nu}} - \frac{1}{\sqrt{|\mathbf{g}|}} \partial_\lambda \left( \sqrt{|\mathbf{g}|} \frac{\partial \hat{\mathcal{L}}}{\partial_\lambda g_{\mu\nu}} \right) \right], \quad (2.8)$$

where  $|\mathbf{g}|$  is the determinant of a metric  $g_{\mu\nu}$  (we finally take the Minkowski limit  $g_{\mu\nu} \rightarrow \eta_{\mu\nu}$  as we are working in the Cartesian coordinates now). In terms of the variables  $\hat{A}_\mu, \hat{\psi}$ , the symmetric energy-momentum  $\hat{T}^{\mu\nu}$  can be explicitly expressed as

$$\begin{aligned} \hat{T}^{\mu\nu} = & \frac{1}{4} \eta^{\mu\nu} \hat{F}^{\rho\sigma} \hat{F}_{\rho\sigma} - \hat{F}^\mu{}_\rho \hat{F}^{\nu\rho} \\ & - \frac{1}{2} \eta^{\mu\nu} (\partial_\lambda \hat{A}^\lambda)^2 - \eta^{\mu\nu} \hat{A}^\rho \partial_\rho \partial_\sigma \hat{A}^\sigma + \hat{A}^\mu \partial^\nu \partial_\lambda \hat{A}^\lambda + \hat{A}^\nu \partial^\mu \partial_\lambda \hat{A}^\lambda \\ & + \frac{i}{4} \hat{\psi} \left[ \gamma^\mu (\vec{\partial}^\nu + ie\hat{A}^\nu) + \gamma^\nu (\vec{\partial}^\mu + ie\hat{A}^\mu) - (\vec{\partial}^\nu - ie\hat{A}^\nu) \gamma^\mu - (\vec{\partial}^\mu - ie\hat{A}^\mu) \gamma^\nu \right] \hat{\psi}. \end{aligned} \quad (2.9)$$

The conservation law for the symmetric energy-momentum tensor  $\hat{T}^{\mu\nu}$  reads

$$\partial_\mu \hat{T}^{\mu\nu} = J_\mu \hat{F}^{\mu\nu} + \hat{A}^\nu \partial_\mu J^\mu. \quad (2.10)$$

The RHS is an energy supply from the external source  $J^\mu$ . Again, we note that the above conservation law is a strict operator relation.

The diagonal components of the symmetric energy-momentum tensor give the definition of the energy density  $\hat{\epsilon}$  and the pressure  $\hat{P}_{x,y,z}$  of the system; namely,

$$\hat{\epsilon} \equiv \hat{T}^{tt}, \quad \hat{P}_i \equiv \hat{T}^{ii} \quad (i = x, y, z). \quad (2.11)$$

---

<sup>1</sup>In general, the *symmetric* energy-momentum tensor is not the same as the *canonical* energy-momentum tensor (which is not necessarily symmetric) obtained by the Noether theorem. In the Minkowski spacetime coordinates, the difference between the two is given by the so-called Belinfante-Rosenfeld tensor [144, 145], which is related to the spin angular momentum of the system.

### 2.1.2 assumptions on the system

The above arguments are general in the sense that they do not depend on details of a system. It is, however, difficult to formulate the Schwinger mechanism under such a fully generic case, which is actually an on-going subject of this research area. To avoid the difficulty, let us make some simplifications:

(i) (Homogeneity in space)

We restrict our attention to the case where only a homogeneous classical electric field is present. If we define the  $z$ -axis by the direction of the electric field, then one can write the classical gauge field  $A_\mu$  in the following form without loss of generality by fixing the residual gauge freedom as

$$A^\mu(x) = (0, 0, 0, A(t)) = (0, 0, 0, - \int_{-\infty}^t dt' E(t')). \quad (2.12)$$

In terms of the classical source  $J^\mu$ , this assumption is equivalent to assume that the source is homogeneous in space and has a current component in the  $z$ -direction only  $J^\mu(x) = \delta^{\mu z} J(t)$ .

(ii) (Vacuum initial condition)

We assume that the initial state is given by a vacuum  $|\text{state}; \text{in}\rangle = |\text{vac}; \text{in}\rangle$ , i.e., there are no particles initially.

(iii) (Adiabatic hypothesis)

We assume that, at asymptotic times  $t \rightarrow \pm\infty$ , there are no classical electromagnetic fields, and the classical gauge field  $A_\mu$  becomes merely a pure gauge by adiabatically switching off the source  $J^\mu$  at the asymptotic times.

The first assumption is, indeed, a strong limitation. Extension to spatially inhomogeneous gauge fields may be straightforward if one neglects backreaction effects [137, 147]. If one considers backreaction, however, it brings some difficulties. The most problematic one is the regularization. As was imagined from Introduction and is explained in the following, it is essential to compute an expectation value of a current operator  $\langle \hat{j} \rangle$  to formulate the backreaction problem within quantum field theory. The expectation value is, unfortunately, divergent and hence one has to regularize it to make sense. The problem is that there is no plausible way known so far to regulate such divergences when there exists a *spacetime* dependent background. If the background depends on time only, then, one can safely regulate divergences via, for instance, the normal ordering procedure [34] or the adiabatic regularization [51].

The second assumption is needed in order that the assumption (i) is consistent with the time-evolution of the system. Indeed, the assumption (i) together with equations of motion (at mean field level) requires that the charge density of the system must vanish.

The third assumption is very useful in employing a canonical quantization procedure in Section 2.1.4. It is only when there are no interactions, where one can uniquely define the notion of particles and the corresponding vacuum state.

### 2.1.3 mean field approximation

It is difficult to directly follow the real-time dynamics of the system defined by the Lagrangian  $\hat{\mathcal{L}}_{\text{QED}}$ ; this is because it contains a non-linear interaction which is higher than the cubic order in the quantum fluctuations, i.e.,  $e\hat{\psi}\hat{A}\hat{\psi}$ . As a workaround of this difficulty, let us consider mean field approximation: We replace the non-linear term (higher than the cubic order in the quantum fluctuations) by its expectation value as

$$e\hat{\psi}\hat{A}\hat{\psi} \rightarrow e\hat{a}_\mu \langle \hat{\psi}\gamma^\mu\hat{\psi} \rangle = \hat{a}_\mu \langle \hat{j}^\mu \rangle, \quad (2.13)$$

or

$$\begin{aligned} \hat{\mathcal{L}}_{\text{QED}} \rightarrow & \hat{\psi}[i\hat{\not{D}} - e\hat{A} - m_e]\hat{\psi} \\ & - \frac{1}{4}F^{\mu\nu}F_{\mu\nu} - J^\mu A_\mu - \frac{1}{2}(\partial_\mu A^\mu)^2 \\ & - \frac{1}{2}F_{\mu\nu}\hat{f}^{\mu\nu} - (\partial_\mu A^\mu)(\partial_\nu \hat{a}^\nu) - J^\mu \hat{a}_\mu - \hat{a}_\mu \langle \hat{j}^\mu \rangle \\ & - \frac{1}{4}\hat{f}^{\mu\nu}\hat{f}_{\mu\nu} - \frac{1}{2}(\partial_\mu \hat{a}^\mu)^2. \end{aligned} \quad (2.14)$$

This approximation is equivalent to discarding the fluctuating term  $\hat{j}^\mu - \langle \hat{j}^\mu \rangle$ . This is justifiable when the classical value of the current  $\langle \hat{j}^\mu \rangle$  is large enough, which is formally realized, for instance, in the limit of large number of fermions (i.e., suppose that we have more than one electron)  $N_f \rightarrow \infty$  [51].

Strictly speaking, the above mean field treatment is *ill-defined* because an expectation value of two-point functions, such as the current  $\langle \hat{j}^\mu \rangle$ , generally diverges because of vacuum contributions. Thus, one has to regularize the divergence by subtracting the unwanted vacuum contributions for our mean field treatment to make sense. For now, let us assume that this is correctly done; we postpone this problem until Section 2.1.5, where divergences are regulated by normal ordering procedure [34].

#### equations of motion

One can immediately derive equations of motion from the mean field Lagrangian (2.14), which read

$$0 = \partial_\nu \partial^\nu \hat{a}^\mu, \quad (2.15)$$

$$0 = [i\hat{\not{D}} - e\hat{A} - m_e]\hat{\psi}, \quad (2.16)$$

$$\langle \hat{j}^\mu \rangle + J^\mu = \partial_\nu \partial^\nu A^\mu. \quad (2.17)$$

The first two are the equations for the quantum fluctuations  $\hat{a}_\mu, \hat{\psi}$ . Thanks to the mean field treatment, these two equations are linear in the quantum fluctuations. This enables us to canonically quantize the fluctuations  $\hat{a}_\mu, \hat{\psi}$ , and to directly compute an expectation value of the corresponding number operator. Notice that the equation for  $\hat{a}_\mu$  is the same as the free one, and thus no particle production occurs for this fluctuation. This is because photons have no electric charge, and do not couple to the classical gauge field  $A_\mu$ . Hence, we do not consider the fluctuation  $\hat{a}_\mu$  in the following discussion for simplicity. On the contrary, the electron field  $\hat{\psi}$  does couple to the classical gauge field  $A_\mu$  through the interaction term  $e\hat{A}\hat{\psi}$ , which represents a multiple scattering between the classical field and electrons. This term is responsible for electron (and positron) production; see Section 2.1.4 for the detail.

The third equation is for the classical gauge field  $A_\mu$ . The physical meaning of this equation is that the electromagnetic current due to produced electrons  $\langle \hat{j}^\mu \rangle$  (the source term on the LHS) screens the original classical gauge field  $A_\mu$  through the Maxwell equation. In this way, one can formulate the backreaction problem in QED. An important point here is that one has to go beyond the one-loop treatment to include the backreaction; it is the quantum interactions of the cubic order in the quantum fluctuation that are responsible for the backreaction in QED.

By recalling the assumption (i) (i.e., homogeneity of the system) made in Section 2.1.2, one can simplify the third equation (2.17) as

$$0 = \langle \hat{j}^t \rangle = \langle \hat{j}^x \rangle = \langle \hat{j}^y \rangle, \quad (2.18)$$

$$\langle \hat{j}^z \rangle + J^z = \frac{d^2 A}{dt^2} = -\frac{dE}{dt}. \quad (2.19)$$

Equation (2.18) tells us that the local charge density of produced particles  $\langle \hat{j}^t \rangle$  is always zero. This is a manifestation of the charge symmetry in QED. Indeed, we shall see in Section 2.1.4 that electrons and positrons are simultaneously created and that the number of electrons and of positrons are the same.

### conservation law

Under the mean field treatment, the conservation laws, Eqs. (2.7) and (2.10), do not hold at the *operator* level; nevertheless, they do hold at the *mean field* level. This is because the mean field approximation does not change the expectation value of the Lagrangian. By using the equations of motion within our mean field treatment, Eqs. (2.15)-(2.17), one can explicitly show the conservation law for the electromagnetic current,

$$0 = \partial_\mu \langle \hat{j}^\mu \rangle, \quad (2.20)$$

and for the symmetric energy-momentum tensor,

$$\partial_\mu \langle \hat{T}^{\mu\nu} \rangle = J_\mu F^{\mu\nu} + A^\nu \partial_\mu J^\mu. \quad (2.21)$$

If the system is homogeneous in space as we have assumed in (i) in Section 2.1.2, the conservation law for  $\langle \hat{j}^\mu \rangle$  reads

$$0 = \partial_t \langle \hat{j}^t \rangle, \quad (2.22)$$

which trivially follows from Eq. (2.18). On the other hand, the conservation laws for  $\langle \hat{T}^{\mu\nu} \rangle$  (2.21) can be simplified as

$$\partial_t \langle \hat{\epsilon} \rangle = -EJ^z, \quad (2.23)$$

which is nothing but the energy conservation law under an external current  $J^z$ .

## 2.1.4 canonical quantization and particle production

In this subsection, we canonically quantize the fluctuation  $\hat{\psi}$  in the presence of the classical gauge field  $A_\mu$ , and compute particle spectra produced from the classical field.

In the canonical quantization procedure, it is important to identify what are *correct* positive/negative frequency mode functions. In the usual quantum field theory of free fields, one can easily identify the correct positive/negative frequency mode functions by the plane wave solutions  $\propto e^{\mp i p^0 t} e^{i \mathbf{p} \cdot \mathbf{x}}$  (i.e., eigenfunctions of the translational operator  $i \partial_\mu$ ) because of the Poincaré invariance. If interactions are present, however, the Poincaré invariance is broken (i.e., non-zero energy and momentum are supplied from the interactions), so that there is no guiding principle to identify the positive/negative frequency mode functions.

In our problem, the classical gauge field  $A_\mu$  becomes merely a pure gauge and no interaction occurs at asymptotic times  $t \rightarrow \pm\infty$  (assumption (iii) in Section 2.1.2). In this case, the canonical quantization procedure at the asymptotic times is doable without any ambiguity because one can identify the positive/negative frequency mode functions at the corresponding asymptotic time by the plane wave solutions as usual; this program is addressed in the first half of this subsection. For intermediate regions  $-\infty < t < \infty$ , however, interactions prevent us from uniquely identifying the positive/negative frequency mode functions. Hence, ambiguities must come in during the canonical quantization procedure, that is, the definition of a particle and of a vacuum must be ambiguous. Nevertheless, it is very useful to make a *working definition* of positive/negative frequency mode functions for intermediate regions in order to describe dynamics of particle production. This is also important in regulating our mean field theory, for which one has to identify the unwanted vacuum contributions to subtract. In the last half of this subsection, we shall make such a working definition by assuming that the classical gauge field is sufficiently adiabatic<sup>2</sup>.

---

<sup>2</sup>This kind of problems frequently appear in the context of cosmological particle production, where the curved spacetime plays a role of the classical gauge field, and the adiabatic approach is frequently applied in this research area as well [50].

### canonical quantization at asymptotic times and particle spectrum at $t \rightarrow \infty$

The homogeneity of the system (assumption (i) in Section 2.1.2) enables us to Fourier expand the fluctuation  $\hat{\psi}$  by positive/negative frequency mode functions  $_{\pm}\psi_{\mathbf{p},s}^{(\text{as})}$  (as = in for  $t \rightarrow -\infty$  and out for  $t \rightarrow \infty$ ) as

$$\hat{\psi}(x) = \sum_s \int d^3\mathbf{p} \left[ {}_+\psi_{\mathbf{p},s}^{(\text{as})}(t) \hat{a}_{\mathbf{p},s}^{(\text{as})} + {}_-\psi_{\mathbf{p},s}^{(\text{as})}(t) \hat{b}_{-\mathbf{p},s}^{(\text{as})\dagger} \right] \frac{e^{i\mathbf{p}\cdot\mathbf{x}}}{(2\pi)^{3/2}}, \quad (2.24)$$

where  $\mathbf{p}$  labels *canonical* momenta, and  $s$  labels spin degrees of freedom. We normalize the mode functions by

$$({}_{\pm}\psi_{\mathbf{p},s}^{(\text{as})} | {}_{\pm}\psi_{\mathbf{p},s'}^{(\text{as})})_{\text{F}} = \delta_{ss'}, \quad ({}_{\pm}\psi_{\mathbf{p},s}^{(\text{as})} | {}_{\mp}\psi_{\mathbf{p},s'}^{(\text{as})})_{\text{F}} = 0 \quad (2.25)$$

for each as = in, out. Here, the fermion inner product  $(\psi_1 | \psi_2)_{\text{F}}$  is denoted by

$$(\psi_1 | \psi_2)_{\text{F}} \equiv \psi_1^{\dagger} \psi_2, \quad (2.26)$$

which stays constant during the whole spacetime evolution as long as the fermionic quantities  $\psi_1, \psi_2$  obey the same Dirac equation (2.16).

The positive/negative frequency mode functions are identified as solutions of the equation of motion (2.16) with *plane wave boundary conditions* at  $t \rightarrow \pm\infty$ : By noting that the classical gauge field  $A_{\mu}$  becomes merely a pure gauge and no interaction occurs at the asymptotic times  $t \rightarrow \pm\infty$ , it is natural to require that the positive/negative frequency mode functions coincide with those of free fields at each asymptotic time; namely, we require the following boundary conditions for the mode functions:

$$\begin{pmatrix} {}_+\psi_{\mathbf{p},s}^{(\text{in})} \\ {}_-\psi_{\mathbf{p},s}^{(\text{in})} \end{pmatrix} \xrightarrow{t \rightarrow -\infty} \begin{pmatrix} u_{\mathbf{p}-e\mathbf{A},s} \exp \left[ -i \int_{-\infty}^t \omega_{\mathbf{p}-e\mathbf{A}} dt \right] \\ v_{-\mathbf{p}+e\mathbf{A},s} \exp \left[ +i \int_{-\infty}^t \omega_{\mathbf{p}-e\mathbf{A}} dt \right] \end{pmatrix}, \quad (2.27)$$

$$\begin{pmatrix} {}_+\psi_{\mathbf{p},s}^{(\text{out})} \\ {}_-\psi_{\mathbf{p},s}^{(\text{out})} \end{pmatrix} \xrightarrow{t \rightarrow \infty} \begin{pmatrix} u_{\mathbf{p}-e\mathbf{A},s} \exp \left[ -i \int_{-\infty}^t \omega_{\mathbf{p}-e\mathbf{A}} dt \right] \\ v_{-\mathbf{p}+e\mathbf{A},s} \exp \left[ +i \int_{-\infty}^t \omega_{\mathbf{p}-e\mathbf{A}} dt \right] \end{pmatrix}. \quad (2.28)$$

Here,  $\omega_{\mathbf{p}-e\mathbf{A}} \equiv \sqrt{(\mathbf{p} - e\mathbf{A})^2 + m_e^2}$  is the on-shell energy of an electron.  $u_{\mathbf{p},s}, v_{\mathbf{p},s}$  are the free-spinors of electrons and positrons, respectively, normalized as

$$u_{\mathbf{p},s}^{\dagger} u_{\mathbf{p},s'} = v_{\mathbf{p},s}^{\dagger} v_{\mathbf{p},s'} = \delta_{ss'}, \quad u_{\mathbf{p},s}^{\dagger} v_{-\mathbf{p},s'} = 0. \quad (2.29)$$

For details of the free-spinors  $u_{\mathbf{p},s}, v_{\mathbf{p},s}$ , see Appendix A.1.

Now, we impose canonical commutation relations

$$\{\hat{\psi}(t, \mathbf{x}), \hat{\psi}^{\dagger}(t, \mathbf{x}')\} = \delta^3(\mathbf{x} - \mathbf{x}'), \quad \{\hat{\psi}(t, \mathbf{x}), \hat{\psi}(t, \mathbf{x}')\} = 0 \quad (2.30)$$

to obtain annihilation operators at each asymptotic time,  $\hat{a}^{(\text{as})}$  and  $\hat{b}^{(\text{as})}$ , for the positive and the negative frequency mode, respectively. The anti-commutation relations for the annihilation operators read

$$\{a_{\mathbf{p},s}^{(\text{as})}, a_{\mathbf{p}',s'}^{(\text{as})\dagger}\} = \{b_{\mathbf{p},s}^{(\text{as})}, b_{\mathbf{p}',s'}^{(\text{as})\dagger}\} = \delta_{ss'}\delta^3(\mathbf{p} - \mathbf{p}'), \quad (\text{others}) = 0 \quad (2.31)$$

for each as = in, out.

An important point here is that the mode functions  $\pm\psi_{\mathbf{p},s}^{(\text{as})}$  do fully include the multiple interactions with the classical field  $A_\mu$  through the interaction term  $e\mathcal{A}\hat{\psi}$  in the Dirac equation (2.16), and hence the positive (or negative) frequency mode at  $t \rightarrow -\infty$  will evolve into a linear combination of the positive and negative frequency modes at  $t \rightarrow \infty$ . This is essentially the same as what we encounter in an one-dimensional barrier scattering problem where we always have a mixture of in-coming wave and its reflection on one side of the barrier, but the other side consists of out-going wave only. The linear relation between the modes can be described by a Bogoliubov transformation given by

$$\begin{aligned} \begin{pmatrix} \hat{a}_{\mathbf{p},s}^{(\text{out})} \\ \hat{b}_{-\mathbf{p},s}^{(\text{out})\dagger} \end{pmatrix} &= \int d^3\mathbf{x} \frac{e^{-i\mathbf{p}\cdot\mathbf{x}}}{(2\pi)^{3/2}} \begin{pmatrix} (+\psi_{\mathbf{p},s}^{(\text{out})}|\hat{\psi})_{\text{F}} \\ (-\psi_{\mathbf{p},s}^{(\text{out})}|\hat{\psi})_{\text{F}} \end{pmatrix} \\ &= \begin{pmatrix} (+\psi_{\mathbf{p},s}^{(\text{out})}|+\psi_{\mathbf{p},s}^{(\text{in})})_{\text{F}} & (+\psi_{\mathbf{p},s}^{(\text{out})}|-\psi_{\mathbf{p},s}^{(\text{in})})_{\text{F}} \\ (-\psi_{\mathbf{p},s}^{(\text{out})}|+\psi_{\mathbf{p},s}^{(\text{in})})_{\text{F}} & (-\psi_{\mathbf{p},s}^{(\text{out})}|-\psi_{\mathbf{p},s}^{(\text{in})})_{\text{F}} \end{pmatrix} \begin{pmatrix} \hat{a}_{\mathbf{p},s}^{(\text{in})} \\ \hat{b}_{-\mathbf{p},s}^{(\text{in})\dagger} \end{pmatrix} \\ &= \begin{pmatrix} \alpha_{\mathbf{p},s}^{(\text{out})} & \beta_{\mathbf{p},s}^{(\text{out})} \\ -\beta_{\mathbf{p},s}^{(\text{out})*} & \alpha_{\mathbf{p},s}^{(\text{out})*} \end{pmatrix} \begin{pmatrix} \hat{a}_{\mathbf{p},s}^{(\text{in})} \\ \hat{b}_{-\mathbf{p},s}^{(\text{in})\dagger} \end{pmatrix}. \end{aligned} \quad (2.32)$$

In the last line, we have used  $(+\psi_{\mathbf{p},s}^{(\text{out})}|+\psi_{\mathbf{p},s}^{(\text{in})})_{\text{F}} = (-\psi_{\mathbf{p},s}^{(\text{out})}|-\psi_{\mathbf{p},s}^{(\text{in})})_{\text{F}}^*$  and  $(+\psi_{\mathbf{p},s}^{(\text{out})}|-\psi_{\mathbf{p},s}^{(\text{in})})_{\text{F}} = -(-\psi_{\mathbf{p},s}^{(\text{out})}|+\psi_{\mathbf{p},s}^{(\text{in})})_{\text{F}}^*$ , which follows from the orthonormality of  $\pm\psi_{\mathbf{p},s}^{(\text{as})}$  (Eq. (2.25)). The Bogoliubov coefficients  $\alpha^{(\text{out})}, \beta^{(\text{out})}$  satisfy the following normalization:

$$1 = |\alpha_{\mathbf{p},s}^{(\text{out})}|^2 + |\beta_{\mathbf{p},s}^{(\text{out})}|^2 \quad (2.33)$$

Thus, the annihilation operators at  $t \rightarrow -\infty$  and those at  $t \rightarrow \infty$  are inequivalent. This means that the corresponding vacuum state, which satisfies

$$0 = a_{\mathbf{p},s}^{(\text{as})} |\text{vac}; \text{as}\rangle = b_{\mathbf{p},s}^{(\text{as})} |\text{vac}; \text{as}\rangle \quad (\text{as} = \text{in}, \text{out}) \quad (2.34)$$

for arbitrary  $\mathbf{p}$  and  $s$ , are also inequivalent. The inequivalence can be expressed by the Bogoliubov coefficients  $\alpha^{(\text{out})}, \beta^{(\text{out})}$  as

$$\begin{aligned} |\text{vac}; \text{out}\rangle &= \sqrt{P^{(\text{out})}} \prod_{\mathbf{p},s} \exp \left[ -\frac{(2\pi)^3}{V} \frac{\beta_{\mathbf{p},s}^{(\text{out})}}{\alpha_{\mathbf{p},s}^{(\text{out})}} a_{\mathbf{p},s}^{(\text{in})\dagger} b_{-\mathbf{p},s}^{(\text{in})\dagger} \right] |\text{vac}; \text{in}\rangle \\ &= \sqrt{P^{(\text{out})}} \prod_{\mathbf{p},s} \left[ 1 - \frac{(2\pi)^3}{V} \frac{\beta_{\mathbf{p},s}^{(\text{out})}}{\alpha_{\mathbf{p},s}^{(\text{out})}} a_{\mathbf{p},s}^{(\text{in})\dagger} b_{-\mathbf{p},s}^{(\text{in})\dagger} \right] |\text{vac}; \text{in}\rangle. \end{aligned} \quad (2.35)$$

This relation predicts that pair production occurs; the final vacuum  $|\text{vac}; \text{out}\rangle$  at  $t \rightarrow \infty$  starting from the initial vacuum  $|\text{vac}; \text{in}\rangle$  at  $t \rightarrow -\infty$  contains pairs of an electron with momentum  $\mathbf{p}$  and a positron with momentum  $-\mathbf{p}$  with a weight  $\propto \beta_{\mathbf{p},s}/\alpha_{\mathbf{p},s}$ . Because of this pair production, the vacuum persistence probability  $P^{(\text{out})} = |\langle \text{vac}; \text{in} | \text{vac}; \text{out} \rangle|^2 / |\langle \text{vac}; \text{in} | \text{vac}; \text{in} \rangle|^2$  is smaller than unity, and the vacuum decays. By using the normalization condition  $1 = |\langle \text{vac}; \text{out} | \text{vac}; \text{out} \rangle|^2 / |\langle \text{vac}; \text{in} | \text{vac}; \text{in} \rangle|^2$ , one can explicitly write down  $P^{(\text{out})}$  as

$$P^{(\text{out})} = \prod_{\mathbf{p},s} (1 - |\beta_{\mathbf{p},s}^{(\text{out})}|^2) = \exp \left[ -\frac{V}{(2\pi)^3} \sum_s \int d^3\mathbf{p} \sum_{n=1}^{\infty} \frac{|\beta_{\mathbf{p},s}^{(\text{out})}|^{2n}}{n} \right], \quad (2.36)$$

from which one can deduce the (average) vacuum decay rate  $w$  as

$$w = \frac{1}{T} \sum_s \int \frac{d^3\mathbf{p}}{(2\pi)^3} \sum_{n=1}^{\infty} \frac{|\beta_{\mathbf{p},s}^{(\text{out})}|^{2n}}{n} \quad (2.37)$$

One can also directly compute the electron and positron spectra at  $t \rightarrow \infty$  thanks to the above canonical quantization procedure. The electron (positron) spectrum is computed as an expectation value of the corresponding number density operator  $\hat{a}_{\mathbf{p},s}^{(\text{out})\dagger} \hat{a}_{\mathbf{p},s}^{(\text{out})}$  ( $\hat{b}_{\mathbf{p},s}^{(\text{out})\dagger} \hat{b}_{\mathbf{p},s}^{(\text{out})}$ ) by a given initial state  $|\text{vac}; \text{in}\rangle$  as

$$\frac{d^6 N_{e^-}^{(\text{out})}(\mathbf{p}, s)}{d\mathbf{p}^3 d\mathbf{x}^3} \equiv \frac{1}{V} \langle \hat{a}_{\mathbf{p},s}^{(\text{out})\dagger} \hat{a}_{\mathbf{p},s}^{(\text{out})} \rangle = \frac{|\beta_{\mathbf{p},s}^{(\text{out})}|^2}{(2\pi)^3}, \quad (2.38)$$

$$\frac{d^6 N_{e^+}^{(\text{out})}(\mathbf{p}, s)}{d\mathbf{p}^3 d\mathbf{x}^3} \equiv \frac{1}{V} \langle \hat{b}_{\mathbf{p},s}^{(\text{out})\dagger} \hat{b}_{\mathbf{p},s}^{(\text{out})} \rangle = \frac{|\beta_{-\mathbf{p},s}^{(\text{out})}|^2}{(2\pi)^3}. \quad (2.39)$$

An important point here is that deriving the particle spectrum is thus reduced to computing the Bogoliubov coefficient  $\beta_{\mathbf{p},s}$  by solving the Dirac equation (2.16) with proper boundary conditions. Remark that this formalism, which takes into account the interactions with the classical field  $A_\mu$  non-perturbatively by fully solving the equations of motion, does include perturbative contributions as well which can be computed by, for instance, the usual diagrammatic techniques of the  $S$ -matrix [148]. For a specific type of electric fields, one can explicitly check this (see Section 2.3).

Let us comment a little bit more about Eqs. (2.38) and (2.39):

- The total number of produced electrons and of positrons  $\int d^3\mathbf{p} d^6 N_{e^\pm}^{(\text{out})} / d^3\mathbf{p} d\mathbf{x}^3$  are the same; this is the manifestation of the charge symmetry in QED.
- $d^6 N_{e^-}^{(\text{out})}(\mathbf{p}, s) / d\mathbf{p}^3 d\mathbf{x}^3 = d^6 N_{e^+}^{(\text{out})}(-\mathbf{p}, s) / d\mathbf{p}^3 d\mathbf{x}^3$  holds reflecting the fact that an electron and a positron are produced simultaneously so as to satisfy the momentum conservation law  $\mathbf{p} + (-\mathbf{p}) = \mathbf{0}$ , where  $\mathbf{0}$  is the momentum that a vacuum carries.
- The Pauli principle strictly holds as  $(2\pi)^3 d^6 N_{e^\pm}^{(\text{out})} / d\mathbf{p}^3 d\mathbf{x}^3 \leq 1$ , which follows from the normalization condition for the Bogoliubov coefficients (2.33).
- It is evident that the (average) vacuum persistence probability  $w$  and the (average) particle production rate  $\Gamma \equiv (1/T) \int d^3\mathbf{p} d^6 N_{e^\pm}^{(\text{out})} / d^3\mathbf{p} d\mathbf{x}^3$  do not agree with each other.

### canonical quantization and particle spectrum for intermediate regions

Let us define positive/negative frequency mode functions for intermediate regions  $-\infty < t < \infty$ , where interactions with the classical gauge field  $A_\mu$  are still present. To do this, let us *assume* that the classical gauge field is sufficiently adiabatic in time. Then, it is natural to think that *correct* positive/negative frequency mode functions at an intermediate time  $t = t_0$  ( $-\infty < t_0 < \infty$ ) do not deviate significantly from the plane waves at  $t = t_0$  because the deviation should be suppressed by factors of  $\partial_t^n A_\mu / dt^n$  ( $n \geq 1$ ).

This consideration urges us to *define* the positive/negative frequency mode functions at an intermediate time by the following plane wave form:

$$\begin{pmatrix} +\psi_{\mathbf{p},s}^{(t)}(t) \\ -\psi_{\mathbf{p},s}^{(t)}(t) \end{pmatrix} \equiv \begin{pmatrix} u_{\mathbf{p}-e\mathbf{A}(t),s} \exp \left[ -i \int_{-\infty}^t \omega_{\mathbf{p}-e\mathbf{A}(t)} dt \right] \\ v_{-\mathbf{p}+e\mathbf{A}(t),s} \exp \left[ +i \int_{-\infty}^t \omega_{\mathbf{p}-e\mathbf{A}(t)} dt \right] \end{pmatrix}. \quad (2.40)$$

From the normalization condition (2.29) for the free-spinors  $u_{\mathbf{p},s}, v_{\mathbf{p},s}$ , one immediately understands that the intermediate mode functions  $\pm\psi_{\mathbf{p},s}^{(t)}$  are normalized as

$$(\pm\psi_{\mathbf{p},s}^{(t)} | \pm\psi_{\mathbf{p},s'}^{(t)})_{\text{F}} = \delta_{ss'}, \quad (\pm\psi_{\mathbf{p},s}^{(t)} | \mp\psi_{\mathbf{p},s'}^{(t)})_{\text{F}} = 0. \quad (2.41)$$

Notice that in the limit of  $t \rightarrow \pm\infty$ ,  $\pm\psi_{\mathbf{p},s}^{(t)}$  smoothly approaches the correct mode functions at asymptotic times  $\pm\psi_{\mathbf{p},s}^{(\text{as})}$  as

$$\pm\psi_{\mathbf{p},s}^{(t)} \xrightarrow[t \rightarrow -\infty]{} \pm\psi_{\mathbf{p},s}^{(\text{in})}, \quad \pm\psi_{\mathbf{p},s}^{(t)} \xrightarrow[t \rightarrow \infty]{} \pm\psi_{\mathbf{p},s}^{(\text{out})}. \quad (2.42)$$

The corresponding annihilation operators at an intermediate time,  $\hat{a}_{\mathbf{p},s}(t)$  and  $\hat{b}_{\mathbf{p},s}(t)$ , are obtained by expanding the fluctuation  $\hat{\psi}$  by the intermediate mode functions  $\pm\psi_{\mathbf{p},s}^{(t)}$  as

$$\hat{\psi}(x) = \sum_s \int d^3\mathbf{p} \left[ +\psi_{\mathbf{p},s}^{(t)}(t) \hat{a}_{\mathbf{p},s}(t) + -\psi_{\mathbf{p},s}^{(t)}(t) \hat{b}_{-\mathbf{p},s}^\dagger(t) \right] \frac{e^{i\mathbf{p}\cdot\mathbf{x}}}{(2\pi)^{3/2}}. \quad (2.43)$$

The annihilation operators,  $\hat{a}_{\mathbf{p},s}(t)$  and  $\hat{b}_{\mathbf{p},s}(t)$ , are time-dependent because the intermediate mode functions  $\pm\psi_{\mathbf{p},s}^{(t)}$  do not satisfy the original Dirac equation (2.16). Because of the asymptotic behavior of  $\pm\psi_{\mathbf{p},s}^{(t)}$  (2.42), the intermediate annihilation operators smoothly coincide with those at asymptotic times  $t \rightarrow \pm\infty$ . The anti-commutation relations for these annihilation operators can be obtained from the canonical commutation relations for the field operator  $\hat{\psi}$  (2.30) as

$$\{a_{\mathbf{p},s}(t), a_{\mathbf{p}',s'}^\dagger(t)\} = \{b_{\mathbf{p},s}(t), b_{\mathbf{p}',s'}^\dagger(t)\} = \delta_{ss'} \delta^3(\mathbf{p} - \mathbf{p}'), \quad (\text{others}) = 0, \quad (2.44)$$

which are the same as for the asymptotic ones.

Because of the multiple interactions with the classical field  $A_\mu$ , the positive (negative) frequency mode at an intermediate time  $t$  becomes a linear combination of those at  $t \rightarrow -\infty$ . From

the orthonormality condition for  $_{\pm}\psi_{\mathbf{p},s}^{(t_0)}$  (2.41), one again finds that the annihilation operators at an intermediate time are related to those at  $t \rightarrow -\infty$  by a Bogoliubov transformation:

$$\begin{pmatrix} \hat{a}_{\mathbf{p},s}(t) \\ \hat{b}_{-\mathbf{p},s}^{\dagger}(t) \end{pmatrix} = \begin{pmatrix} \alpha_{\mathbf{p},s}(t) & \beta_{\mathbf{p},s}(t) \\ -\beta_{\mathbf{p},s}^*(t) & \alpha_{\mathbf{p},s}^*(t) \end{pmatrix} \begin{pmatrix} \hat{a}_{\mathbf{p}',s'}^{(\text{in})} \\ \hat{b}_{-\mathbf{p}',s'}^{(\text{in})\dagger} \end{pmatrix}. \quad (2.45)$$

Here, the Bogoliubov coefficients are given by

$$\alpha_{\mathbf{p},s}(t) \equiv ({}_{+}\psi_{\mathbf{p},s}^{(t)} | {}_{+}\psi_{\mathbf{p},s}^{(\text{in})})_{\text{F}} = ({}_{-}\psi_{\mathbf{p},s}^{(t)} | {}_{-}\psi_{\mathbf{p},s}^{(\text{in})})_{\text{F}}^*, \quad (2.46)$$

$$\beta_{\mathbf{p},s}(t) \equiv ({}_{+}\psi_{\mathbf{p},s}^{(t)} | {}_{-}\psi_{\mathbf{p},s}^{(\text{in})})_{\text{F}} = -({}_{-}\psi_{\mathbf{p},s}^{(t)} | {}_{+}\psi_{\mathbf{p},s}^{(\text{in})})_{\text{F}}^*, \quad (2.47)$$

and are normalized as

$$1 = |\alpha_{\mathbf{p},s}(t)|^2 + |\beta_{\mathbf{p},s}(t)|^2. \quad (2.48)$$

The Bogoliubov transformation (2.45) coincides with that at  $t \rightarrow \infty$  (2.32) because of Eq. (2.42).

From the Bogoliubov transformation (2.45), one can derive various quantities at intermediate times such as the vacuum persistence probability, electron and positron spectra and so on in the same manner as in the  $t \rightarrow \infty$  case. We do not repeat the derivation here, but just write down the results:

- The intermediate vacuum  $|\text{vac}; t\rangle$ :

$$\begin{aligned} |\text{vac}; t\rangle &= \sqrt{P(t)} \prod_{\mathbf{p},s} \exp \left[ -\frac{(2\pi)^3}{V} \frac{\beta_{\mathbf{p},s}(t)}{\alpha_{\mathbf{p},s}(t)} a_{\mathbf{p},s}^{\dagger}(t) b_{-\mathbf{p},s}^{\dagger}(t) \right] |\text{vac}; \text{in}\rangle \\ &= \sqrt{P(t)} \prod_{\mathbf{p},s} \left[ 1 - \frac{(2\pi)^3}{V} \frac{\beta_{\mathbf{p},s}(t)}{\alpha_{\mathbf{p},s}(t)} a_{\mathbf{p},s}^{\dagger}(t) b_{-\mathbf{p},s}^{\dagger}(t) \right] |\text{vac}; \text{in}\rangle. \end{aligned} \quad (2.49)$$

- The vacuum persistence probability  $P$ :

$$P(t) = \prod_{\mathbf{p},s} (1 - |\beta_{\mathbf{p},s}(t)|^2) = \exp \left[ -\frac{V}{(2\pi)^3} \sum_s \int d^3\mathbf{p} \sum_{n=1}^{\infty} \frac{|\beta_{\mathbf{p},s}(t)|^{2n}}{n} \right]. \quad (2.50)$$

- The vacuum decay rate  $w$ :

$$w(t) = \frac{d}{dt} \sum_s \int \frac{d^3\mathbf{p}}{(2\pi)^3} \sum_{n=1}^{\infty} \frac{|\beta_{\mathbf{p},s}(t)|^{2n}}{n}. \quad (2.51)$$

- The electron and positron spectra  $d^6 N_{e_{\pm}}^{(t)}(\mathbf{p}, s; t)/d\mathbf{p}^3 d\mathbf{x}^3$ :

$$\frac{d^6 N_{e^-}(\mathbf{p}, s; t)}{d\mathbf{p}^3 d\mathbf{x}^3} = \frac{d^6 N_{e^+}(-\mathbf{p}, s; t)}{d\mathbf{p}^3 d\mathbf{x}^3} = \frac{|\beta_{\mathbf{p},s}(t)|^2}{(2\pi)^3}. \quad (2.52)$$

For later purposes, it is useful to investigate the ultraviolet ( $\omega_{\mathbf{p}-e\mathbf{A}} \rightarrow \infty$ ) behavior of the Bogoliubov coefficients  $\alpha_{\mathbf{p},s}, \beta_{\mathbf{p},s}$ . In doing this, we first note that the in-state mode functions  $+\psi_{\mathbf{p},s}^{(\text{in})}$  are related to the intermediate ones  $+\psi_{\mathbf{p},s}^{(t)}$  as

$$\begin{pmatrix} +\psi_{\mathbf{p},s}^{(\text{in})} \\ -\psi_{\mathbf{p},s}^{(\text{in})} \end{pmatrix} = \begin{pmatrix} \alpha_{\mathbf{p},s}(t) & -\beta_{\mathbf{p},s}^*(t) \\ \beta_{\mathbf{p},s}(t) & \alpha_{\mathbf{p},s}^*(t) \end{pmatrix} \begin{pmatrix} +\psi_{\mathbf{p},s}^{(t)} \\ -\psi_{\mathbf{p},s}^{(t)} \end{pmatrix}, \quad (2.53)$$

because

$$+\psi_{\mathbf{p},s}^{(\text{in})}(t)\hat{a}_{\mathbf{p},s}^{(\text{in})} + -\psi_{\mathbf{p},s}^{(\text{in})}(t)\hat{b}_{-\mathbf{p},s}^{(\text{in})\dagger} = +\psi_{\mathbf{p},s}^{(t)}(t)\hat{a}_{\mathbf{p},s}(t) + -\psi_{\mathbf{p},s}^{(t)}(t)\hat{b}_{-\mathbf{p},s}^{(t)\dagger} \quad (2.54)$$

holds. By substituting this Bogoliubov relation into the original Dirac equation (2.16), one obtains a differential equation for the Bogoliubov coefficients  $\alpha_{\mathbf{p},s}, \beta_{\mathbf{p},s}$  as

$$\frac{d}{dt} \begin{pmatrix} \alpha_{\mathbf{p},s} \\ \beta_{\mathbf{p},s} \end{pmatrix} = -\frac{1}{2} \frac{eE}{\omega_{\mathbf{p}-e\mathbf{A}}} \frac{\sqrt{m_e^2 + \mathbf{p}_\perp^2}}{\omega_{\mathbf{p}-e\mathbf{A}}} \exp \left[ 2i \int_{-\infty}^t \omega_{\mathbf{p}-e\mathbf{A}} dt \right] \begin{pmatrix} \beta_{\mathbf{p},s}^* \\ \alpha_{\mathbf{p},s}^* \end{pmatrix}. \quad (2.55)$$

One can iteratively solve Eq. (2.55) order-by-order in  $\omega_{\mathbf{p}}$  to find

$$\alpha_{\mathbf{p},s} = 1 + \mathcal{O}(\omega_{\mathbf{p}-e\mathbf{A}}^{-3}), \quad \beta_{\mathbf{p},s} = \frac{i}{4} \frac{eE}{\omega_{\mathbf{p}-e\mathbf{A}}^2} \frac{\sqrt{m_e^2 + \mathbf{p}_\perp^2}}{\omega_{\mathbf{p}-e\mathbf{A}}} \exp \left[ 2i \int_{-\infty}^t \omega_{\mathbf{p}-e\mathbf{A}} dt \right] + \mathcal{O}(\omega_{\mathbf{p}-e\mathbf{A}}^{-3}). \quad (2.56)$$

Here, we have used  $\pm\psi_{\mathbf{p},s}^{(\text{in})} \xrightarrow{\omega_{\mathbf{p}} \rightarrow \infty} \pm\psi_{\mathbf{p},s}^{(t)}$  in determining the boundary condition  $\alpha_{\mathbf{p},s} \xrightarrow{\omega_{\mathbf{p}} \rightarrow \infty} 1, \beta_{\mathbf{p},s} \xrightarrow{\omega_{\mathbf{p}} \rightarrow \infty} 0$ . Notice that  $|\beta|^2$  falls faster than  $\omega_{\mathbf{p}}^4$ , which guarantees that the total number of produced particles  $\int d^3\mathbf{p} |\beta_{\mathbf{p},s}|^2$  stays finite.

## 2.1.5 regularization

In this subsection, we discuss how to regularize fermionic two-point functions  $\langle \hat{\psi} \Gamma \hat{\psi} \rangle$ , where  $\Gamma$  represents  $1, \gamma^\mu, \partial_\mu, \dots$  and so on. As was mentioned, the regularization is important for our mean field treatment to make sense. The main message of this subsection is that the divergence in the two-point functions originates from vacuum contributions, which are safely subtracted via a normal ordering procedure [34] with respect to the intermediate operators introduced in Eq. (2.43).

To be explicit, let us consider the current  $\langle \hat{j}^z \rangle = \langle \hat{\psi} \gamma^z \hat{\psi} \rangle$  ( $\Gamma = \gamma^z$ ) as an example. Firstly, we examine the divergent structure of the two-point function. To do this, we use the Bogoliubov relation (2.53) to re-express  $\langle \hat{j}^z \rangle$  as

$$\begin{aligned} \langle \hat{j}^z \rangle &= e \sum_s \int \frac{d^3\mathbf{p}}{(2\pi)^3} \bar{\psi}_{\mathbf{p},s}^{(\text{in})} \gamma^z \psi_{\mathbf{p},s}^{(\text{in})} \\ &= e \sum_s \int \frac{d^3\mathbf{p}}{(2\pi)^3} \left[ |\alpha_{\mathbf{p},s}|^2 \bar{\psi}_{\mathbf{p},s}^{(t)} \gamma^z \psi_{\mathbf{p},s}^{(t)} + \alpha_{\mathbf{p},s} \beta_{\mathbf{p},s} \bar{\psi}_{\mathbf{p},s}^{(t)} \gamma^z \psi_{\mathbf{p},s}^{(t)} \right. \\ &\quad \left. + \alpha_{\mathbf{p},s}^* \beta_{\mathbf{p},s}^* \bar{\psi}_{\mathbf{p},s}^{(t)} \gamma^z \psi_{\mathbf{p},s}^{(t)} + |\beta_{\mathbf{p},s}|^2 \bar{\psi}_{\mathbf{p},s}^{(t)} \gamma^z \psi_{\mathbf{p},s}^{(t)} \right]. \quad (2.57) \end{aligned}$$

Using the asymptotic ( $\omega_{\mathbf{p}-e\mathbf{A}} \rightarrow \infty$ ) expressions for the Bogoliubov coefficients (2.56) and computing the spinor product as  ${}_{\pm}\bar{\psi}_{\mathbf{p},s}^{(t)}\gamma^z{}_{\mp}\psi_{\mathbf{p},s}^{(t)} = (\sqrt{m_e^2 + \mathbf{p}_{\perp}^2}/\omega_{\mathbf{p}-e\mathbf{A}}) \exp[\pm 2i \int \omega_{\mathbf{p}-e\mathbf{A}} dt]$ , one can evaluate Eq. (2.57) to find

$$\langle \hat{j}^z \rangle = e \sum_s \int \frac{d^3\mathbf{p}}{(2\pi)^3} [-\bar{\psi}_{\mathbf{p},s}^{(t)}\gamma^z - \psi_{\mathbf{p},s}^{(t)} + \mathcal{O}(\omega_{\mathbf{p}-e\mathbf{A}}^{-3})]. \quad (2.58)$$

By noting that  ${}_{\pm}\bar{\psi}_{\mathbf{p},s}^{(t)}\gamma^z{}_{\pm}\psi_{\mathbf{p},s}^{(t)} = \mp(p_z + eA)/\omega_{\mathbf{p}-e\mathbf{A}}$ , one understands that the first term in Eq. (2.58) cubically  $\sim \Lambda^3$  diverges with  $\Lambda$  being a momentum cutoff. On the other hand, the second term only gives finite contributions<sup>3</sup>. Physically speaking, this divergence comes from vacuum contributions at an intermediate time  $t$  because

$$\langle \text{vac}; t | \hat{j}^z | \text{vac}; t \rangle = e \sum_s \int \frac{d^3\mathbf{p}}{(2\pi)^3} -\bar{\psi}_{\mathbf{p},s}^{(t)}\gamma^z - \psi_{\mathbf{p},s}^{(t)}. \quad (2.59)$$

Now, we are not interested in the vacuum contributions because only the difference from the vacuum value is physically meaningful. This suggests us to re-define  $\langle \hat{j}^z \rangle$  so as to subtract the vacuum contributions as

$$\langle \hat{j}^z \rangle \rightarrow \langle : \hat{j}^z : \rangle \equiv \langle \text{vac}; \text{in} | \hat{j}^z | \text{vac}; \text{in} \rangle - \langle \text{vac}; t | \hat{j}^z | \text{vac}; t \rangle, \quad (2.60)$$

which is now free from the divergence. This subtraction procedure is equivalent to taking a normal ordering of intermediate operators  $c^{(t)}$  as  $: c^{(t)} c^{(t)\dagger} : \equiv c^{(t)} c^{(t)\dagger} - [c^{(t)}, c^{(t)\dagger}] = c^{(t)\dagger} c^{(t)}$ .

The above considerations can straightforwardly be extended to other two-point functions  $\langle \hat{\psi}\Gamma\hat{\psi} \rangle$  as well. That is, one can regularize  $\langle \hat{\psi}\Gamma\hat{\psi} \rangle$  by re-defining  $\langle \hat{\psi}\Gamma\hat{\psi} \rangle \rightarrow \langle : \hat{\psi}\Gamma\hat{\psi} : \rangle$  as

$$\begin{aligned} \langle : \hat{\psi}\Gamma\hat{\psi} : \rangle &\equiv \langle \text{vac}; \text{in} | \hat{\psi}\Gamma\hat{\psi} | \text{vac}; \text{in} \rangle - \langle \text{vac}; t | \hat{\psi}\Gamma\hat{\psi} | \text{vac}; t \rangle \\ &= \sum_s \int \frac{d^3\mathbf{p}}{(2\pi)^3} [\bar{\psi}_{\mathbf{p},s}^{(\text{in})}\Gamma\psi_{\mathbf{p},s}^{(\text{in})} - \bar{\psi}_{\mathbf{p},s}^{(t)}\Gamma\psi_{\mathbf{p},s}^{(t)}]. \end{aligned} \quad (2.61)$$

The above normal ordering regularization is also valid to the Yang-Mills theory discussed in Section 3 and QCD in Section 4.

One of the advantages of this regularization method is that it does not violate the conservation laws. Let us take the energy conservation law (2.23) as an example to see this advantage explicitly. For our homogeneous case, the total energy  $\langle : \hat{\epsilon} : \rangle$  reads

$$\langle : \hat{\epsilon} : \rangle = \langle : \hat{\epsilon}_{(A)} : \rangle + \langle : \hat{\epsilon}_{(\psi)} : \rangle, \quad (2.62)$$

<sup>3</sup>Formally, the second term still contains logarithmic divergences  $\sim \ln \Lambda$ . These divergences can be eliminated via a charge renormalization procedure [53]. In a practical sense, however, the logarithmic divergences are small (for a reasonable cutoff scale  $\Lambda$ ) and do not modify the spacetime evolution of the system significantly. Hence, we do not consider to regulate the logarithmic divergences in the following. This simplification is equivalent to neglecting running coupling effects. We have checked this treatment does no harm by explicitly conducting numerical simulations with and without regulating the logarithmic divergences.

where

$$\langle : \hat{\epsilon}_{(A)} : \rangle = \frac{E^2}{2}, \quad (2.63)$$

$$\langle : \hat{\epsilon}_{(\psi)} : \rangle = \langle : \text{Re}[i\hat{\psi}^\dagger \partial_t \hat{\psi}] : \rangle = -\text{Im} \sum_s \int \frac{d^3 \mathbf{p}}{(2\pi)^3} [\psi_{\mathbf{p},s}^{(\text{in})\dagger} \partial_t \psi_{\mathbf{p},s}^{(\text{in})} - \psi_{\mathbf{p},s}^{(t)\dagger} \partial_t \psi_{\mathbf{p},s}^{(t)}]. \quad (2.64)$$

The energy contribution from the fluctuation  $\hat{a}_\mu$  is obviously zero because it obeys the free field equation of motion (2.15). By using the equations of motion, Eqs. (2.16) and (2.17), and the definition of  $\pm\psi_{\mathbf{p},s}^{(t)}$  (2.40), one finds

$$\partial_t \langle : \hat{\epsilon}_{(A)} : \rangle = -E \langle : \hat{j}^z : \rangle - EJ^z \quad (2.65)$$

$$\begin{aligned} \partial_t \langle : \hat{\epsilon}_{(\psi)} : \rangle &= -\text{Im} \sum_s \int \frac{d^3 \mathbf{p}}{(2\pi)^3} [\psi_{\mathbf{p},s}^{(\text{in})\dagger} \partial_t^2 \psi_{\mathbf{p},s}^{(\text{in})} - \psi_{\mathbf{p},s}^{(t)\dagger} \partial_t^2 \psi_{\mathbf{p},s}^{(t)}] \\ &= eE \sum_s \int \frac{d^3 \mathbf{p}}{(2\pi)^3} [\psi_{\mathbf{p},s}^{(\text{in})\dagger} \gamma^z \psi_{\mathbf{p},s}^{(\text{in})} - \psi_{\mathbf{p},s}^{(t)\dagger} \gamma^z \psi_{\mathbf{p},s}^{(t)}] \\ &= E \langle : \hat{j}^z : \rangle, \end{aligned} \quad (2.66)$$

and hence  $\partial_t \langle : \hat{\epsilon} : \rangle = -EJ^z$  strictly holds.

## 2.2 $e^+e^-$ pair production from a constant electric field

Let us dare neglect the backreaction, i.e., artificially set  $\langle : \hat{j}^z : \rangle = 0$  in the coming three sections, Section 2.2, 2.3, and 2.4; the backreaction problem is discussed in Section 2.5. This simplification may be justified when the quantum contribution  $\langle : \hat{j}^z : \rangle$  is much smaller than the classical one  $J^z$ ; this may be realized at the very early times of the pair creation, where the number of produced particles and the acceleration by the electric field are sufficiently small. Although this simplification violates the strict energy conservation of the system, it enables us to better understand the nature of the pair creation because one can analytically solve the Dirac equation (2.17) for specific configurations of classical fields  $A_\mu$  (or the classical source  $J^\mu$ ).

In this section, we consider the case, where the classical field is given by a constant electric field  $E(t) = E_0$ , i.e.,

$$A(t) = -E_0 t. \quad (2.67)$$

For this case, one can analytically solve the Dirac equation (2.17) (see Appendix A.2 for details), which enables us to analytically compute various quantities such as the vacuum persistence probability  $P^{(\text{out})}$ , the vacuum decay rate  $w$ , the electron and positron spectra, and so on.

One can analytically compute the Bogoliubov coefficient at  $t \rightarrow \infty$  (see Appendix A.2 for

details) as

$$\alpha_{\mathbf{p},s}^{(\text{out})} = \frac{\sqrt{\pi \frac{m_e^2 + \mathbf{p}_\perp^2}{|eE_0|}} \exp \left[ -\pi \frac{m_e^2 + \mathbf{p}_\perp^2}{4|eE_0|} \right]}{\Gamma \left( 1 - i \frac{m_e^2 + \mathbf{p}_\perp^2}{2|eE_0|} \right)}, \quad \beta_{\mathbf{p},s}^{(\text{out})} = \exp \left[ -\pi \frac{m_e^2 + \mathbf{p}_\perp^2}{2|eE_0|} \right]. \quad (2.68)$$

### 2.2.1 particle spectrum at $t \rightarrow \infty$

From Eqs. (2.38) and (2.39), one obtains the electron and positron spectra at  $t \rightarrow \infty$  by squaring Eq. (2.68) as

$$\frac{d^6 N_{e^\pm}^{(\text{out})}(\mathbf{p}, s)}{d^3 \mathbf{p} d\mathbf{x}^3} = \frac{1}{(2\pi)^3} \exp \left[ -\pi \frac{m_e^2 + \mathbf{p}_\perp^2}{|eE_0|} \right]. \quad (2.69)$$

As is evident from the exponential factor, one understands that the pair creation is genuinely non-perturbative if the electric field is constant in time. This is because the typical frequency of the constant electric field is vanishing, so that infinite number of photons involve to excite real particles from a vacuum.

Equation (2.69) does not have a canonical momentum  $p_z$ -dependence. Physically speaking, this is because all the produced particles are accelerated by the electric field with infinite duration to obtain an infinite kinetic momentum  $P_z = p_z + eE_0 t \xrightarrow{t \rightarrow \infty} \infty$ , no matter what values of their canonical momentum  $p_z$  are. Because of this independence,  $p_z$ -integration of the spectra diverges. To estimate the degree of divergence, we assume that the pair creation occurs at around  $P_z \sim 0$ , where the pair creation threshold  $\sim \omega_{\mathbf{p}}$  takes its minimum. Then, one finds that the time  $t_0$  when pair creation occurs and the canonical momentum  $p_z$  of the produced particle are correlated with each other as  $p_z \sim -eE_0 t_0$ . Thus, we have

$$\int dp_z \sim |eE_0| \int dt_0 = |eE_0| T. \quad (2.70)$$

Note that this estimate has been used in many articles on pair creation from a constant electric field. In order to obtain  $p_z$ -dependent spectra and to examine the validity of this estimate, one has to compute intermediate spectra at  $-\infty < t < \infty$ ; this is done in Section 2.4.

Now, we can integrate the particle spectra  $d^6 N_{e^\pm}^{(\text{out})}/d^3 \mathbf{p} d\mathbf{x}^3$  to obtain the (average) particle production rate  $\Gamma$

$$\begin{aligned} \Gamma_{e^\pm} &\equiv \frac{1}{T} \sum_s \int d^3 \mathbf{p} \frac{d^6 N_{e^\pm}^{(\text{out})}}{d^3 \mathbf{p} d\mathbf{x}^3} \\ &= \frac{1}{T} \sum_s \int \frac{d^3 \mathbf{p}}{(2\pi)^3} \exp \left[ -\pi \frac{m_e^2 + \mathbf{p}_\perp^2}{|eE_0|} \right] \\ &\sim \frac{|eE_0|}{(2\pi)^3} \sum_s \int d^2 \mathbf{p}_\perp \exp \left[ -\pi \frac{m_e^2 + \mathbf{p}_\perp^2}{|eE_0|} \right] \\ &= \frac{|eE_0|^2}{4\pi^3} \exp \left[ -\pi \frac{m_e^2}{|eE_0|} \right], \end{aligned} \quad (2.71)$$

which is the same as the pair production rate originally obtained by Nikishov (1.5) (note that Nikishov [8] also utilized the estimate (2.70)).

### 2.2.2 vacuum persistence probability at $t \rightarrow \infty$

With the help of the estimate Eq. (2.70), one can evaluate Eq. (2.37) to find an expression for the (average) vacuum decay rate  $w$  under a constant electric field as

$$\begin{aligned}
 w &= \frac{1}{T} \sum_s \int \frac{d^3\mathbf{p}}{(2\pi)^3} \sum_{n=1}^{\infty} \frac{\exp\left[-n\pi \frac{m_e^2 + \mathbf{p}_\perp^2}{|eE_0|}\right]}{n} \\
 &\sim \frac{|eE_0|}{(2\pi)^3} \sum_s \int d^2\mathbf{p}_\perp \sum_{n=1}^{\infty} \frac{\exp\left[-n\pi \frac{m_e^2 + \mathbf{p}_\perp^2}{|eE_0|}\right]}{n} \\
 &= \frac{|eE_0|}{4\pi^3} \sum_{n=1}^{\infty} \frac{\exp\left[-n\pi \frac{m_e^2}{|eE_0|}\right]}{n^2}, \tag{2.72}
 \end{aligned}$$

which is nothing but the Schwinger formula for the vacuum decay rate (1.4) (note that Schwinger [6] also utilized the estimate (2.70)).

## 2.3 Finite pulse effects

In the last subsection, we have seen that the pair production is genuinely non-perturbative if the electric field is constant in time, and only a single dimensionless parameter  $|eE_0|/m_e^2$  characterizes the pair production because there are only two dimensionful parameters  $m_e, eE_0$ . The situation changes if we add another dimensionful parameter in the system. In particular, time-dependence of the field is important in realistic situations such as intense laser experiments and ultra-relativistic heavy ion collisions. Now, suppose that the electric field has a finite lifetime  $\tau$ . Then, since we have three dimensionful parameters  $m_e, eE_0, \tau$ , one can construct two dimensionless parameters out of the three to characterize the system. In this subsection, we will see that the pair production mechanism is largely affected by changing two dimensionless parameters. In particular, we will explicitly show that an interplay between non-perturbative and perturbative pair production occurs, whose transition is characterized by  $\gamma \equiv |eE_0|\tau/m_e, \nu \equiv |eE_0|\tau^2$ . In addition to this, we will see that the particle production is enhanced in the perturbative regime compared to a naive estimate from the non-perturbative Schwinger formula for a constant electric field.

The rest of this section is organized as follows: In Section 2.3.1, we derive a formula for the electron spectra produced from a classical electric field within the lowest order perturbation theory, and discuss how the perturbative particle production mechanism differs from the non-perturbative one. In Section 2.3.2, we consider a specific type of pulsed electric fields (Sauter-type electric field). The advantage of this particular choice of electric fields is that one can



energy  $\omega_{\mathbf{p}} > m_e$ , the number of produced electrons and positrons vanishes if  $|\omega| < 2m_e$  (“2” comes from the fact that the an electron and a positron are always produced as a pair), which means that the pair creation does not occur when the energy supplied by a single photon is below this threshold. This is certainly true for a constant electric field  $\omega \rightarrow 0$ , no matter how strong the electric field is (within the perturbation theory). For a general time-dependent electric field, the number of produced particles is non-vanishing even for a single photon as long as the electric field has a nonzero Fourier spectrum  $\tilde{E}(\omega)$  above the threshold  $\omega \geq 2m_e$ . It is also important to note that the formula (2.76) depends on  $eE/m_e$  in positive powers, which is in contrast to the exponential dependence as was seen in the non-perturbative particle production formula (2.69).

The total number of produced particles,  $d^3N_{e^\pm}^{(\text{out})}/d\mathbf{x}^3$ , is obtained after integrating over  $\mathbf{p}$  as

$$\frac{d^3N_{e^\pm}^{(\text{out})}}{d^3\mathbf{x}} = \frac{1}{(4\pi)^2} \int_{2m_e}^{\infty} d\omega \sqrt{1 - \frac{4m_e^2}{\omega^2}} \frac{1}{3} \left( 2 + \frac{4m_e^2}{\omega^2} \right) |e\tilde{E}(\omega)|^2. \quad (2.77)$$

The  $\omega$  integral is not possible in general unless we specify the electric field  $\tilde{E}$ .

### 2.3.2 comparison of perturbative and non-perturbative evaluation

From now, we consider a special case where the electric field is applied as a pulse in time. In particular, we work with a Sauter-type pulsed field [142] with height  $E_0$  and width  $\tau$ :

$$A(t) = -E_0\tau \tanh(t/\tau) \quad \text{or} \quad E(t) = E_0 \text{sech}^2(t/\tau). \quad (2.78)$$

An advantage of this particular choice of electric fields is one can analytically evaluate both the non-perturbative formulas (2.38) and (2.39) the perturbative one (2.77). Thus, by directly comparing these two evaluations, one can discuss, in particular, how the interplay between the perturbative and non-perturbative particle production occurs with changing the parameters  $m_e, eE_0, \tau$ .

#### perturbative evaluation

We substitute the Sauter-type electric field (2.78) into Eqs. (2.76) and (2.77) to get the number density  $d^6N_{e^\pm}^{(\text{out})}/d\mathbf{p}^3 d\mathbf{x}^3$  and the total number  $d^3N_{e^\pm}^{(\text{out})}/d\mathbf{x}^3$ , respectively, in the lowest-order perturbation theory. By using

$$\tilde{E}(\omega) = -i\omega \tilde{A}(\omega) = \frac{i\pi E_0 \tau^2 \omega}{\sinh \frac{\pi\tau\omega}{2}}, \quad (2.79)$$

we find that the number density  $d^6N_{e^\pm}^{(\text{out})}/d\mathbf{p}^3 d\mathbf{x}^3$  is given by

$$\frac{d^6N_{e^-}^{(\text{out})}(\mathbf{p}, s)}{d\mathbf{p}^3 d\mathbf{x}^3} = \frac{d^6N_{e^+}^{(\text{out})}(-\mathbf{p}, s)}{d\mathbf{p}^3 d\mathbf{x}^3} = \frac{1}{(2\pi)^3} \left( 1 - \frac{p_z^2}{\omega_{\mathbf{p}}^2} \right) \left| \frac{eE_0}{\omega_{\mathbf{p}}^2} \right|^2 \frac{(\pi\omega_{\mathbf{p}}\tau)^4}{\pi^2 |\sinh[\pi\omega_{\mathbf{p}}\tau]|^2}. \quad (2.80)$$

We obtain a non-vanishing result because the Fourier spectrum of the Sauter-type field  $\tilde{E}(\omega)$  is nonzero at any value of  $\omega$ , in particular in the region  $\omega \geq 2m_e$ . Also, the total number  $d^3N_{e^\pm}^{(\text{out})}/d\mathbf{x}^3$  is given by

$$\frac{d^3N_{e^\pm}^{(\text{out})}}{d\mathbf{x}^3} = m_e^3 \left| \frac{eE_0}{m_e^2} \right|^2 f(\pi m_e \tau), \quad (2.81)$$

where  $f$  is given by

$$f(x) \equiv \frac{x^4}{2\pi^4} \int_1^\infty d\omega \omega^2 \sqrt{1 - \frac{1}{\omega^2}} \frac{1}{3} \left( 2 + \frac{1}{\omega^2} \right) \frac{1}{|\sinh(\omega x)|^2}, \quad (2.82)$$

which behaves asymptotically as

$$f(x) \sim \begin{cases} \frac{x}{18\pi^2} & (x \lesssim 1) \\ \frac{x^{5/2}}{2\pi^{7/2}} \left( 1 + \frac{7}{16} \frac{1}{x} \right) e^{-2x} & (x \gtrsim 1) \end{cases}. \quad (2.83)$$

It is important to point out that the total number (2.81) does not depend on the mass  $m_e$  in the short pulse limit  $\pi m_e \tau \rightarrow 0$  as  $d^3N_{e^\pm}^{(\text{out})}/d\mathbf{x}^3 \sim \tau \times |eE_0|/18\pi$ . This is because the typical frequency of the Sauter-type pulse  $\sim 1/\tau \gg m_e$  becomes so hard that it can excite arbitrary heavy particles from the vacuum. The factor  $\tau$  can easily be understood as the total time of the interaction with the pulse.

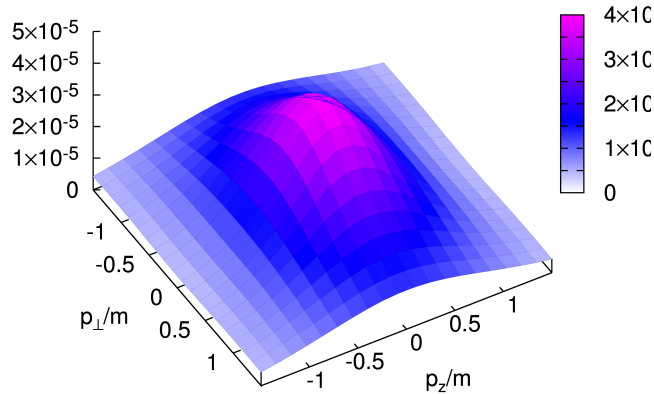


Figure 2.1: The momentum  $\mathbf{p}$ -dependence of the number density of electrons  $d^6N_{e^-}^{(\text{out})}/d\mathbf{p}^3 d\mathbf{x}^3$  (2.80) for a particular parameter  $|eE_0|/m_e^2 = 10$ ,  $m_e \tau = 0.01$ .

Figure 2.1 shows the momentum  $\mathbf{p}$ -dependence of the electron number density  $d^6N_{e^-}^{(\text{out})}/d\mathbf{p}^3 d\mathbf{x}^3$  (2.80) for  $|eE_0|/m_e^2 = 10$  and  $m_e \tau = 0.01$  as an example. We see that the peak is located at

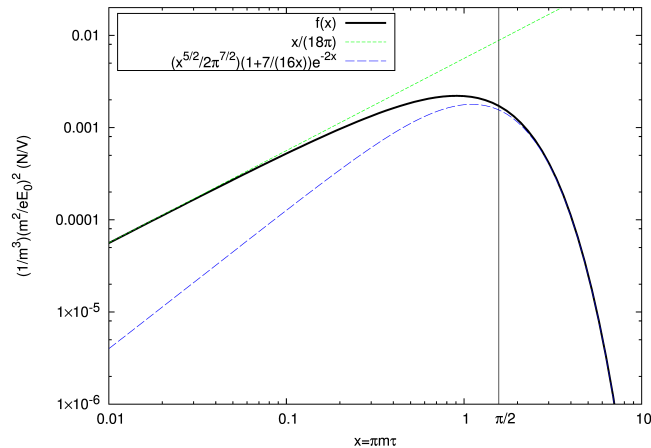


Figure 2.2: The total number  $d^3 N_{e^\pm}^{(\text{out})}/d\mathbf{x}^3$  as a function of  $\pi m_e \tau$  in the lowest-order perturbation theory (2.81) (solid line). Two asymptotic forms (2.83) are shown in dashed and dotted lines. The vertical black line indicates the point  $1/\tau = 2m_e$ .

$\mathbf{p} = \mathbf{0}$ , which reflects the fact that the energy threshold for creating one  $e^+e^-$  pair  $\sim 2\omega_{\mathbf{p}} \equiv \mathcal{E}_{\text{thr}}$  takes its minimum  $\mathcal{E}_{\text{thr}} = 2m_e$  at  $\mathbf{p} = \mathbf{0}$ . We also find that the distribution decays exponentially for large  $|\mathbf{p}_\perp|$  as

$$\frac{d^6 N_{e^-}^{(\text{out})}}{d\mathbf{p}^3 d\mathbf{x}^3} \xrightarrow{p_\perp \gg p_z, m} \frac{1}{2\pi} \left| \frac{eE_0}{m_e^2} \right|^2 (m_e \tau)^4 e^{-2\pi |\mathbf{p}_\perp| \tau}. \quad (2.84)$$

The  $\mathbf{p}_\perp$ -dependence is solely determined by the pulse duration  $\tau$ , which is not the case for the non-perturbative Schwinger mechanism (2.69), where the  $\mathbf{p}_\perp$ -dependence is determined by  $eE_0$  only. For sufficiently small  $\tau \lesssim 1/\sqrt{|eE_0|}$ , the spectrum becomes harder than what one naively expects from the non-perturbative Schwinger formula (2.69) because the typical frequency of the Sauter-type pulse  $\sim 1/\tau$  becomes sufficiently hard.

Figure 2.2 shows the  $\tau$ -dependence of the total number  $d^3 N_{e^\pm}^{(\text{out})}/d\mathbf{x}^3$ . We find that  $d^3 N_{e^\pm}^{(\text{out})}/d\mathbf{x}^3$  increases monotonically for small  $m_e \tau$ , and it takes its maximum at around  $m_e \tau = 1/2$ . After that, it decreases exponentially with increasing  $\tau$  for large  $m_e \tau \gtrsim 1/2$ . The emergence of the threshold duration  $m_e \tau = 1/2$  can be understood as follows: Since the threshold energy of the pair creation is  $\mathcal{E}_{\text{thr}} \sim 2m_e$ , the electric field must supply energy  $\Omega$  larger than  $2m_e$  for the pair creation to occur. In our computation based on the lowest-order perturbation theory, the energy  $\Omega$  is supplied by a single (virtual) photon from the electric field  $E$ . Since the typical energy  $\omega$  of a photon which forms the Sauter-type electric field is  $\omega \sim 1/\tau$ , we find  $\Omega \sim (\text{number of photons}) \times (\text{typical photon energy}) \sim 1 \times \omega \sim 1/\tau$ . Thus,  $\Omega \gtrsim 2m_e$ , i.e.,  $m_e \tau \lesssim 1/2$  is required for the pair creation in the lowest order perturbation theory. The upper limit  $m_e \tau = 1/2$  is shown as a vertical line in Fig. 2.2. In this way, one can understand that pair creation from a single photon occurs when the pulse duration  $\tau$  is short enough.

### non-perturbative evaluation

One can obtain analytic solutions to the Dirac equation in the presence of the Sauter-type electric field (see Appendix A.3 for details), which enables us to compute the number of produced particles via the formulas (2.38) and (2.39). After some calculations, one finds

$$\begin{aligned} & \frac{d^6 N_{e^-}^{(\text{out})}(\mathbf{p}, s)}{d\mathbf{p}^3 d\mathbf{x}^3} \\ &= \frac{d^6 N_{e^+}^{(\text{out})}(-\mathbf{p}, s)}{d\mathbf{p}^3 d\mathbf{x}^3} \\ &= \frac{\sinh\left[\frac{\pi\tau}{2}(2eE_0\tau + \omega_{\mathbf{p}-e\mathbf{E}_0\tau} - \omega_{\mathbf{p}+e\mathbf{E}_0\tau})\right] \sinh\left[\frac{\pi\tau}{2}(2eE_0\tau - \omega_{\mathbf{p}-e\mathbf{E}_0\tau} + \omega_{\mathbf{p}+e\mathbf{E}_0\tau})\right]}{\sinh[\pi\tau\omega_{\mathbf{p}-e\mathbf{E}_0\tau}] \sinh[\pi\tau\omega_{\mathbf{p}+e\mathbf{E}_0\tau}]}. \end{aligned} \quad (2.85)$$

Here, the momentum label  $p_z$  is the *canonical* momentum  $p_z$ , and the corresponding electron mode originally has the *kinetic* longitudinal momentum  $p_z - eE_0\tau$  in the infinite past and  $p_z + eE_0\tau$  in the infinite future. We stress that this result is clearly non-perturbative with respect to the coupling constant  $e$ , i.e., takes into account an infinite number of interactions with the electric field, while the lowest order perturbation, whose result is proportional to  $e^2$  (Eq. (2.80)), includes only a single interaction with the electric field.

The total number of produced particles,  $d^3 N_{e^\pm}^{(\text{out})}/d\mathbf{x}^3$ , is obtained after integration over the momentum  $\mathbf{p}$ . This is numerically feasible.

### comparison of the perturbative and non-perturbative evaluations

We compare the non-perturbative evaluation (2.85) with the perturbative one (2.80) and (2.81), and results are displayed in Figs. 2.3, 2.4, and 2.5.

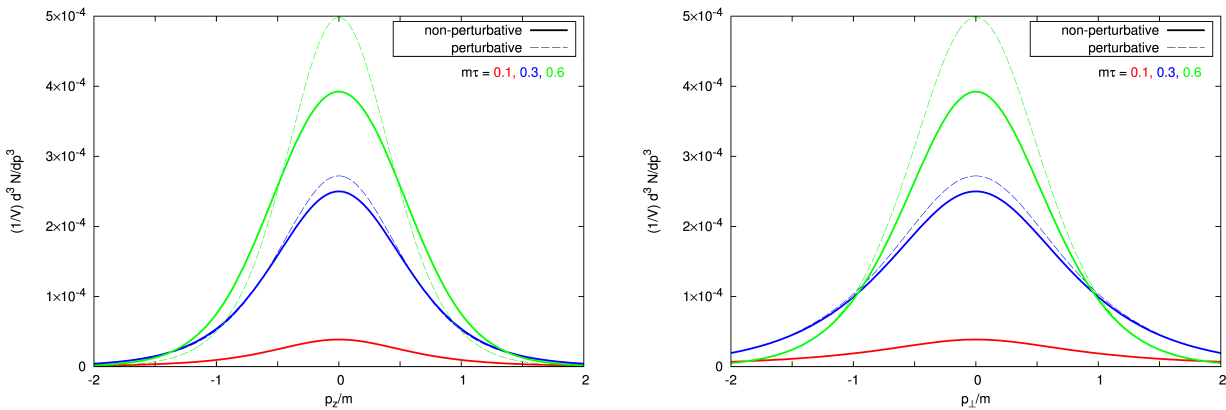


Figure 2.3: A comparison of the number density of electrons  $d^6 N_{e^-}^{(\text{out})}/d\mathbf{p}^3 d\mathbf{x}^3$ . Solid lines represent the non-perturbative result (2.85), and dashed lines represent the perturbative result (2.80) at  $|eE_0|/m_e^2 = 1$ . [Left] The  $p_z$ -dependence at  $\mathbf{p}_\perp/m_e = \mathbf{0}$  with various duration  $m_e\tau$ . Right:  $|\mathbf{p}_\perp|$ -dependence at  $p_z/m_e = 0$  with various duration  $m_e\tau$ .

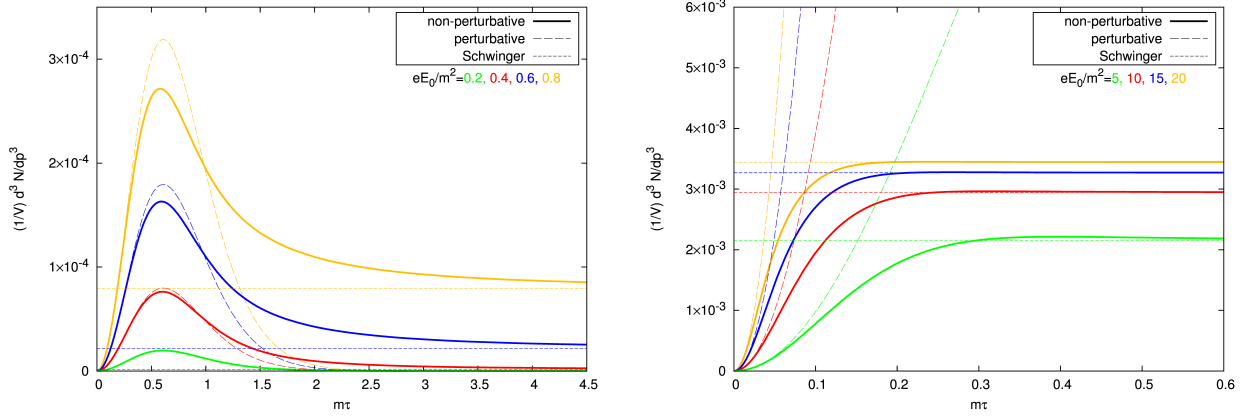


Figure 2.4: A comparison of  $\tau$  dependence of the number density of electrons  $d^6 N_{e^-}^{(out)} / d\mathbf{p}^3 d\mathbf{x}^3$  at  $p_z/m_e = |\mathbf{p}_\perp|/m_e = 0$  for the subcritical field strength  $|eE_0|/m_e^2 = 0.2, 0.4, 0.6$  and  $0.8$  (left), and for supercritical field strength  $|eE_0|/m_e^2 = 5, 10, 15$  and  $20$  (right). Solid lines represent the non-perturbative result (2.85), and dashed lines represent the perturbative result (2.80). The horizontal lines indicate Schwinger's result (2.69) obtained in a constant electric field.

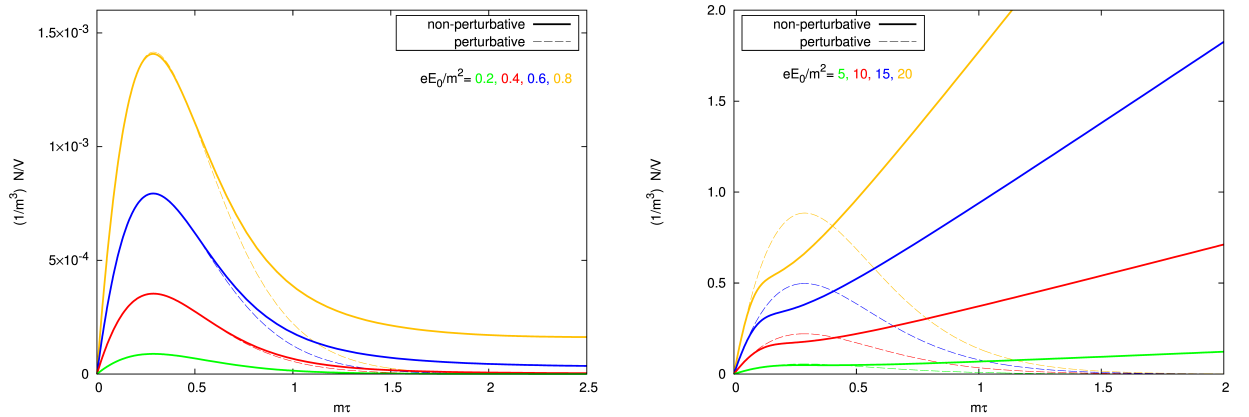


Figure 2.5: A comparison of the total number  $d^3 N_{e^\pm}^{(out)} / d\mathbf{x}^3$  as a function of the duration  $m_e \tau$  for subcritical field strength  $|eE_0|/m_e^2 = 0.2, 0.4, 0.6$  and  $0.8$  (left), and for supercritical field strength  $|eE_0|/m_e^2 = 5, 10, 15$  and  $20$  (right). Dashed lines represent the perturbative result (2.81) and solid lines represent the non-perturbative result obtained by numerically integrating (2.85) over  $\mathbf{p}$ .

Figure 2.3 shows the comparison of the momentum  $p_z$ - and  $|\mathbf{p}_\perp$ |-dependence of the number density of electrons  $d^6 N_{e^-}^{(\text{out})}/d\mathbf{p}^3 d\mathbf{x}^3$ . The peak strength of the field is taken as  $|eE_0|/m_e^2 = 1$ . Three lines are for different values of the duration  $\tau$ . We show only relatively short pulse cases:  $m_e\tau = 0.1, 0.3, \text{ and } 0.6$ . We immediately observe that the non-perturbative evaluation (2.85) and the perturbative one (2.80) coincide with each other for *short* pulses. The deviation becomes larger as  $\tau$  increases, which can be explicitly seen in Fig. 2.4. There,  $\tau$  dependence is shown for different values of the peak strength. The left panel is for the subcritical<sup>4</sup> field strength  $|eE_0|/m_e^2 = 0.2, 0.4, 0.6 \text{ and } 0.8$ , and the right panel is for the supercritical field strength  $|eE_0|/m_e^2 = 5, 10, 15 \text{ and } 20$ . We again observe the agreement of the two evaluations for *short* pulses  $m_e\tau \ll 1$  no matter how large the field strength  $|eE_0|/m_e^2$  is. However, the size of the agreement region in  $\tau$  heavily depends on the field strength  $|eE_0|/m_e^2$ . For subcritical field strength  $|eE_0|/m_e^2 \lesssim 1$ , perturbative contribution dominates the non-perturbative result even when the pulse is not *very short*  $m_e\tau \sim 1$ . On the other hand, for supercritical field strength  $|eE_0|/m_e^2 \gtrsim 1$ , perturbative description is applicable only for *very short* pulse region  $m_e\tau \ll 1$ . We will clarify the reason for this behavior in the later discussion. An important point here is that, for any field strength  $|eE_0|/m_e^2$ , there surely exists a region (*short* pulse region) where pair creation can be understood as a purely perturbative phenomenon. We can also observe that there is a clear deviation between the two in the *long* pulse region where the non-perturbative result approaches Schwinger's result (horizontal lines). In particular, the deviation is larger for supercritical field  $|eE_0|/m_e^2 \gtrsim 1$ . This can be understood as follows: Notice first that the perturbative evaluation always approaches zero in the long pulse limit  $m_e\tau \gg 1$  because the typical energies of a (virtual) photon which forms the Sauter-type field  $\omega \sim 1/\tau \rightarrow 0$  for large  $\tau$  and thus not enough to create a pair. On the other hand, Schwinger's formula valid in the long pulse region says that pair creation for subcritical field strength is exponentially suppressed  $d^6 N_{e^\pm}^{(\text{out})}/d\mathbf{p}^3 d\mathbf{x}^3 \propto \exp[-\pi m_e^2/|eE_0|]$ . Therefore, the deviation between the two is almost negligible for weak field strength  $|eE_0|/m_e^2 \lesssim 1$ , while it increases with increasing peak strength  $|eE_0|/m_e^2$  in the supercritical regime  $|eE_0|/m_e^2 \gtrsim 1$ .

The same tendency is found in the comparison of the total number  $d^3 N_{e^\pm}^{(\text{out})}/d\mathbf{x}^3$  as shown in Fig. 2.5. Interestingly, the peak structure in the *short* pulse region is reproduced by the perturbative result quite well. Although for small  $p_z$  the perturbative value of the density  $d^3 N_{e^-}^{(\text{out})}/d\mathbf{x}^3 d^3\mathbf{p}$  is somewhat larger than the non-perturbative one, while it becomes smaller for large  $p_z$  (see the left panel of Fig. 2.3), these differences cancel out with each other in integration over  $p_z$ . Thus we have a nice agreement in the total number  $d^3 N_{e^\pm}^{(\text{out})}/d\mathbf{x}^3$  as displayed in Fig. 2.5.

Figure 2.4 also shows an interesting behavior. For relatively short pulses  $m_e\tau \lesssim 1$  with subcritical field strength  $|eE_0|/m_e^2 \lesssim 1$  (left panel), the results of the Sauter-type field are enhanced

---

<sup>4</sup>We tentatively use the words ‘‘supercritical’’ and ‘‘subcritical’’ for the cases  $|eE_0|/m_e^2 > 1$  and  $|eE_0|/m_e^2 < 1$ , respectively, but precisely speaking, the condition  $|eE_0|/m_e^2 = 1$  (valid for a constant electric field) does not play the same role for finite pulses.

as compared to Schwinger's value (horizontal lines). Since the pair creation in this region is dominated by the perturbative contribution, this enhancement should be understood as a purely perturbative effect. It shows up because Schwinger's non-perturbative result  $d^6 N_{e\pm}^{(\text{out})}/d\mathbf{p}^3 d\mathbf{x}^3 \propto \exp[-\pi m_e^2/|eE_0|]$  is exponentially small for subcritical field strength  $|eE_0|/m_e^2 \lesssim 1$ , while the perturbative result is only power-suppressed as  $d^6 N_{e\pm}^{(\text{out})}/d\mathbf{p}^3 d\mathbf{x}^3 \propto |eE_0/m_e^2|^2$  (see Eq. (2.76)). By using the perturbative formula for  $d^6 N_{e\pm}^{(\text{out})}/d\mathbf{p}^3 d\mathbf{x}^3$  (2.80), we immediately find that the peak position  $\tau_{\text{peak}}$  is given by  $2 = (\pi\omega_{\mathbf{p}}\tau_{\text{peak}}) \coth[\pi\omega_{\mathbf{p}}\tau_{\text{peak}}]$  or  $\omega_{\mathbf{p}}\tau_{\text{peak}} \sim 0.61$ , which does not depend on the field strength  $|eE_0|$  as is seen in Fig. 2.4. Accordingly, the peak value is given by  $d^6 N_{e\pm}^{(\text{out})}/d\mathbf{p}^3 d\mathbf{x}^3 \sim (5.0 \times 10^{-4}) \times (1 - p_z^2/\omega_{\mathbf{p}}^2)|eE_0/\omega_{\mathbf{p}}^2|^2$ .

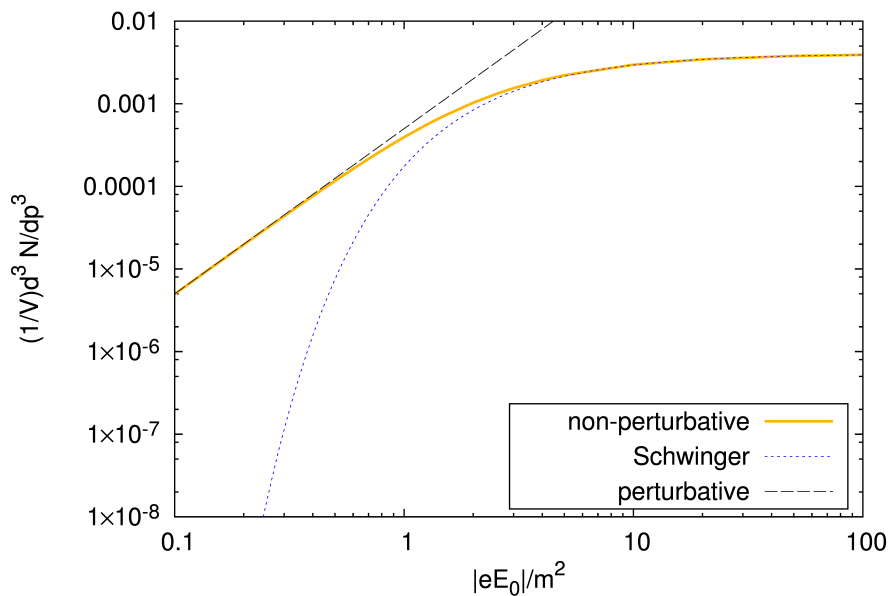


Figure 2.6: The peak value  $\max_{\tau} \left[ d^6 N_{e\pm}^{(\text{out})}/d\mathbf{p}^3 d\mathbf{x}^3 \right]$  of the non-perturbative evaluation (2.85) (solid line) as a function of the field strength  $|eE_0|/m_e^2$ . For comparison, Schwinger's value and an estimate  $d^6 N_{e\pm}^{(\text{out})}/d\mathbf{p}^3 d\mathbf{x}^3|_{\text{peak}} \sim (5.0 \times 10^{-4}) \times (1 - p_z^2/\omega_{\mathbf{p}}^2)|eE_0/\omega_{\mathbf{p}}^2|^2$  obtained from the perturbative evaluation (2.80) are shown in dotted and dashed lines, respectively. Parameters are set to  $p_z/m = |\mathbf{p}_{\perp}|/m = 0$ .

The peak value,  $\max_{\tau} \left[ d^6 N_{e\pm}^{(\text{out})}/d\mathbf{p}^3 d\mathbf{x}^3 \right]$ , at  $\mathbf{p} = \mathbf{0}$  is displayed in Fig. 2.6 as a function of the field strength  $|eE_0|/m_e^2$ , together with Schwinger's value and the peak value of the perturbative contribution. The extrapolation of Schwinger's value to the weak field case  $|eE_0|/m_e^2 \lesssim 1$  underestimates the pair creation in the Sauter-type pulsed field; the pair creation from the vacuum in the region  $|eE_0|/m_e^2 \lesssim 1, m_e\tau \lesssim 1$  is actually more abundant than Schwinger's value, owing to the perturbative contribution with a single photon. Indeed, the compact formula for the perturbative peak nicely describes the enhancement for the subcritical fields, which is explicitly depicted with a dashed line in Fig. 2.6. Similar behavior was found in Refs. [149, 150], which however regarded this peak as a result of non-perturbative physics.

Now we return to the question: To what extent are we able to say a pulse is *short*? To answer this, we expand the non-perturbative result (2.85) by the pulse duration  $\tau$ . More precisely, we expand (2.85) by the following two dimensionless parameters,

$$\nu \equiv |eE_0|\tau^2, \quad \gamma \equiv \frac{|eE_0|\tau}{m_e}, \quad (2.86)$$

because there are two dimensionful quantities  $|eE_0|$ ,  $m_e$  in addition to  $\tau$ . The result is

Eq. (2.85)

$$\begin{aligned} &= \frac{\sinh\left[\frac{\pi\nu}{2\gamma}\left(2\gamma + \sqrt{\gamma^2 - 2\frac{p_z}{\omega_p}\gamma + 1} - \sqrt{\gamma^2 + 2\frac{p_z}{\omega_p}\gamma + 1}\right)\right] \sinh\left[\frac{\pi\nu}{2\gamma}\left(2\gamma - \sqrt{\gamma^2 - 2\frac{p_z}{\omega_p}\gamma + 1} + \sqrt{\gamma^2 + 2\frac{p_z}{\omega_p}\gamma + 1}\right)\right]}{\sinh\left[\frac{\pi\nu}{\gamma}\sqrt{\gamma^2 - 2\frac{p_z}{\omega_p}\gamma + 1}\right] \sinh\left[\frac{\pi\nu}{\gamma}\sqrt{\gamma^2 + 2\frac{p_z}{\omega_p}\gamma + 1}\right]} \\ &\rightarrow \begin{cases} \frac{1}{(2\pi)^3} \left(1 - \frac{p_z^2}{\omega_p^2}\right) \left|\frac{eE_0}{\omega_p^2}\right|^2 \frac{(\pi\omega_p\tau)^4}{\pi^2 |\sinh[\pi\omega_p\tau]|^2} & (\nu, \gamma \ll 1) \\ \exp\left[-\frac{\pi(m^2 + \mathbf{p}_\perp^2)}{|eE_0|}\right] & (\nu, \gamma \gg 1). \end{cases} \quad (2.87) \end{aligned}$$

The asymptotic forms (2.87) exactly reproduce the perturbative result (2.80) for  $\nu, \gamma \ll 1$  and the non-perturbative expression (2.69) for the Schwinger mechanism for a constant electric field for  $\nu, \gamma \gg 1$ . Thus, we conclude that pulses, such that the condition  $\nu, \gamma \ll 1$ , i.e.,  $m_e\tau \ll \sqrt{m_e^2/|eE_0|}, m_e^2/|eE_0|$  is satisfied, are so *short* that pair creation becomes purely perturbative, where the *lowest* order perturbation theory works very nicely. On the other hand, pulses, such that the condition  $\nu, \gamma \gg 1$ , i.e.,  $m_e\tau \gg \sqrt{m_e^2/|eE_0|}, m_e^2/|eE_0|$  is satisfied, are so *long* that pair creation becomes non-perturbative, where perturbation theory completely breaks down. We can also say that for *middle* pulses, such that neither condition  $\nu, \gamma \gg 1$  nor  $\nu, \gamma \ll 1$  is satisfied, perturbation theory is still applicable; however, the lowest-order perturbation theory does not work because higher-order corrections  $\mathcal{O}(|eE|^n)$  ( $n > 1$ ) become important. We summarize our picture in Fig. 2.7.

These considerations clearly show that in order to investigate the non-perturbative nature of pair creation, we must require not only the strength  $|eE_0|/m_e^2 \gtrsim 1$  but also a sufficient duration  $m_e\tau \gg \sqrt{m_e^2/|eE_0|}, m_e^2/|eE_0|$ ; otherwise pair creation from the vacuum can be understood simply as a perturbative phenomenon.

The discussion given above is a natural result if we consider the meaning of the dimensionless parameters  $\nu, \gamma$ . Recall the fact that the work  $W$  done by a pulsed electric field with height  $E_0$  and width  $\tau$  is given by  $W \sim |eE_0|\tau$  and that the typical energy  $\omega$  of a photon that forms the pulsed background field is given by  $\omega \sim 1/\tau$ . Then, we can understand the physical meaning of  $\nu, \gamma$  as follows:  $\nu \sim W/\omega$  is the number of (virtual) photons of the electric field involved in a scattering process.  $\gamma \sim W/m_e \sim \nu\omega/m_e$  is the work done by the electric field scaled by the typical energy scale of the system  $m_e$ . Keeping these in mind, we can interpret that the perturbative condition  $\nu, \gamma \ll 1$  corresponds to the case where both the number of photons

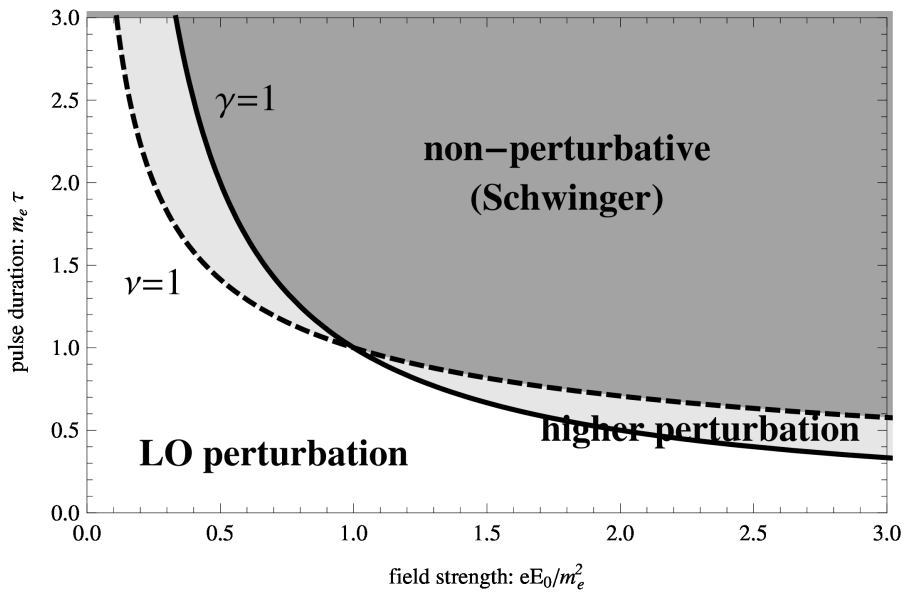


Figure 2.7: Sketch of the appropriate picture for pair creation from the vacuum for various pulses with height  $E_0$  and width  $\tau$ .  $m_e$  is the electron mass.

involved in a scattering process  $\nu$  and its correction to the system  $\gamma$  are very small. This is obviously a natural criterion for the lowest order perturbation theory to work. We can also interpret the non-perturbative condition  $\nu, \gamma \gg 1$  in the same way.

It is interesting to compare our discussion with Ref. [39] (see also Section 1.1.2), which claims that the Keldysh parameter  $\gamma_K = |eE_0|/(m_e\omega)$  discriminates whether the system is perturbative or non-perturbative. Note that their discussion is limited to the case where (i) an oscillating electric field  $E(t) = E_0 \sin \omega t$ , (ii)  $\omega$  is sufficiently small compared to the electron mass  $\omega/m_e \ll 1$ , and (iii) the electric field is sufficiently weak  $|eE_0|/m_e^2 \ll 1$ . If we assume that the typical frequency  $\omega$  of a pulsed electric field is given by the inverse of the pulse duration  $\omega \sim 1/\tau$ , we find that our discussion obtained in a pulsed electric field (see Fig. 2.7) agrees with Ref. [39] as long as the limitation (iii) is satisfied. In such a condition,  $\gamma$  determines the “perturbativeness” of the system in our discussion and is equivalent to the Keldysh parameter because  $\gamma = \frac{|eE_0|}{m_e(1/\tau)} \sim |eE_0|/(m_e\omega) = \gamma_K$ .

## 2.4 Dynamical evolution without backreaction

In the preceding two sections, Section 2.2 and 2.3, we have investigated the particle spectra at  $t \rightarrow \infty$  only. In this section, in order to understand dynamical aspects of pair creation, let us compute particle spectra at intermediate times  $-\infty < t < \infty$  by employing the canonical quantization procedure explained in Section 2.1.4 for a constant electric field initiated at time

$t = 0$ :

$$E(t) = E_0\theta(t), \quad \text{or} \quad A(t) = -E_0t\theta(t). \quad (2.88)$$

An advantage of this particular electric field is that one can analytically solve the Dirac equation (2.17) if one neglects the backreaction. Since we know the plane wave solutions  $\pm\psi_{\mathbf{p},s}^{(\text{plane})}$  (see Appendix A.1 for details) and the solutions under a constant electric field with infinite duration  $\pm\psi_{\mathbf{p},s}^{(\text{const;out})}$  (see Appendix A.2 for details), we can easily construct analytical mode functions  $\pm\psi_{\mathbf{p},s}^{(\text{in})}$  for this case (2.88) by smoothly connecting the two solutions  $\pm\psi_{\mathbf{p},s}^{(\text{plane})}$ ,  $\pm\psi_{\mathbf{p},s}^{(\text{const;out})}$  at the boundary  $t = 0$ . By noting that  $\pm\psi_{\mathbf{p},s}^{(t)} = \pm\psi_{\mathbf{p},s}^{(\text{plane})}$  for  $t < 0$  (where  $A(t) = 0$  holds), one obtains

$$\begin{pmatrix} +\psi_{\mathbf{p},s}^{(\text{in})} \\ -\psi_{\mathbf{p},s}^{(\text{in})} \end{pmatrix} = \begin{cases} \begin{pmatrix} +\psi_{\mathbf{p},s}^{(t)} \\ -\psi_{\mathbf{p},s}^{(t)} \end{pmatrix} & (t < 0) \\ \begin{pmatrix} \tilde{\alpha}_{\mathbf{p},s}(t_0) & -\tilde{\beta}_{\mathbf{p},s}^*(t_0) \\ \tilde{\beta}_{\mathbf{p},s}(t_0) & \tilde{\alpha}_{\mathbf{p},s}^*(t_0) \end{pmatrix} \begin{pmatrix} +\psi_{\mathbf{p},s}^{(\text{const;out})}(t) \\ -\psi_{\mathbf{p},s}^{(\text{const;out})}(t) \end{pmatrix} & (t > 0) \end{cases}. \quad (2.89)$$

The coefficients  $\tilde{\alpha}_{\mathbf{p},s}, \tilde{\beta}_{\mathbf{p},s}$  are given by

$$\begin{aligned} \tilde{\alpha}_{\mathbf{p},s}(t) &\equiv (+\psi_{\mathbf{p},s}^{(\text{const;out})}(t)|_+\psi_{\mathbf{p},s}^{(t)}(t))_{\text{F}} \\ &= \exp\left[-i\int_{-\infty}^t \omega_{\mathbf{p}+e\mathbf{E}_0t} dt\right] \exp\left[-\pi\frac{m_e^2 + \mathbf{p}_\perp^2}{8|eE_0|}\right] \\ &\quad \times \left[ \frac{1}{\sqrt{2}} \sqrt{1 + \frac{p_z + eE_0t}{\omega_{\mathbf{p}+e\mathbf{E}_0t}}} e^{i\pi/8} D_{i\frac{m_e^2 + \mathbf{p}_\perp^2}{2|eE_0|}}(e^{-i\pi/4} \sqrt{\frac{2}{|eE_0|}}(p_z + eE_0t)) \right. \\ &\quad \left. + \frac{1}{\sqrt{2}} \sqrt{1 - \frac{p_z + eE_0t}{\omega_{\mathbf{p}+e\mathbf{E}_0t}}} e^{-i\pi/8} \sqrt{\frac{m_e^2 + \mathbf{p}_\perp^2}{2|eE_0|}} D_{i\frac{m_e^2 + \mathbf{p}_\perp^2}{2|eE_0|} - 1}(e^{-i\pi/4} \sqrt{\frac{2}{|eE_0|}}(p_z + eE_0t)) \right], \end{aligned} \quad (2.90)$$

$$\begin{aligned} \tilde{\beta}_{\mathbf{p},s}(t) &\equiv (+\psi_{\mathbf{p},s}^{(\text{const;out})}(t)|_-\psi_{\mathbf{p},s}^{(t)}(t))_{\text{F}} \\ &= \exp\left[+i\int_{-\infty}^t \omega_{\mathbf{p}+e\mathbf{E}_0t} dt\right] \exp\left[-\pi\frac{m_e^2 + \mathbf{p}_\perp^2}{8|eE_0|}\right] \\ &\quad \times \left[ \frac{1}{\sqrt{2}} \sqrt{1 - \frac{p_z + E_0t}{\omega_{\mathbf{p}+e\mathbf{E}_0t}}} e^{i\pi/8} D_{i\frac{m_e^2 + \mathbf{p}_\perp^2}{2|eE_0|}}(e^{-i\pi/4} \sqrt{\frac{2}{|eE_0|}}(p_z + eE_0t)) \right. \\ &\quad \left. - \frac{1}{\sqrt{2}} \sqrt{1 + \frac{p_z + eE_0t}{\omega_{\mathbf{p}+e\mathbf{E}_0t}}} e^{-i\pi/8} \sqrt{\frac{m_e^2 + \mathbf{p}_\perp^2}{2|eE_0|}} D_{i\frac{m_e^2 + \mathbf{p}_\perp^2}{2|eE_0|} - 1}(e^{-i\pi/4} \sqrt{\frac{2}{|eE_0|}}(p_z + eE_0t)) \right]. \end{aligned} \quad (2.91)$$

The time-dependent Bogoliubov coefficients  $\alpha_{\mathbf{p},s}(t), \beta_{\mathbf{p},s}(t)$  are obtained by expanding the in-state mode functions  $\pm\psi_{\mathbf{p},s}^{(\text{in})}$  with the intermediate ones  $\pm\psi_{\mathbf{p},s}^{(t)}$ . By using Eqs. (2.46) and (2.47), one immediately obtains

$$\alpha_{\mathbf{p},s}(t) = \tilde{\alpha}_{\mathbf{p},s}(t_0)\tilde{\alpha}_{\mathbf{p},s}^*(t) + \tilde{\beta}_{\mathbf{p},s}(t_0)\tilde{\beta}_{\mathbf{p},s}^*(t), \quad (2.92)$$

$$\beta_{\mathbf{p},s}(t) = \tilde{\beta}_{\mathbf{p},s}(t_0)\tilde{\alpha}_{\mathbf{p},s}^*(t) - \tilde{\alpha}_{\mathbf{p},s}^*(t_0)\tilde{\beta}_{\mathbf{p},s}(t). \quad (2.93)$$

Below, we compute the time-evolution of particle spectra  $(2\pi)^3 d^6 N_{e^-} / d\mathbf{p}^3 d\mathbf{x}^3 = |\beta_{\mathbf{p},s}|^2$  and total number  $d^3 N_{e^\pm} / d\mathbf{x}^3 = \int d^3 \mathbf{p} |\beta_{\mathbf{p},s}|^2 / (2\pi)^3$ . We shall see that the intermediate spectra reveal the  $p_z$ -dependence of pair creation and that naturally recover the asymptotic  $t \rightarrow \infty$  result. We shall also see that the total number of produced particles increases ultimately as time goes as  $\propto t$ . This is simply because we neglect the backreaction, and particles are endlessly created from the electric field violating the total energy conservation of the system; we will remedy this problem in Section 2.5.

### 2.4.1 electron distribution

Electron spectrum  $(2\pi)^3 d^6 N_{e^-} / d\mathbf{p}^3 d\mathbf{x}^3 = |\beta_{\mathbf{p},s}|^2$  is plotted in Figs. 2.8 and 2.9. For the sake of simplicity, we consider the massless limit  $m_e / \sqrt{|eE_0|} = 0$  (or the strong field limit  $|eE_0| \rightarrow \infty$ ) here.

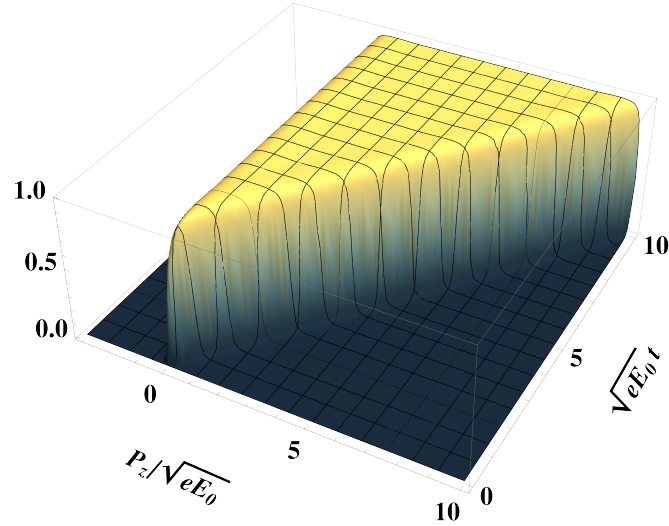


Figure 2.8: The time-evolution of the longitudinal kinetic momentum  $P_z = p_z - eA$  distribution  $(2\pi)^3 d^6 N_{e^-} / d\mathbf{p}^3 d\mathbf{x}^3$  for a fixed transverse momentum  $|\mathbf{p}_\perp| / \sqrt{|eE_0|} = 0.1$ . The mass  $m_e$  is set to  $m_e / \sqrt{|eE_0|} = 0$ .

Figure 2.8 shows the longitudinal kinetic momentum  $P_z = p_z - eA$  dependence of the spectrum  $(2\pi)^3 d^6 N_{e^-} / d\mathbf{p}^3 d\mathbf{x}^3$  at a fixed transverse momentum  $|\mathbf{p}_\perp| / \sqrt{|eE_0|} = 0$ . We observe a triangle-shaped distribution. The physical meaning of this distribution is evident: Electrons are constantly created at around  $\mathbf{P} \sim \mathbf{0}$ , where the pair creation threshold  $\omega_{\mathbf{P}}$  takes its minimum. After they are created, the electrons are accelerated uniformly by the electric field as  $dP_z/dt = eE_0$ . We also find that the Pauli principle is strictly satisfied and the distribution is saturated as  $(2\pi)^3 d^6 N_{e^-} / d\mathbf{p}^3 d\mathbf{x}^3 \sim 1$ . This is consistent with the asymptotic formula (2.71):  $(2\pi)^3 d^6 N_{e^-}(t = \infty) / d\mathbf{p}^3 d\mathbf{x}^3 = \exp[-\pi(m_e^2 + \mathbf{p}_\perp^2) / |eE_0|] \sim 1$ .

We study the transverse  $|\mathbf{p}_\perp|$ -dependence of the spectrum in more detail in Fig. 2.9. There,

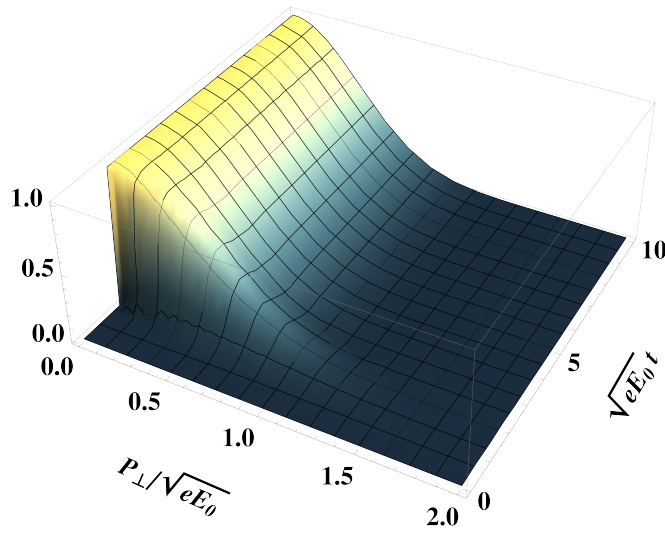


Figure 2.9: The time-evolution of the transverse  $|\mathbf{p}_\perp|$ -distribution  $(2\pi)^3 d^6 N_{e^-}/d\mathbf{p}^3 d\mathbf{x}^3$  for a fixed longitudinal kinetic momentum  $P_z = p_z + eE_0 t = 1.5 \times \sqrt{|eE_0|}$ . The mass  $m_e$  is set to  $m_e/\sqrt{|eE_0|} = 0$ .

the time-evolution of the transverse distribution  $(2\pi)^3 d^6 N_{e^-}/d\mathbf{p}^3 d\mathbf{x}^3$  at a fixed longitudinal kinetic momentum  $P_z/\sqrt{|eE_0|} = 1.5$  is plotted. From this figure, one again understands that the distribution is well reproduced by the asymptotic formula (2.71) shortly after the switch on of the electric field ( $\sqrt{|eE_0|}t \gtrsim 2.0$  in the figure). In the transient regime ( $\sqrt{|eE_0|}t \lesssim 2.0$  in the figure), however, the spectrum does not agree with the asymptotic formula: The distribution has a hard  $|\mathbf{p}_\perp|$ -dependence compared to the asymptotic one (2.71). This is relevant to the finite pulse effects discussed in Section 2.3 because the sudden switch-on of the field at  $t = 0$  contains hard frequencies to excite hard particles (see Eq. (2.84)).

Collecting all the above observations, one understands that the spectra  $(2\pi)^3 d^6 N_{e^\pm}/d\mathbf{p}^3 d\mathbf{x}^3$  are well approximated by

$$\frac{d^6 N_{e^\pm}}{d\mathbf{p}^3 d\mathbf{x}^3} \sim \frac{1}{(2\pi)^3} \exp \left[ -\pi \frac{m_e^2 + \mathbf{p}_\perp^2}{|eE(t)|} \right] \theta(\mp p_z (p_z \mp eA(t))). \quad (2.94)$$

Notice that positrons are accelerated by the electric field in the opposite direction of electrons. The approximation (2.94) is valid as long as time-derivatives of the electric field  $d^n E/dt^n$  are sufficiently small and quantum interferences among electrons are absent. One inevitably encounters the quantum interferences if one considers pair creation in the presence of other particles occupying the same phase space point (e.g. pair creation in a thermal bath [34, 91] and with backreaction [34, 54, 91, 151]). We shall briefly discuss the quantum interferences in the next section.

### 2.4.2 total number of electrons

The total number of produced particles for a single spin and flavor  $d^3 N_{e\pm}/d\mathbf{x}^3 = \int d^3 \mathbf{p} |\beta_{\mathbf{p},s}|^2 / (2\pi)^3$  is plotted in the left panel of Fig. 2.10. From this figure, one finds that the total number grows in proportion to the time  $\sqrt{|eE_0|}t$ , which implies that particles are constantly produced from the constant electric field. This feature is consistent with the estimate (2.71). On the other hand, the estimate (2.71) slightly underestimates the observed numbers. This is because the sudden switch-on of the field at  $t = 0$  creates additional particles which is not included in the non-perturbative Schwinger formula for a constant electric field. These particles can be seen at the excess from the estimate at early times.

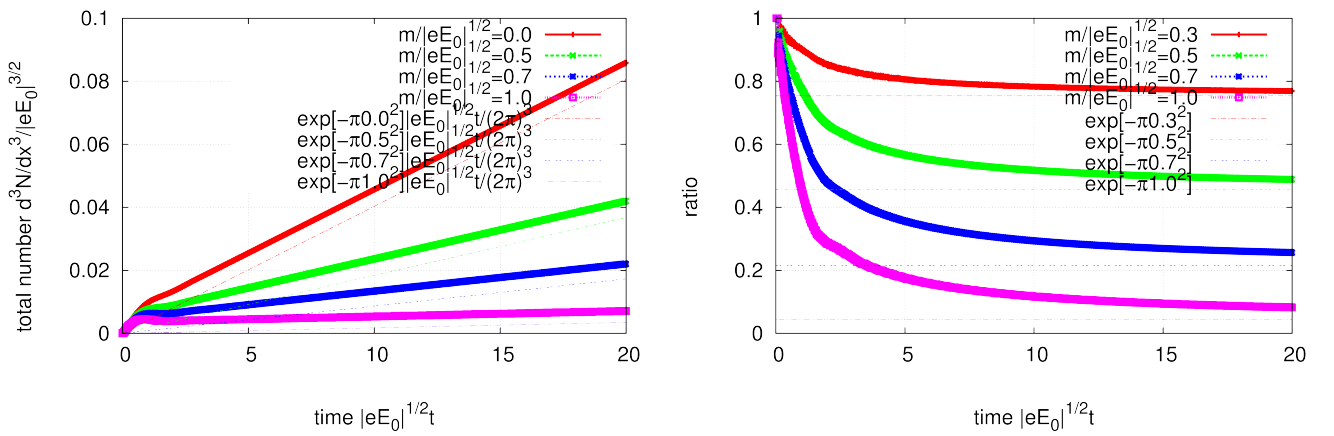


Figure 2.10: The total number of produced electrons: [Left] The time-evolution of the total number of produced electrons for a single spin and flavor  $d^3 N_{e\pm}/d\mathbf{x}^3$ . The color labels the electron mass  $m_e$  or the field strength  $eE_0$  as  $m_e/\sqrt{|eE_0|} = 0.0$  (red), 0.5 (green), 0.7 (blue), 1.0 (purple). The thin lines represent the estimate from the asymptotic formula (2.71). [Right] The ratio  $R$  of the massive electron (or finite field strength  $|eE_0| < \infty$ ) yield to the massless (or infinite field strength  $|eE_0| \rightarrow \infty$ ) one:  $R \equiv (d^3 N_{e\pm}[m_e/\sqrt{|eE_0|} \neq 0]/d\mathbf{x}^3)/(d^3 N_{e\pm}[m_e/\sqrt{|eE_0|} = 0]/d\mathbf{x}^3)$ . The color again labels  $m_e/\sqrt{|eE_0|}$  as 0.3 (red), 0.5 (green), 0.7 (blue), 1.0 (purple). Thin lines represent the estimates from the asymptotic formula (2.71) as  $R^{(\text{out})} = \exp[-\pi m_e^2/|eE_0|]$ .

In the right panel of Fig. 2.10, we plotted the ratio  $R$  of the massive electron (or finite field strength  $|eE_0| < \infty$ ) yield to the massless (or infinite field strength  $|eE_0| \rightarrow \infty$ ) one:  $R \equiv (d^3 N_{e\pm}[m_e/\sqrt{|eE_0|} \neq 0]/d\mathbf{x}^3)/(d^3 N_{e\pm}[m_e/\sqrt{|eE_0|} = 0]/d\mathbf{x}^3)$ . The asymptotic formula (2.71) tempts us to naively expect that the ratio takes values around  $R^{(\text{out})} = \exp[-\pi m_e^2/|eE_0|]$ . The figure, however, shows that this expectation is definitely wrong for early times. This is because of the finite pulse effects discussed in Section 2.3. The perturbative pair creation always raises up the ratio  $R$  because the typical frequency of the field at early times is so hard that it can excite arbitrary heavy particles from the vacuum (see Eq. (2.81)). On the other

hand, the naive estimate becomes accurate for later times, although the time scale depends on the mass  $m_e$  or the field strength  $eE_0$ . Indeed, one can observe that heavier mass (or weaker field strength) requires longer times for converging to the estimate  $R^{(\text{out})}$ . This aspect can be understood in terms of the Keldysh parameter  $\gamma_K = |eE_0|t/m_e$ , which is one of the dimensionless parameters characterizing the interplay between the non-perturbative Schwinger particle production ( $\gamma_K \gg 1$ ) and the perturbative one ( $\gamma_K \ll 1$ ) (see Fig. 2.7): The Keldysh parameter becomes smaller for larger (smaller) values of  $m_e$  ( $eE_0$ ), and thus larger time  $t$  is required to realize  $\gamma_K \gg 1$ .

## 2.5 Dynamical evolution with backreaction

In the last three sections, Section 2.2, 2.3, and 2.4, we have neglected the backreaction by artificially setting  $\langle : \hat{j}^z : \rangle = 0$  and kept the electric field strength  $E$  fixed. As was addressed, this treatment is unphysical because it violates the strict energy conservation of the system, and is justifiable only at the very beginning of the time-evolution of the system.

In this section, we discuss backreaction effects: By numerically solving the equations of motion (2.15)-(2.17), we compute the time-evolution of the electron distribution function, the field strength, the total number of produced particles, and thermodynamic quantities such as energy density and pressure of the system.

### 2.5.1 setup

We consider the case where there is a homogeneous electric field initially  $t = t_0 = 0$  as

$$A(t_0) = 0, \quad E(t_0) = E_0, \quad \frac{dE(t_0)}{dt} = 0. \quad (2.95)$$

We never supply any external source  $J^\mu$  during the time-evolution, i.e.,  $J^\mu = 0$ . For the sake of simplicity, the coupling constant  $e$  is set to be unity in the following.

### 2.5.2 electron distribution

Figures 2.11 and 2.12 display the time-evolution of the electron number density  $d^6 N_{e^-}/d\mathbf{p}^3 d\mathbf{x}^3$ , where  $m_e/|eE_0| = 0$  is taken for simplicity.

Figure 2.11 displays the time-evolution of the kinetic longitudinal momentum  $P_z = p_z - eA$  dependence of the electron number density  $d^6 N_{e^-}/d\mathbf{p}^3 d\mathbf{x}^3$ . Obviously, the result is distinct from that without the backreaction (see Fig. 2.8). They coincide with each other only at the beginning  $\sqrt{|eE_0|}t \lesssim 10$ . Thus, one understands that the backreaction effects (or quantum effects higher than one-loop order) are crucial in describing the time-evolution of the system. Interestingly, Fig. 2.11 exhibits an oscillating behavior [34, 52, 53, 54, 91] (see Fig. 2.13 also), which is an analogue of the plasma oscillation well known in the context of plasma physics [152]:

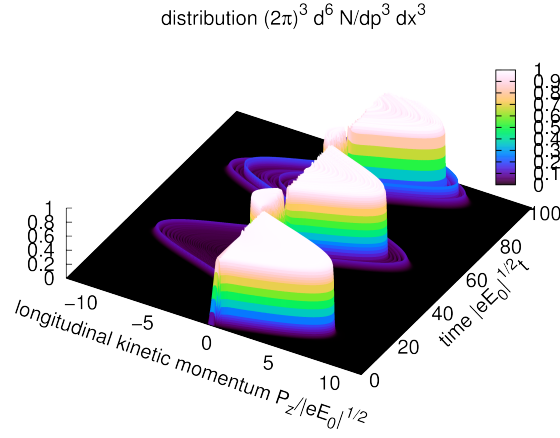


Figure 2.11: The kinetic longitudinal distribution of electrons  $d^6 N_{e^-} / dp^3 dx^3$  at a fixed transverse momentum  $\mathbf{p}_\perp / \sqrt{|eE_0|} = 0.045$  for  $m_e / |eE_0| = 0$ .

Suppose that we have  $E_0 > 0$  initially. The electric field creates particles via the Schwinger mechanism, and after that those particles are accelerated according to the classical equation of motion,  $dP_z/dt = eE$ , in the positive direction. Hence, the current (or the longitudinal kinetic momentum  $P_z$ ) is positive  $\langle \hat{j}^z \rangle > 0$  in early times, and it diminishes the original electric field via the Maxwell equation (2.19) as  $-dE/dt = \langle \hat{j}^z \rangle > 0$ . After some times  $t_{\text{osc}}$ , the electric field is completely screened out  $E(t_{\text{osc}}) = 0$ . At this time  $t_{\text{osi}}$ , the current still flows in the positive direction  $\langle \hat{j}^z \rangle > 0$ , and further decreases the electric field strength as  $E < 0$ . The negative electric field strength, then, decelerates the particles to diminish the current, which eventually becomes zero and flips its sign as  $\langle \hat{j}^z \rangle < 0$ . At this point, the electric field strength takes its minimum, and begins to grow in accordance with the Maxwell equation (2.19) as  $-dE/dt = \langle \hat{j}^z \rangle < 0$ . Repeating these steps again and again, the oscillating behavior appears.

Figure 2.12, shows the time-evolution of the transverse  $\mathbf{p}_\perp$  distribution  $d^6 N_{e^-} / dp^3 dx^3$  at a fixed kinetic longitudinal momentum  $P_z / \sqrt{|eE_0|} = 1.5$ . We first observe that the spectrum periodically “disappears” because of the plasma oscillation. Apart from that, the transverse  $\mathbf{p}_\perp$ -dependence is largely consistent with a Gaussian  $\sim \exp[-\pi(m_e^2 + \mathbf{p}_\perp^2) / |eE_0|]$  as the asymptotic formula (2.71) predicts. The deviation from the Gaussian is because of the decay of the electric field (see Fig. 2.13) and of quantum interference. The quantum interferences occur and the spectrum is heavily distorted when the created particles come back to the phase space where the pair production takes place  $\mathbf{P} \sim \mathbf{0}$ . This is essentially because the phase of the particles coming back  $\sim \exp[-iS_{\text{cl}}]$ , where  $S_{\text{cl}}$  is the classical action, and that of newly produced anti-particles  $\sim \exp[+iS_{\text{cl}}]$  are not the same. An overlap of these particles having different phases results in an interference term in the distribution  $\sim |\exp[-iS_{\text{cl}}] + e^{i\theta} \exp[+iS_{\text{cl}}]|^2 = 2 + 2 \cos(S_{\text{cl}} + \theta/2) (e^{i\theta})$

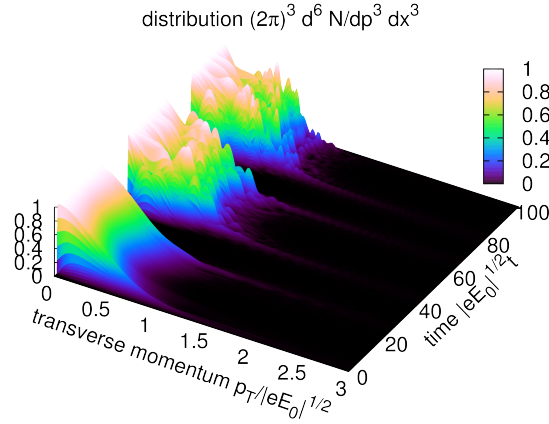


Figure 2.12: The transverse distribution of electrons  $d^6 N_{e^-}/d\mathbf{p}^3 d\mathbf{x}^3$  at a fixed kinetic longitudinal momentum  $P_z = p_z - eA = 1.5\sqrt{|eE_0|}$  for  $m_e/|eE_0| = 0$ .

is a constant relative phase factor), which rapidly oscillates in the phase space. The quantum interferences disorder the system to increase the entropy, and are important for the seemingly irreversibility of the system [151].

Now, let us quantitatively estimate the time scale of the oscillation  $t_{\text{osc}}$  [91]: From the above arguments (or the discussion without the backreaction (2.94)), one may approximate the distribution function  $d^6 N_{e^\pm}/d\mathbf{p}^3 d\mathbf{x}^3$  by neglecting the quantum interferences and setting  $E(t) \sim E_0$  as

$$\frac{d^6 N_{e^\pm}}{d\mathbf{p}^3 d\mathbf{x}^3} \sim \frac{1}{(2\pi)^3} \exp\left[-\pi \frac{m_e^2 + \mathbf{p}_\perp^2}{|eE_0|}\right] \theta(\mp p_z(p_z \mp eA(t))). \quad (2.96)$$

We furthermore approximate the current  $\langle : \hat{j}^z : \rangle$  by assuming that the quantum interferences are again negligible and particles are ultra-relativistic in the longitudinal direction  $\omega_{\mathbf{P}} \sim |\mathbf{P}|$  as

$$\begin{aligned} \langle : \hat{j}^z : \rangle &\sim \sum_{e^\pm} (\pm e) \sum_s \int d^3 \mathbf{p} \frac{p_z \mp eA}{\omega_{\mathbf{p} \mp eA}} \frac{d^6 N_{e^\pm}}{d\mathbf{p}^3 d\mathbf{x}^3} \\ &\sim \sum_{e^\pm} (\pm e) \sum_s \int d^3 \mathbf{p} \operatorname{sgn}(p_z \mp eA) \frac{d^6 N_{e^\pm}}{d\mathbf{p}^3 d\mathbf{x}^3} \\ &\sim \frac{e^3}{2\pi^3} E_0 \exp\left[-\pi \frac{m_e^2}{|eE_0|}\right] A(t) \quad (\because \text{Eq. (2.96)}). \end{aligned} \quad (2.97)$$

By substituting the last expression (2.97) into the equation of motion (2.19), one gets

$$E(t) = E_0 \cos\left[\frac{\pi}{2} \frac{t}{t_{\text{osc}}}\right], \quad (2.98)$$

where  $t_{\text{osc}}$  is the time when the electric field passes zero (or the longitudinal kinetic momentum flips its sign) for the first time:

$$\sqrt{|eE_0|}t_{\text{osc}} = \frac{\pi^2}{e} \sqrt{\frac{\pi}{2}} \exp \left[ \frac{\pi}{2} \frac{m_e^2}{|eE_0|} \right]. \quad (2.99)$$

The estimate (2.99) reads  $\sqrt{|eE_0|}t_{\text{osc}} \sim 12$  for  $m_e/\sqrt{|eE_0|} = 0$ , and is in good agreement with the result displayed in Fig. 2.11. Notice that Eq. (2.98) expects that the electric field  $E(t)$  does not decay in time, but simply oscillates with a constant amplitude  $E_0$ . As we shall see in Fig. 2.13, however, this expectation is definitely wrong: The electric field not only oscillates in time but also decays. What is missing is the quantum interferences we have neglected in the derivation of Eq. (2.98), which tells us the importance of the quantum interference in the seeming irreversibility of the system. On the other hand, Eq. (2.98) does reproduce well the oscillating behavior of the electric field. This is because the plasma oscillation is purely classical dynamics, and is well captured by the approximations made during the derivation.

### 2.5.3 decay of electric field

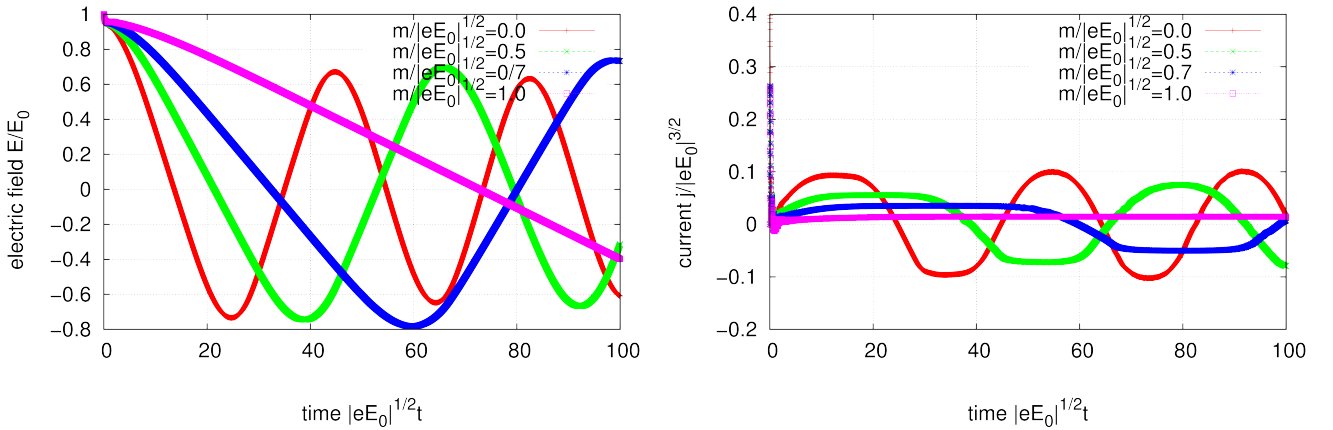


Figure 2.13: [Left] The time-evolution of the electric field strength  $E(t)$ . Different colors indicate different initial field strength  $E_0$  (or the electron mass  $m_e$ ) as  $m_e/\sqrt{|eE_0|} = 0.0$  (red), 0.5 (green), 0.7 (blue), and 1.0 (purple). [Right] The time-evolution of the current  $\langle \hat{j}^z \rangle$  of the produced particles. The colors again indicate the values of  $m_e/\sqrt{|eE_0|}$  as in the left panel.

Figure 2.13 displays the time-evolution of the electric field strength  $E$  (left) together with that of the current  $\langle \hat{j}^z \rangle$  (right). One again observes the plasma oscillation in the time-evolution of the electric field strength and that of the current as was explained in Section 2.5.2. As was estimated in Eq. (2.99), the typical time scale of the oscillation  $t_{\text{osc}}$  exponentially grows with increasing the ratio  $m_e^2/|eE_0|$ . This is because the production of particles that generate the current to screen the electric field is exponentially suppressed by an inverse power of  $m_e^2/|eE_0|$ .

Another important point is that the electric field decays. This means that the energy of the classical field is converted into quantum particles as we shall explicitly see in Section 2.5.5. We note that the speed of the decay is rather slow in QED. This is because electrons are subjected to the Pauli principle so that the total number of electrons do not grow so much as we shall see in Section 2.5.4, i.e., the energy of the classical field can be converted into electrons only slowly. This is not the case for boson production, which is relevant in QCD. There, gluons are abundantly produced so that the energy of a classical color field is efficiently converted into particle degrees of freedom (see Section 4.3).

Note that the electric field is sufficiently adiabatic in time. Indeed, for the infinite field strength (or the massless) limit  $m_e/\sqrt{|eE_0|} = 0$ , the typical value of the dimensionless parameters  $\nu, \gamma$  (see Eq. (2.86)) read  $\nu \sim \sqrt{|eE_0|}t_{\text{osc}} \sim 100 \gg 1, \gamma \sim \sqrt{|eE_0|}t_{\text{osc}} \times (m_e/\sqrt{|eE_0|})^{-1} \rightarrow \infty$ . These values of  $\nu, \gamma$  guarantee that the effects of the time-dependence of the electric field are weak and the pair production is purely non-perturbative as was discussed in Section 2.3.

### 2.5.4 total number of electrons

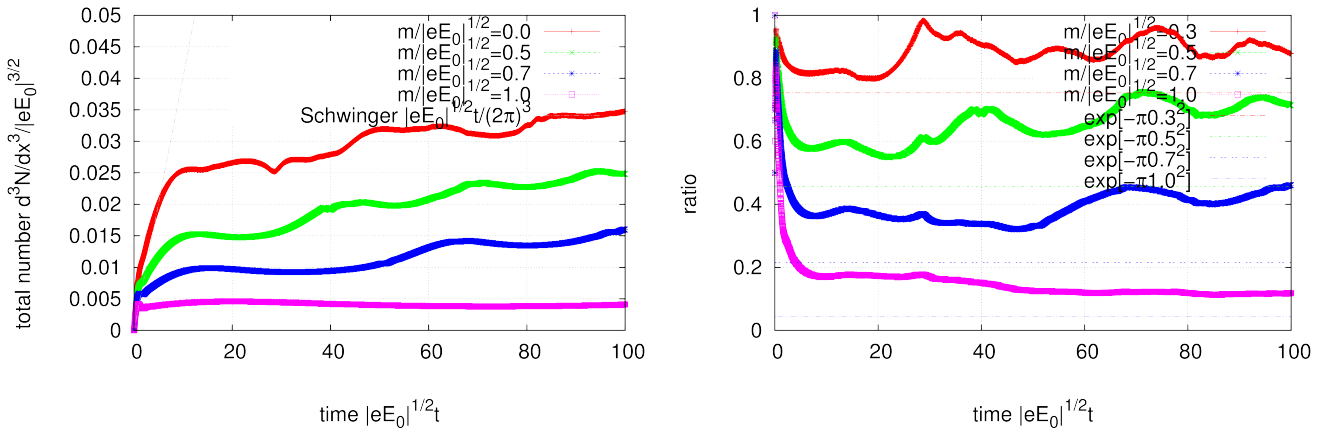


Figure 2.14: The total number of produced particles: [Left] The time-evolution of the total number of produced electrons for a single spin and flavor  $d^3N_{e\pm}/d\mathbf{x}^3$ . The color labels the electron mass  $m_e$  or the field strength  $eE_0$  as  $m_e/\sqrt{|eE_0|} = 0.0$  (red), 0.5 (green), 0.7 (blue), 1.0 (purple). The thin line represents the estimate from the asymptotic formula (2.71) in the infinite field strength (or massless) limit  $m_e/\sqrt{|eE_0|} = 0.0$ . [Right] The ratio  $R$  of the massive electron (or finite field strength  $|eE_0| < \infty$ ) yield to the massless (or infinite field strength  $|eE_0| \rightarrow \infty$ ) one:  $R \equiv (d^3N_{e\pm}[m_e/\sqrt{|eE_0|} \neq 0]/d\mathbf{x}^3)/(d^3N_{e\pm}[m_e/\sqrt{|eE_0|} = 0]/d\mathbf{x}^3)$ . The color again labels  $m_e/\sqrt{|eE_0|}$  as 0.3 (red), 0.5 (green), 0.7 (blue), 1.0 (purple). Thin lines represent an estimate from the asymptotic formula (2.71) as  $R^{(\text{out})} = \exp[-\pi m_e^2/|eE_0|]$ .

The total number of produced particles for a single spin and flavor  $d^3N_{e\pm}/d\mathbf{x}^3 = \int d^3\mathbf{p}|\beta_{\mathbf{p},s}|^2/(2\pi)^3$  is plotted in the left panel of Fig. 2.14 for various values of the initial field strength  $E_0$  or the

electron mass  $m_e$ . When compared to the result without the backreaction in Section 2.4.2, one finds that they coincide with each other only for  $\sqrt{|eE_0|}t \lesssim 10$ , which implies that the backreaction effects are negligible at the beginning of the pair production. At later times  $\sqrt{|eE_0|}t \gtrsim 10$ , they start to deviate because of the backreaction. Indeed, only smaller numbers of particles are produced when the backreaction is turned on because the average value of the field strength is much smaller than the initial one  $E_0$  due to the decay and to the plasma oscillation as were observed in Fig. 2.13. Also, the Pauli blocking is important: The Pauli principle forbids electron production at the phase space point which is already occupied by another electron. The plasma oscillation strongly bounds the longitudinal momentum extension of the phase space density of electrons (see Fig. 2.11), which is in contrast to the case without the backreaction, where electrons are accelerated by the electric field uniformly (see Fig. 2.8) to get much larger momentum than that of newly produced electrons.

The right panel of Fig. 2.14 displays the ratio  $R$  of the massive electron (or a finite initial field strength  $|eE_0| < \infty$ ) yield to the massless (or an infinite initial field strength  $|eE_0| \rightarrow \infty$ ) one:  $R \equiv (d^3 N_{e^\pm}[m_e/\sqrt{|eE_0|} \neq 0]/d\mathbf{x}^3)/(d^3 N_{e^\pm}[m_e/\sqrt{|eE_0|} = 0]/d\mathbf{x}^3)$ . We note that the same quantity without the backreaction was plotted in Fig. 2.10. We again observe that the result deviates from the naive expectation of the asymptotic formula (2.71)  $R^{(\text{out})} = \exp[-\pi m_e^2/|eE_0|]$ , which is represented by the thin lines in the figure. Interestingly, the deviation is larger than that without the backreaction (see Fig. 2.10). This is because the backreaction effects are larger for lighter electron mass (or stronger initial field strength), where stronger current flows. Hence, particle production is more strongly suppressed for lighter electron mass (or stronger initial field strength), so that the ratio  $R$  becomes larger than that without the backreaction.

### 2.5.5 energy density

Figure. 2.15 shows the time-evolution of the energy  $\langle : \hat{\epsilon} : \rangle = \langle : \hat{\epsilon}_{(A)} : \rangle + \langle : \hat{\epsilon}_{(\psi)} : \rangle$ , where  $\langle : \hat{\epsilon}_{(A)} : \rangle$  (Eq. (2.63)) is the energy of the classical electric field and  $\langle : \hat{\epsilon}_{(\psi)} : \rangle$  (Eq. (2.64)) is that of the matter (electrons and positrons).

The left panel of Fig. 2.15 displays the energy balance between  $\langle : \hat{\epsilon}_{(A)} : \rangle$  and  $\langle : \hat{\epsilon}_{(\psi)} : \rangle$ . The figure shows that the energy of the classical electric field  $\langle : \hat{\epsilon}_{(A)} : \rangle$  is smoothly converted into that of quantum particles  $\langle : \hat{\epsilon}_{(\psi)} : \rangle$ . The conversion process is seemingly irreversible, and the energy of the classical field decreases as time goes. Notice that the energy conservation law (2.23) strictly holds during the time-evolution.

The time-evolution of the matter energy  $\langle : \hat{\epsilon}_{(\psi)} : \rangle$  is further investigated in the right panel of Fig. 2.15. One observes that the matter energy does not increase monotonically, but oscillates in time. This is because pair creation and annihilation occur at around  $\mathbf{P} \sim \mathbf{0}$  periodically because of the plasma oscillation explained in Section 2.5.2.

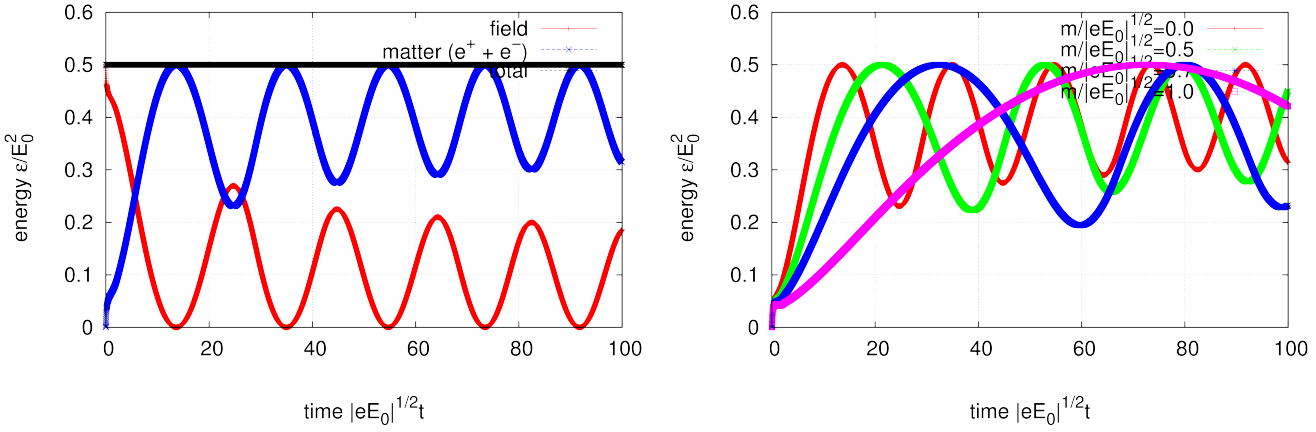


Figure 2.15: The time-evolution of the energy density  $\langle : \hat{\varepsilon} : \rangle = \langle : \hat{\varepsilon}_{(A)} : \rangle + \langle : \hat{\varepsilon}_{(\psi)} : \rangle$ . [Left] The energy balance between the matter  $\langle : \hat{\varepsilon}_{(\psi)} : \rangle$  (blue) and the classical electric field  $\langle : \hat{\varepsilon}_{(A)} : \rangle$  (red). The black line is the sum of these two contributions  $\langle : \hat{\varepsilon} : \rangle$ , and is constant because of the energy conservation. [Right] The energy of the matter  $\langle : \hat{\varepsilon}_{(\psi)} : \rangle$  for various values of the initial field strength (or the electron mass) as  $m_e/\sqrt{|eE_0|} = 0.0$  (red), 0.5 (green), 0.7 (blue), and 1.0 (purple).

### 2.5.6 pressure

The transverse pressure  $\langle : \hat{P}_\perp : \rangle \equiv (\langle : \hat{P}_x : \rangle + \langle : \hat{P}_y : \rangle)/2$  and the longitudinal pressure  $\langle : \hat{P}_z : \rangle$  are plotted in Figs. 2.16 and 2.17, respectively. In the figures, the pressure  $\langle : \hat{P}_{\perp,z} : \rangle$  are further split into the classical field part  $\langle : \hat{P}_{\perp,z(A)} : \rangle$  and the matter (electrons and positrons) part  $\langle : \hat{P}_{\perp,z(\psi)} : \rangle$  as (see Eq. (2.9))

$$\begin{aligned} \langle : \hat{P}_{\perp(A)} : \rangle &= \frac{E^2}{2}, \\ \langle : \hat{P}_{\perp(\psi)} : \rangle &= \left\langle : -i\text{Re} \left[ \hat{\psi} \frac{\gamma^x \partial_x + \gamma^y \partial_y}{2} \hat{\psi} \right] : \right\rangle, \end{aligned} \quad (2.100)$$

and

$$\begin{aligned} \langle : \hat{P}_{z(A)} : \rangle &= -\frac{E^2}{2}, \\ \langle : \hat{P}_{z(\psi)} : \rangle &= \left\langle : -i\text{Re} \left[ \hat{\psi} \gamma^z (\partial_z - ieA) \hat{\psi} \right] : \right\rangle. \end{aligned} \quad (2.101)$$

From Figs. 2.16 and 2.17, one again notices that the classical field degree of freedom is smoothly converted into those of quantum particles. One also finds the matter part of the transverse pressure  $\langle : \hat{P}_{\perp(\psi)} : \rangle$  is negligible, and hence the total pressure  $\langle : \hat{P}_\perp : \rangle$  is dominated by the classical field contribution  $\langle : \hat{P}_{\perp(A)} : \rangle$ . This is because the transverse distribution of produced particles form almost the Gaussian distribution  $\sim \exp[-\pi(m_e^2 + \mathbf{p}_\perp^2)/|eE|]$  (see Section 2.5.2) so that they typically have small transverse momentum  $(m_e^2 + \mathbf{p}_\perp^2)/|eE| \lesssim 1$ . On the

contrary to this, the longitudinal pressure of the matter  $\langle : \hat{P}_{z(\psi)} : \rangle$  dominates the total pressure  $\langle : \hat{P}_z : \rangle$  because the longitudinal acceleration by the classical electric field is significant.

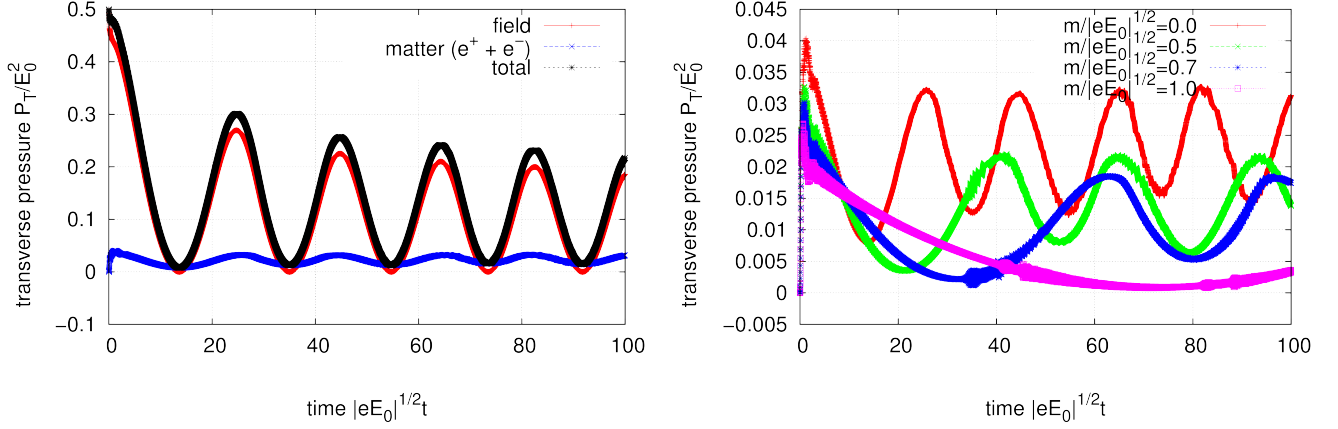


Figure 2.16: The time-evolution of the transverse pressure  $\langle : \hat{P}_{\perp} : \rangle = \langle : \hat{P}_{\perp(A)} : \rangle + \langle : \hat{P}_{\perp(\psi)} : \rangle$ . [Left] The total pressure  $\langle : \hat{P}_{\perp} : \rangle$  (black) together with the matter  $\langle : \hat{P}_{\perp(\psi)} : \rangle$  (blue) and the classical electric field  $\langle : \hat{P}_{\perp(A)} : \rangle$  (red) contributions. [Right] The transverse pressure of the matter  $\langle : \hat{P}_{\perp(\psi)} : \rangle$  for various values of the initial field strength (or the electron mass) as  $m_e/\sqrt{|eE_0|} = 0.0$  (red), 0.5 (green), 0.7 (blue), and 1.0 (purple).

As is evident from Eqs. (2.100) and (2.101), the classical part of the longitudinal pressure  $\langle : \hat{P}_{z(A)} : \rangle$  is negative and the system is highly anisotropic initially. In other words, the system is far from equilibrium. In order to investigate how the system equilibrates (or does not equilibrate) through the decoherence of the classical field, we compare the total pressures,  $\langle : \hat{P}_{\perp} : \rangle$  and  $\langle : \hat{P}_z : \rangle$ , and examine isotropization of the system. The result is plotted in Fig. 2.18, where the initial field strength or the electron mass is set to be  $m_e/\sqrt{|eE_0|} = 0$  for simplicity; it only changes the time-scale of the result. The figure shows that the degree of the anisotropy is relaxed through the decoherence. In particular, the longitudinal pressure  $\langle : \hat{P}_z : \rangle$  becomes positive because the matter contribution  $\langle : \hat{P}_{z(\psi)} : \rangle$ , which is always positive because of their longitudinal motion, dominates the total pressure  $\langle : \hat{P}_z : \rangle$ . However, complete isotropization is not achieved in our mean field treatment formulated in Section 2.1. This is because our framework does not take into account collisions between created particles, i.e., collisions. In order to take into account collisional effects, one needs to go beyond the mean field treatment.

## 2.6 Brief summary

We briefly summarize the main results of this chapter:

- We formulated the Schwinger mechanism in QED within mean field approximation including backreaction from produced electrons to the classical field (see Section 2.1).

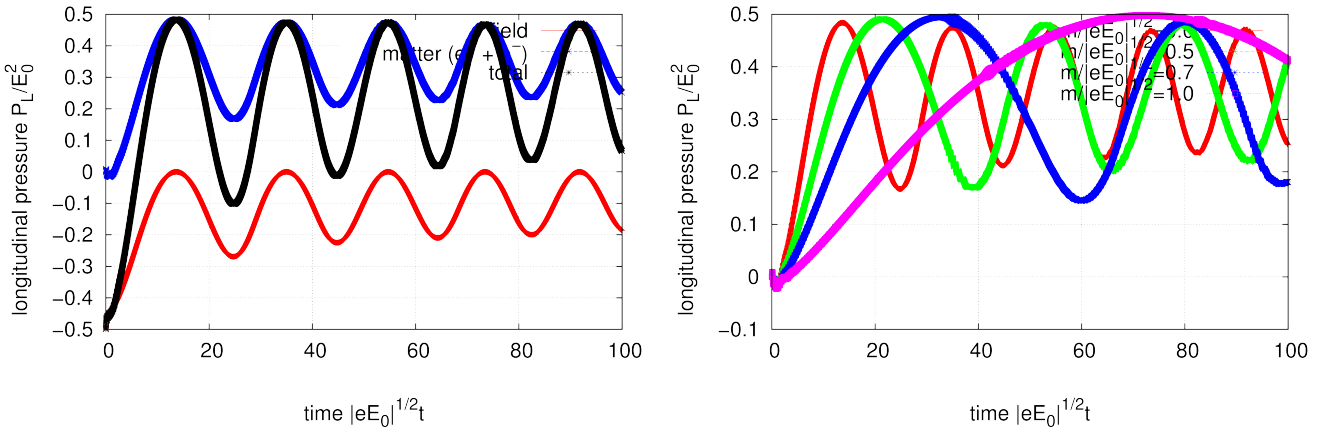


Figure 2.17: The time-evolution of the longitudinal pressure  $\langle : \hat{P}_z : \rangle = \langle : \hat{P}_{z(A)} : \rangle + \langle : \hat{P}_{z(\psi)} : \rangle$ . [Left] The total pressure  $\langle : \hat{P}_z : \rangle$  (black) together with the matter  $\langle : \hat{P}_{z(\psi)} : \rangle$  (blue) and the classical electric field  $\langle : \hat{P}_{z(A)} : \rangle$  (red) contributions. [Right] The longitudinal pressure of the matter  $\langle : \hat{P}_{z(\psi)} : \rangle$  for various values of the initial field strength (or the electron mass) as  $m_e/\sqrt{|eE_0|} = 0.0$  (red), 0.5 (green), 0.7 (blue), and 1.0 (purple).

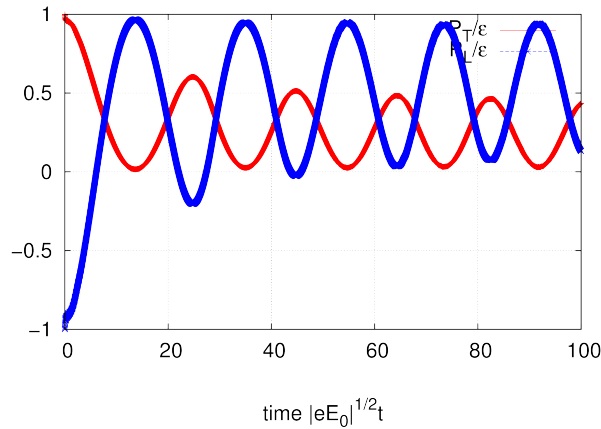


Figure 2.18: Isotropization of the system. The total transverse and longitudinal pressure scaled by the total energy,  $\langle : \hat{P}_\perp : \rangle / \langle : \hat{\epsilon} : \rangle$  and  $\langle : \hat{P}_z : \rangle / \langle : \hat{\epsilon} : \rangle$ , are plotted in red and blue line, respectively.

- We applied the formalism to a constant electric field ignoring backreaction in Section 2.2 and 2.4: We analytically traced the time-evolution of the electron distribution function to find that the electron production is consistent with the well-known Schwinger formula.
- Time-dependence of the background field largely affects the particle production mechanism. In particular, an interplay between perturbative and non-perturbative particle production occurs because of the time-dependence. By employing a Sauter-type pulsed electric field with duration  $\tau$  and strength  $E_0$ , we analytically showed in Section 2.3 that (i) two dimensionless parameters  $\nu = |eE_0|\tau^2$ ,  $\gamma = |eE_0|\tau/m_e$  control the interplay, and (ii) the electron production is strongly enhanced in the perturbative regime.
- Backreaction effects were discussed in Section 2.5, where we found that the electron spectrum is dramatically modified from the naive Schwinger formula. In particular, we found that (i) the classical plasma oscillation occurs; (ii) the quantum interferences among electrons strongly distort the electron spectrum; and (iii) the Pauli principle suppresses the electron production.
- Because of the backreaction, the initial field energy is smoothly converted into particle degrees of freedom and the field attenuates, although the time-scale is rather slow in QED (see Fig. 2.15).
- A longitudinal classical electric field is highly anisotropic. The degree of the anisotropy is relaxed as the classical field decoheres into electrons via the Schwinger mechanism. However, the complete isotropization is never achieved as was plotted in Fig. 2.18 because our mean field treatment neglects scatterings and collisions between produced electrons.



## Chapter 3

# Schwinger Mechanism in $SU_c(N_c = 2)$ Yang-Mills theory

As a first step towards formulating the Schwinger mechanism in QCD, we consider the  $SU_c(N_c = 2)$  Yang-Mills theory without quarks in this chapter. In Section 3.1, we formulate the Schwinger mechanism in the  $SU_c(N_c = 2)$  Yang-Mills theory including backreaction from gluon and ghost fluctuations by extending the mean field framework developed in QED (Section 2.1). In Section 3.2 and 3.3, we analytically and numerically apply the formalism to discuss how the Schwinger mechanism in the Yang-Mills theory is similar to and/or different from that in QED: In Section 3.2, we consider a constant color electric field neglecting backreaction. By analytically tracing the time-evolution of the gluon spectrum, we will see that the gluon spectrum is consistent with the Schwinger formula for a constant electric field. In Section 3.3, we treat the backreaction numerically, and will see that the backreaction dramatically affects the time-evolution of the system. In particular, we shall see that the boson statistics of gluons strongly enhances the gluon production, and the classical gauge field decays much faster than in QED.

### 3.1 Formalism

#### 3.1.1 $SU_c(N_c = 2)$ Yang-Mills theory under a classical gauge field

##### Lagrangian

Let us consider the  $SU_c(N_c = 2)$  pure Yang-Mills theory, which is described by the Lagrangian  $\hat{\mathcal{L}}_{\text{YM}}$ :

$$\hat{\mathcal{L}}_{\text{YM}} = \hat{\mathcal{L}}_{(\text{g})} + \hat{\mathcal{L}}_{(\text{GF+FP})} + \hat{\mathcal{L}}_{(\text{ext})}, \quad (3.1)$$

where

$$\hat{\mathcal{L}}_{(\text{g})} = -\frac{1}{2} \text{tr}_c[\hat{F}^{\mu\nu} \hat{F}_{\mu\nu}], \quad (3.2)$$

$$\hat{\mathcal{L}}_{(\text{ext})} = 2 \text{tr}_c[J^\mu \hat{A}_\mu] \quad (3.3)$$

are contributions from the gluon field  $\hat{A}_\mu$ , and a classical external source  $J^\mu$ , respectively.  $g$  is the strong coupling constant. The non-Abelian field strength  $\hat{F}_{\mu\nu}$  is introduced as  $\hat{F}_{\mu\nu} \equiv \partial_\mu \hat{A}_\nu - \partial_\nu \hat{A}_\mu + ig[\hat{A}_\mu, \hat{A}_\nu]$ .  $\text{tr}_c$  is a trace operation in the color space. We normalize generators  $t_a$  ( $a = 1, \dots, N_c^2 - 1$ ) of  $SU_c(N_c = 2)$  by  $\text{tr}_c[t_a t_b] = \delta_{ab}/2$ . The remaining Lagrangian  $\hat{\mathcal{L}}_{(\text{GF}+\text{FP})}$  represents the contribution from the gauge-fixing and the ghost fields  $\hat{c}, \hat{\bar{c}}$ , and is given by [153]

$$\hat{\mathcal{L}}_{(\text{GF}+\text{FP})} = -2i \text{tr}_c[\delta_{\text{BRS}}(\hat{c}\hat{\theta})]. \quad (3.4)$$

Here,  $\delta_{\text{BRS}}$  denotes the BRS transformation (where *BRS* refers to Becchi, Rouet and Stora [154]):

$$\begin{cases} \delta_{\text{BRS}}\hat{A}_\mu = \hat{D}_\mu\hat{c} \\ \delta_{\text{BRS}}\hat{c} = -ig\hat{c}^2 \\ \delta_{\text{BRS}}\hat{\bar{c}} = i\hat{B} \\ \delta_{\text{BRS}}\hat{B} = 0 \end{cases}, \quad (3.5)$$

where  $\hat{D}_\mu$  is the covariant derivative with respect to the gauge field  $\hat{A}_\mu$  as  $\hat{D}_\mu\hat{\bullet} \equiv \partial_\mu\hat{\bullet} + ig[\hat{A}_\mu, \hat{\bullet}]$ , and  $\hat{B}$  is the so-called Nakanishi-Lautrap (NL) field [155, 156]. Notice that the BRS transformation is nil-potent  $\delta_{\text{BRS}}^2 = 0$ , which guarantees the BRS invariance of the Yang-Mills Lagrangian  $\hat{\mathcal{L}}_{\text{YM}}$ . The choice of the gauge fixing function  $\hat{\theta}$  is arbitrary in principle, but it is convenient to take a specific function as

$$\hat{\theta} = \hat{\vartheta}[\hat{A}] + \frac{1}{2}\hat{B}. \quad (3.6)$$

The newly introduced function  $\hat{\vartheta}$  is an arbitrary function depending on the gauge field  $\hat{A}$  only (for the explicit expression of  $\hat{\vartheta}$  used in this thesis, see Eq. (3.20)). Under this choice of the gauge fixing function  $\hat{\theta}$ ,  $\hat{\mathcal{L}}_{(\text{GF}+\text{FP})}$  reads

$$\hat{\mathcal{L}}_{(\text{GF}+\text{FP})} = 2\text{tr}_c \left[ \hat{B}\hat{\vartheta} + \frac{1}{2}\hat{B}^2 + i\hat{\bar{c}}\delta_{\text{BRS}}\hat{\vartheta} \right]. \quad (3.7)$$

Now that the Euler-Lagrange equation for the NL field  $\hat{B}$  is  $0 = \hat{\vartheta} + \hat{B}$ , one can safely replace the NL field  $\hat{B}$  by  $-\hat{\vartheta}$  to obtain

$$\hat{\mathcal{L}}_{(\text{GF}+\text{FP})} = \underbrace{-\text{tr}_c[\hat{\vartheta}^2]}_{\equiv \hat{\mathcal{L}}_{(\text{GF})}} + \underbrace{2i \text{tr}_c[\hat{\bar{c}}\delta_{\text{BRS}}\hat{\vartheta}]}_{\equiv \hat{\mathcal{L}}_{(\text{FP})}}. \quad (3.8)$$

### Color basis

In order to avoid some complexities coming from the non-Abelian algebra of  $SU_c(N_c = 2)$ , it is useful to expand the color space (gluons  $\hat{A}_\mu$  and ghosts  $\hat{c}, \hat{\bar{c}}$ ) by ladder operators (or a Cartan-Weyl basis of  $SU_c(N_c = 2)$ ), instead of the usual Pauli matrices  $\{\sigma_a\}$ . Namely, we consider the

following particular generators,  $H, E$ , as

$$\begin{aligned} H &\equiv \sigma_3 = \frac{1}{2} \begin{pmatrix} 1 & 0 \\ 0 & -1 \end{pmatrix}, \\ E &\equiv \frac{\sigma_1 + i\sigma_2}{\sqrt{2}} = \frac{1}{\sqrt{2}} \begin{pmatrix} 0 & 1 \\ 0 & 0 \end{pmatrix}. \end{aligned} \quad (3.9)$$

These generators  $H, E$  satisfy the following algebra:

$$\mathrm{tr}_c[H^2] = \mathrm{tr}_c[EE^\dagger] = \frac{1}{2}, \quad \mathrm{tr}_c[HE] = \mathrm{tr}_c[E^2] = 0, \quad (3.10)$$

and

$$[H, E] = E, \quad [E, E^\dagger] = H. \quad (3.11)$$

### Abelian dominance assumption

From now, we adopt the *Abelian dominance assumption* for simplicity: We assume that the Abelian components  $\propto H$  dominate the classical current  $J^\mu$  and the classical field  $\langle \hat{A}_\mu \rangle$  generated by the classical current. Under this assumption, one may neglect non-Abelian components  $\propto E, E^\dagger$  in the classical current  $J^\mu$  and the classical gauge field  $\langle \hat{A}_\mu \rangle$  to write

$$J_\mu(x) = \bar{J}_\mu(x)H, \quad \langle \hat{A}_\mu(x) \rangle = \bar{A}_\mu(x)H, \quad (3.12)$$

The Abelian dominance assumption is justified when non-Abelian commutators, in which we are interested, vanish as  $ig[\bullet, *] \rightarrow 0$ . Formally, this criterion is fulfilled in the small coupling constant limit  $g \rightarrow 0^1$ . Under this assumption, the problem is reduced to essentially an Abelian one, and thus one can formulate the Schwinger mechanism in the Yang-Mills theory in an analogous manner in QED explained in Section 2.1.

### expansion around a classical field

Now, we are interested in how the classical gauge field  $\bar{A}_\mu$  affects the quantum mechanical evolution of the system. In order to make this situation manifest, we decompose the total gauge field  $\hat{A}_\mu$  and the ghost fields  $\hat{c}, \hat{\bar{c}}$  into the Abelian classical field  $\langle \hat{A}_\mu \rangle = \bar{A}_\mu H$  and quantum

<sup>1</sup>Strictly speaking, one has to take care about how the unspecified quantities  $\bullet, *$  depend on the coupling constant  $g$ . For example, in the CGC framework one is interested in a commutator of the classical fields  $A_\mu$ . In CGC, the strength of the classical field  $A_\mu$  grows as  $\sim 1/g$  with  $g \rightarrow 0$ , so that the commutator  $ig[A_\mu, A_\nu]$  does not vanish in the small coupling constant limit  $g \rightarrow 0$ . Thus, one cannot theoretically justify the Abelian dominance assumption with the smallness of the coupling constant  $g$  in this example. It is, however, interesting to note that the Abelian dominance assumption for the classical field  $A_\mu$  is largely consistent with a full numerical simulation of the classical Yang-Mills equation initiated by a CGC initial condition [140].

fluctuations around it,  $\hat{a}_\mu, \hat{\mathcal{A}}_\mu, \hat{C}, \hat{\bar{C}}$  as

$$\hat{A}_\mu = (\bar{A}_\mu + \hat{a}_\mu)H + \hat{\mathcal{A}}_\mu E + \hat{\mathcal{A}}_\mu^\dagger E^\dagger, \quad (3.13)$$

$$\begin{pmatrix} \hat{c} \\ \hat{\bar{c}} \end{pmatrix} = \begin{pmatrix} \hat{C} \\ \hat{\bar{C}} \end{pmatrix} H + \begin{pmatrix} \hat{C} \\ \hat{\bar{C}} \end{pmatrix} E + \begin{pmatrix} \hat{C}^\dagger \\ \hat{\bar{C}}^\dagger \end{pmatrix} E^\dagger. \quad (3.14)$$

Under this decomposition, one can expand the field strength tensor  $\hat{F}_{\mu\nu}$  as

$$\hat{F}_{\mu\nu} = (\bar{F}_{\mu\nu} + \hat{f}_{\mu\nu} + \delta\hat{f}_{\mu\nu})H + [(\hat{\mathcal{F}}_{\mu\nu} + \delta\hat{\mathcal{F}}_{\mu\nu})E + (\text{h.c.})], \quad (3.15)$$

where

$$\begin{cases} \bar{F}_{\mu\nu} & \equiv \partial_\mu \bar{A}_\nu - \partial_\nu \bar{A}_\mu \\ \hat{f}_{\mu\nu} & \equiv \partial_\mu \hat{a}_\nu - \partial_\nu \hat{a}_\mu \\ \delta\hat{f}_{\mu\nu} & \equiv ig(\hat{\mathcal{A}}_\nu^\dagger \hat{\mathcal{A}}_\mu - \hat{\mathcal{A}}_\mu^\dagger \hat{\mathcal{A}}_\nu) \\ \hat{\mathcal{F}}_{\mu\nu} & \equiv \bar{D}_\mu \hat{\mathcal{A}}_\nu - \bar{D}_\nu \hat{\mathcal{A}}_\mu \\ \delta\hat{\mathcal{F}}_{\mu\nu} & \equiv ig(\hat{a}_\mu \hat{\mathcal{A}}_\nu - \hat{a}_\nu \hat{\mathcal{A}}_\mu) \end{cases}. \quad (3.16)$$

Here,  $\bar{D}_\mu$  is the covariant derivative with respect to the classical gauge field denoted by

$$\bar{D}_\mu \equiv \partial_\mu + ig\bar{A}_\mu. \quad (3.17)$$

Now, the Yang-Mills Lagrangian (3.1) reads

$$\begin{aligned} \hat{\mathcal{L}}_{(\text{g})} &= -\frac{1}{4}\bar{F}_{\mu\nu}\bar{F}^{\mu\nu} \\ &\quad -\frac{1}{2}\bar{F}^{\mu\nu}\hat{f}_{\mu\nu} \\ &\quad -\frac{1}{4}\hat{f}_{\mu\nu}\hat{f}^{\mu\nu} - \frac{1}{2}\left[\hat{\mathcal{F}}_{\mu\nu}^\dagger\hat{\mathcal{F}}^{\mu\nu} + \bar{F}^{\mu\nu}\delta\hat{f}^{\mu\nu}\right] \\ &\quad -\frac{1}{2}\hat{f}_{\mu\nu}\delta\hat{f}^{\mu\nu} - \frac{1}{2}\left[\hat{\mathcal{F}}_{\mu\nu}^\dagger\delta\hat{\mathcal{F}}^{\mu\nu} + \delta\hat{\mathcal{F}}^{\mu\nu\dagger}\hat{\mathcal{F}}_{\mu\nu}\right] \\ &\quad -\frac{1}{4}\delta\hat{f}_{\mu\nu}\delta\hat{f}^{\mu\nu} - \frac{1}{2}\delta\hat{\mathcal{F}}_{\mu\nu}^\dagger\delta\hat{\mathcal{F}}^{\mu\nu}, \end{aligned} \quad (3.18)$$

$$\hat{\mathcal{L}}_{(\text{ext})} = \bar{J}^\mu \bar{A}_\mu + \bar{J}^\mu \hat{a}_\mu. \quad (3.19)$$

### gauge fixing and ghost term

Under the Abelian dominance approximation, it is convenient to fix the gauge along the Abelian direction of the gauge field  $2\text{tr}_c[H\hat{A}_\mu] = \bar{A}_\mu + \hat{a}_\mu$ . Namely, we consider the following gauge fixing function  $\hat{\vartheta}$ :

$$\hat{\vartheta} = \partial^\mu (\bar{A}_\mu + \hat{a}_\mu)H + \left[ (\partial_\mu + ig(\bar{A}_\mu + \hat{a}_\mu)) \hat{\mathcal{A}}^\mu E + (\text{h.c.}) \right]. \quad (3.20)$$

Under this choice of the gauge fixing function, the gauge fixing Lagrangian  $\hat{\mathcal{L}}_{(\text{GF})}$  and the ghost Lagrangian  $\hat{\mathcal{L}}_{(\text{FP})}$  read

$$\begin{aligned}\hat{\mathcal{L}}_{(\text{GF})} = & -\frac{1}{2}(\partial^\mu \bar{A}_\mu)^2 \\ & -(\partial^\mu \hat{a}_\mu)(\partial^\nu \bar{A}_\nu) \\ & -\frac{1}{2}(\partial^\mu \hat{a}_\mu)^2 - |\bar{D}_\mu \hat{\mathcal{A}}^\mu|^2 \\ & -ig\hat{a}_\mu \left[ (\bar{D}_\nu \hat{\mathcal{A}}^\nu)^\dagger \hat{\mathcal{A}}^\mu - \hat{\mathcal{A}}^{\mu\dagger} (\bar{D}_\nu \hat{\mathcal{A}}^\nu) \right] \\ & -g^2 \hat{a}_\mu \hat{a}_\nu \hat{\mathcal{A}}^\mu \hat{\mathcal{A}}^{\nu\dagger},\end{aligned}\tag{3.21}$$

$$\begin{aligned}\hat{\mathcal{L}}_{(\text{FP})} = & i\hat{\mathcal{C}}\partial_\mu\partial^\mu\hat{\mathcal{C}} + i\left[\hat{\mathcal{C}}^\dagger\left(\bar{D}_\mu\bar{D}^\mu\hat{\mathcal{C}}\right) - \left(\bar{D}_\mu\bar{D}^\mu\hat{\mathcal{C}}\right)^\dagger\hat{\mathcal{C}}\right] \\ & -g\left[2\hat{a}_\mu\left(\hat{\mathcal{C}}^\dagger(\bar{D}^\mu\hat{\mathcal{C}}) + (\bar{D}^\mu\hat{\mathcal{C}})^\dagger\hat{\mathcal{C}}\right) + (\partial^\mu\hat{a}_\mu)(\hat{\mathcal{C}}^\dagger\hat{\mathcal{C}} + \hat{\mathcal{C}}^\dagger\hat{\mathcal{C}})\right] \\ & -g\left[\hat{\mathcal{A}}_\mu\hat{\mathcal{C}}(\bar{D}^\mu\hat{\mathcal{C}})^\dagger - \hat{\mathcal{A}}_\mu^\dagger\hat{\mathcal{C}}(\bar{D}^\mu\hat{\mathcal{C}}) + (\bar{D}^\mu\hat{\mathcal{A}}_\mu)^\dagger(\hat{\mathcal{C}}\hat{\mathcal{C}} - \hat{\mathcal{C}}^\dagger\hat{\mathcal{C}}) - (\bar{D}^\mu\hat{\mathcal{A}}_\mu)(\hat{\mathcal{C}}^\dagger\hat{\mathcal{C}} - \hat{\mathcal{C}}^\dagger\hat{\mathcal{C}})\right] \\ & -ig^2\left[\hat{\mathcal{A}}^\mu\hat{\mathcal{A}}_\mu\hat{\mathcal{C}}^\dagger\hat{\mathcal{C}} - \hat{\mathcal{A}}^\mu\hat{\mathcal{A}}_\mu^\dagger(\hat{\mathcal{C}}^\dagger\hat{\mathcal{C}} - \hat{\mathcal{C}}^\dagger\hat{\mathcal{C}}) + \hat{\mathcal{A}}^{\mu\dagger}\hat{\mathcal{A}}_\mu^\dagger\hat{\mathcal{C}}\hat{\mathcal{C}}\right] \\ & + ig^2(\hat{a}_\mu\hat{a}^\mu)(\hat{\mathcal{C}}^\dagger\hat{\mathcal{C}} - \hat{\mathcal{C}}^\dagger\hat{\mathcal{C}}) + ig^2\hat{a}^\mu\left[\hat{\mathcal{A}}_\mu^\dagger\hat{\mathcal{C}}\hat{\mathcal{C}} + \hat{\mathcal{A}}_\mu\hat{\mathcal{C}}^\dagger\hat{\mathcal{C}}\right].\end{aligned}\tag{3.22}$$

Note that in the limit of  $\hat{a}_\mu \rightarrow 0$ , the gauge fixing and ghost Lagrangian  $\hat{\mathcal{L}}_{(\text{GF})}, \hat{\mathcal{L}}_{(\text{FP})}$  reduce to the well-known covariant background gauge fixing term and the corresponding ghost term, which are useful as long as the backreaction is neglected. The gauge-dependence of our results presented below must be investigated further, but we leave this topic as a future work.

### conserved quantities

There exist some conserved quantities associated with symmetries in the Yang-Mills Lagrangian  $\hat{\mathcal{L}}_{\text{YM}}$  (3.1):

color current  $\hat{j}^\mu$

Even after the gauge is fixed by Eq. (3.20), the Yang-Mills Lagrangian  $\hat{\mathcal{L}}_{\text{YM}}$  (3.1) is invariant under a global color rotation around the Abelian  $H$ -direction in the color space:

$$\hat{A}_\mu \rightarrow U\hat{A}_\mu U^\dagger, \quad \begin{pmatrix} \hat{\mathcal{C}} \\ \hat{\mathcal{C}}^\dagger \end{pmatrix} \rightarrow U \begin{pmatrix} \hat{\mathcal{C}} \\ \hat{\mathcal{C}}^\dagger \end{pmatrix} U^\dagger,\tag{3.23}$$

where

$$U = \exp[-ig\theta H].\tag{3.24}$$

The conserved quantity associated with this symmetry is the color current (in the  $H$ -direction)  $\hat{j}^\mu$ , which is obtained via the Noether theorem [143]. The vacuum expectation value of the

current  $\langle : \hat{j}^\mu : \rangle$  reads

$$\begin{aligned} \langle : \hat{j}^\mu : \rangle = & -\partial^\nu \langle : \delta f_{\mu\nu} : \rangle + ig \left\langle : \hat{\mathcal{A}}_\nu^\dagger \left( \bar{D}^\mu \hat{\mathcal{A}}^\nu \right) - \left( \bar{D}^\mu \hat{\mathcal{A}}^\nu \right)^\dagger \hat{\mathcal{A}}_\nu : \right\rangle \\ & - g \left\langle : \hat{\mathcal{C}}^\dagger \left( \bar{D}_\mu \hat{\mathcal{C}} \right) + \left( \bar{D}_\mu \hat{\mathcal{C}} \right)^\dagger \hat{\mathcal{C}} - \left( \bar{D}_\mu \hat{\mathcal{C}} \right)^\dagger \hat{\mathcal{C}} - \hat{\mathcal{C}}^\dagger \left( \bar{D}_\mu \hat{\mathcal{C}} \right) : \right\rangle. \end{aligned} \quad (3.25)$$

Here, the divergence is eliminated by the normal ordering procedure as was explained in Section 2.1.5.

The conservation law for  $\langle : \hat{j}^\mu : \rangle$  is

$$0 = \partial_\mu \langle : \hat{j}^\mu : \rangle. \quad (3.26)$$

symmetric energy-momentum tensor  $\hat{T}^{\mu\nu}$

As in QED (see Section 2.1.1), the symmetric energy-momentum tensor  $\hat{T}^{\mu\nu}$  for the Yang-Mills Lagrangian (3.1) associated with the translational invariance of the system can be obtained by Eq. (2.8). The vacuum expectation value of the symmetric energy-momentum tensor  $\langle : \hat{T}^{\mu\nu} : \rangle$  reads

$$\begin{aligned} \langle : \hat{T}_{\mu\nu} : \rangle = & \eta^{\mu\nu} \left[ \frac{1}{4} \bar{F}^{\rho\sigma} \bar{F}_{\rho\sigma} - \frac{1}{2} (\partial_\lambda \bar{A}^\lambda)^2 - \bar{A}^\rho \partial_\rho \partial_\sigma \bar{A}^\sigma \right] - [\bar{F}^\mu{}_\lambda \bar{F}^{\nu\lambda} - \bar{A}^\mu \partial^\nu \partial_\lambda \bar{A}^\lambda - \bar{A}^\nu \partial^\mu \partial_\lambda \bar{A}^\lambda] \\ & + \eta^{\mu\nu} \text{Re} \left\langle : \frac{1}{4} \hat{f}^{\rho\sigma} \hat{f}_{\rho\sigma} - \frac{1}{4} [M_{(a)}^2]^{\rho\sigma} \hat{a}_\rho \hat{a}_\sigma - \frac{1}{2} (\partial_\lambda \hat{a}^\lambda)^2 - \hat{a}^\rho \partial_\rho \partial_\sigma \hat{a}^\sigma : \right\rangle \\ & - \text{Re} \left\langle : \hat{f}^\mu{}_\lambda \hat{f}^{\nu\lambda} - \frac{1}{2} [[M_{(a)}^2]^{\mu\rho} \hat{a}^\nu \hat{a}_\rho + [M_{(a)}^2]^{\nu\rho} \hat{a}^\mu \hat{a}_\rho] - \hat{a}^\mu \partial^\nu \partial_\lambda \hat{a}^\lambda - \hat{a}^\nu \partial^\mu \partial_\lambda \hat{a}^\lambda : \right\rangle \\ & + 2 \times \left( \eta^{\mu\nu} \text{Re} \left\langle : \frac{1}{4} \hat{\mathcal{F}}_{\rho\sigma}^\dagger \hat{\mathcal{F}}^{\rho\sigma} - \frac{1}{4} [M_{(\mathcal{A})}]^{\rho\sigma} \hat{\mathcal{A}}_\rho^\dagger \hat{\mathcal{A}}_\sigma - \frac{1}{2} |\bar{D}_\lambda \hat{\mathcal{A}}^\lambda|^2 - \hat{\mathcal{A}}^{\rho\dagger} (\bar{D}_\rho \bar{D}_\sigma \hat{\mathcal{A}}^\sigma) : \right\rangle \right. \\ & \left. - \text{Re} \left\langle : \hat{\mathcal{F}}_{\lambda}^{\mu\dagger} \hat{\mathcal{F}}^{\nu\lambda} - \frac{1}{2} [[M_{(\mathcal{A})}]^{\mu\lambda} \hat{\mathcal{A}}^{\nu\dagger} \hat{\mathcal{A}}_\lambda + [M_{(\mathcal{A})}]^{\nu\lambda} \hat{\mathcal{A}}^{\mu\dagger} \hat{\mathcal{A}}_\lambda] \right. \right. \\ & \left. \left. - \hat{\mathcal{A}}^{\mu\dagger} (\bar{D}^\nu \bar{D}_\lambda \hat{\mathcal{A}}^\lambda) - \hat{\mathcal{A}}^{\nu\dagger} (\bar{D}^\mu \bar{D}_\lambda \hat{\mathcal{A}}^\lambda) : \right\rangle \right) \\ & + \text{Re} \left\langle : i \times [\eta^{\mu\nu} (\partial_\lambda \hat{\mathcal{C}}) (\partial^\lambda \hat{\mathcal{C}}) - (\partial^\mu \hat{\mathcal{C}}) (\partial^\nu \hat{\mathcal{C}}) - (\partial^\nu \hat{\mathcal{C}}) (\partial^\mu \hat{\mathcal{C}})] : \right\rangle \\ & + 2 \times \left( \eta^{\mu\nu} \text{Re} \left\langle : i \times \left[ (\bar{D}_\lambda \hat{\mathcal{C}})^\dagger (\bar{D}^\lambda \hat{\mathcal{C}}) - \frac{1}{2} M_{(\mathcal{C})} \hat{\mathcal{C}}^\dagger \hat{\mathcal{C}} \right] : \right\rangle \right. \\ & \left. - \text{Re} \left\langle : i \times \left[ (\bar{D}^\mu \hat{\mathcal{C}})^\dagger (\bar{D}^\nu \mathcal{C}) + (\bar{D}^\nu \hat{\mathcal{C}})^\dagger (\bar{D}^\mu \mathcal{C}) \right] : \right\rangle \right), \end{aligned} \quad (3.27)$$

where we introduced effective mass terms  $M_{(a)}^2, M_{(\mathcal{A})}^2, M_{(\mathcal{C})}^2$  whose explicit expressions are given later in Eq. (3.35).

The conservation law for  $\langle : \hat{T}_{\mu\nu} : \rangle$  is

$$\partial_\mu \langle : \hat{T}_{\mu\nu} : \rangle = \bar{J}_\mu \bar{F}^{\mu\nu} + \bar{A}^\nu \partial_\mu \bar{J}^\mu, \quad (3.28)$$

which is free from non-Abelian commutators and is the same as the Abelian one (2.21) because of the Abelian dominance assumption (3.12).

As in QED (See Section 2.1.1), we define the energy density  $\langle : \hat{\epsilon} : \rangle$ , the transverse pressure  $\langle : \hat{P}_\perp : \rangle$ , and the longitudinal pressure  $\langle : \hat{P}_z : \rangle$  by the diagonal components of the symmetric energy-momentum tensor  $\langle : \hat{T}^{\mu\nu} : \rangle$  (3.27) as

$$\begin{aligned} \langle : \hat{\epsilon} : \rangle &\equiv \langle : \hat{T}^{tt} : \rangle, \\ \langle : \hat{P}_\perp : \rangle &\equiv \frac{\langle : \hat{T}^{xx} + \hat{T}^{yy} : \rangle}{2}, \\ \langle : \hat{P}_z : \rangle &\equiv \langle : \hat{T}^{zz} : \rangle. \end{aligned} \quad (3.29)$$

### 3.1.2 assumptions on the system

In addition to the Abelian dominance assumption made in Eq. (3.12), we furthermore assume the same three assumptions made in the QED study (see Section 2.1.2): (i) Homogeneity in space by assuming the classical gauge field  $\bar{A}_\mu$  is given by

$$\bar{A}^\mu(x) = (0, 0, 0, \bar{A}(t)) = (0, 0, 0, - \int_{-\infty}^t dt' \bar{E}(t')); \quad (3.30)$$

(ii) Vacuum initial condition  $|\text{state}; \text{in}\rangle = |\text{vac}; \text{in}\rangle$ ; and (iii) Adiabatic hypothesis by requiring  $\partial_t \bar{E} \xrightarrow{t \rightarrow \pm\infty} 0$ .

### 3.1.3 mean field approximation

mean field approximation

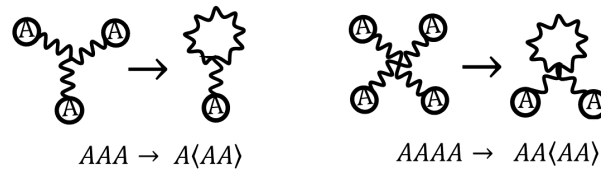


Figure 3.1: A diagrammatic illustration of the mean field treatment for gluons  $\hat{\mathcal{A}}$  as an example.

As in the QED study (see Section 2.1.3), we adopt mean field approximation for the non-linear interactions in  $\hat{\mathcal{L}}_{\text{YM}}$ . As is pictorially illustrated in Fig. 3.1, we approximate the higher order terms beyond the cubic order in the fluctuations by taking an expectation value of a product of two fluctuations in higher order terms to obtain an effective Lagrangian which is

at most quadratic order in the quantum fluctuations. In taking an expectation value of two fluctuations, we assume that only the following two-point functions are non-vanishing as

$$\begin{aligned} ig \langle : \hat{a}_\mu \hat{a}_\nu : \rangle &\equiv \pi_{\mu\nu}, \\ ig \langle : \hat{\mathcal{A}}_\mu^\dagger \hat{\mathcal{A}}_\nu : \rangle &\equiv \Pi_{\mu\nu}, \\ g \langle : \hat{\mathcal{C}}^\dagger \hat{\mathcal{C}} - \hat{\mathcal{C}}^\dagger \hat{\mathcal{C}} : \rangle &\equiv \varphi, \end{aligned} \quad (3.31)$$

and that all the other two-point functions such as  $\langle \hat{a}_\mu \hat{\mathcal{A}}_\nu \rangle, \langle \hat{\mathcal{C}} \hat{\mathcal{A}}_\mu \rangle, \dots$  are vanishing. This assumption says that the quantum fluctuations do not mix with each other during the spacetime evolution. We note that this assumption is surely consistent with equations of motion (3.36)-(3.40) derived later. All the non-linear effects are effectively represented by the two-point functions,  $\pi_{\mu\nu}, \Pi_{\mu\nu}, \varphi$ , which are self-consistently solved throughout the computation.

As an example of the mean field treatment, let us consider a quartic term of  $\hat{\mathcal{A}}$  described by  $(ig)^2 \hat{\mathcal{A}}_\mu^\dagger \hat{\mathcal{A}}_\nu \hat{\mathcal{A}}_\rho^\dagger \hat{\mathcal{A}}_\sigma$ . We approximate this term by replacing all the possible combinations of two fluctuations out of the four in the term by their expectation value as

$$\begin{aligned} (ig)^2 \hat{\mathcal{A}}_\mu^\dagger \hat{\mathcal{A}}_\nu \hat{\mathcal{A}}_\rho^\dagger \hat{\mathcal{A}}_\sigma &\rightarrow ig \hat{\mathcal{A}}_\mu^\dagger \hat{\mathcal{A}}_\nu \Pi_{\rho\sigma} + \Pi_{\mu\nu} ig \hat{\mathcal{A}}_\rho^\dagger \hat{\mathcal{A}}_\sigma + ig \hat{\mathcal{A}}_\mu^\dagger \hat{\mathcal{A}}_\sigma \Pi_{\rho\nu} + \Pi_{\mu\sigma} ig \hat{\mathcal{A}}_\rho^\dagger \hat{\mathcal{A}}_\nu \\ &\quad - [\Pi_{\mu\nu} \Pi_{\rho\sigma} + \Pi_{\mu\sigma} \Pi_{\rho\nu}], \end{aligned} \quad (3.32)$$

where the last term  $\Pi_{\mu\nu} \Pi_{\rho\sigma} + \Pi_{\mu\sigma} \Pi_{\rho\nu}$  is inserted so that the expectation value of the term,

$$(ig)^2 \langle : \hat{\mathcal{A}}_\mu^\dagger \hat{\mathcal{A}}_\nu \hat{\mathcal{A}}_\rho^\dagger \hat{\mathcal{A}}_\sigma : \rangle = \Pi_{\mu\nu} \Pi_{\rho\sigma} + \Pi_{\mu\sigma} \Pi_{\rho\nu}, \quad (3.33)$$

is not affected by the mean field treatment.

As a result of the mean field treatment, the Yang-Mills Lagrangian (3.1) is approximated as

$$\begin{aligned} \hat{\mathcal{L}}_{\text{YM}} &\rightarrow -\frac{1}{4} \bar{F}_{\mu\nu} \bar{F}^{\mu\nu} - \frac{1}{2} (\partial_\mu \bar{A}^\mu)^2 + g (\partial^\mu \bar{A}^\nu) \text{Re}[\Pi_{\mu\nu}] + \bar{J}^\mu \bar{A}_\mu \\ &\quad - (\partial^\mu \hat{a}_\mu) (\partial^\nu \bar{A}_\nu) - \frac{1}{2} \left[ \bar{F}^{\mu\nu} + \langle : \delta \hat{f}^{\mu\nu} : \rangle \right] \hat{f}_{\mu\nu} + \hat{a}_\mu \left[ \langle : \hat{j}^\mu : \rangle + \bar{J}^\mu \right] - g \partial^\mu \left[ \hat{a}_\mu \langle : \hat{\mathcal{C}}^\dagger \hat{\mathcal{C}} + \hat{\mathcal{C}}^\dagger \hat{\mathcal{C}} : \rangle \right] \\ &\quad - \frac{1}{4} \hat{f}_{\mu\nu} \hat{f}^{\mu\nu} - \frac{1}{2} (\partial^\mu \hat{a}_\mu)^2 + \frac{1}{2} [M_{(a)}^2]^{\mu\nu} \left( \hat{a}_\mu \hat{a}_\nu - \frac{1}{2ig} \pi_{\mu\nu} \right) \\ &\quad - \frac{1}{2} \hat{\mathcal{F}}^{\mu\nu\dagger} \hat{\mathcal{F}}_{\mu\nu} - |\bar{D}_\mu \hat{\mathcal{A}}^\mu|^2 + [M_{(\mathcal{A})}^2]^{\mu\nu} \left( \hat{\mathcal{A}}_\mu^\dagger \hat{\mathcal{A}}_\nu - \frac{1}{2ig} \Pi_{\mu\nu} \right) \\ &\quad + i \hat{\mathcal{C}} \partial_\mu \partial^\mu \hat{\mathcal{C}} \\ &\quad + i \hat{\mathcal{C}}^\dagger \left[ \bar{D}_\mu \bar{D}^\mu + M_{(\mathcal{C})}^2 \right] \hat{\mathcal{C}} - i \left( [\bar{D}_\mu \bar{D}^\mu + M_{(\mathcal{C})}^2] \hat{\mathcal{C}} \right)^\dagger \hat{\mathcal{C}} + \frac{1}{2ig} M_{(\mathcal{C})}^2 \varphi, \end{aligned} \quad (3.34)$$

where

$$\begin{aligned} [M_{(a)}^2]^{\mu\nu} &= 2ig \left[ \Pi_\lambda^\lambda - \varphi \right] \eta^{\mu\nu}, \\ [M_{(\mathcal{A})}^2]^{\mu\nu} &= 2ig \bar{F}^{\mu\nu} - ig \left[ (2\Pi^{\mu\nu} - \Pi^{\nu\mu}) - \eta^{\mu\nu} (\Pi_\lambda^\lambda + \pi_\lambda^\lambda + \varphi) \right], \\ M_{(\mathcal{C})}^2 &= -ig \left[ \Pi_\lambda^\lambda - \pi_\lambda^\lambda \right]. \end{aligned} \quad (3.35)$$

represent effective masses squared for the corresponding particles. These mass terms are dynamically generated from the gluon and the ghost condensates  $\pi_{\mu\nu}, \Pi_{\mu\nu}, \varphi$ . The imaginary part of the effective masses is responsible for scatterings and collisions between particles, which are important for thermalization of the system. As the original Lagrangian  $\hat{\mathcal{L}}_{\text{YM}}$  is BRS invariant, the dynamically generated mass terms do not break the BRS invariance of the system although the condensates  $\pi_{\mu\nu}, \Pi_{\mu\nu}, \varphi$  generally depend on the gauge one chooses.

### equations of motion

The mean-field-approximated Lagrangian (3.34) is quadratic in the quantum fluctuations and thus corresponding equations of motion are now linear, which is easy to handle. From the mean field Lagrangian (3.34), one obtains

$$\langle : \hat{j}_\mu : \rangle + \bar{J}_\mu = \partial^\nu \left[ \partial_\nu \bar{A}_\mu + \langle : \delta \hat{f}_{\nu\mu} : \rangle \right], \quad (3.36)$$

$$0 = [\partial^\rho \partial_\rho \eta^{\mu\nu} + [M_{(a)}^2]^{\mu\nu}] \hat{a}_\nu, \quad (3.37)$$

$$0 = [\bar{D}^\rho \bar{D}_\rho \eta^{\mu\nu} + [M_{\mathcal{A}}^2]^{\mu\nu}] \hat{\mathcal{A}}_\nu, \quad (3.38)$$

$$0 = \partial^\rho \partial_\rho \overset{(-)}{C}, \quad (3.39)$$

$$0 = [\bar{D}^\rho \bar{D}_\rho + M_{(\mathcal{C})}^2] \overset{(-)}{C}. \quad (3.40)$$

Equation (3.36) describes the backreaction to the classical gauge field  $\bar{A}_\mu$ , i.e., the color electromagnetic field on the RHS is screened by the sources on the LHS. As we are assuming the Abelian dominance (3.12), this equation is essentially the same as the Maxwell equation that we encountered in the QED problem (Eq. (2.17)). The difference is the appearance of the term  $\partial^\nu \langle : \delta \hat{f}_{\nu\mu} : \rangle$ , which appears because the produced off-diagonal gluons  $\hat{\mathcal{A}}$  have a non-vanishing color charge so that they can produce another electromagnetic field in the  $H$ -direction in addition to the original classical electromagnetic field  $\bar{F}_{\mu\nu}$ . The other four equations (3.37)-(3.40) determine the spacetime evolution of the quantum fluctuations  $\hat{a}_\mu, \hat{\mathcal{A}}_\mu, \overset{(-)}{C}, \overset{(-)}{\mathcal{C}}$ , respectively.

Equation (3.39) for the ghost field  $\overset{(-)}{C}$  is nothing but the free field equation, and no particle production occurs for this fluctuation  $\overset{(-)}{C}$  as for photons in QED. Thus, we do not consider  $\overset{(-)}{C}$  in the following discussion for simplicity.

If we assume homogeneity in space (assumption (i) in Section 3.1.2), it is convenient to define the gluon polarization by the direction of the classical electric field as

$$\bar{F}^{\mu\nu} \epsilon_{\sigma,\nu} = \epsilon_\sigma^\mu \quad \text{with} \quad \Lambda_\sigma = \begin{cases} \bar{E} & (\sigma = 0) \\ 0 & (\sigma = 1, 2) \\ -\bar{E} & (\sigma = 3) \end{cases}, \quad (3.41)$$

where  $\epsilon_{\sigma,\mu}$  ( $\sigma = 0, 1, 2, 3$ ) represent the polarization vector of gluons, and are normalized as

$$\eta^{\mu\nu} \epsilon_{\sigma,\mu}^* \epsilon_{\sigma',\nu} = - \begin{pmatrix} 0 & 0 & 0 & 1 \\ 0 & 1 & 0 & 0 \\ 0 & 0 & 1 & 0 \\ 1 & 0 & 0 & 0 \end{pmatrix} \equiv -\xi_{\sigma\sigma'}, \quad \sum_{\sigma\sigma'} \xi_{\sigma\sigma'} \epsilon_{\sigma,\mu}^* \epsilon_{\sigma',\nu} = -\eta_{\mu\nu}. \quad (3.42)$$

Without loss of generality, one can require  $\epsilon_{\sigma,\mu}$  to be independent of the spacetime coordinates  $x^\mu$ . Notice that the indefinite metric  $\xi_{\sigma\sigma'}$  has off-diagonal components  $\xi_{03} = \xi_{30} = 1$ . Because of this property, the 0-th and the 3-rd polarization modes of gluons become unphysical and they do not appear in the physical spectrum as we will see later in Section 3.1.4. Now, we expand the gluon field  $\hat{a}_\mu, \hat{\mathcal{A}}_\mu$  in terms of the polarization vector  $\epsilon_{\sigma,\mu}$  as

$$\begin{pmatrix} \hat{a}_\mu \\ \hat{\mathcal{A}}_\mu \end{pmatrix} = \sum_{\sigma} \epsilon_{\sigma,\mu} \begin{pmatrix} \hat{a}_\sigma \\ \hat{\mathcal{A}}_\sigma \end{pmatrix}. \quad (3.43)$$

In terms of the polarization label  $\sigma$ , one can rewrite the gluon equations (3.37) and (3.38) as

$$0 = [\partial_\mu \partial^\mu + M_{(a)\sigma}^2] \hat{a}_\sigma \quad (3.44)$$

$$0 = [\bar{D}_\mu \bar{D}^\mu + M_{(\mathcal{A})\sigma}^2] \hat{\mathcal{A}}_\sigma. \quad (3.45)$$

Here, the effective masses  $M_{(a)\sigma}^2, M_{(\mathcal{A})\sigma}^2$  in terms of the polarization label  $\sigma$  are given by

$$M_{(a)\sigma}^2 = [M_{(a)}^2]_{tt} = -[M_{(a)}^2]_{xx} = -[M_{(a)}^2]_{yy} = -[M_{(a)}^2]_{zz}, \quad (3.46)$$

and

$$\begin{cases} M_{(\mathcal{A})0}^2 \equiv [M_{(\mathcal{A})}^2]_{tz} - [M_{(\mathcal{A})}^2]_{zz} \\ M_{(\mathcal{A})1}^2 \equiv -[M_{(\mathcal{A})}^2]_{xx} \\ M_{(\mathcal{A})2}^2 \equiv -[M_{(\mathcal{A})}^2]_{yy} \\ M_{(\mathcal{A})3}^2 \equiv -[M_{(\mathcal{A})}^2]_{tz} - [M_{(\mathcal{A})}^2]_{zz} \end{cases}. \quad (3.47)$$

Notice that  $M_{(a)\sigma}^2$  for the diagonal gluons is always real, while only the physical  $\sigma = 1, 2$  modes of  $M_{(\mathcal{A})\sigma}^2$  for the off-diagonal gluons are real.  $M_{(\mathcal{A})\sigma}^2$  for the unphysical  $\sigma = 0, 3$  modes are complex in general, and are related with each other by  $[M_{(\mathcal{A})0}^2]^* = M_{(\mathcal{A})3}^2$ .

Under the spatial homogeneity, the backreaction equation (3.36) is further simplified as

$$\begin{aligned} 0 &= \langle : \hat{j}_t : \rangle = \langle : \hat{j}_x : \rangle = \langle : \hat{j}_y : \rangle, \\ -\frac{d}{dt}(\bar{E} + \delta\bar{E}) &= \langle : \hat{j}^z : \rangle + \bar{J}^z, \end{aligned} \quad (3.48)$$

where

$$\delta\bar{E} \equiv \langle : \delta\hat{f}_{tz} : \rangle = -2g\text{Re}[\Pi_{tz}] \quad (3.49)$$

represents an electric field produced by the produced colored gluons  $\hat{\mathcal{A}}$ .

### conservation law

As in the QED study (see Section 2.1.4), the mean field approximation preserves the conservation law at the mean field level, so that the conservation law for the current  $\langle : \hat{j}_\mu : \rangle$  (3.26) and the symmetric energy-momentum tensor  $\hat{T}_{\mu\nu}$  (3.28) still hold.

For a homogeneous system (assumption (i) in Section 3.1.2), the conservation laws (4.28) and (4.30) can be simplified as

$$0 = \partial_t \langle : \hat{j}_t : \rangle, \quad (3.50)$$

and

$$\partial_t \langle : \hat{\epsilon} : \rangle = -E \bar{J}^z. \quad (3.51)$$

Notice that Eq. (3.50) is trivial because Eq. (3.48) says  $\langle \hat{j}_t \rangle = 0$ .

### 3.1.4 canonical quantization and particle production

Since the equations of motion (3.37)-(3.40) are linear in the quantum fluctuations, one can safely employ the canonical quantization procedure. The canonical quantization of gluons and ghosts in the presence of the classical gauge field is done in essentially the same way as that in QED (see Section 2.1.4) [83], although there are slight differences due to the different quantum statistics of gluons and ghosts. Here, we only consider the canonical quantization at intermediate times  $-\infty < t < \infty$  because it naturally coincides with that at the asymptotic times  $t \rightarrow \pm\infty$ .

#### canonical quantization of gluons

The canonical quantization of gluons can be done in essentially the same way as that of electrons (see Section 2.1.4), although there are some differences because of the boson statistics of gluons.

Because of the spatial homogeneity (assumption (i) in Section 3.1.2), it is useful to Fourier expand the fluctuations  $\hat{a}_\mu, \hat{\mathcal{A}}_\mu$  in solving their equations of motion (3.44) and (3.45) as

$$\hat{a}_\sigma = \int d^3\mathbf{p} \left[ +a_{\sigma,\mathbf{p}}^{(t)}(t) \hat{c}_{\sigma,\mathbf{p}}(t) + -a_{\sigma,\mathbf{p}}^{(t)}(t) \hat{c}_{\sigma,-\mathbf{p}}^\dagger(t) \right] \frac{e^{i\mathbf{p}\cdot\mathbf{x}}}{(2\pi)^{3/2}}, \quad (3.52)$$

$$\hat{\mathcal{A}}_\sigma = \int d^3\mathbf{p} \left[ +\mathcal{A}_{\sigma,\mathbf{p}}^{(t)}(t) \hat{\mathbf{c}}_{\sigma,\mathbf{p}}(t) + -\mathcal{A}_{\sigma,\mathbf{p}}^{(t)} \hat{\mathbf{d}}_{\sigma,-\mathbf{p}}^\dagger(t) \right] \frac{e^{i\mathbf{p}\cdot\mathbf{x}}}{(2\pi)^{3/2}}. \quad (3.53)$$

Note that the fluctuation  $\hat{a}_\sigma$  is real so that  $+a_{\sigma,\mathbf{p}}^{(t)} = [-a_{\sigma,-\mathbf{p}}^{(t)}]^*$  always holds. Here, the positive/negative frequency mode functions at intermediate times  $\pm a_{\sigma,\mathbf{p}}^{(t)}, \pm \mathcal{A}_{\sigma,\mathbf{p}}^{(t)}$  are defined by the same principle that we employed for electrons (see Section 2.1.4 for the details). That is, we require  $\pm a_{\sigma,\mathbf{p}}^{(t)}, \pm \mathcal{A}_{\sigma,\mathbf{p}}^{(t)}$  to be plane waves at the instant of an intermediate time (for details of the

plane wave solutions, see Appendix B.1). Namely, we define the mode functions at  $t = t_0$  by the following plane-wave-like functions as

$$\left( \begin{array}{c} \pm a_{\sigma, \mathbf{p}}^{(t_0)}(t_0) \\ d_{\pm} a_{\sigma, \mathbf{p}}^{(t_0)}(t_0) \\ dt \end{array} \right) \equiv \left( \begin{array}{c} 1 \\ \sqrt{2|\mathbf{p}|} \\ \mp i \sqrt{\frac{|\mathbf{p}|}{2}} \end{array} \right) \exp \left[ \mp i \int_{-\infty}^{t_0} |\mathbf{p}| dt \right], \quad (3.54)$$

$$\left( \begin{array}{c} \pm \mathcal{A}_{\sigma, \mathbf{p}}^{(t_0)}(t_0) \\ d_{\pm} \mathcal{A}_{\sigma, \mathbf{p}}^{(t_0)}(t_0) \\ dt \end{array} \right) \equiv \left( \begin{array}{c} 1 \\ \sqrt{2|\mathbf{p} - g\bar{\mathbf{A}}(t_0)|} \\ \mp i \sqrt{\frac{|\mathbf{p} - g\bar{\mathbf{A}}(t_0)|}{2}} \end{array} \right) \exp \left[ \mp i \int_{-\infty}^{t_0} |\mathbf{p} - g\bar{\mathbf{A}}(t)| dt \right], \quad (3.55)$$

As the fluctuation  $\hat{\mathcal{A}}_{\sigma}$  has the color charge  $g$ , while  $\hat{a}_{\sigma}$  is chargeless, their kinetic momentum  $\mathbf{P}$  is given by  $\mathbf{p} - g\bar{\mathbf{A}}$  and  $\mathbf{p}$ , respectively. In contrast to the plane-wave-like functions for the Dirac equation (2.40), as the Klein-Gordon equation is a second order differential equation, one needs not only a value at the time  $t = t_0$  but also its derivative in uniquely expanding the field operators. Here, we normalize the mode functions  $\pm a_{\sigma, \mathbf{p}}^{(t)}$ ,  $\pm \mathcal{A}_{\sigma, \mathbf{p}}^{(t)}$  as

$$\sum_{\sigma'} \xi_{\sigma\sigma'} (\pm a_{\sigma, \mathbf{p}}^{(t)} | \pm a_{\sigma', \mathbf{p}}^{(t)})_{\text{B}} = \pm 1, \quad \sum_{\sigma'} \xi_{\sigma\sigma'} (\pm a_{\sigma, \mathbf{p}}^{(t)} | \mp a_{\sigma', \mathbf{p}}^{(t)})_{\text{B}} = 0, \quad (3.56)$$

$$\sum_{\sigma'} \xi_{\sigma\sigma'} (\pm \mathcal{A}_{\sigma, \mathbf{p}}^{(t)} | \pm \mathcal{A}_{\sigma', \mathbf{p}}^{(t)})_{\text{B}} = \pm 1, \quad \sum_{\sigma'} \xi_{\sigma\sigma'} (\pm \mathcal{A}_{\sigma, \mathbf{p}}^{(t)} | \mp \mathcal{A}_{\sigma', \mathbf{p}}^{(t)})_{\text{B}} = 0, \quad (3.57)$$

where the boson inner product  $(\phi_1 | \phi_2)_{\text{B}}$  is

$$(\phi_1 | \phi_2)_{\text{B}} \equiv i \phi_1^* \overset{\leftrightarrow}{\partial}_t \phi_2 = i [\phi_1^* (\partial_t \phi_2) - (\partial_t \phi_1)^* \phi_2], \quad (3.58)$$

which is conserved if  $\phi_1, \phi_2$  obey the same Klein-Gordon equation. Now, we impose canonical commutation relations

$$\begin{aligned} [\hat{a}_{\mu}(t, \mathbf{x}), \partial_t \hat{a}_{\nu}(t, \mathbf{x}')] &= -i \eta_{\mu\nu} \delta^3(\mathbf{x} - \mathbf{x}'), \\ [\hat{a}_{\mu}(t, \mathbf{x}), \hat{a}_{\nu}(t, \mathbf{x}')] &= [\partial_t \hat{a}_{\mu}(t, \mathbf{x}), \partial_t \hat{a}_{\nu}(t, \mathbf{x}')] = 0, \end{aligned} \quad (3.59)$$

$$\begin{aligned} [\hat{\mathcal{A}}_{\mu}(t, \mathbf{x}), \partial_t \hat{\mathcal{A}}_{\nu}^{\dagger}(t, \mathbf{x}')] &= -i \eta_{\mu\nu} \delta^3(\mathbf{x} - \mathbf{x}'), \\ [\hat{\mathcal{A}}_{\mu}(t, \mathbf{x}), \hat{\mathcal{A}}_{\nu}^{\dagger}(t, \mathbf{x}')] &= [\partial_t \hat{\mathcal{A}}_{\mu}(t, \mathbf{x}), \partial_t \hat{\mathcal{A}}_{\nu}^{\dagger}(t, \mathbf{x}')] = 0, \end{aligned} \quad (3.60)$$

to obtain commutation relations for the intermediate annihilation operators  $\hat{c}_{\sigma, \mathbf{p}}$  for  $\hat{a}$  and  $\hat{\mathbf{c}}_{\sigma, \mathbf{p}}, \hat{\mathbf{d}}_{\sigma, \mathbf{p}}$  for  $\hat{\mathcal{A}}$  as

$$\begin{aligned} [\hat{c}_{\sigma, \mathbf{p}}, \hat{c}_{\sigma', \mathbf{p}'}^{\dagger}] &= \xi_{\sigma\sigma'} \delta^3(\mathbf{p} - \mathbf{p}'), \\ [\hat{\mathbf{c}}_{\sigma, \mathbf{p}}, \hat{\mathbf{c}}_{\sigma', \mathbf{p}'}^{\dagger}] &= [\hat{\mathbf{d}}_{\sigma, \mathbf{p}}, \hat{\mathbf{d}}_{\sigma', \mathbf{p}'}^{\dagger}] = \xi_{\sigma\sigma'} \delta^3(\mathbf{p} - \mathbf{p}'), \\ (\text{others}) &= 0. \end{aligned} \quad (3.61)$$

Noting that the indefinite metric  $\xi_{\sigma\sigma'}$  is not diagonal as Eq. (3.42),  $\sigma = 0, 3$  modes of gluons commute with each other.

The positive/negative frequency mode functions at an intermediate time  $\pm a_{\sigma,\mathbf{p}}^{(t)}, \pm \mathcal{A}_{\sigma,\mathbf{p}}^{(t)}$  smoothly approach the correct mode functions at the asymptotic times  $\pm a_{\sigma,\mathbf{p}}^{(\text{as})}, \pm \mathcal{A}_{\sigma,\mathbf{p}}^{(\text{as})}$  (as = in/out) in the limit of  $t \rightarrow \pm\infty$  because of the adiabatic hypothesis (assumption (iii) made in Section 3.1.2):

$$\begin{pmatrix} \pm a_{\sigma,\mathbf{p}}^{(t)} \\ \pm \mathcal{A}_{\sigma,\mathbf{p}}^{(t)} \end{pmatrix} \xrightarrow{t \rightarrow -\infty} \begin{pmatrix} \pm a_{\sigma,\mathbf{p}}^{(\text{in})} \\ \pm \mathcal{A}_{\sigma,\mathbf{p}}^{(\text{in})} \end{pmatrix}, \quad \begin{pmatrix} \pm a_{\sigma,\mathbf{p}}^{(t)} \\ \pm \mathcal{A}_{\sigma,\mathbf{p}}^{(t)} \end{pmatrix} \xrightarrow{t \rightarrow \infty} \begin{pmatrix} \pm a_{\sigma,\mathbf{p}}^{(\text{out})} \\ \pm \mathcal{A}_{\sigma,\mathbf{p}}^{(\text{out})} \end{pmatrix}. \quad (3.62)$$

Hence, one can obtain the annihilation operators at the asymptotic times  $\hat{c}_{\sigma,\mathbf{p}}^{(\text{as})}, \hat{\mathbf{c}}_{\sigma,\mathbf{p}}^{(\text{as})}, \hat{\mathbf{d}}_{\sigma,\mathbf{p}}^{(\text{as})}$  by taking  $t \rightarrow \pm\infty$  limit of the time-dependent annihilation operators  $\hat{c}_{\sigma,\mathbf{p}}, \hat{\mathbf{c}}_{\sigma,\mathbf{p}}, \hat{\mathbf{d}}_{\sigma,\mathbf{p}}$  as

$$\begin{pmatrix} \hat{c}_{\sigma,\mathbf{p}}^{(\text{in})} \\ \hat{\mathbf{c}}_{\sigma,\mathbf{p}}^{(\text{in})} \\ \hat{\mathbf{d}}_{\sigma,\mathbf{p}}^{(\text{in})} \end{pmatrix} = \lim_{t \rightarrow -\infty} \begin{pmatrix} \hat{c}_{\sigma,\mathbf{p}}(t) \\ \hat{\mathbf{c}}_{\sigma,\mathbf{p}}(t) \\ \hat{\mathbf{d}}_{\sigma,\mathbf{p}}(t) \end{pmatrix}, \quad \begin{pmatrix} \hat{c}_{\sigma,\mathbf{p}}^{(\text{out})} \\ \hat{\mathbf{c}}_{\sigma,\mathbf{p}}^{(\text{out})} \\ \hat{\mathbf{d}}_{\sigma,\mathbf{p}}^{(\text{out})} \end{pmatrix} = \lim_{t \rightarrow \infty} \begin{pmatrix} \hat{c}_{\sigma,\mathbf{p}}(t) \\ \hat{\mathbf{c}}_{\sigma,\mathbf{p}}(t) \\ \hat{\mathbf{d}}_{\sigma,\mathbf{p}}(t) \end{pmatrix}. \quad (3.63)$$

The Bogoliubov transformation between the in-state annihilation operators  $\hat{c}_{\sigma,\mathbf{p}}^{(\text{in})}, \hat{\mathbf{c}}_{\sigma,\mathbf{p}}^{(\text{in})}, \hat{\mathbf{d}}_{\sigma,\mathbf{p}}^{(\text{in})}$  and those at intermediate times  $\hat{c}_{\sigma,\mathbf{p}}, \hat{\mathbf{c}}_{\sigma,\mathbf{p}}, \hat{\mathbf{d}}_{\sigma,\mathbf{p}}$  is given by

$$\begin{pmatrix} \hat{c}_{\sigma,\mathbf{p}}(t) \\ \hat{c}_{\sigma,-\mathbf{p}}^\dagger(t) \end{pmatrix} = \begin{pmatrix} \alpha_{(a)\sigma,\mathbf{p}}(t) & \beta_{(a)\sigma,\mathbf{p}}(t) \\ \beta_{(a)\sigma,\mathbf{p}}^*(t) & \alpha_{(a)\sigma,\mathbf{p}}^*(t) \end{pmatrix} \begin{pmatrix} \hat{c}_{\sigma,\mathbf{p}}^{(\text{in})} \\ \hat{c}_{\sigma,-\mathbf{p}}^{(\text{in})\dagger} \end{pmatrix}, \quad (3.64)$$

$$\begin{pmatrix} \hat{\mathbf{c}}_{\sigma,\mathbf{p}}(t) \\ \hat{\mathbf{d}}_{\sigma,-\mathbf{p}}^\dagger(t) \end{pmatrix} = \begin{pmatrix} \alpha_{(\mathcal{A})\sigma,\mathbf{p}}(t) & \beta_{(\mathcal{A})\sigma,\mathbf{p}}(t) \\ \beta_{(\mathcal{A})\sigma,\mathbf{p}}^*(t) & \alpha_{(\mathcal{A})\sigma,\mathbf{p}}^*(t) \end{pmatrix} \begin{pmatrix} \hat{\mathbf{c}}_{\sigma,\mathbf{p}}^{(\text{in})} \\ \hat{\mathbf{d}}_{\sigma,-\mathbf{p}}^{(\text{in})\dagger} \end{pmatrix}, \quad (3.65)$$

where

$$\begin{aligned} \alpha_{(a)\sigma,\mathbf{p}}(t) &\equiv (+a_{\sigma,\mathbf{p}}^{(t)} | +a_{\sigma,\mathbf{p}}^{(\text{in})})_{\text{B}} = -(-a_{\sigma,\mathbf{p}}^{(t)} | -a_{\sigma,\mathbf{p}}^{(\text{in})})_{\text{B}}^* \\ &= \frac{i}{\sqrt{2|\mathbf{p}|}} \left[ \frac{d_+ a_{\sigma,\mathbf{p}}^{(\text{in})}}{dt} - i|\mathbf{p}| + a_{\sigma,\mathbf{p}}^{(\text{in})} \right] \exp \left[ +i \int_{-\infty}^t |\mathbf{p}| dt \right], \\ \beta_{(a)\sigma,\mathbf{p}}(t) &\equiv (+a_{\sigma,\mathbf{p}}^{(t)} | -a_{\sigma,\mathbf{p}}^{(\text{in})})_{\text{B}} = -(-a_{\sigma,\mathbf{p}}^{(t)} | +a_{\sigma,\mathbf{p}}^{(\text{in})})_{\text{B}}^* \\ &= \frac{i}{\sqrt{2|\mathbf{p}|}} \left[ \frac{d_- a_{\sigma,\mathbf{p}}^{(\text{in})}}{dt} - i|\mathbf{p}| - a_{\sigma,\mathbf{p}}^{(\text{in})} \right] \exp \left[ +i \int_{-\infty}^t |\mathbf{p}| dt \right] \end{aligned} \quad (3.66)$$

and

$$\begin{aligned} \alpha_{(\mathcal{A})\sigma,\mathbf{p}}(t) &\equiv (+\mathcal{A}_{\sigma,\mathbf{p}}^{(t)} | +\mathcal{A}_{\sigma,\mathbf{p}}^{(\text{in})})_{\text{B}} = -(-\mathcal{A}_{\sigma,\mathbf{p}}^{(t)} | -\mathcal{A}_{\sigma,\mathbf{p}}^{(\text{in})})_{\text{B}}^* \\ &= \frac{i}{\sqrt{2|\mathbf{p} - g\bar{\mathbf{A}}|}} \left[ \frac{d_+ \mathcal{A}_{\sigma,\mathbf{p}}^{(\text{in})}}{dt} - i|\mathbf{p} - g\bar{\mathbf{A}}| + \mathcal{A}_{\sigma,\mathbf{p}}^{(\text{in})} \right] \exp \left[ +i \int_{-\infty}^t |\mathbf{p} - g\bar{\mathbf{A}}| dt \right], \\ \beta_{(\mathcal{A})\sigma,\mathbf{p}}(t) &\equiv (+\mathcal{A}_{\sigma,\mathbf{p}}^{(t)} | -\mathcal{A}_{\sigma,\mathbf{p}}^{(\text{in})})_{\text{B}} = -(-\mathcal{A}_{\sigma,\mathbf{p}}^{(t)} | +\mathcal{A}_{\sigma,\mathbf{p}}^{(\text{in})})_{\text{B}}^* \\ &= \frac{i}{\sqrt{2|\mathbf{p} - g\bar{\mathbf{A}}|}} \left[ \frac{d_- \mathcal{A}_{\sigma,\mathbf{p}}^{(\text{in})}}{dt} - i|\mathbf{p} - g\bar{\mathbf{A}}| - \mathcal{A}_{\sigma,\mathbf{p}}^{(\text{in})} \right] \exp \left[ +i \int_{-\infty}^t |\mathbf{p} - g\bar{\mathbf{A}}| dt \right]. \end{aligned} \quad (3.67)$$

The Bogoliubov coefficients are normalized as

$$\begin{aligned} 1 &= |\alpha_{(a)\sigma,\mathbf{p}}(t)|^2 - |\beta_{(a)\sigma,\mathbf{p}}(t)|^2, \\ &= |\alpha_{(\mathcal{A})\sigma,\mathbf{p}}(t)|^2 - |\beta_{(\mathcal{A})\sigma,\mathbf{p}}(t)|^2. \end{aligned} \quad (3.68)$$

Notice that we have a minus sign in front of  $|\beta|^2$ , which is in contrast to the plus sign for electrons (2.32). This is because of the boson statistics of gluons, and  $|\beta|^2$  can be larger than unity. We also note that the Bogoliubov coefficient  $\beta_{(a)\sigma,\mathbf{p}}$  for chargeless  $\hat{a}_\sigma$  gluons can be non-zero because colored  $\mathcal{A}_\sigma$  gluons can merge into  $\hat{a}_\sigma$  gluons through the mass term  $M_{(a)}$ . This means that particle production of  $\hat{a}_\sigma$  modes can occur, which is in contrast to QED, where photon production does not occur (within the mean field treatment).

Finally, let us discuss the ultraviolet ( $|\mathbf{p}| \rightarrow \infty$ ) behavior of the Bogoliubov coefficients  $\alpha_{(a)\sigma,\mathbf{p}}, \beta_{(a)\sigma,\mathbf{p}}, \alpha_{(\mathcal{A})\sigma,\mathbf{p}}, \beta_{(\mathcal{A})\sigma,\mathbf{p}}$ . For this purpose, we first note that the in-state Fourier modes  $\pm\phi^{(\text{in})} = \pm a_{\sigma,\mathbf{p}}^{(\text{in})}$  or  $\pm \mathcal{A}_{\sigma,\mathbf{p}}^{(\text{in})}$  satisfy the following Klein-Gordon equation (see Eqs. (3.37) and (3.38))

$$0 = [\partial_t^2 + \mathbf{P}^2 + M^2]_{\pm}\phi^{(\text{in})}(t), \quad (3.69)$$

where  $\mathbf{P}^2, M^2$  is the kinetic momentum and the effective mass for the corresponding particle, respectively. By substituting the Bogoliubov relation between the in-state Fourier modes  $\pm\phi^{(\text{in})}$  and those at intermediate times  $\pm\phi^{(t)}$  (see Eqs. (3.54) and (3.55)),

$$\frac{d^n}{dt^n} \begin{pmatrix} +\phi^{(\text{in})} \\ -\phi^{(\text{in})} \end{pmatrix} = \begin{pmatrix} \alpha & \beta^* \\ \beta & \alpha^* \end{pmatrix} \frac{d^n}{dt^n} \begin{pmatrix} +\phi^{(t)} \\ -\phi^{(t)} \end{pmatrix} \quad (n = 0, 1), \quad (3.70)$$

into this equation (3.69), one obtains a differential equation for the Bogoliubov coefficients  $\alpha, \beta$  as

$$\frac{d}{dt} \begin{pmatrix} \alpha \\ \beta^* \end{pmatrix} = \frac{|\mathbf{P}|}{2} \begin{pmatrix} -i\frac{M^2}{|\mathbf{P}|^2} & \left[ \frac{1}{|\mathbf{P}|^2} \frac{d|\mathbf{P}|}{dt} - i\frac{M^2}{|\mathbf{P}|^2} \right] e^{+2i \int_{-\infty}^t |\mathbf{P}| dt} \\ \left[ \frac{1}{|\mathbf{P}|^2} \frac{d|\mathbf{P}|}{dt} + i\frac{M^2}{|\mathbf{P}|^2} \right] e^{+2i \int_{-\infty}^t |\mathbf{P}| dt} & i\frac{M^2}{|\mathbf{P}|^2} \end{pmatrix} \begin{pmatrix} \alpha \\ \beta^* \end{pmatrix}. \quad (3.71)$$

One can iteratively solve this equation (3.71) order-by-order in  $\mathbf{P}$ . By requiring  $\alpha \xrightarrow{|\mathbf{P}| \rightarrow \infty} 1, \beta \xrightarrow{|\mathbf{P}| \rightarrow \infty} 0$ , one gets

$$\begin{aligned} \alpha &= \left[ 1 - \frac{i}{4} \frac{1}{|\mathbf{P}|^2} \frac{d|\mathbf{P}|}{dt} + \mathcal{O}(|\mathbf{P}|^{-3}) \right] \exp \left[ -i \int_{-\infty}^t \left\{ \frac{M^2}{2|\mathbf{P}|} - \frac{1}{4} \frac{1}{|\mathbf{P}|^2} \frac{d^2|\mathbf{P}|}{dt^2} + \mathcal{O}(|\mathbf{P}|^{-3}) \right\} dt \right], \\ \beta &= \left[ -\frac{i}{4} \left\{ \frac{1}{|\mathbf{P}|^2} \frac{d|\mathbf{P}|}{dt} + i\frac{M^2}{|\mathbf{P}|^2} \right\} + \mathcal{O}(|\mathbf{P}|^{-3}) \right] \\ &\quad \times \exp \left[ +i \int_{-\infty}^t \left\{ 2|\mathbf{P}| + \frac{M^2}{2|\mathbf{P}|} - \frac{1}{4} \frac{1}{|\mathbf{P}|^2} \frac{d^2|\mathbf{P}|}{dt^2} + \mathcal{O}(|\mathbf{P}|^{-3}) \right\} dt \right]. \end{aligned} \quad (3.72)$$

As for electrons (Eq. (2.56)),  $|\beta|^2$  falls faster than  $|\mathbf{p}|^4$ , which guarantees finiteness of the total number of produced gluons. With the use of the asymptotic formula (3.72), one can show that the normal ordering procedure  $\langle \hat{\bullet} \rangle \rightarrow \langle : \hat{\bullet} : \rangle$  explained in Section 2.1.5 surely regulates divergences in gluon two-point functions.

### canonical quantization of ghosts

Lastly, we consider the canonical quantization of ghosts. This program is essentially the same as done in the gluon case, although there are slight differences because of unusual anti-commutative nature of ghosts.

By noting the spatial homogeneity of the system (assumption (i) in Section 3.1.2), we Fourier expand the fluctuations  $\hat{\mathcal{C}}, \hat{\bar{\mathcal{C}}}$  to solve the equation of motion (3.40) as

$$\begin{pmatrix} \hat{\mathcal{C}} \\ \hat{\bar{\mathcal{C}}} \end{pmatrix} = \int d^3\mathbf{p} \left[ {}_+\mathcal{C}_{\mathbf{p}}^{(t)}(t) \begin{pmatrix} \hat{\mathbf{e}}_{\mathbf{p}}(t) \\ \hat{\mathbf{e}}_{\mathbf{p}}(t) \end{pmatrix} + {}_-\mathcal{C}_{\mathbf{p}}^{(t)}(t) \begin{pmatrix} \hat{\mathbf{f}}_{-\mathbf{p}}(t) \\ \hat{\mathbf{f}}_{-\mathbf{p}}(t) \end{pmatrix} \right] \frac{e^{i\mathbf{p}\cdot\mathbf{x}}}{(2\pi)^{3/2}}, \quad (3.73)$$

the positive/negative frequency mode functions at intermediate times  $\pm\mathcal{C}_{\mathbf{p}}^{(t)}$  are defined in the same way as those for bosons (3.54) and (3.55); namely

$$\begin{pmatrix} \pm\mathcal{C}_{\mathbf{p}}^{(t)}(t) \\ \frac{d\pm\mathcal{C}_{\mathbf{p}}^{(t)}(t)}{dt} \end{pmatrix} \equiv \begin{pmatrix} 1 \\ \sqrt{2|\mathbf{p} - g\mathbf{A}(t)|} \\ \mp i\sqrt{\frac{|\mathbf{p} - g\mathbf{A}(t)|}{2}} \end{pmatrix} \exp \left[ \mp i \int_{-\infty}^t |\mathbf{p} - q_A^{(\text{ad.})}\mathbf{A}(t)| dt \right]. \quad (3.74)$$

We consider a normalization condition for the mode function  $\pm\mathcal{C}_{\mathbf{p}}^{(t)}$  given by

$$({}_\pm\mathcal{C}_{\mathbf{p}}^{(t)} | {}_\pm\mathcal{C}_{\mathbf{p}}^{(t)})_{\text{B}} = \pm 1, \quad ({}_\pm\mathcal{C}_{\mathbf{p}}^{(t)} | {}_\mp\mathcal{C}_{\mathbf{p}}^{(t)})_{\text{B}} = 0. \quad (3.75)$$

Now, we impose a canonical commutation relation for the ghost modes  $\hat{\mathcal{C}}, \hat{\bar{\mathcal{C}}}$  as

$$\begin{aligned} \left\{ \begin{pmatrix} \hat{\mathcal{C}} \\ \hat{\pi} \end{pmatrix} (t, \mathbf{x}), \begin{pmatrix} \hat{\mathcal{C}} \\ \hat{\pi} \end{pmatrix} (t, \mathbf{x}') \right\} &= i\delta^3(\mathbf{p} - \mathbf{p}'), \\ \left\{ \begin{pmatrix} \hat{\mathcal{C}} \\ \hat{\mathcal{C}} \end{pmatrix} (t, \mathbf{x}), \begin{pmatrix} \hat{\mathcal{C}} \\ \hat{\mathcal{C}} \end{pmatrix} (t, \mathbf{x}') \right\} &= \left\{ \begin{pmatrix} \hat{\pi} \\ \hat{\pi} \end{pmatrix} (t, \mathbf{x}), \begin{pmatrix} \hat{\pi} \\ \hat{\pi} \end{pmatrix} (t, \mathbf{x}') \right\} = 0, \end{aligned} \quad (3.76)$$

where  $\begin{pmatrix} \hat{\mathcal{C}} \\ \hat{\pi} \end{pmatrix}$  is the canonical conjugate field to the ghost field  $\hat{\mathcal{C}}$  as  $\hat{\pi} = -i\partial_t\hat{\mathcal{C}}^\dagger$  and  $\hat{\bar{\pi}} = i\partial_t\hat{\bar{\mathcal{C}}}^\dagger$ . Then, we obtain anti-commutation relations for the intermediate annihilation operators  $\begin{pmatrix} \hat{\mathcal{C}} \\ \hat{\mathbf{e}}_{\mathbf{p}}, \hat{\mathbf{f}}_{\mathbf{p}} \end{pmatrix}$  as

$$i\delta^3(\mathbf{p} - \mathbf{p}') = \left\{ \hat{\mathbf{e}}_{\mathbf{p}}, \hat{\mathbf{e}}_{\mathbf{p}'}^\dagger \right\} = \left\{ \hat{\mathbf{f}}_{\mathbf{p}}, \hat{\mathbf{f}}_{\mathbf{p}'}^\dagger \right\}, \quad (\text{others}) = 0. \quad (3.77)$$

Notice that  $\begin{pmatrix} \hat{\mathcal{C}} \\ \hat{\mathbf{e}}_{\mathbf{p}}, \hat{\mathbf{e}}_{\mathbf{p}}^\dagger \end{pmatrix}$  and  $\begin{pmatrix} \hat{\mathcal{C}} \\ \hat{\mathbf{f}}_{\mathbf{p}}, \hat{\mathbf{f}}_{\mathbf{p}}^\dagger \end{pmatrix}$  anti-commute with each other because of the canonical commutation relation (3.76) for ghosts. Thanks to this property, it is assured that the unphysical ghosts are never produced and do not appear in the physical spectrum as we shall see later.

Just as in the electron and the gluon cases, the positive/negative frequency mode functions at the asymptotic times  $\pm\mathcal{C}_{\mathbf{p}}^{(\text{as})}$  (as = in/out) and the corresponding annihilation operators  $\hat{\mathbf{e}}_{\mathbf{p}}, \hat{\mathbf{f}}_{\mathbf{p}}$  can be obtained by taking the  $t \rightarrow \pm\infty$  limit of those at intermediate times. Namely,

$$\pm\mathcal{C}_{\mathbf{p}}^{(t)} \xrightarrow[t \rightarrow -\infty]{} \pm\mathcal{C}_{\mathbf{p}}^{(\text{in})}, \quad \pm\mathcal{C}_{\mathbf{p}}^{(t)} \xrightarrow[t \rightarrow \infty]{} \pm\mathcal{C}_{\mathbf{p}}^{(\text{out})}, \quad (3.78)$$

and

$$\begin{pmatrix} \hat{\mathbf{e}}_{\mathbf{p}} \\ \hat{\mathbf{f}}_{\mathbf{p}} \end{pmatrix} \xrightarrow[t \rightarrow -\infty]{} \begin{pmatrix} \hat{\mathbf{e}}_{\mathbf{p}}^{(\text{in})} \\ \hat{\mathbf{f}}_{\mathbf{p}}^{(\text{in})} \end{pmatrix}, \quad \begin{pmatrix} \hat{\mathbf{e}}_{\mathbf{p}} \\ \hat{\mathbf{f}}_{\mathbf{p}} \end{pmatrix} \xrightarrow[t \rightarrow \infty]{} \begin{pmatrix} \hat{\mathbf{e}}_{\mathbf{p}}^{(\text{out})} \\ \hat{\mathbf{f}}_{\mathbf{p}}^{(\text{out})} \end{pmatrix}. \quad (3.79)$$

The in-state annihilation operators  $\hat{\mathbf{e}}_{\mathbf{p}}^{(\text{in})}, \hat{\mathbf{f}}_{\mathbf{p}}^{(\text{in})}$  and those at intermediate times  $\hat{\mathbf{e}}_{\mathbf{p}}, \hat{\mathbf{f}}_{\mathbf{p}}$  are not independent of each other, and their relationship is given by the following Bogoliubov transformation:

$$\begin{pmatrix} \hat{\mathbf{e}}_{\mathbf{p}}(t) \\ \hat{\mathbf{f}}_{-\mathbf{p}}(t) \end{pmatrix} = \begin{pmatrix} \alpha_{(c)\mathbf{p}}(t) & \beta_{(c)\mathbf{p}}(t) \\ \beta_{(c)\mathbf{p}}^*(t) & \alpha_{(c)\mathbf{p}}^*(t) \end{pmatrix} \begin{pmatrix} \hat{\mathbf{e}}_{\mathbf{p}}^{(\text{in})} \\ \hat{\mathbf{f}}_{-\mathbf{p}}^{(\text{in})\dagger} \end{pmatrix}, \quad (3.80)$$

where

$$\begin{aligned} \alpha_{(c)\mathbf{p}}(t) &\equiv ({}_+\mathcal{C}_{\mathbf{p}}^{(t)} | {}_+\mathcal{C}_{\mathbf{p}}^{(\text{in})})_{\text{B}} = -({}_-\mathcal{C}_{\mathbf{p}}^{(t)} | {}_-\mathcal{C}_{\mathbf{p}}^{(\text{in})})_{\text{B}}^* \\ &= \frac{i}{\sqrt{2|\mathbf{p} - g\bar{\mathbf{A}}|}} \left[ \frac{d_+\mathcal{C}_{\mathbf{p}}^{(\text{in})}}{dt} - i|\mathbf{p} - g\bar{\mathbf{A}}| {}_+\mathcal{C}_{\mathbf{p}}^{(\text{in})} \right] \exp \left[ +i \int_{-\infty}^t |\mathbf{p} - g\bar{\mathbf{A}}| dt \right], \\ \beta_{(c)\mathbf{p}}(t) &\equiv ({}_+\mathcal{C}_{\mathbf{p}}^{(t)} | {}_-\mathcal{C}_{\mathbf{p}}^{(\text{in})})_{\text{B}} = -({}_-\mathcal{C}_{\mathbf{p}}^{(t)} | {}_+\mathcal{C}_{\mathbf{p}}^{(\text{in})})_{\text{B}}^* \\ &= \frac{i}{\sqrt{2|\mathbf{p} - g\bar{\mathbf{A}}|}} \left[ \frac{d_-\mathcal{C}_{\mathbf{p}}^{(\text{in})}}{dt} - i|\mathbf{p} - g\bar{\mathbf{A}}| {}_-\mathcal{C}_{\mathbf{p}}^{(\text{in})} \right] \exp \left[ +i \int_{-\infty}^t |\mathbf{p} - g\bar{\mathbf{A}}| dt \right]. \end{aligned} \quad (3.81)$$

The Bogoliubov coefficients are normalized as

$$1 = |\alpha_{(c)\mathbf{p}}(t)|^2 - |\beta_{(c)\mathbf{p}}(t)|^2. \quad (3.82)$$

As the mode functions obey the Klein-Gordon equation, it is obvious that the ultraviolet ( $|\mathbf{p}| \rightarrow \infty$ ) behavior of the Bogoliubov coefficients  $\alpha_{(c)\mathbf{p}}, \beta_{(c)\mathbf{p}}$  are given by Eq. (3.72) as those for gluons, by which one can justify the use of the normal ordering procedure in regulating ghost two-point functions.

### particle production

Now, we have the intermediate annihilation operators  $\hat{c}_{\sigma,\mathbf{p}}$  for chargeless gluons  $\hat{a}_{\sigma}$ ;  $\hat{\mathbf{c}}_{\sigma,\mathbf{p}}, \hat{\mathbf{d}}_{\sigma,\mathbf{p}}$  for charged gluons  $\hat{\mathcal{A}}_{\sigma}$  with the color charge  $g$  and  $-g$ , respectively;  $\hat{\mathbf{e}}_{\mathbf{p}}, \hat{\mathbf{f}}_{\mathbf{p}}$  for charged ghosts

$\hat{\mathcal{C}}$  with the color charge  $g$  and  $-g$ , respectively; and  $\hat{\mathbf{e}}_{\mathbf{p}}, \hat{\mathbf{f}}_{\mathbf{p}}$  for charged anti-ghosts  $\hat{\bar{\mathcal{C}}}$  with the color charge  $g$  and  $-g$ , respectively. From these annihilation operators, one can construct a vacuum state  $|\text{vac}; t\rangle$  at an intermediate time  $t$ . By noting that the annihilation operators  $\hat{c}_{\sigma, \mathbf{p}}, \hat{\mathbf{c}}_{\sigma, \mathbf{p}}, \hat{\mathbf{d}}_{\sigma, \mathbf{p}}, \hat{\mathbf{e}}_{\mathbf{p}}, \hat{\mathbf{f}}_{\mathbf{p}}, \hat{\bar{\mathbf{e}}}_{\mathbf{p}}, \hat{\bar{\mathbf{f}}}_{\mathbf{p}}$  do not mix up with each other during the whole spacetime evolution (because the equations of motion (3.37)-(3.40) are linear within our mean field treatment), one can decompose the vacuum state  $|\text{vac}; t\rangle$  into a product of vacua for each fluctuation as

$$|\text{vac}; t\rangle = |\text{vac}_{(a)}; t\rangle \otimes |\text{vac}_{(\mathcal{A})}; t\rangle \otimes |\text{vac}_{(c)}; t\rangle, \quad (3.83)$$

where each vacuum satisfies

$$\begin{aligned} 0 &= \hat{c}_{\sigma, \mathbf{p}} |\text{vac}_{(a)}; t\rangle, \\ 0 &= \hat{\mathbf{c}}_{\sigma, \mathbf{p}} |\text{vac}_{(\mathcal{A})}; t\rangle = \hat{\mathbf{d}}_{\sigma, \mathbf{p}} |\text{vac}_{(\mathcal{A})}; t\rangle, \\ 0 &= \hat{\mathbf{e}}_{\mathbf{p}} |\text{vac}_{(c)}; t\rangle = \hat{\mathbf{f}}_{\mathbf{p}} |\text{vac}_{(c)}; t\rangle = \hat{\bar{\mathbf{e}}}_{\mathbf{p}} |\text{vac}_{(c)}; t\rangle = \hat{\bar{\mathbf{f}}}_{\mathbf{p}} |\text{vac}_{(c)}; t\rangle \end{aligned} \quad (3.84)$$

for all values of the quantum numbers  $\sigma, \mathbf{p}$ . One can naturally construct the in-vacuum  $|\text{vac}; \text{in}\rangle$  by taking the  $t \rightarrow -\infty$  limit of  $|\text{vac}; t\rangle$  as

$$|\text{vac}; \text{in}\rangle = \lim_{t \rightarrow -\infty} |\text{vac}; t\rangle = \lim_{t \rightarrow -\infty} |\text{vac}_{(a)}; t\rangle \otimes |\text{vac}_{(\mathcal{A})}; t\rangle \otimes |\text{vac}_{(c)}; t\rangle. \quad (3.85)$$

The number of produced particles are obtained as an in-vacuum  $|\text{vac}; \text{in}\rangle$  expectation value of the corresponding number operator; namely

$$\frac{d^6 N_{g_0}(\sigma, \mathbf{p}; t)}{d\mathbf{p}^3 d\mathbf{x}^3} = \frac{1}{V} \langle \hat{c}_{\sigma, \mathbf{p}}^\dagger \hat{c}_{\sigma, \mathbf{p}} \rangle = \begin{cases} 0 & (\sigma = 0, 3) \\ \frac{|\beta_{(a)\sigma, \mathbf{p}}|^2}{(2\pi)^3} & (\sigma = 1, 2) \end{cases} \quad (3.86)$$

for chargeless gluons;

$$\begin{aligned} \frac{d^6 N_{g_+}(\sigma, \mathbf{p}; t)}{d\mathbf{p}^3 d\mathbf{x}^3} &= \frac{1}{V} \langle \hat{\mathbf{c}}_{\sigma, \mathbf{p}}^\dagger \hat{\mathbf{c}}_{\sigma, \mathbf{p}} \rangle = \begin{cases} 0 & (\sigma = 0, 3) \\ \frac{|\beta_{(\mathcal{A})\sigma, \mathbf{p}}|^2}{(2\pi)^3} & (\sigma = 1, 2) \end{cases} \\ \frac{d^6 N_{g_-}(\sigma, \mathbf{p}; t)}{d\mathbf{p}^3 d\mathbf{x}^3} &= \frac{1}{V} \langle \hat{\mathbf{d}}_{\sigma, \mathbf{p}}^\dagger \hat{\mathbf{d}}_{\sigma, \mathbf{p}} \rangle = \begin{cases} 0 & (\sigma = 0, 3) \\ \frac{|\beta_{(\mathcal{A})\sigma, -\mathbf{p}}|^2}{(2\pi)^3} & (\sigma = 1, 2) \end{cases} \end{aligned} \quad (3.87)$$

for charged gluons with the color charge  $g$  and  $-g$ , respectively; and

$$\begin{aligned} \frac{d^6 N_{\text{gh}_+}^{(-)}(\mathbf{p}; t)}{d\mathbf{p}^3 d\mathbf{x}^3} &= \frac{1}{V} \left\langle \begin{pmatrix} (-)^\dagger & (-) \\ \mathbf{e} & \mathbf{p} \end{pmatrix} \begin{pmatrix} (-) \\ \mathbf{e} & \mathbf{p} \end{pmatrix} \right\rangle = 0, \\ \frac{d^6 N_{\text{gh}_-}^{(-)}(\mathbf{p}; t)}{d\mathbf{p}^3 d\mathbf{x}^3} &= \frac{1}{V} \left\langle \begin{pmatrix} (-)^\dagger & (-) \\ \mathbf{f} & \mathbf{p} \end{pmatrix} \begin{pmatrix} (-) \\ \mathbf{f} & \mathbf{p} \end{pmatrix} \right\rangle = 0 \end{aligned} \quad (3.88)$$

for charged ghosts (anti-ghosts) with the color charge  $g$  and  $-g$ , respectively. In deriving the gluon spectra (3.86) and (3.87), we used that  $\sigma = 0, 3$  modes of gluons commute with each other because of the commutation relation (3.61). Also, for the ghost and anti-ghost spectra (3.88), the use is made of Eq. (3.77) which says that ghosts (anti-ghosts) anti-commute with themselves. No production of  $\sigma = 0, 3$  modes of gluons and ghosts is a reasonable result because two out of the four polarization modes of gluons and ghosts are unphysical particles, and must not appear in the physical spectra. In contrast to the electron spectra (2.38) and (2.39), gluons are not subjected to the Pauli principle because of the minus sign in the normalization condition for the Bogoliubov coefficients (3.68), and the phase space density can exceed unity.

### 3.1.5 massless approximation

Within the mean field treatment explained in Section 3.1.3, we found that dynamical mass terms  $M_{(a)}, M_{(\mathcal{A})}, M_{(c)}$  appear in the equations of motion (3.37)-(3.40) because of self-interactions among gluons. Physically speaking, these mass terms are responsible for scatterings and collisions of produced particles, and hence are important in describing the thermalization of the system. However, the problem is that the mass terms have a complicated expression and are somewhat difficult to evaluate. Furthermore, as the mass terms originate from the quartic interaction of the Yang-Mills Lagrangian, they are higher-order in the coupling  $g$  compared to the other terms and might be negligible in the small coupling constant limit  $g \rightarrow 0$ . In view of these circumstances, we dare neglect the mass terms and set  $M_{(a)} = M_{(\mathcal{A})} = M_{(c)} = 0$  (which we shall call *massless approximation*) in the following as the first study of the Schwinger mechanism in QCD including backreaction effects. This simplification dramatically simplifies the equations of motion (3.36)-(3.40), and thus one can develop a better understanding of the problem. We stress that this simplification does not violate the current conservation law (3.26) nor the energy conservation law (3.28).

Under the massless approximation  $M_{(a)} = M_{(\mathcal{A})} = M_{(c)} = 0$ , the equations of motion (3.36)-(3.40) for a homogeneous system read

$$-\frac{d\bar{E}}{dt} = \langle : \hat{j}^z : \rangle + \bar{J}^z, \quad (3.89)$$

$$0 = \partial^\rho \partial_\rho \hat{a}_\sigma, \quad (3.90)$$

$$0 = \bar{D}^\rho \bar{D}_\rho \hat{A}_\sigma, \quad (3.91)$$

$$0 = \partial^\rho \partial_\rho \hat{C}^{(-)}, \quad (3.92)$$

$$0 = \bar{D}^\rho \bar{D}_\rho \hat{C}^{(-)}. \quad (3.93)$$

Note that  $\delta\bar{E} = 0$  holds in the massless approximation. Now that not only the fluctuation  $\hat{C}^{(-)}$  but also the fluctuation  $\hat{a}_\sigma$  becomes trivial, we do not consider them in the following. Notice

that the equations for charged gluons  $\hat{A}_\sigma$  (3.91) and charged ghosts  $\hat{\mathcal{C}}, \hat{\bar{\mathcal{C}}}$  (3.93) are now the same as the one for massless charged scalar particles with spin 0.

The massless approximation does no harm to the canonical quantization procedure explained in Section 3.1.4. In the following sections, Section 3.2 and 3.3, we discuss the time-evolution of the system within this massless approximation.

## 3.2 Gluon production from a constant color electric field

For now, we neglect the backreaction and treat the classical electric field as a background by artificially setting  $\langle : \hat{j}_\mu : \rangle = 0$ . The backreaction effects will be discussed in Section 3.3. This treatment is, unfortunately, unphysical because it apparently violates the energy conservation of the system and is justifiable only at the very beginning of the pair production process. Nevertheless, this treatment is very useful in understanding the basics of the gluon production and how it is different from the electron production discussed in Chapter 2 because one can analytically compute the gluon spectrum for some particular types of electric fields.

### 3.2.1 gluon distribution

In this section, we consider a constant color electric field initiated at  $t = t_0 = 0$ , which is given by

$$\bar{E}(t) = \bar{E}_0 \theta(t), \quad \text{or} \quad \bar{A}(t) = -\bar{E}_0 t \theta(t). \quad (3.94)$$

Under this field configuration, we compute the intermediate gluon spectrum  $(2\pi)^3 d^6 N_{g\pm} / d\mathbf{p}^3 d\mathbf{x}^3 = |\beta_{(\mathcal{A})\sigma, \pm \mathbf{p}}|^2$  for the physical  $\sigma = 1, 2$  modes (see Eq. (3.87)). One can analytically evaluate the intermediate Bogoliubov coefficient  $\beta_{(\mathcal{A})\sigma, \mathbf{p}}$  because the equation of motion (3.91) is analytically solvable: This can be done easily by smoothly connecting the plane wave solutions  $\pm \mathcal{A}_{\sigma, \mathbf{p}}^{(\text{plane})}$  (see Appendix B.1) and solutions under a constant color electric field with infinite duration  $\pm \mathcal{A}_{\sigma, \mathbf{p}}^{(\text{const}; \text{out})}$  (see Appendix B.2) at the boundary  $t = t_0$ . By noting  $\pm \mathcal{A}_{\sigma, \mathbf{p}}^{(\text{plane})} = \pm \mathcal{A}_{\sigma, \mathbf{p}}^{(t)}$  for  $t < 0$  where  $\bar{A} = 0$ , one obtains

$$\begin{pmatrix} +\mathcal{A}_{\sigma, \mathbf{p}}^{(\text{in})} \\ -\mathcal{A}_{\sigma, \mathbf{p}}^{(\text{in})} \end{pmatrix} = \begin{cases} \begin{pmatrix} +\mathcal{A}_{\sigma, \mathbf{p}}^{(t)} \\ -\mathcal{A}_{\sigma, \mathbf{p}}^{(t)} \end{pmatrix} & (t < t_0) \\ \begin{pmatrix} \tilde{\alpha}_{\sigma, \mathbf{p}}(t_0) & \tilde{\beta}_{\sigma, \mathbf{p}}^*(t_0) \\ \tilde{\beta}_{\sigma, \mathbf{p}}(t_0) & \tilde{\alpha}_{\sigma, \mathbf{p}}^*(t_0) \end{pmatrix} \begin{pmatrix} +\mathcal{A}_{\sigma, \mathbf{p}}^{(\text{const}; \text{out})} \\ -\mathcal{A}_{\sigma, \mathbf{p}}^{(\text{const}; \text{out})} \end{pmatrix} & (t > t_0) \end{cases}, \quad (3.95)$$

where the coefficients  $\tilde{\alpha}_{\sigma,\mathbf{p}}, \tilde{\beta}_{\sigma,\mathbf{p}}$  are given by

$$\begin{aligned} \tilde{\alpha}_{\sigma,\mathbf{p}}(t) &\equiv ({}_+\mathcal{A}_{\sigma,\mathbf{p}}^{\text{(const;out)}}(t)|_+\mathcal{A}_{\sigma,\mathbf{p}}^{(t)}(t))_{\text{B}} \\ &= \frac{-i}{\sqrt{2|\mathbf{p} + g\bar{\mathbf{E}}_0 t|}} \frac{\exp\left[-\pi \frac{\mathbf{p}_\perp^2}{8|g\bar{\mathbf{E}}_0|}\right]}{(2|g\bar{\mathbf{E}}_0|)^{1/4}} \exp\left[-i \int_{-\infty}^t |\mathbf{p} + g\bar{\mathbf{E}}_0 t| dt\right] \\ &\quad \times \left[ (|\mathbf{p} + g\bar{\mathbf{E}}_0 t| - (p_z + g\bar{E}_0 t)) D_{i \frac{\mathbf{p}_\perp^2}{2|g\bar{\mathbf{E}}_0|} - 1/2} \left(e^{-i\pi/4} \sqrt{\frac{2}{|g\bar{\mathbf{E}}_0|}} (g\bar{E}_0 t + p_z)\right) \right. \\ &\quad \left. + e^{i\pi/4} \sqrt{2|g\bar{\mathbf{E}}_0|} D_{i \frac{\mathbf{p}_\perp^2}{2|g\bar{\mathbf{E}}_0|} + 1/2} \left(e^{-i\pi/4} \sqrt{\frac{2}{|g\bar{\mathbf{E}}_0|}} (g\bar{E}_0 t + p_z)\right) \right], \end{aligned} \quad (3.96)$$

$$\begin{aligned} \tilde{\beta}_{\sigma,\mathbf{p}}(t) &\equiv ({}_+\mathcal{A}_{\sigma,\mathbf{p}}^{\text{(const;out)}}(t)|_-\mathcal{A}_{\sigma,\mathbf{p}}^{(t)}(t))_{\text{B}} \\ &= \frac{i}{\sqrt{2|\mathbf{p} + g\bar{\mathbf{E}}_0 t|}} \frac{\exp\left[-\pi \frac{\mathbf{p}_\perp^2}{8|g\bar{\mathbf{E}}_0|}\right]}{(2|g\bar{\mathbf{E}}_0|)^{1/4}} \exp\left[+i \int_{-\infty}^t |\mathbf{p} + g\bar{\mathbf{E}}_0 t| dt\right] \\ &\quad \times \left[ (|\mathbf{p} + g\bar{\mathbf{E}}_0 t| + (p_z + g\bar{E}_0 t)) D_{i \frac{\mathbf{p}_\perp^2}{2|g\bar{\mathbf{E}}_0|} - 1/2} \left(e^{-i\pi/4} \sqrt{\frac{2}{|g\bar{\mathbf{E}}_0|}} (g\bar{E}_0 t + p_z)\right) \right. \\ &\quad \left. - e^{i\pi/4} \sqrt{2|g\bar{\mathbf{E}}_0|} D_{i \frac{\mathbf{p}_\perp^2}{2|g\bar{\mathbf{E}}_0|} + 1/2} \left(e^{-i\pi/4} \sqrt{\frac{2}{|g\bar{\mathbf{E}}_0|}} (g\bar{E}_0 t + p_z)\right) \right]. \end{aligned} \quad (3.97)$$

The intermediate Bogoliubov coefficients  $\alpha_{\sigma,\mathbf{p}}, \beta_{\sigma,\mathbf{p}}$  can be computed by Eq. (3.67), and one finds that

$$\begin{aligned} \alpha_{(\mathcal{A})\sigma,\mathbf{p}} &= \tilde{\alpha}_{\sigma,\mathbf{p}}(t_0) \tilde{\alpha}_{\sigma,\mathbf{p}}^*(t) - \tilde{\beta}_{\sigma,\mathbf{p}}^*(t_0) \tilde{\beta}_{\sigma,\mathbf{p}}(t), \\ \beta_{(\mathcal{A})\sigma,\mathbf{p}} &= \tilde{\beta}_{\sigma,\mathbf{p}}(t_0) \tilde{\alpha}_{\sigma,\mathbf{p}}^*(t) - \tilde{\alpha}_{\sigma,\mathbf{p}}^*(t_0) \tilde{\beta}_{\sigma,\mathbf{p}}(t). \end{aligned} \quad (3.98)$$

### analytic formula at $t \rightarrow \infty$

The analytical expression for the intermediate Bogoliubov coefficient  $\beta_{(\mathcal{A})\sigma,\mathbf{p}}$  (3.98) looks somewhat complicated, however, it takes a remarkably simple form in the infinite future  $t \rightarrow \infty$  (or the infinite longitudinal kinetic momentum  $P_z = p_z + gEt \rightarrow \infty$ ). By noting the asymptotic formula for the parabolic cylinder functions  $D_\nu(z)$ , [162]

$$D_\nu(z) \xrightarrow{|z| \rightarrow \infty} \begin{cases} z^\nu e^{-z^2/4} & (|\arg z| < 3\pi/4) \\ z^\nu e^{-z^2/4} - \frac{\sqrt{2\pi}}{\Gamma(-\nu)} e^{i\nu\pi} z^{-\nu-1} e^{z^2/4} & (\pi/4 < \arg z < 5\pi/4) \\ z^\nu e^{-z^2/4} - \frac{\sqrt{2\pi}}{\Gamma(-\nu)} e^{-i\nu\pi} z^{-\nu-1} e^{z^2/4} & (-5\pi/4 < \arg z < -\pi/4) \end{cases}, \quad (3.99)$$

one finds

$$\beta_{(\mathcal{A})\sigma,\mathbf{p}} \xrightarrow{t \rightarrow \infty} i \exp\left[-\pi \frac{\mathbf{p}_\perp^2}{2|g\bar{\mathbf{E}}_0|}\right]. \quad (3.100)$$

Hence, the gluon spectrum in the infinite future  $t \rightarrow \infty$  becomes

$$\frac{d^6 N_{\mathbf{g}\pm}}{d\mathbf{p}^3 d\mathbf{x}^3} \xrightarrow{t \rightarrow \infty} \frac{1}{(2\pi)^3} \exp\left[-\pi \frac{\mathbf{p}_\perp^2}{|g\bar{\mathbf{E}}_0|}\right]. \quad (3.101)$$

This expression is the same as the electron spectrum (2.69), which implies that the gluon production in an Abelian dominated constant color electric field is essentially the same as the electron production in QED. The situation will dramatically change when quantum interferences, which depend on the quantum statistics of particles, come into play; see Section 3.3, where backreaction and resulting quantum interferences are treated.

### dynamical evolution

We directly evaluate the Bogoliubov coefficient  $\beta_{\sigma,\mathbf{p}}$  (3.98) to discuss the intermediate gluon spectrum  $(2\pi)^3 d^6 N_{g\pm}/d\mathbf{p}^3 d\mathbf{x}^3 = |\beta_{(\mathcal{A})\sigma,\mathbf{p}}|^2$ . The results are plotted in Figs. 3.2 and 3.3: Figure 3.2 shows longitudinal kinetic momentum  $P_z = p_z - g\bar{A}$  distribution  $(2\pi)^3 d^6 N_{g\pm}/d\mathbf{p}^3 d\mathbf{x}^3 = |\beta_{(\mathcal{A})\sigma,\mathbf{p}}|^2$  for a fixed transverse momentum  $|\mathbf{p}_\perp|/\sqrt{|g\bar{E}_0|} = 0.1$ , and Fig. 3.3 shows the transverse momentum  $\mathbf{p}_\perp$ -distribution for a fixed longitudinal kinetic momentum  $P_z = p_z + g\bar{E}_0 t = 3 \times \sqrt{|g\bar{E}_0|}$ .

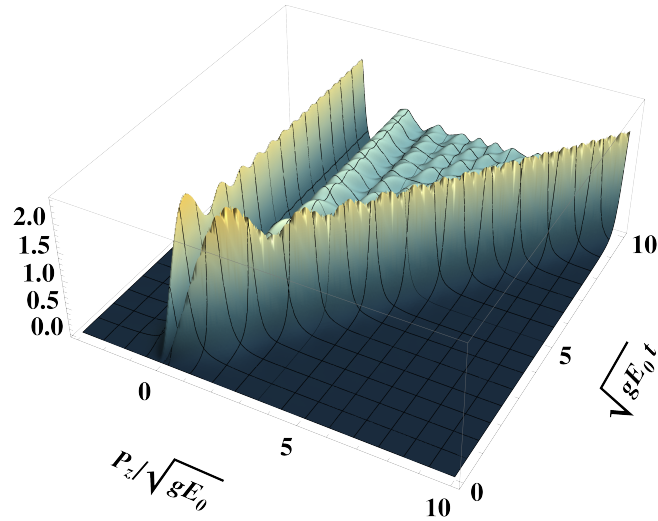


Figure 3.2: The time-evolution of the longitudinal kinetic momentum  $P_z = p_z - g\bar{A}$  distribution  $(2\pi)^3 d^6 N_{g\pm}/d\mathbf{p}^3 d\mathbf{x}^3 = |\beta_{(\mathcal{A})\sigma,\mathbf{p}}|^2$  for a fixed transverse momentum  $|\mathbf{p}_\perp|/\sqrt{|g\bar{E}_0|} = 0.1$ .

The essential features of the gluon production (without backreaction) are the same as in the electron production discussed in Section 2.4: Gluons are constantly produced at  $\mathbf{P} \sim 0$ , where the production threshold  $\sim |\mathbf{P}|$  becomes smallest. After gluons are created, they are accelerated in the longitudinal direction by the electric field according to the classical equation of motion  $d\mathbf{P}/dt = g\bar{\mathbf{E}}_0$ . The transverse distribution is given by a Gaussian, and is consistent with the asymptotic formula (3.101). Thus, the gluon distribution  $d^6 N_{g\pm}/d\mathbf{p}^3 d\mathbf{x}^3$  is nicely approximated by

$$\frac{d^6 N_{g\pm}}{d\mathbf{p}^3 d\mathbf{x}^3} \sim \frac{1}{(2\pi)^3} \exp \left[ -\pi \frac{\mathbf{p}_\perp^2}{|g\bar{\mathbf{E}}(t)|} \theta(\mp p_z (p_z \mp g\bar{A}(t))) \right], \quad (3.102)$$

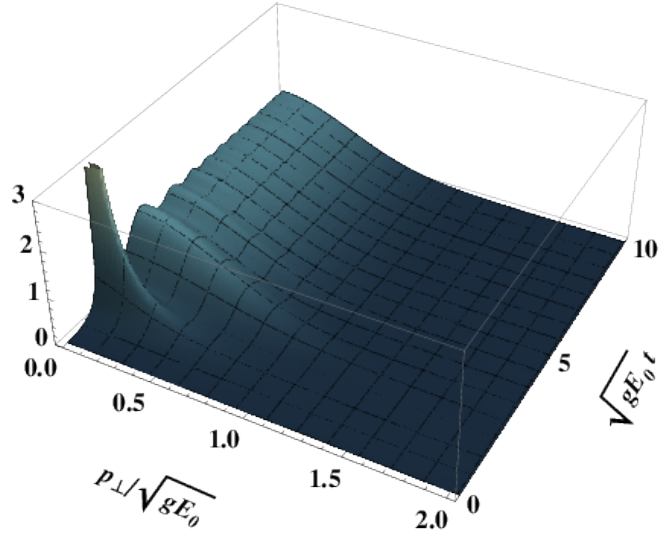


Figure 3.3: The time-evolution of the transverse momentum  $\mathbf{p}_\perp$ -distribution  $(2\pi)^3 d^6 N_{g_\pm} / d\mathbf{p}^3 d\mathbf{x}^3 = |\beta_{(\mathcal{A})\sigma, \mathbf{p}}|^2$  for a fixed longitudinal kinetic momentum  $P_z = p_z + g\bar{E}_0 t = 3 \times \sqrt{|g\bar{E}_0|}$ .

which is the same as for the electrons (2.94).

### 3.2.2 total number of gluons

#### analytical estimate at $t \rightarrow \infty$

The analytic formula for the gluon distribution at  $t \rightarrow \infty$  (3.101) has no  $p_z$ -dependence, and so the  $p_z$ -integration diverges. We estimate the degree of the divergence in the same way as what we did for the electron production (2.70). That is, by estimating  $\int dp_z \sim |g\bar{E}_0|T$  (which is consistent with the longitudinal kinetic distribution, Fig. 3.2, and the approximation (3.102)), we find the total number of produced gluons with the color charge  $\pm g$  for a single physical polarization  $\sigma = 1$  or 2 as

$$\frac{d^3 N_{g_\pm}}{d\mathbf{x}^3} \xrightarrow{t \rightarrow \infty} \frac{|g\bar{E}_0|^2 T}{(2\pi)^3} \exp \left[ -\pi \frac{\mathbf{p}_\perp^2}{|g\bar{E}_0|} \right]. \quad (3.103)$$

#### dynamical evolution

We numerically integrate the Bogoliubov coefficient  $\beta_{\sigma, \mathbf{p}}$  (3.98) over the momentum  $\mathbf{p}$  to study the time-evolution of the total number of gluons produced  $d^3 N_{g_\pm} / d\mathbf{x}^3 = \int d^3 \mathbf{p} |\beta_{(\mathcal{A})\sigma, \mathbf{p}}|^2 / (2\pi)^3$ .

The result is shown in Fig. 3.4. We find that the gluon production is in good agreement with the estimate (3.103) as for the electron production (see Section 2.4.2). It is interesting to note that the agreement is better than in the case of the electron production (see Fig. 2.10). One can understand this difference in terms of the perturbative particle production mechanism

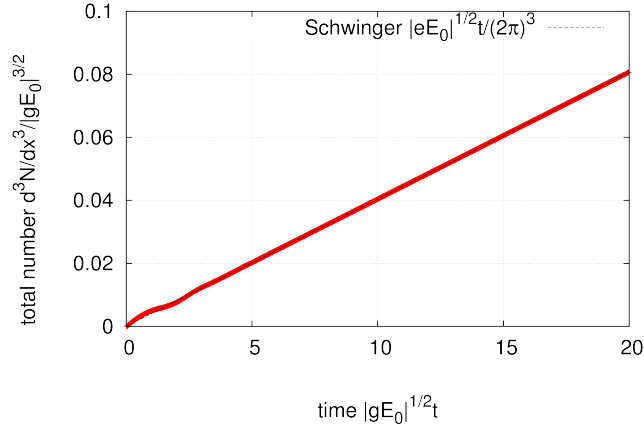


Figure 3.4: The total number of gluons produced  $d^3 N_{g_{\pm}}/d^3 x$  with the color charge  $\pm g$  per unit physical polarization. The dashed line is the estimate (3.103).

which dominates particle production at early times (see Section 2.3). As in Section 2.3.1, one can compute the  $S$ -matrix element,  $S \equiv \langle g_+(\sigma, \mathbf{p})g_-(\sigma', \mathbf{p}'); \text{out}|\text{vac}; \text{in} \rangle$ , within the lowest order perturbation theory to perturbatively evaluate the total number of gluons produced with a particular physical polarization  $\sigma$  from the classical gauge field  $\bar{A}_\mu$  as

$$\begin{aligned} \frac{d^3 N_{g_{\pm}}}{d^3 x} &= \sum_{\sigma'} \int d^3 \mathbf{p} d^3 \mathbf{p}' |\langle g_+(\sigma, \mathbf{p})g_-(\sigma', \mathbf{p}'); \text{out}|\text{vac}; \text{in} \rangle|^2 \\ &= \frac{1}{48\pi^2} \int_0^\infty d\omega |g\tilde{E}(\omega)|^2, \end{aligned} \quad (3.104)$$

where  $\tilde{E}(\omega)$  is the Fourier component of the electric field  $\tilde{E}(\omega) \equiv \int dt E(t)e^{i\omega t}$ . By comparing the electron formula (2.77),  $d^3 N_{e^\pm}/d^3 x \xrightarrow{m_e \rightarrow 0} 1/(24\pi^2) \int_0^\infty d\omega |e\tilde{E}(\omega)|^2$ , one understands that the perturbative enhancement at early times of the gluon production amounts to just a half of that of the electron (for the same electric field strength  $|eE| = |g\bar{E}|$ ). Hence, the gluon production is not enhanced so much at the early times and the excess from the naive estimate (3.103) becomes smaller compared to the electron case.

### 3.3 Dynamical evolution with backreaction

In this section, we consider backreaction effects: By numerically solving the equations of motion (3.89)-(3.93), we discuss the dynamical evolution of the gluon distribution function, the electric field strength, the total number of produced gluons, and thermodynamic quantities including energy density and pressure of the system.

### 3.3.1 setup

We consider a spatially homogeneous system without any classical source  $\bar{J}^\mu = 0$ . As an initial condition at  $t = t_0 = 0$ , we consider an electric field described by

$$\bar{A}(t_0) = 0, \quad \bar{E}(t_0) = \bar{E}_0, \quad \frac{d\bar{E}(t_0)}{dt} = 0. \quad (3.105)$$

For the sake of simplicity, we set the strength of the coupling constant  $g$  as  $g = 1$ .

### 3.3.2 gluon distribution

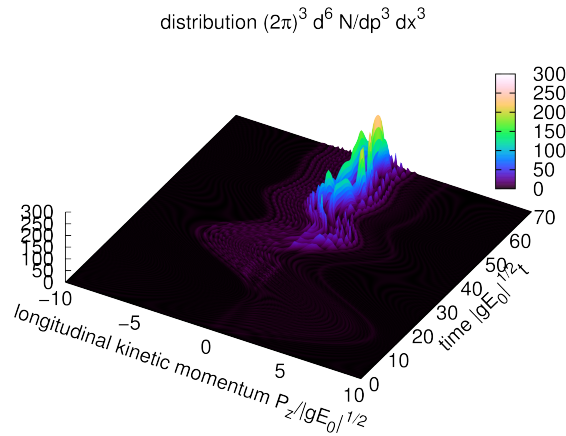


Figure 3.5: The longitudinal kinetic momentum  $P_z = p_z - g\bar{A}$  dependence of the gluon distribution  $d^6N_{g_+}/d\mathbf{p}^3 d\mathbf{x}^3$  at a fixed transverse momentum  $|\mathbf{p}_\perp|/\sqrt{|g\bar{E}_0|} = 0.1$ .

The time-evolution of the gluon distribution  $d^6N_{g_+}/d\mathbf{p}^3 d\mathbf{x}^3$  is plotted in Figs. 3.5 and 3.6. One observes once again that the plasma oscillation occurs just as in the electron case (see Section 2.5.2). Quantum interferences also occur when the newly produced gluons and the previously produced gluons meet at the same phase space point around  $\mathbf{P} \sim \mathbf{0}$  in the oscillational motion. As a result, the gluon spectrum is strongly distorted, which may indicate that entropy is irreversibly produced as was so for the electron production. What is remarkable here is that the gluon distribution is dramatically enhanced due to the quantum interferences (the Bose enhancement [34]) whenever the “old” gluons come back to  $\mathbf{P} \sim \mathbf{0}$  where the gluon production constantly takes place. This is in contrast to the electron production, which is restricted by the Pauli principle and hence whose phase space density never exceeds unity. Because of the quantum interferences, the naive formula (3.102) for the gluon distribution function without backreaction is valid only at relatively early times  $t \lesssim t_{\text{osc}}$ , where  $t_{\text{osc}}$  is the typical time-scale of the plasma oscillation (the time when the longitudinal momentum extension of the gluon

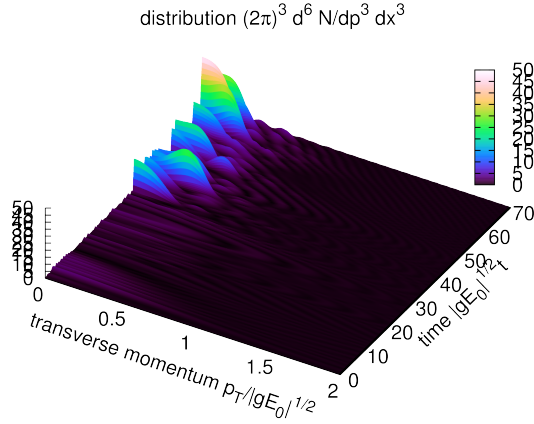


Figure 3.6: The transverse momentum  $\mathbf{p}_\perp$ -dependence of the gluon distribution  $d^6 N_{g_+} / d\mathbf{p}^3 d\mathbf{x}^3$  at a fixed kinetic longitudinal momentum  $P_z = p_z - g\bar{A} = 1.2 \times \sqrt{|g\bar{E}_0|}$ .

distribution takes its maximum for the first time, i.e., when the electric field strength crosses zero for the first time). The time-scale of the oscillation  $t_{\text{osc}}$  may roughly be estimated in the same way as that for electrons (2.99). By neglecting the quantum interferences, one gets

$$\sqrt{|g\bar{E}_0|} t_{\text{osc}} \sim \frac{\pi^2}{g} \sqrt{\frac{\pi}{2}} \sim 12 \quad (\text{for } g = 1), \quad (3.106)$$

which indeed turns out to be consistent with the figure.

We stress that because of the quantum interferences, i.e., the Bose enhancement and the Pauli blocking, the gluon (or boson in general) production is much more abundant than the electron (or fermion) production (see Section 3.3.4), and hence the initial *field* energy is more efficiently converted into the gluon *particle* degree of freedom as we shall see in Section 3.3.3 - 3.3.5.

### 3.3.3 decay of color electric field

Figure 3.7 displays the time-evolution of the electric field strength (left) and the current  $\langle : \hat{j}^z : \rangle$  (right). We again observe for  $\sqrt{|g\bar{E}_0|} t \lesssim 50$  that the electric field strength and the current show the plasma oscillation as was discussed in Section 2.5.3. What is more important here is that the time-scale of the decay is much faster than the electron case (see Fig. 2.13). This is because the gluon production is much more abundant than the electron one because of the Bose enhancement of the gluon production (see Section 3.3.2) and the suppression of the electron production by the Pauli blocking (see Section 2.5.2). Another notable point is that both the electric field and the current show rapid oscillations at later times  $\sqrt{|g\bar{E}_0|} t \gtrsim 50$ . By noting that the gluon spectrum at later times (see Figs. 3.5 and 3.6) is strongly distorted by the

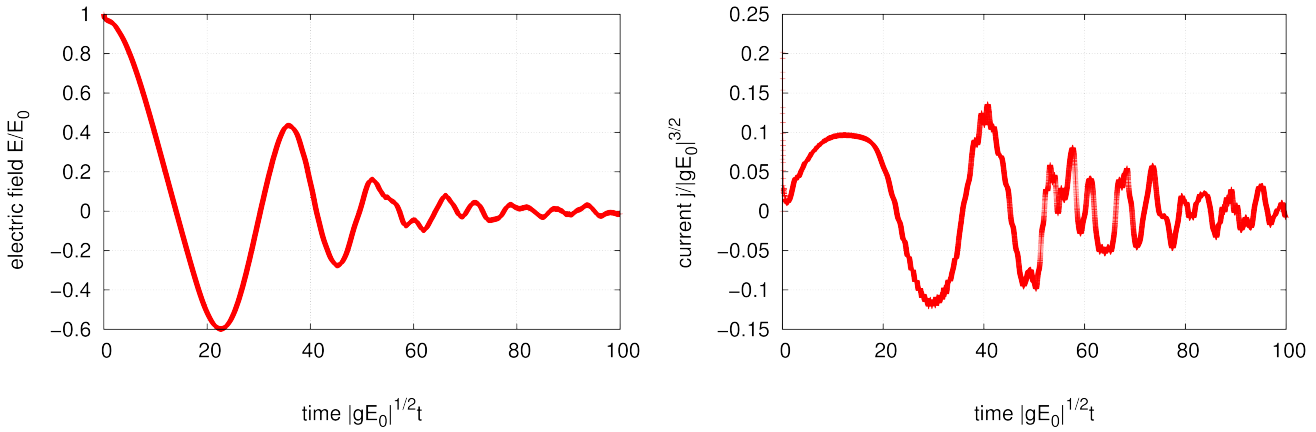


Figure 3.7: [Left] The time-evolution of the electric field strength  $\bar{E}(t)$ . [Right] The time-evolution of the current  $\langle : \hat{j}^z : \rangle$ .

quantum interferences, one understands that the rapid oscillation is not due to the plasma oscillation, which is purely a classical effect, but is due to a quantum effect arising from the quantum interferences.

### 3.3.4 total number of gluons

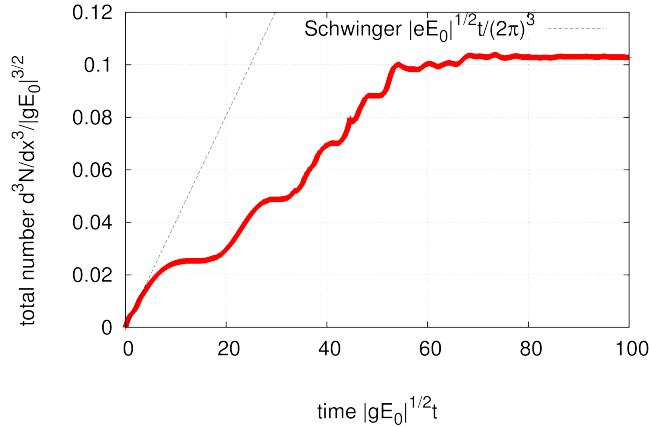


Figure 3.8: The total number of produced gluons  $d^3N_{g_{\pm}}/d\mathbf{x}^3$  with the color charge  $\pm g$  for a single physical polarization. The dashed line is the estimate (3.103) without the backreaction.

In Fig. 3.8, we plotted the total number of gluons produced  $d^3N_{g_{\pm}}/d\mathbf{x}^3$  with the color charge  $\pm g$  for a single physical polarization  $\sigma = 1$  or  $2$ . Just as in the electron production (2.5.4), the result (red thick line) coincides with that neglecting the backreaction (dashed black line) only at the beginning of the gluon production process  $\sqrt{g\bar{E}_0}t \lesssim 10$ . If one compares this result with

that of electrons, Fig. 2.14, one finds that the gluon production is much more abundant than the electron one: The electron production is strongly suppressed by the Pauli blocking, while the gluon production is, in contrast, enhanced by the Bose enhancement.

### 3.3.5 energy density

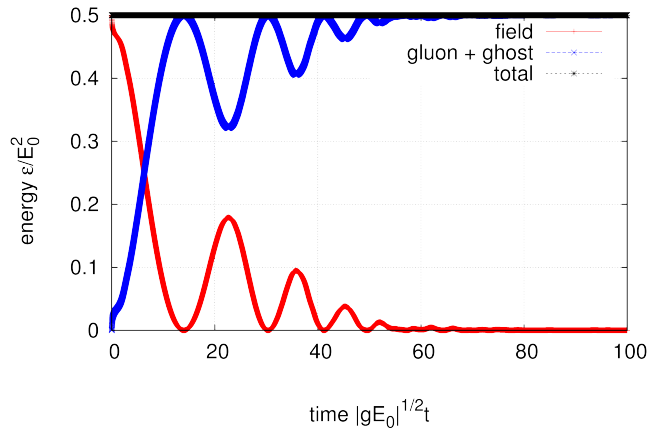


Figure 3.9: The energy balance between the classical field (blue) and the quantum particles, i.e., gluons and ghosts (red). The total energy of the system is strictly conserved as indicated by the black line.

Figure 3.9 shows the energy balance between the classical electric field  $\bar{A}$  and the sum of the physical  $\sigma = 1, 2$  gluons  $\hat{\mathcal{A}}_\sigma$ ; unphysical contributions from  $\sigma = 0, 3$  gluons  $\hat{\mathcal{A}}_\sigma$ , and ghosts  $\hat{\mathcal{C}}^{(-)}$  exactly cancel out with each other because they obey the same equation of motion (3.91) and (3.93). One immediately notices that the initial *field* energy is quickly converted into gluon *particles*. The time-scale of the conversion is much faster than the electron production (see Fig. 2.5.5) because of the different quantum statistics as was repeatedly addressed in this section.

We note that the energy conservation is strictly satisfied during the whole time-evolution.

### 3.3.6 pressure

We plotted the transverse and longitudinal pressures  $\langle : \hat{P}_\perp : \rangle, \langle : \hat{P}_z : \rangle$  of the system in Fig. 3.10. The basic features of the figure is the same as the QED one (see Figs. 2.16 and 2.17), although the typical time-scale of the transition from the classical field regime to the quantum particle regime is much shorter:

- The transverse pressure of particles is negligible because they are created with soft transverse momenta  $\mathbf{p}_\perp \sim \mathbf{0}$  as was seen in Fig. 3.6. Hence, the total transverse pressure of the system dies away as the classical field decoheres into particles.

- The longitudinal pressure of particles is sizable because the classical electric field significantly accelerates the particles in the longitudinal direction. Hence, the total longitudinal pressure of the system is dominated by particles as the classical electric field decoheres into particles.

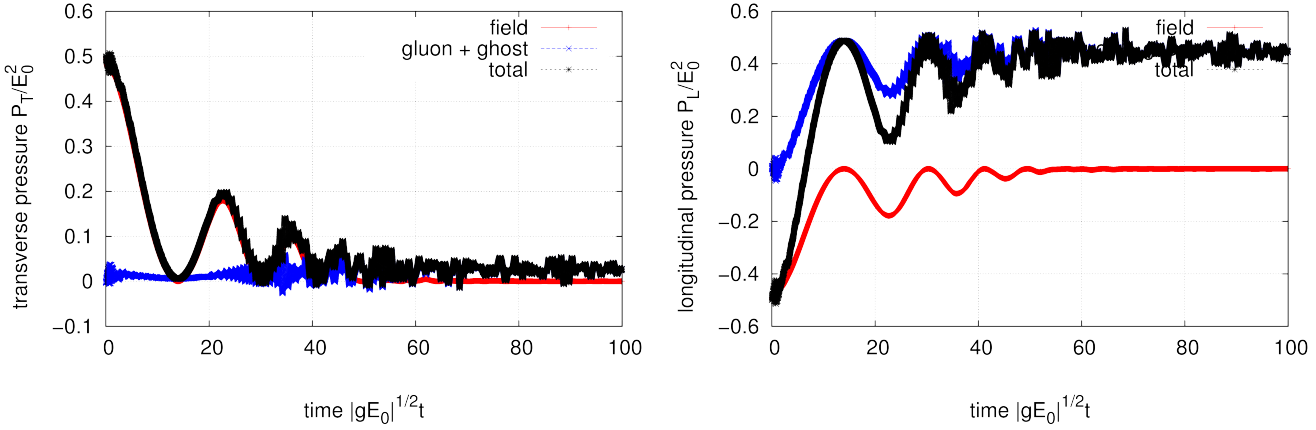


Figure 3.10: The time-evolution of the transverse pressure  $\langle : \hat{P}_\perp : \rangle$  (left) and the longitudinal pressure  $\langle : \hat{P}_z : \rangle$  (right) from the classical field (blue) and the quantum particles, i.e., gluons and ghosts (red). The black line is the sum of these two, i.e, the total transverse/longitudinal pressure of the system.

In Fig. 3.11, we characterize the anisotropy of the system by the total transverse and longitudinal pressure scaled by the total energy,  $\langle : \hat{P}_\perp : \rangle / \langle : \hat{\epsilon} : \rangle$  and  $\langle : \hat{P}_z : \rangle / \langle : \hat{\epsilon} : \rangle$  as in the QED study (see Fig. 2.18). We observe that the initial anisotropy of the system  $\langle : \hat{P}_\perp : \rangle / \langle : \hat{\epsilon} : \rangle = 1/2$ ,  $\langle : \hat{P}_z : \rangle / \langle : \hat{\epsilon} : \rangle = -1/2$  is relaxed with relatively shorter time-scale compared to the QED study. However, the complete isotropization of the system cannot be achieved within the massless approximation, by which we neglect scatterings and collisions between produced gluons.

### 3.4 Brief summary

We briefly summarize the main results of this chapter:

- We formulated the Schwinger mechanism in the  $SU_c(N_c = 2)$  pure Yang-Mills theory including backreaction from gluon and ghost fluctuations to the classical gauge field. This was done in Section 3.1 by extending the mean field framework developed in QED (Section 2.1).
- Without backreaction (see Section 3.2), we analytically evaluated the time-evolution of the gluon spectrum under a constant color electric field background to find that the gluon

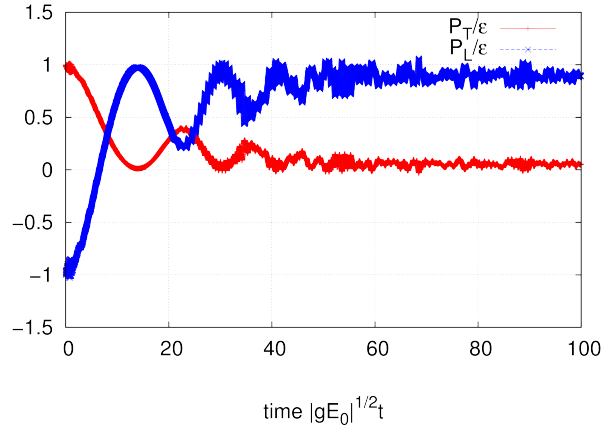


Figure 3.11: Isotropization of the system. The total transverse and longitudinal pressure scaled by the total energy,  $\langle : \hat{P}_\perp : \rangle / \langle : \hat{\epsilon} : \rangle$  and  $\langle : \hat{P}_z : \rangle / \langle : \hat{\epsilon} : \rangle$ , are plotted in red and blue line, respectively.

spectrum almost agrees with the well-known Schwinger formula for a constant electric field.

- Once backreaction is taken into account (see Section 3.3), the classical plasma oscillation and the quantum interferences among gluons occur, and the gluon production is dramatically modified from the naive Schwinger formula for a constant electric field.
- The quantum interferences strongly enhance the gluon production (the Bose enhancement), which accelerates the decoherence of the classical gauge field (see Section 3.3).
- Within the mean field treatment together with the massless approximation (see Section 3.1.5), the system never isotropitizes (i.e., thermalizes) although the degree of the anisotropy is relaxed as was plotted in Fig. 3.11.



## Chapter 4

# Schwinger Mechanism in Quantum Chromodynamics

In this chapter, we extend the previous  $SU(N_c = 2)$  pure Yang-Mills study (see Chapter 3) to QCD with  $N_c = 3$  colors and  $N_f$  flavors of quarks. In Section 4.1, we formulate the Schwinger mechanism in QCD by applying the mean field approximation and the massless approximation developed in Chapter 3. In Section 4.2 and 4.3, we extensively study the Schwinger mechanism in QCD by applying the formalism: In Section 4.2, quark and gluon production is analytically investigated by neglecting backreaction, and similarities/differences between the two production are clarified. In Section 4.3, backreaction effects are taken into account numerically. By tracing the time-evolution of the quark and gluon distribution functions; the color electric field strength; the total number of quarks and gluons produced; and the thermodynamics quantities such as the energy density and the pressure, we reveal the dynamics of how an initial classical field decoheres into quantum quarks and gluons within a realistic QCD framework.

## 4.1 Formalism

### 4.1.1 QCD under a classical gauge field

#### Lagrangian

In the rest of this thesis, we consider the  $SU_c(N_c = 3) \otimes SU_f(N_f)$  QCD Lagrangian  $\hat{\mathcal{L}}_{\text{QCD}}$ :

$$\hat{\mathcal{L}}_{\text{QCD}} = \hat{\mathcal{L}}_{(q)} + \hat{\mathcal{L}}_{(g)} + \hat{\mathcal{L}}_{(\text{GF})} + \hat{\mathcal{L}}_{(\text{FP})} + \hat{\mathcal{L}}_{(\text{ext})}, \quad (4.1)$$

where

$$\hat{\mathcal{L}}_{(q)} = \sum_f \hat{\psi}_f [i\hat{\not{\partial}} - g\hat{A} - m_f] \hat{\psi}_f, \quad (4.2)$$

$$\hat{\mathcal{L}}_{(g)} = -\frac{1}{2} \text{tr}_c [\hat{F}^{\mu\nu} \hat{F}_{\mu\nu}], \quad (4.3)$$

$$\hat{\mathcal{L}}_{(\text{GF})} = -\text{tr}_c [\hat{\vartheta}^2], \quad (4.4)$$

$$\hat{\mathcal{L}}_{(\text{FP})} = 2i \operatorname{tr}_c[\hat{c}\delta_{\text{BRS}}\hat{\vartheta}], \quad (4.5)$$

$$\hat{\mathcal{L}}_{(\text{ext})} = 2\operatorname{tr}_c[J^\mu \hat{A}_\mu] \quad (4.6)$$

are contributions from the quark field  $\hat{\psi}_f$  of flavor  $f$ , the gluon field  $\hat{A}_\mu$ , the gauge fixing term, the ghost fields  $\hat{c}, \hat{\bar{c}}$ , and a classical external source  $J^\mu$ , respectively.  $\hat{\vartheta}$  is the gauge fixing function as was introduced in Eq. (3.6).

### Cartan-Weyl basis of $SU(3)$

We expand the color space by the Cartan-Weyl basis  $\{H_\alpha, E_A, E_A^\dagger\}$ , instead of the usual Gell-Mann matrices  $\{\lambda_a\}$ , so as to avoid some complexities coming from the non-Abelian algebra of  $SU_c(N_c = 3)$ ,

The Cartan-Weyl basis of  $SU_c(N_c)$  is a generalization of the ladder operators in  $SU_c(N_c = 2)$ . The Cartan-Weyl basis consists of Abelian generators of  $SU_c(N_c = 3)$  which belongs to the Cartan subalgebra  $H_\alpha$  ( $\alpha = 1, \dots, N_c - 1$ ) and non-Abelian generators  $E_A$  ( $A = 1, \dots, N_c(N_c - 1)/2$ ) that are eigen-generators of  $H_\alpha$  as  $[H_\alpha, E_A] = v_{\alpha,A} E_A$  (where  $v_{\alpha,A}$  is the so-called root vector). The choice of a Cartan-Weyl basis is not unique, but it is convenient here to choose

$$\begin{aligned} H_1 \equiv \lambda_3 &= \frac{1}{2} \begin{pmatrix} 1 & 0 & 0 \\ 0 & -1 & 0 \\ 0 & 0 & 0 \end{pmatrix}, \\ H_2 \equiv \lambda_8 &= \frac{1}{2\sqrt{3}} \begin{pmatrix} 1 & 0 & 0 \\ 0 & 1 & 0 \\ 0 & 0 & -2 \end{pmatrix}, \\ E_1 \equiv \frac{\lambda_6 + i\lambda_7}{2} &= \frac{1}{\sqrt{2}} \begin{pmatrix} 0 & 0 & 0 \\ 0 & 0 & 1 \\ 0 & 0 & 0 \end{pmatrix}, \\ E_2 \equiv \frac{\lambda_4 - i\lambda_5}{2} &= \frac{1}{\sqrt{2}} \begin{pmatrix} 0 & 0 & 0 \\ 0 & 0 & 0 \\ 1 & 0 & 0 \end{pmatrix}, \\ E_3 \equiv \frac{\lambda_1 + i\lambda_2}{2} &= \frac{1}{\sqrt{2}} \begin{pmatrix} 0 & 1 & 0 \\ 0 & 0 & 0 \\ 0 & 0 & 0 \end{pmatrix}. \end{aligned} \quad (4.7)$$

These matrices satisfy the following algebra:

$$\begin{aligned} \operatorname{tr}_c[H_\alpha H_\beta] &= \frac{\delta_{\alpha\beta}}{2}, \\ \operatorname{tr}_c[E_A E_B^\dagger] &= \frac{\delta_{AB}}{2}, \\ \operatorname{tr}_c[H_\alpha E_A] &= \operatorname{tr}_c[E_A E_B] = 0, \end{aligned} \quad (4.8)$$

and

$$\begin{aligned}
[H_\alpha, H_\beta] &= 0, \\
[H_\alpha, E_A] &= v_{\alpha,A} E_A, \\
[E_A, E_B] &= \sum_C \frac{\epsilon_{ABC}}{\sqrt{2}} E_C^\dagger, \\
[E_A, E_B^\dagger] &= \delta_{AB} \sum_\alpha v_{\alpha,A} H_\alpha,
\end{aligned} \tag{4.9}$$

where  $\epsilon_{ABC}$  is the completely anti-symmetric tensor normalized by  $\epsilon_{123} = 1$ . The root vector  $v_{\alpha,A}$  is given by

$$\begin{aligned}
v_{\alpha,1} &= (H_\alpha)_{22} - (H_\alpha)_{33} = \begin{pmatrix} -1/2 \\ \sqrt{3}/2 \end{pmatrix}_\alpha, \\
v_{\alpha,2} &= (H_\alpha)_{33} - (H_\alpha)_{11} = \begin{pmatrix} -1/2 \\ -\sqrt{3}/2 \end{pmatrix}_\alpha, \\
v_{\alpha,3} &= (H_\alpha)_{11} - (H_\alpha)_{22} = \begin{pmatrix} 1 \\ 0 \end{pmatrix}_\alpha.
\end{aligned} \tag{4.10}$$

### Abelian dominance assumption

As in the Yang-Mills study (see Chapter 3), let us assume the Abelian dominance for simplicity. We neglect non-Abelian components  $\propto E_A, E_A^\dagger$  in the classical current  $J^\mu$  and the classical gauge field  $\langle \hat{A}_\mu \rangle$ , and write

$$J_\mu(x) = \bar{J}_\mu(x) \sum_\alpha w_\alpha H_\alpha, \quad \langle \hat{A}_\mu(x) \rangle = \bar{A}_\mu(x) \sum_\alpha w_\alpha H_\alpha. \tag{4.11}$$

In contrast to the  $SU_c(N_c = 2)$  case, as  $SU_c(N_c = 3)$  has rank  $N_c - 1 = 2$ , we have two weight factors  $w_1, w_2$  that characterize the color orientation of the Abelian current  $J^\mu$  and gauge field  $\langle \hat{A}_\mu \rangle$ .

### expansion around a classical field

We decompose the total gauge field  $\hat{A}_\mu$  and the ghost fields  $\hat{c}, \hat{\bar{c}}$  into the Abelian classical field  $\langle \hat{A}_\mu \rangle = \bar{A}_\mu \sum_\alpha w_\alpha H_\alpha$  and quantum fluctuations around it,  $\hat{a}_{\alpha,\mu}, \hat{\mathcal{A}}_{A,\mu}, \begin{pmatrix} \hat{c} \\ \hat{c} \end{pmatrix}_A, \begin{pmatrix} \hat{\bar{c}} \\ \hat{\bar{c}} \end{pmatrix}_A$  as

$$\hat{A}_\mu = \sum_\alpha (w_\alpha \bar{A}_\mu + \hat{a}_{\alpha,\mu}) H_\alpha + \sum_A \left[ \hat{\mathcal{A}}_{A,\mu} E_A + \hat{\mathcal{A}}_{A,\mu}^\dagger E_A^\dagger \right], \tag{4.12}$$

$$\begin{pmatrix} \hat{c} \\ \hat{\bar{c}} \end{pmatrix} = \sum_\alpha \begin{pmatrix} \hat{C}_\alpha \\ \hat{\bar{C}}_\alpha \end{pmatrix} H_\alpha + \sum_A \left[ \begin{pmatrix} \hat{C}_A \\ \hat{\bar{C}}_A \end{pmatrix} E_A + \begin{pmatrix} \hat{C}_A^\dagger \\ \hat{\bar{C}}_A^\dagger \end{pmatrix} E_A^\dagger \right]. \tag{4.13}$$

### gauge fixing and ghost term

Under the Abelian dominance approximation, it is convenient to fix the gauge along the Abelian direction of the gauge field  $2\text{tr}_c[H_\alpha \hat{A}_\mu] = w_\alpha \bar{A}_\mu + \hat{a}_{\alpha,\mu}$ . Namely, we consider the following gauge fixing function  $\hat{v}$ :

$$\hat{v} = \sum_{\alpha} \partial^\mu (w_\alpha \bar{A}_\mu + \hat{a}_{\alpha,\mu}) H_\alpha + \sum_A \left[ \left( \partial_\mu + ig \sum_{\alpha} v_{\alpha,A} (w_\alpha \bar{A}_\mu + \hat{a}_{\alpha,\mu}) \right) \hat{\mathcal{A}}_A^\mu E_A + (\text{h.c.}) \right]. \quad (4.14)$$

Under this choice of the gauge fixing function, the gauge fixing Lagrangian  $\hat{\mathcal{L}}_{(\text{GF})}$  and the ghost Lagrangian  $\hat{\mathcal{L}}_{(\text{FP})}$  read

$$\begin{aligned} \hat{\mathcal{L}}_{(\text{GF})} = & -\frac{1}{2} (\partial^\mu \bar{A}_\mu)^2 \\ & - \sum_{\alpha} w_{\alpha} (\partial^\mu \hat{a}_{\alpha,\mu}) (\partial^\nu \bar{A}_\nu) \\ & - \frac{1}{2} \sum_{\alpha} (\partial^\mu \hat{a}_{\alpha,\mu})^2 - \sum_A |D_{A,\mu} \hat{\mathcal{A}}_A^\mu|^2 \\ & - \sum_{\alpha} a_{\alpha,\mu} \sum_A ig v_{\alpha,A} \left[ (D_{A,\nu} \hat{\mathcal{A}}_A^\nu)^\dagger \hat{\mathcal{A}}_A^\mu - \hat{\mathcal{A}}_A^{\mu\dagger} (D_{A,\nu} \hat{\mathcal{A}}_A^\nu) \right] \\ & - g^2 \sum_{\alpha\beta} \sum_A v_{\alpha,A} v_{\beta,A} \hat{a}_{\alpha,\mu} \hat{a}_{\beta,\nu} \hat{\mathcal{A}}_A^\mu \hat{\mathcal{A}}_A^{\nu\dagger}, \end{aligned} \quad (4.15)$$

$$\begin{aligned} \hat{\mathcal{L}}_{(\text{FP})} = & i \sum_{\alpha} \hat{C}_\alpha \partial_\mu \partial^\mu \hat{C}_\alpha + i \sum_A \left[ \hat{C}_A^\dagger (D_{A,\mu} D_A^\mu \hat{C}_A) - (D_{A,\mu} D_A^\mu \hat{C}_A)^\dagger \hat{C}_A \right] \\ & - g \sum_{\alpha} \sum_A v_{\alpha,A} \left[ 2a_{\alpha,\mu} \left( \hat{C}_A^\dagger (D_A^\mu \hat{C}_A) + (D_A^\mu \hat{C}_A)^\dagger \hat{C}_A \right) + (\partial^\mu \hat{a}_{\alpha,\mu}) (\hat{C}_A^\dagger \hat{C}_A + \hat{C}_A^\dagger \hat{C}_A) \right] \\ & - g \sum_{\alpha} \sum_A v_{\alpha,A} \left[ \hat{\mathcal{A}}_{A,\mu} \hat{C}_\alpha (D_A^\mu \hat{C}_A)^\dagger - \hat{\mathcal{A}}_{A,\mu}^\dagger \hat{C}_\alpha (D_A^\mu \hat{C}_A) \right. \\ & \quad \left. + (D_A^\mu \hat{\mathcal{A}}_{A,\mu})^\dagger (\hat{C}_A \hat{C}_\alpha - \hat{C}_\alpha \hat{C}_A) - (D_A^\mu \hat{\mathcal{A}}_{A,\mu}) (\hat{C}_A^\dagger \hat{C}_\alpha - \hat{C}_\alpha^\dagger \hat{C}_A) \right] \\ & + g \sum_{ABC} \frac{\epsilon_{ABC}}{\sqrt{2}} \left[ (D_A^\mu (\hat{\mathcal{A}}_{B,\mu}^\dagger \hat{C}_C^\dagger))^\dagger \hat{C}_A + \hat{C}_A^\dagger (D_A^\mu (\hat{\mathcal{A}}_{B,\mu}^\dagger \hat{C}_C^\dagger)) \right] \\ & - ig^2 \sum_{\alpha} \sum_{AB} v_{\alpha,A} v_{\alpha,B} \left[ \hat{\mathcal{A}}_A^\mu \hat{\mathcal{A}}_{B,\mu} \hat{C}_A^\dagger \hat{C}_B^\dagger - \hat{\mathcal{A}}_A^\mu \hat{\mathcal{A}}_{B,\mu}^\dagger (\hat{C}_A^\dagger \hat{C}_B - \hat{C}_A \hat{C}_B) + \hat{\mathcal{A}}_A^{\mu\dagger} \hat{\mathcal{A}}_{B,\mu}^\dagger \hat{C}_A \hat{C}_B \right] \\ & + ig^2 \sum_{\alpha\beta} \sum_A v_{\alpha,A} v_{\beta,A} (\hat{a}_{\alpha,\mu} \hat{a}_{\beta}^\mu) (\hat{C}_A^\dagger \hat{C}_A - \hat{C}_A^\dagger \hat{C}_A) \\ & + ig^2 \sum_{\alpha\beta} \sum_A v_{\alpha,A} v_{\beta,A} a_{\beta}^\mu \left[ \hat{\mathcal{A}}_{A,\mu}^\dagger \hat{C}_A \hat{C}_\alpha + \hat{\mathcal{A}}_{A,\mu} \hat{C}_\alpha^\dagger \hat{C}_\alpha \right] \\ & - ig^2 \sum_{\alpha} \sum_{ABC} \frac{\epsilon_{ABC}}{\sqrt{2}} v_{\alpha,A} a_{\alpha}^\mu \left[ \hat{\mathcal{A}}_{B,\mu} \hat{C}_C \hat{C}_A - \hat{\mathcal{A}}_{B,\mu}^\dagger \hat{C}_A^\dagger \hat{C}_C^\dagger \right]. \end{aligned} \quad (4.16)$$

### 4.1.2 assumptions on the system

In addition to the Abelian dominance assumption (4.11), we furthermore assume the same three assumptions made in the previous studies (see Section 2.1.2 and 3.1.2): (i) Homogeneity in space by assuming the classical gauge field  $\bar{A}_\mu$  is given by

$$\bar{A}^\mu(x) = (0, 0, 0, \bar{A}(t)) = (0, 0, 0, - \int_{-\infty}^t dt' \bar{E}(t')); \quad (4.17)$$

(ii) Vacuum initial condition  $|\text{state}; \text{in}\rangle = |\text{vac}; \text{in}\rangle$ ; and (iii) Adiabatic hypothesis by requiring  $\partial_t \bar{E} \xrightarrow{t \rightarrow \pm\infty} 0$ .

### 4.1.3 mean field and massless approximation

The QCD Lagrangian (4.1) is so complicated to evaluate as it is. As a workaround of this difficulty, we again apply the mean field approximation (see Section 2.1.3 and 3.1.3) and the massless approximation (see Section 3.1.5) as the first study of the Schwinger mechanism in QCD including backreaction effects.

#### Lagrangian

By applying the two approximations, the QCD Lagrangian (4.1) is approximated as

$$\begin{aligned} \hat{\mathcal{L}}_{\text{QCD}} \rightarrow & \hat{\psi}_{f,i} [i\hat{\not{D}} - q_i^{(\text{fund.})} \bar{A} - m_f] \hat{\psi}_{f,i} \\ & - \frac{1}{4} \bar{F}_{\mu\nu} \bar{F}^{\mu\nu} - \frac{1}{2} (\partial_\mu \bar{A}^\mu)^2 + \bar{J}^\mu \bar{A}_\mu \\ & - \sum_\alpha w_\alpha (\partial^\mu \hat{a}_{\alpha,\mu}) (\partial^\nu \bar{A}_\nu) - \frac{1}{2} \bar{F}^{\mu\nu} \sum_\alpha w_\alpha \hat{f}_{\alpha,\mu\nu} \\ & \quad + \sum_\alpha \hat{a}_{\alpha,\mu} \left[ \langle \hat{j}_\alpha^\mu \rangle + w_\alpha \bar{J}_\alpha^\mu \right] - g \sum_{\alpha,A} v_{\alpha,A} \partial^\mu \left[ \hat{a}_{\alpha,\mu} \langle \hat{\mathcal{C}}_A^\dagger \hat{\mathcal{C}}_A + \hat{\mathcal{C}}_A^\dagger \hat{\mathcal{C}}_A \rangle \right] \\ & - \frac{1}{4} \sum_\alpha \hat{f}_{\alpha,\mu\nu} \hat{f}_\alpha^{\mu\nu} - \frac{1}{2} \sum_\alpha (\partial^\mu \hat{a}_{\alpha,\mu})^2 \\ & - \frac{1}{2} \sum_A \hat{\mathcal{F}}_A^{\mu\nu\dagger} \hat{\mathcal{F}}_{A,\mu\nu} - \sum_A |\bar{D}_{A,\mu} \hat{\mathcal{A}}_A^\mu|^2 \\ & + i \sum_\alpha \hat{\mathcal{C}}_\alpha \partial_\mu \partial^\mu \hat{\mathcal{C}}_\alpha + i \sum_A \hat{\mathcal{C}}_A^\dagger [\bar{D}_{A,\mu} \bar{D}_A^\mu] \hat{\mathcal{C}}_A - i \sum_A \left( [\bar{D}_{A,\mu} \bar{D}_A^\mu] \hat{\mathcal{C}}_A \right)^\dagger \hat{\mathcal{C}}_A, \quad (4.18) \end{aligned}$$

where the color indices  $i, j = 1, \dots, N_c$  for the fundamental representation (quarks  $\hat{\psi}_{f,i}$ ) are explicitly written.

$D_{A,\mu}$  is the covariant derivative for the adjoint representations with respect to the classical gauge field  $\bar{A}_\mu$  given by

$$\bar{D}_{A,\mu} \equiv \partial_\mu + iq_A^{(\text{ad.})} \bar{A}_\mu. \quad (4.19)$$

Here,  $q_A^{(\text{ad.})}$  represents an effective color charge for the adjoint presentations (gluons  $\hat{\mathcal{A}}_{A,\mu}, \hat{\mathcal{A}}_{A,\mu}^\dagger$  and ghosts  $\hat{\mathcal{C}}_A, \hat{\mathcal{C}}_A$ ) given by

$$q_A^{(\text{ad.})} \equiv g \sum_{\alpha} w_{\alpha} v_{\alpha,A} = g \begin{pmatrix} \cos(\theta + 4\pi/3) \\ \cos(\theta + 2\pi/3) \\ \cos \theta \end{pmatrix}_A, \quad (4.20)$$

where the ‘‘color angle’’  $\theta$ , which characterizes the color orientation of the classical gauge field  $\langle \hat{A}_{\mu} \rangle$ , is defined by

$$\frac{w_2}{w_1} \equiv \tan \theta. \quad (4.21)$$

On the other hand,  $q_i^{(\text{fund.})}$  represents an effective color charge for the fundamental representations, and is given by

$$q_i^{(\text{fund.})} \equiv g \sum_{\alpha} w_{\alpha} (H_{\alpha})_{ii} = \frac{-1}{\sqrt{3}} g \begin{pmatrix} \sin(\theta + 4\pi/3) \\ \sin(\theta + 2\pi/3) \\ \sin \theta \end{pmatrix}_i. \quad (4.22)$$

Although these two charges  $q_A^{(\text{ad.})}, q_i^{(\text{fund.})}$  are gauge-dependent, the squared sum of the charges are gauge-independent as [137, 157, 158] as

$$\begin{aligned} \sum_A |q_A^{(\text{ad.})}|^2 &= \frac{g^2 N_c}{2} = \frac{3g^2}{2}, \\ \sum_i |q_i^{(\text{fund.})}|^2 &= \frac{g^2}{2}. \end{aligned} \quad (4.23)$$

The squared sum of  $q_A^{(\text{ad.})}$  is larger than that of  $q_i^{(\text{fund.})}$ , intuitively because there are (approximately)  $N_c$  times as many colors of gluons ( $N_c(N_c - 1)$ ) as those of quarks ( $N_c$ ).

$\hat{f}_{\alpha,\mu\nu}$  and  $\hat{\mathcal{F}}_{A,\mu\nu}$  are fluctuation part of Abelian and non-Abelian components of the total field strength tensor  $\hat{F}_{\mu\nu}$ , respectively, given by

$$\begin{aligned} \hat{f}_{\alpha,\mu\nu} &\equiv \partial_{\mu} \hat{a}_{\alpha,\nu} - \partial_{\nu} \hat{a}_{\alpha,\mu}, \\ \hat{\mathcal{F}}_{A,\mu\nu} &\equiv \bar{D}_{A,\mu} \hat{\mathcal{A}}_{A,\nu} - \bar{D}_{A,\nu} \hat{\mathcal{A}}_{A,\mu}, \end{aligned} \quad (4.24)$$

which are  $SU_c(N_c = 3)$  extensions of Eq. (3.16).

$\langle : \hat{j}_{\alpha}^{\mu} : \rangle$  is a vacuum expectation value of the color current associated with a global color rotation around the Abelian  $H_{\alpha}$ -directions, whose explicit expression is given in Eq. (4.27). We again take the normal ordering  $\langle \hat{\bullet} \rangle \rightarrow \langle : \hat{\bullet} : \rangle$  to eliminate the unwanted vacuum divergences (see Section 2.1.5).

### conserved quantities

The approximated Lagrangian (4.18) has certain symmetries and conserved currents associated with them.

#### color current $\hat{j}_\alpha^\mu$

The approximated Lagrangian (4.18) is invariant under a global color rotation around the Abelian  $H_\alpha$ -directions of the color space:

$$\begin{aligned}\hat{\psi}_f &\rightarrow U\hat{\psi}_f, \\ \hat{A}_\mu &\rightarrow U\hat{A}_\mu U^\dagger, \\ \begin{pmatrix} \hat{c} \\ \hat{\bar{c}} \end{pmatrix} &\rightarrow U \begin{pmatrix} \hat{c} \\ \hat{\bar{c}} \end{pmatrix} U^\dagger,\end{aligned}\tag{4.25}$$

where

$$U = \exp\left[-ig \sum_\alpha \theta_\alpha H_\alpha\right].\tag{4.26}$$

The conserved quantity associated with this symmetry is the color current (in the  $H_\alpha$ -directions)  $\hat{j}_\alpha^\mu$ . From the Noether theorem [143], one can compute its vacuum expectation value  $\langle : \hat{j}_\alpha^\mu : \rangle$  as

$$\begin{aligned}\langle : \hat{j}_\alpha^\mu : \rangle &= g \sum_f \sum_i (H_\alpha)_{ii} \langle : \hat{\psi}_{f,i} \gamma^\mu \hat{\psi}_{f,i} : \rangle \\ &\quad ig \sum_A v_{\alpha,A} \left\langle : \hat{\mathcal{A}}_{A,\nu}^\dagger \left( \bar{D}_A^\mu \hat{\mathcal{A}}_A^\nu \right) - \left( \bar{D}_A^\mu \hat{\mathcal{A}}_A^\nu \right)^\dagger \hat{\mathcal{A}}_{A,\nu} : \right\rangle \\ &\quad - g \sum_A v_{\alpha,A} \left\langle : \hat{\mathcal{C}}_A^\dagger \left( \bar{D}_{A,\mu} \hat{\mathcal{C}}_A \right) + \left( \bar{D}_{A,\mu} \hat{\mathcal{C}}_A \right)^\dagger \hat{\mathcal{C}}_A - \left( \bar{D}_{A,\mu} \hat{\mathcal{C}}_A \right)^\dagger \hat{\mathcal{C}}_A - \hat{\mathcal{C}}_A^\dagger \left( \bar{D}_{A,\mu} \hat{\mathcal{C}}_A \right) : \right\rangle.\end{aligned}\tag{4.27}$$

The conservation law for  $\langle : \hat{j}_\alpha^\mu : \rangle$  is

$$0 = \partial_\mu \langle : \hat{j}_\alpha^\mu : \rangle.\tag{4.28}$$

#### symmetric energy-momentum tensor $\hat{T}^{\mu\nu}$

The translational invariance of the approximated Lagrangian (4.18) assures us that the symmetric energy-momentum tensor  $\hat{T}^{\mu\nu}$  defined by Eq. (2.8) is conserved. The vacuum expectation

value of the symmetric energy-momentum tensor  $\langle : \hat{T}^{\mu\nu} : \rangle$  is

$$\begin{aligned}
\langle : \hat{T}_{\mu\nu} : \rangle = & \eta^{\mu\nu} \left[ \frac{1}{4} \bar{F}^{\rho\sigma} \bar{F}_{\rho\sigma} - \frac{1}{2} (\partial_\lambda \bar{A}^\lambda)^2 - \bar{A}^\rho \partial_\rho \partial_\sigma \bar{A}^\sigma \right] - [\bar{F}^\mu{}_\lambda \bar{F}^{\nu\lambda} - \bar{A}^\mu \partial^\nu \partial_\lambda \bar{A}^\lambda - \bar{A}^\nu \partial^\mu \partial_\lambda \bar{A}^\lambda] \\
& + \eta^{\mu\nu} \sum_\alpha \text{Re} \left\langle : \frac{1}{4} \hat{f}_\alpha^{\rho\sigma} \hat{f}_{\alpha,\rho\sigma} - \frac{1}{2} (\partial_\lambda \hat{a}_\alpha^\lambda)^2 - \hat{a}_\alpha^\rho \partial_\rho \partial_\sigma \hat{a}_\alpha^\sigma : \right\rangle \\
& \quad - \sum_\alpha \text{Re} \left\langle : \hat{f}_{\alpha,\lambda}{}^\mu \hat{f}_\alpha{}^{\lambda\nu} - \hat{a}_\alpha^\mu \partial^\nu \partial_\lambda \hat{a}_\alpha^\lambda - \hat{a}_\alpha^\nu \partial^\mu \partial_\lambda \hat{a}_\alpha^\lambda : \right\rangle \\
& + 2 \times \left( \eta^{\mu\nu} \sum_A \text{Re} \left\langle : \frac{1}{4} \hat{\mathcal{F}}_{A,\rho\sigma}^\dagger \hat{\mathcal{F}}_A{}^{\rho\sigma} - \frac{1}{2} \left| \bar{D}_{A,\lambda} \hat{\mathcal{A}}_A{}^\lambda \right|^2 - \hat{\mathcal{A}}_A{}^{\rho\dagger} (\bar{D}_{A,\rho} \bar{D}_{A,\sigma} \hat{\mathcal{A}}_A{}^\sigma) : \right\rangle \right. \\
& \quad \left. - \sum_A \text{Re} \left\langle : \hat{\mathcal{F}}_{A,\lambda}{}^{\mu\dagger} \hat{\mathcal{F}}_A{}^{\lambda\nu} - \hat{\mathcal{A}}_A{}^{\mu\dagger} (\bar{D}_A{}^\nu \bar{D}_{A,\lambda} \hat{\mathcal{A}}_A{}^\lambda) - \hat{\mathcal{A}}_A{}^{\nu\dagger} (\bar{D}_A{}^\mu \bar{D}_{A,\lambda} \hat{\mathcal{A}}_A{}^\lambda) : \right\rangle \right) \\
& + \sum_\alpha \text{Re} \left\langle : i \times \left[ \eta^{\mu\nu} (\partial_\lambda \hat{C}_\alpha) (\partial^\lambda \hat{C}_\alpha) - (\partial^\mu \hat{C}_\alpha) (\partial^\nu \hat{C}_\alpha) - (\partial^\nu \hat{C}_\alpha) (\partial^\mu \hat{C}_\alpha) \right] : \right\rangle \\
& + 2 \times \sum_A \text{Re} \left\langle : i \left[ \eta^{\mu\nu} (\bar{D}_{A,\lambda} \hat{C}_A)^\dagger (\bar{D}_A{}^\lambda \hat{C}_A) - (\bar{D}_A{}^\mu \hat{C}_A)^\dagger (\bar{D}_A{}^\nu \hat{C}_A) - (\bar{D}_A{}^\nu \hat{C}_A)^\dagger (\bar{D}_A{}^\mu \hat{C}_A) \right] : \right\rangle,
\end{aligned} \tag{4.29}$$

which is conserved as

$$\partial_\mu \langle : \hat{T}^{\mu\nu} : \rangle = \bar{J}_\mu \bar{F}^{\mu\nu} + \bar{A}^\nu \partial_\mu \bar{J}^\mu. \tag{4.30}$$

We define the energy density and the transverse/longitudinal pressure of the system by the diagonal components of the symmetric energy-momentum tensor as

$$\begin{aligned}
\langle : \hat{\epsilon} : \rangle & \equiv \langle : \hat{T}^{tt} : \rangle, \\
\langle : \hat{P}_\perp : \rangle & \equiv \frac{\langle : \hat{T}^{xx} + \hat{T}^{yy} : \rangle}{2}, \\
\langle : \hat{P}_z : \rangle & \equiv \langle : \hat{T}^{zz} : \rangle.
\end{aligned} \tag{4.31}$$

## equations of motion

From the approximated Lagrangian (4.18), one obtains a set of linear equations of motion:

$$\sum_\alpha w_\alpha \langle : \hat{j}_{\alpha,\mu} : \rangle + \bar{J}_\mu = \partial^\nu \partial_\nu \bar{A}_\mu, \tag{4.32}$$

$$0 = [i\hat{\not{D}} - q_i^{(\text{fund.})} \bar{A} - m_f] \hat{\psi}_{f,i}, \tag{4.33}$$

$$0 = \partial^\mu \partial_\mu \hat{a}_{\alpha,\sigma}, \tag{4.34}$$

$$0 = \bar{D}_A{}^\mu \bar{D}_{A,\mu} \hat{\mathcal{A}}_{A,\sigma}, \tag{4.35}$$

$$0 = \partial^\mu \partial_\mu \hat{C}_\alpha, \tag{4.36}$$

$$0 = \bar{D}_A{}^\mu \bar{D}_{A,\mu} \hat{C}_A, \tag{4.37}$$

As the fluctuations  $\hat{a}_{\alpha,\mu}, \hat{C}_\alpha$  are chargeless and do not couple to the classical gauge field  $\bar{A}_\mu$ , no particle production occurs for these fluctuations. Hence, we do not consider them in the following. The first equation (4.32) describes the backreaction effects from the produced particles. For a spatially homogeneous system as was assumed in assumption (i) in Section 4.1.2, it reads

$$0 = \langle : \hat{j}_{\alpha,t} : \rangle = \langle : \hat{j}_{\alpha,x} : \rangle = \langle : \hat{j}_{\alpha,y} : \rangle, \\ -\frac{d\bar{E}}{dt} = \sum_{\alpha} w_{\alpha} \langle : \hat{j}_{\alpha}^z : \rangle. \quad (4.38)$$

#### 4.1.4 canonical quantization and particle production

Since the equations of motion (4.33)-(4.37) are linear in the quantum fluctuations, one can apply the canonical quantization procedure to compute the number of particles produced from the classical gauge field  $\bar{A}_\mu$ . The canonical quantization procedure can be done in completely the same manner as that for electrons (or fermions) in Section 2.1.4 and that for gluons and ghosts (or bosons) in Section 3.1.4. Hence, we do not repeat the details of the canonical quantization procedure, and we briefly write down results only.

##### quarks

We Fourier expand the quark field operator  $\hat{\psi}_i$  as

$$\hat{\psi}_{f,i} = \sum_s \int d^3\mathbf{p} \left[ +\psi_{f,i,\mathbf{p},s}^{(t)} \hat{a}_{f,i,\mathbf{p},s}(t) + -\psi_{f,i,\mathbf{p},s}^{(t)} \hat{b}_{f,i,-\mathbf{p},s}^\dagger(t) \right], \quad (4.39)$$

where

$$\begin{pmatrix} +\psi_{f,i,\mathbf{p},s}^{(t)} \\ -\psi_{f,i,\mathbf{p},s}^{(t)} \end{pmatrix} \equiv \begin{pmatrix} u_{\mathbf{p}-q_i^{(\text{fund.})}} \bar{\mathbf{A}}(t) \exp \left[ -i \int_{-\infty}^t \omega_{\mathbf{p}-q_i^{(\text{fund.})}} \bar{\mathbf{A}}(t) dt \right] \\ v_{-\mathbf{p}+q_i^{(\text{fund.})}} \bar{\mathbf{A}}(t) \exp \left[ +i \int_{-\infty}^t \omega_{\mathbf{p}-q_i^{(\text{fund.})}} \bar{\mathbf{A}}(t) dt \right] \end{pmatrix} \quad (4.40)$$

denotes positive/negative frequency mode functions at an intermediate time  $-\infty < t < \infty$ . The normalization condition for the mode functions is

$$(\pm \psi_{f,i,\mathbf{p},s}^{(t)} | \pm \psi_{f,i,\mathbf{p},s'}^{(t)})_{\text{F}} = \delta_{ss'}, \quad (\pm \psi_{f,i,\mathbf{p},s}^{(t)} | \mp \psi_{f,i,\mathbf{p},s'}^{(t)})_{\text{F}} = 0. \quad (4.41)$$

By imposing canonical commutation relations

$$\{\hat{\psi}_{f,i}(t, \mathbf{x}), \hat{\psi}_{f',i'}^\dagger(t, \mathbf{x}')\} = \delta_{ff'} \delta_{ii'} \delta^3(\mathbf{x} - \mathbf{x}'), \quad \{\hat{\psi}_{f,i}(t, \mathbf{x}), \hat{\psi}_{f',i'}(t, \mathbf{x}')\} = 0, \quad (4.42)$$

one obtains anti-commutation relations for the annihilation operators  $\hat{a}_{f,i,\mathbf{p},s}, \hat{b}_{f,i,\mathbf{p},s}$  as

$$\{\hat{a}_{f,i,\mathbf{p},s}, \hat{a}_{f',i',\mathbf{p}',s'}^\dagger\} = \{\hat{b}_{f,i,\mathbf{p},s}, \hat{b}_{f',i',\mathbf{p}',s'}^\dagger\} = \delta_{ff'} \delta_{ii'} \delta_{ss'} \delta^3(\mathbf{p} - \mathbf{p}'), \quad (\text{others}) = 0. \quad (4.43)$$

The vacuum at an intermediate time  $|\text{vac};t\rangle$  is a state such that it is annihilated by the annihilation operators  $\hat{a}_{f,i,\mathbf{p},s}, \hat{b}_{f,i,\mathbf{p},s}$  as

$$0 = \hat{a}_{f,i,\mathbf{p},s} |\text{vac};t\rangle = \hat{b}_{f,i,\mathbf{p},s} |\text{vac};t\rangle \quad (4.44)$$

for all values of  $f, i, \mathbf{p}, s$ .

The positive/negative frequency mode functions  $\pm\psi_{f,i,\mathbf{p},s}^{(t)}$ , the annihilation operators  $\hat{a}_{f,i,\mathbf{p},s}, \hat{b}_{f,i,\mathbf{p},s}$ , and the vacuum  $|\text{vac};t\rangle$  at an intermediate time smoothly approach the correct mode functions  $\pm\psi_{\mathbf{p},s}^{(\text{as})}$ , the annihilation operators  $\hat{a}_{f,i,\mathbf{p},s}^{(\text{in})}, \hat{b}_{f,i,\mathbf{p},s}^{(\text{in})}$ , and the vacuum  $|\text{vac};\text{as}\rangle$  at the asymptotic times (as = in/out) in the limit of  $t \rightarrow \pm\infty$  as

$$\pm\psi_{f,i,\mathbf{p},s}^{(t)} \xrightarrow{t \rightarrow -\infty} \pm\psi_{f,i,\mathbf{p},s}^{(\text{in})}, \quad \pm\psi_{f,i,\mathbf{p},s}^{(t)} \xrightarrow{t \rightarrow \infty} \pm\psi_{f,i,\mathbf{p},s}^{(\text{out})}, \quad (4.45)$$

$$\begin{pmatrix} \hat{a}_{f,i,\mathbf{p},s}^{(\text{in})} \\ \hat{b}_{f,i,\mathbf{p},s}^{(\text{in})} \end{pmatrix} = \lim_{t \rightarrow -\infty} \begin{pmatrix} \hat{a}_{f,i,\mathbf{p},s}(t) \\ \hat{b}_{f,i,\mathbf{p},s}(t) \end{pmatrix}, \quad \begin{pmatrix} \hat{a}_{f,i,\mathbf{p},s}^{(\text{out})} \\ \hat{b}_{f,i,\mathbf{p},s}^{(\text{out})} \end{pmatrix} = \lim_{t \rightarrow \infty} \begin{pmatrix} \hat{a}_{f,i,\mathbf{p},s}(t) \\ \hat{b}_{f,i,\mathbf{p},s}(t) \end{pmatrix}, \quad (4.46)$$

and

$$|\text{vac};t\rangle \xrightarrow{t \rightarrow -\infty} |\text{vac};\text{in}\rangle, \quad |\text{vac};t\rangle \xrightarrow{t \rightarrow \infty} |\text{vac};\text{out}\rangle. \quad (4.47)$$

The Bogoliubov transformation between the in-state annihilation operators  $\hat{a}_{f,i,\mathbf{p},s}^{(\text{in})}, \hat{b}_{f,i,\mathbf{p},s}^{(\text{in})}$  and those at intermediate times  $\hat{a}_{f,i,\mathbf{p},s}, \hat{b}_{f,i,\mathbf{p},s}$  are given by

$$\begin{pmatrix} \hat{a}_{f,i,\mathbf{p},s}(t) \\ \hat{b}_{f,i,-\mathbf{p},s}^\dagger(t) \end{pmatrix} = \begin{pmatrix} \alpha_{(\psi)f,i,\mathbf{p},s}(t) & \beta_{(\psi)f,i,\mathbf{p},s}(t) \\ -\beta_{(\psi)f,i,\mathbf{p},s}^*(t) & \alpha_{(\psi)f,i,\mathbf{p},s}^*(t) \end{pmatrix} \begin{pmatrix} \hat{a}_{f,i,\mathbf{p},s}^{(\text{in})} \\ \hat{b}_{f,i,-\mathbf{p},s}^{(\text{in})\dagger} \end{pmatrix}, \quad (4.48)$$

where

$$\alpha_{(\psi)f,i,\mathbf{p},s}(t) \equiv (+\psi_{f,i,\mathbf{p},s}^{(t)} | +\psi_{f,i,\mathbf{p},s}^{(\text{in})})_{\text{F}} = (-\psi_{f,i,\mathbf{p},s}^{(t)} | -\psi_{f,i,\mathbf{p},s}^{(\text{in})})_{\text{F}}^*, \quad (4.49)$$

$$\beta_{(\psi)f,i,\mathbf{p},s}(t) \equiv (+\psi_{f,i,\mathbf{p},s}^{(t)} | -\psi_{f,i,\mathbf{p},s}^{(\text{in})})_{\text{F}} = -(-\psi_{f,i,\mathbf{p},s}^{(t)} | +\psi_{f,i,\mathbf{p},s}^{(\text{in})})_{\text{F}}^*. \quad (4.50)$$

The Bogoliubov coefficients are normalized as

$$1 = |\alpha_{(\psi)f,i,\mathbf{p},s}(t)|^2 + |\beta_{(\psi)f,i,\mathbf{p},s}(t)|^2, \quad (4.51)$$

The number of produced quarks and anti-quarks are obtained as an in-vacuum  $|\text{vac};\text{in}\rangle$  expectation value of number operator  $\hat{a}_{i,f,\mathbf{p},s}^\dagger \hat{a}_{i,f,\mathbf{p},s}$  and  $\hat{b}_{i,f,\mathbf{p},s}^\dagger \hat{b}_{i,f,\mathbf{p},s}$ , respectively, as

$$\begin{aligned} \frac{d^6 N_{\text{q}}(i, f, \mathbf{p}, s; t)}{d\mathbf{p}^3 d\mathbf{x}^3} &= \frac{1}{V} \langle \hat{a}_{i,f,\mathbf{p},s}^\dagger \hat{a}_{i,f,\mathbf{p},s} \rangle = \frac{|\beta_{(\psi)i,f,\mathbf{p},s}|^2}{(2\pi)^3}, \\ \frac{d^6 N_{\bar{\text{q}}}(i, f, \mathbf{p}, s; t)}{d\mathbf{p}^3 d\mathbf{x}^3} &= \frac{1}{V} \langle \hat{b}_{i,f,\mathbf{p},s}^\dagger \hat{b}_{i,f,\mathbf{p},s} \rangle = \frac{|\beta_{(\psi)i,f,-\mathbf{p},s}|^2}{(2\pi)^3}. \end{aligned} \quad (4.52)$$

## gluons

By Fourier expanding the fluctuation  $\hat{\mathcal{A}}_{A,\mu}$  as

$$\hat{\mathcal{A}}_{A,\mu} = \sum_{\sigma} \int d^3\mathbf{p} \left[ +\mathcal{A}_{A,\sigma,\mathbf{p}}^{(t)} \hat{\mathbf{c}}_{A,\sigma,\mathbf{p}}(t) + -\mathcal{A}_{A,\sigma,\mathbf{p}}^{(t)} \hat{\mathbf{d}}_{A,\sigma,-\mathbf{p}}^{\dagger}(t) \right] \frac{e^{i\mathbf{p}\cdot\mathbf{x}}}{(2\pi)^{3/2}}, \quad (4.53)$$

where  $\epsilon_{\sigma,\mu}$  is the polarization vector introduced in Eq. (3.42). The positive/negative frequency mode functions for intermediate times  $\pm\mathcal{A}_{A,\sigma,\mathbf{p}}^{(t)}$  are defined by

$$\left( \frac{\pm\mathcal{A}_{A,\sigma,\mathbf{p}}^{(t_0)}}{d\pm\mathcal{A}_{A,\sigma,\mathbf{p}}^{(t_0)}/dt} \right) \equiv \left( \frac{1}{\sqrt{2|\mathbf{p} - q_A^{(\text{ad.})}\bar{\mathbf{A}}(t_0)|}} \right) \exp \left[ \mp i \int_{-\infty}^{t_0} |\mathbf{p} - q_A^{(\text{ad.})}\bar{\mathbf{A}}(t)| dt \right], \quad (4.54)$$

We normalize the mode functions  $\pm\mathcal{A}_{A,\sigma,\mathbf{p}}^{(t)}$  by

$$\sum_{\sigma'} \xi_{\sigma\sigma'} (\pm\mathcal{A}_{A,\sigma,\mathbf{p}}^{(t)} | \pm\mathcal{A}_{A,\sigma',\mathbf{p}}^{(t)})_{\text{B}} = \pm 1, \quad \sum_{\sigma'} \xi_{\sigma\sigma'} (\pm\mathcal{A}_{A,\sigma,\mathbf{p}}^{(t)} | \mp\mathcal{A}_{A,\sigma',\mathbf{p}}^{(t)})_{\text{B}} = 0. \quad (4.55)$$

We impose canonical commutation relations

$$\begin{aligned} [\hat{\mathcal{A}}_{A,\mu}(t, \mathbf{x}), \partial_t \hat{\mathcal{A}}_{B,\nu}^{\dagger}(t, \mathbf{x}')] &= -i\eta_{\mu\nu} \delta_{AB} \delta^3(\mathbf{x} - \mathbf{x}'), \\ [\hat{\mathcal{A}}_{A,\mu}(t, \mathbf{x}), \hat{\mathcal{A}}_{B,\nu}^{\dagger}(t, \mathbf{x}')] &= [\partial_t \hat{\mathcal{A}}_{A,\mu}(t, \mathbf{x}), \partial_t \hat{\mathcal{A}}_{B,\nu}(t, \mathbf{x}')] = 0, \end{aligned} \quad (4.56)$$

to obtain commutation relations for the intermediate annihilation operators  $\hat{\mathbf{c}}_{A,\sigma,\mathbf{p}}, \hat{\mathbf{d}}_{A,\sigma,\mathbf{p}}$  as

$$\begin{aligned} [\hat{\mathbf{c}}_{A,\sigma,\mathbf{p}}, \hat{\mathbf{c}}_{A',\sigma',\mathbf{p}'}^{\dagger}] &= [\hat{\mathbf{d}}_{A,\sigma,\mathbf{p}}, \hat{\mathbf{d}}_{A',\sigma',\mathbf{p}'}^{\dagger}] = \delta_{AA'} \xi_{\sigma\sigma'} \delta^3(\mathbf{p} - \mathbf{p}'), \\ (\text{others}) &= 0, \end{aligned} \quad (4.57)$$

where the indefinite metric  $\xi_{\sigma\sigma'}$  was introduced in Eq. (3.42).

The vacuum at an intermediate time  $|\text{vac};t\rangle$  is a state such that it is annihilated by the annihilation operators  $\hat{\mathbf{c}}_{A,\sigma,\mathbf{p}}, \hat{\mathbf{d}}_{A,\sigma,\mathbf{p}}$  as

$$0 = \hat{\mathbf{c}}_{A,\sigma,\mathbf{p}} |\text{vac};t\rangle = \hat{\mathbf{d}}_{A,\sigma,\mathbf{p}} |\text{vac};t\rangle \quad (4.58)$$

for all values of  $A, \sigma, \mathbf{p}$ .

The positive/negative frequency mode functions  $\pm\mathcal{A}_{A,\sigma,\mathbf{p}}^{(\text{as})}$ , the annihilation operators  $\hat{\mathbf{c}}_{A,\sigma,\mathbf{p}}^{(\text{as})}, \hat{\mathbf{d}}_{A,\sigma,\mathbf{p}}^{(\text{as})}$ , and the vacuum  $|\text{vac};\text{as}\rangle$  at the asymptotic times (as = in/out) are obtained by taking  $t \rightarrow \pm\infty$  limit of those at an intermediate time as

$$\pm\mathcal{A}_{A,\sigma,\mathbf{p}}^{(t)} \xrightarrow{t \rightarrow -\infty} \pm\mathcal{A}_{A,\sigma,\mathbf{p}}^{(\text{in})}, \quad \pm\mathcal{A}_{A,\sigma,\mathbf{p}}^{(t)} \xrightarrow{t \rightarrow \infty} \pm\mathcal{A}_{A,\sigma,\mathbf{p}}^{(\text{out})}, \quad (4.59)$$

$$\begin{pmatrix} \hat{\mathbf{c}}_{A,\sigma,\mathbf{p}}^{(\text{in})} \\ \hat{\mathbf{d}}_{A,\sigma,\mathbf{p}}^{(\text{in})} \end{pmatrix} = \lim_{t \rightarrow -\infty} \begin{pmatrix} \hat{\mathbf{c}}_{A,\sigma,\mathbf{p}}(t) \\ \hat{\mathbf{d}}_{A,\sigma,\mathbf{p}}(t) \end{pmatrix}, \quad \begin{pmatrix} \hat{\mathbf{c}}_{A,\sigma,\mathbf{p}}^{(\text{out})} \\ \hat{\mathbf{d}}_{A,\sigma,\mathbf{p}}^{(\text{out})} \end{pmatrix} = \lim_{t \rightarrow \infty} \begin{pmatrix} \hat{\mathbf{c}}_{A,\sigma,\mathbf{p}}(t) \\ \hat{\mathbf{d}}_{A,\sigma,\mathbf{p}}(t) \end{pmatrix}, \quad (4.60)$$

and

$$|\text{vac}; t\rangle \xrightarrow[t \rightarrow -\infty]{} |\text{vac}; \text{in}\rangle, \quad |\text{vac}; t\rangle \xrightarrow[t \rightarrow \infty]{} |\text{vac}; \text{out}\rangle. \quad (4.61)$$

The in-state annihilation operators  $\hat{\mathbf{c}}_{A,\sigma,\mathbf{p}}^{(\text{in})}$ ,  $\hat{\mathbf{d}}_{A,\sigma,\mathbf{p}}^{(\text{in})}$  and those at intermediate times  $\hat{c}_{\alpha,\sigma,\mathbf{p}}$ ,  $\hat{\mathbf{c}}_{A,\sigma,\mathbf{p}}$ ,  $\hat{\mathbf{d}}_{A,\sigma,\mathbf{p}}$  are not independent of each other, and their relationship can be expressed by the following Bogoliubov transformation:

$$\begin{pmatrix} \hat{\mathbf{c}}_{A,\sigma,\mathbf{p}}(t) \\ \hat{\mathbf{d}}_{A,\sigma,-\mathbf{p}}^\dagger(t) \end{pmatrix} = \begin{pmatrix} \alpha_{(\mathcal{A})A,\sigma,\mathbf{p}}(t) & \beta_{(\mathcal{A})A,\sigma,\mathbf{p}}(t) \\ \beta_{(\mathcal{A})A,\sigma,\mathbf{p}}^*(t) & \alpha_{(\mathcal{A})A,\sigma,\mathbf{p}}^*(t) \end{pmatrix} \begin{pmatrix} \hat{\mathbf{c}}_{A,\sigma,\mathbf{p}}^{(\text{in})} \\ \hat{\mathbf{d}}_{A,\sigma,-\mathbf{p}}^{(\text{in})\dagger} \end{pmatrix}, \quad (4.62)$$

where

$$\begin{aligned} \alpha_{(\mathcal{A})A,\sigma,\mathbf{p}}(t) &\equiv (+\mathcal{A}_{A,\sigma,\mathbf{p}}^{(t)} | +\mathcal{A}_{A,\sigma,\mathbf{p}}^{(\text{in})})_{\text{B}} = -(-\mathcal{A}_{A,\sigma,\mathbf{p}}^{(t)} | -\mathcal{A}_{A,\sigma,\mathbf{p}}^{(\text{in})})_{\text{B}}^* \\ &= \frac{i}{\sqrt{2|\mathbf{p} - q_A^{(\text{ad.})} \bar{\mathbf{A}}|}} \left[ \frac{d_+ \mathcal{A}_{A,\sigma,\mathbf{p}}^{(\text{in})}}{dt} - i|\mathbf{p} - q_A^{(\text{ad.})} \bar{\mathbf{A}} | +\mathcal{A}_{A,\sigma,\mathbf{p}}^{(\text{in})} \right] \exp \left[ +i \int_{-\infty}^t |\mathbf{p} - q_A^{(\text{ad.})} \bar{\mathbf{A}}| dt \right], \\ \beta_{(\mathcal{A})A,\sigma,\mathbf{p}}(t) &\equiv (+\mathcal{A}_{A,\sigma,\mathbf{p}}^{(t)} | -\mathcal{A}_{A,\sigma,\mathbf{p}}^{(\text{in})})_{\text{B}} = -(-\mathcal{A}_{A,\sigma,\mathbf{p}}^{(t)} | +\mathcal{A}_{A,\sigma,\mathbf{p}}^{(\text{in})})_{\text{B}}^* \\ &= \frac{i}{\sqrt{2|\mathbf{p} - q_A^{(\text{ad.})} \bar{\mathbf{A}}|}} \left[ \frac{d_- \mathcal{A}_{A,\sigma,\mathbf{p}}^{(\text{in})}}{dt} - i|\mathbf{p} - q_A^{(\text{ad.})} \bar{\mathbf{A}} | -\mathcal{A}_{A,\sigma,\mathbf{p}}^{(\text{in})} \right] \exp \left[ +i \int_{-\infty}^t |\mathbf{p} - q_A^{(\text{ad.})} \bar{\mathbf{A}}| dt \right]. \end{aligned} \quad (4.63)$$

The normalization condition for the Bogoliubov coefficients is

$$1 = |\alpha_{(\mathcal{A})A,\sigma,\mathbf{p}}(t)|^2 - |\beta_{(\mathcal{A})A,\sigma,\mathbf{p}}(t)|^2. \quad (4.64)$$

The number of produced gluons can be computed as an in-vacuum  $|\text{vac}; \text{in}\rangle$  expectation value of number operators  $\hat{\mathbf{c}}_{A,\sigma,\mathbf{p}}^\dagger \hat{\mathbf{c}}_{A,\sigma,\mathbf{p}}$  and  $\hat{\mathbf{d}}_{A,\sigma,\mathbf{p}}^\dagger \hat{\mathbf{d}}_{A,\sigma,\mathbf{p}}$  for charged gluons with the color charge  $q_A^{(\text{ad.})}$  and  $-q_A^{(\text{ad.})}$ , respectively, as

$$\begin{aligned} \frac{d^6 N_{\text{g}_+}(A, \sigma, \mathbf{p}; t)}{d\mathbf{p}^3 d\mathbf{x}^3} &= \frac{1}{V} \langle \hat{\mathbf{c}}_{A,\sigma,\mathbf{p}}^\dagger \hat{\mathbf{c}}_{A,\sigma,\mathbf{p}} \rangle = \begin{cases} 0 & (\sigma = 0, 3) \\ \frac{|\beta_{(\mathcal{A})A,\sigma,\mathbf{p}}|^2}{(2\pi)^3} & (\sigma = 1, 2) \end{cases} \\ \frac{d^6 N_{\text{g}_-}(A, \sigma, \mathbf{p}; t)}{d\mathbf{p}^3 d\mathbf{x}^3} &= \frac{1}{V} \langle \hat{\mathbf{d}}_{A,\sigma,\mathbf{p}}^\dagger \hat{\mathbf{d}}_{A,\sigma,\mathbf{p}} \rangle = \begin{cases} 0 & (\sigma = 0, 3) \\ \frac{|\beta_{(\mathcal{A})A,\sigma,-\mathbf{p}}|^2}{(2\pi)^3} & (\sigma = 1, 2) \end{cases}. \end{aligned} \quad (4.65)$$

**ghosts**

We Fourier expand the fluctuations  $\hat{\mathcal{C}}_A, \hat{\bar{\mathcal{C}}}_A$  as

$$\begin{pmatrix} \hat{\mathcal{C}}_A \\ \hat{\bar{\mathcal{C}}}_A \end{pmatrix} = \int d^3 \mathbf{p} \left[ +\mathcal{C}_{A,\mathbf{p}}^{(t)}(t) \begin{pmatrix} \hat{\mathbf{c}}_{A,\mathbf{p}}(t) \\ \hat{\mathbf{c}}_{A,\mathbf{p}}(t) \end{pmatrix} + -\mathcal{C}_{A,\mathbf{p}}^{(t)}(t) \begin{pmatrix} \hat{\mathbf{f}}_{A,-\mathbf{p}}(t) \\ \hat{\mathbf{f}}_{A,-\mathbf{p}}(t) \end{pmatrix} \right] \frac{e^{i\mathbf{p}\cdot\mathbf{x}}}{(2\pi)^{3/2}}, \quad (4.66)$$

where the positive/negative frequency mode functions for intermediate times  $\pm\mathcal{C}_{A,\mathbf{p}}^{(t)}$  are

$$\begin{pmatrix} \pm\mathcal{C}_{A,\mathbf{p}}^{(t)} \\ \frac{d_{\pm}\mathcal{C}_{A,\mathbf{p}}^{(t)}}{dt} \end{pmatrix} \equiv \begin{pmatrix} 1 \\ \sqrt{2|\mathbf{p} - q_A^{(\text{ad.})}\bar{\mathbf{A}}(t)|} \\ \mp i\sqrt{\frac{|\mathbf{p} - q_A^{(\text{ad.})}\bar{\mathbf{A}}(t)|}{2}} \end{pmatrix} \exp \left[ \mp i \int_{-\infty}^t |\mathbf{p} - q_A^{(\text{ad.})}\bar{\mathbf{A}}(t)| dt \right]. \quad (4.67)$$

The normalization condition for the mode function  $\pm\mathcal{C}_{A,\mathbf{p}}^{(t)}$  is

$$(\pm\mathcal{C}_{A,\mathbf{p}}^{(t)} | \pm\mathcal{C}_{A,\mathbf{p}}^{(t)})_{\text{B}} = \pm 1, \quad (\pm\mathcal{C}_{A,\mathbf{p}}^{(t)} | \mp\mathcal{C}_{A,\mathbf{p}}^{(t)})_{\text{B}} = 0. \quad (4.68)$$

Now, we impose canonical commutation relations for the ghost modes  $\hat{\mathcal{C}}_A, \hat{\pi}_A$  as

$$\begin{aligned} \left\{ \hat{\mathcal{C}}_A(t, \mathbf{x}), \hat{\pi}_{A'}(t, \mathbf{x}') \right\} &= i\delta_{AA'}\delta^3(\mathbf{p} - \mathbf{p}'), \\ \left\{ \hat{\mathcal{C}}_A(t, \mathbf{x}), \hat{\mathcal{C}}_{A'}(t, \mathbf{x}') \right\} &= \left\{ \hat{\pi}_A(t, \mathbf{x}), \hat{\pi}_{A'}(t, \mathbf{x}') \right\} = 0, \end{aligned} \quad (4.69)$$

where  $\hat{\pi}_A$  is the canonical conjugate field to the ghost field  $\hat{\mathcal{C}}_A$  as  $\hat{\pi}_A = -i\partial_t\hat{\mathcal{C}}_A^\dagger$  and  $\hat{\pi}_A = i\partial_t\hat{\mathcal{C}}_A^\dagger$ . Then, we obtain anti-commutation relations for the intermediate annihilation operators  $\hat{\mathbf{e}}_{A,\mathbf{p}}, \hat{\mathbf{f}}_{A,\mathbf{p}}$  as

$$i\delta_{AA'}\delta^3(\mathbf{p} - \mathbf{p}') = \left\{ \hat{\mathbf{e}}_{A,\mathbf{p}}, \hat{\mathbf{e}}_{A',\mathbf{p}'}^\dagger \right\} = \left\{ \hat{\mathbf{f}}_{A,\mathbf{p}}, \hat{\mathbf{f}}_{A',\mathbf{p}'}^\dagger \right\}, \quad (\text{others}) = 0. \quad (4.70)$$

The corresponding vacuum state  $|\text{vac};t\rangle$  must be annihilated by  $\hat{\mathbf{e}}_{A,\mathbf{p}}, \hat{\mathbf{f}}_{A,\mathbf{p}}$  as

$$0 = \hat{\mathbf{e}}_{A,\mathbf{p}} |\text{vac};t\rangle = \hat{\mathbf{f}}_{A,\mathbf{p}} |\text{vac};t\rangle \quad (4.71)$$

for all values of  $A, \mathbf{p}, s$ .

The positive/negative frequency mode functions  $\pm\mathcal{C}_{A,\mathbf{p},s}^{(t)}$ , the annihilation operators  $\hat{\mathbf{e}}_{A,\mathbf{p}}, \hat{\mathbf{f}}_{A,\mathbf{p}}$ , and the vacuum  $|\text{vac};t\rangle$  at an intermediate time smoothly approach those at the asymptotic times (as = in/out) in the limit of  $t \rightarrow \pm\infty$  as

$$\pm\mathcal{C}_{A,\mathbf{p}}^{(t)} \xrightarrow{t \rightarrow -\infty} \pm\mathcal{C}_{A,\mathbf{p}}^{(\text{in})}, \quad \pm\mathcal{C}_{A,\mathbf{p}}^{(t)} \xrightarrow{t \rightarrow \infty} \pm\mathcal{C}_{A,\mathbf{p}}^{(\text{out})}, \quad (4.72)$$

$$\begin{pmatrix} \hat{\mathbf{e}}_{A,\mathbf{p}} \\ \hat{\mathbf{f}}_{A,\mathbf{p}} \end{pmatrix} \xrightarrow{t \rightarrow -\infty} \begin{pmatrix} \hat{\mathbf{e}}_{A,\mathbf{p}}^{(\text{in})} \\ \hat{\mathbf{f}}_{A,\mathbf{p}}^{(\text{in})} \end{pmatrix}, \quad \begin{pmatrix} \hat{\mathbf{e}}_{A,\mathbf{p}} \\ \hat{\mathbf{f}}_{A,\mathbf{p}} \end{pmatrix} \xrightarrow{t \rightarrow \infty} \begin{pmatrix} \hat{\mathbf{e}}_{A,\mathbf{p}}^{(\text{out})} \\ \hat{\mathbf{f}}_{A,\mathbf{p}}^{(\text{out})} \end{pmatrix}, \quad (4.73)$$

and

$$|\text{vac}; t\rangle \xrightarrow[t \rightarrow -\infty]{} |\text{vac}; \text{in}\rangle, \quad |\text{vac}; t\rangle \xrightarrow[t \rightarrow \infty]{} |\text{vac}; \text{out}\rangle. \quad (4.74)$$

The in-state annihilation operators  $\hat{\mathbf{e}}_{A,\mathbf{p}}^{(-)\text{(in)}}$ ,  $\hat{\mathbf{f}}_{A,\mathbf{p}}^{(-)\text{(in)}}$  and those at intermediate times  $\hat{\mathbf{e}}_{A,\mathbf{p}}^{(-)}$ ,  $\hat{\mathbf{f}}_{A,\mathbf{p}}^{(-)}$  are related with each other by a Bogoliubov transformation:

$$\begin{pmatrix} \hat{\mathbf{e}}_{A,\mathbf{p}}^{(-)}(t) \\ \hat{\mathbf{f}}_{A,-\mathbf{p}}^{(-)\dagger}(t) \end{pmatrix} = \begin{pmatrix} \alpha_{(C)A,\mathbf{p}}(t) & \beta_{(C)A,\mathbf{p}}(t) \\ \beta_{(C)A,\mathbf{p}}^*(t) & \alpha_{(C)A,\mathbf{p}}^*(t) \end{pmatrix} \begin{pmatrix} \hat{\mathbf{e}}_{A,\mathbf{p}}^{(-)\text{(in)}} \\ \hat{\mathbf{f}}_{A,-\mathbf{p}}^{(-)\text{(in)\dagger}} \end{pmatrix}. \quad (4.75)$$

Here, the Bogoliubov coefficients are given by

$$\begin{aligned} \alpha_{(C)A,\mathbf{p}}(t) &\equiv (+\mathcal{C}_{A,\mathbf{p}}^{(t)} | +\mathcal{C}_{A,\mathbf{p}}^{(\text{in})})_{\text{B}} = -(-\mathcal{C}_{A,\mathbf{p}}^{(t)} | -\mathcal{C}_{A,\mathbf{p}}^{(\text{in})})_{\text{B}}^* \\ &= \frac{i}{\sqrt{2|\mathbf{p} - q_A^{(\text{ad.})}\bar{\mathbf{A}}|}} \left[ \frac{d_+ \mathcal{C}_{A,\mathbf{p}}^{(\text{in})}}{dt} - i|\mathbf{p} - q_A^{(\text{ad.})}\bar{\mathbf{A}}| + \mathcal{C}_{A,\mathbf{p}}^{(\text{in})} \right] \exp \left[ +i \int_{-\infty}^t |\mathbf{p} - q_A^{(\text{ad.})}\bar{\mathbf{A}}| dt \right], \\ \beta_{(C)A,\mathbf{p}}(t) &\equiv (+\mathcal{C}_{A,\mathbf{p}}^{(t)} | -\mathcal{C}_{A,\mathbf{p}}^{(\text{in})})_{\text{B}} = -(-\mathcal{C}_{A,\mathbf{p}}^{(t)} | +\mathcal{C}_{A,\mathbf{p}}^{(\text{in})})_{\text{B}}^* \\ &= \frac{i}{\sqrt{2|\mathbf{p} - q_A^{(\text{ad.})}\bar{\mathbf{A}}|}} \left[ \frac{d_- \mathcal{C}_{A,\mathbf{p}}^{(\text{in})}}{dt} - i|\mathbf{p} - q_A^{(\text{ad.})}\bar{\mathbf{A}}| - \mathcal{C}_{A,\mathbf{p}}^{(\text{in})} \right] \exp \left[ +i \int_{-\infty}^t |\mathbf{p} - q_A^{(\text{ad.})}\bar{\mathbf{A}}| dt \right], \end{aligned} \quad (4.76)$$

and are normalized as

$$1 = |\alpha_{(C)A,\mathbf{p}}(t)|^2 - |\beta_{(C)A,\mathbf{p}}(t)|^2. \quad (4.77)$$

From the canonical quantization procedure briefly described above, one can easily show that ghosts are never produced. Indeed, the number of produced ghosts and anti-ghosts are obtained as an in-vacuum  $|\text{vac}; \text{in}\rangle$  expectation value of number operators  $\hat{\mathbf{e}}_{A,\mathbf{p}}^{(-)\dagger} \hat{\mathbf{e}}_{A,\mathbf{p}}^{(-)}$  and  $\hat{\mathbf{f}}_{A,\mathbf{p}}^{(-)\dagger} \hat{\mathbf{f}}_{A,\mathbf{p}}^{(-)}$  for charged ghosts (anti-ghosts) with the color charge  $q_A^{(\text{ad.})}$  and  $-q_A^{(\text{ad.})}$ , respectively, as

$$\begin{aligned} \frac{d^6 N_{\text{gh}_+}^{(-)}(A, \mathbf{p}; t)}{d\mathbf{p}^3 d\mathbf{x}^3} &= \frac{1}{V} \left\langle \hat{\mathbf{e}}_{A,\mathbf{p}}^{(-)\dagger} \hat{\mathbf{e}}_{A,\mathbf{p}}^{(-)} \right\rangle = 0, \\ \frac{d^6 N_{\text{gh}_-}^{(-)}(A, \mathbf{p}; t)}{d\mathbf{p}^3 d\mathbf{x}^3} &= \frac{1}{V} \left\langle \hat{\mathbf{f}}_{A,\mathbf{p}}^{(-)\dagger} \hat{\mathbf{f}}_{A,\mathbf{p}}^{(-)} \right\rangle = 0. \end{aligned} \quad (4.78)$$

## 4.2 Quark and gluon production from a constant color electric field

In this section, we consider a constant color electric field  $\bar{A}_\mu$  initiated at  $t = t_0 = 0$  described by

$$\bar{E}(t) = \bar{E}_0, \quad \text{or} \quad \bar{A}(t) = -\bar{E}_0 t \theta(t). \quad (4.79)$$

By ignoring the backreaction and keeping the electric field strength fixed, we analytically follow the time-evolution of the quark and the gluon spectra. The analytical calculation can be done in the same ways as were explained in Section 2.4 and 3.2 because the equation of motion for the quark field  $\hat{\psi}_{f,i}$  (4.33) and the charged gluon field  $\hat{\mathcal{A}}_{A,\sigma}$  (4.35) are the same as what we encountered in QED (2.16) and the  $SU_c(N_c = 2)$  Yang-Mills theory (3.91), respectively, except for the additional labels  $f, i, A$ .

As were discussed in Section 2.5 within QED and 3.2 within the  $SU_c(N_c = 2)$  pure Yang-Mills theory, the neglect of the backreaction is actually problematic (e.g. violation of the energy conservation), and is justifiable only at the very beginning of the particle production process, where the number of produced particles and/or the acceleration by the classical field is negligible. The backreaction effects for our QCD problem will be discussed in Section 4.3.

### 4.2.1 quark and gluon distribution

One can easily solve Eqs. (4.33) and (4.35) under the constant electric field (4.79) in the same manner as were explained in Section 2.4 and 3.2, respectively. As a result, one obtains an analytical expression for the quark and the gluon distribution function  $d^6 N_{(-)}/d\mathbf{p}^3 d\mathbf{x}^3$ ,  $d^6 N_{g\pm}/d\mathbf{p}^3 d\mathbf{x}^3$ , respectively, as

$$\frac{d^6 N_q(f, i, \mathbf{p})}{d\mathbf{p}^3 d\mathbf{x}^3} = \frac{d^6 N_{\bar{q}}(f, i, -\mathbf{p})}{d\mathbf{p}^3 d\mathbf{x}^3} = \frac{1}{(2\pi)^3} \left| \tilde{\beta}_{(\psi)f,i,\mathbf{p},s}(t_0) \tilde{\alpha}_{(\psi)f,i,\mathbf{p},s}^*(t) - \tilde{\alpha}_{(\psi)f,i,\mathbf{p},s}^*(t_0) \tilde{\beta}_{(\psi)f,i,\mathbf{p},s}(t) \right|^2, \quad (4.80)$$

$$\frac{d^6 N_{g\pm}(A, \sigma, \pm\mathbf{p})}{d\mathbf{p}^3 d\mathbf{x}^3} = \frac{1}{(2\pi)^3} \left| \tilde{\beta}_{(A)A,\sigma,\mathbf{p}}(t_0) \tilde{\alpha}_{(A)A,\sigma,\mathbf{p}}^*(t) - \tilde{\alpha}_{(A)A,\sigma,\mathbf{p}}^*(t_0) \tilde{\beta}_{(A)A,\sigma,\mathbf{p}}(t) \right|^2. \quad (4.81)$$

Here, the coefficients  $\tilde{\alpha}, \tilde{\beta}$  are given by

$$\begin{aligned} \tilde{\alpha}_{(\psi)f,i,\mathbf{p},s}(t) = & \exp \left[ -i \int_{-\infty}^t \omega_{\mathbf{p}+q_i^{(\text{fund.})} \bar{\mathbf{E}}_0 t} dt \right] \exp \left[ -\pi \frac{m_f^2 + \mathbf{p}_\perp^2}{8 |q_i^{(\text{fund.})} \bar{\mathbf{E}}_0|} \right] \\ & \times \left[ \frac{1}{\sqrt{2}} \sqrt{1 + \frac{p_z + q_i^{(\text{fund.})} \bar{\mathbf{E}}_0 t}{\omega_{\mathbf{p}+q_i^{(\text{fund.})} \bar{\mathbf{E}}_0 t}} e^{i\pi/8} D_{i \frac{m_f^2 + \mathbf{p}_\perp^2}{2|q_i^{(\text{fund.})} \bar{\mathbf{E}}_0|}} (e^{-i\pi/4} \sqrt{\frac{2}{|q_i^{(\text{fund.})} \bar{\mathbf{E}}_0|}} (p_z + q_i^{(\text{fund.})} \bar{\mathbf{E}}_0 t)) \right] \end{aligned}$$

$$+ \frac{1}{\sqrt{2}} \sqrt{1 - \frac{p_z + q_i^{(\text{fund.})} \bar{E}_0 t}{\omega_{\mathbf{p}+q_i^{(\text{fund.})} \bar{E}_0 t}} e^{-i\pi/8}} \sqrt{\frac{m_f^2 + \mathbf{p}_\perp^2}{2|q_i^{(\text{fund.})} \bar{E}_0|}} \\ \times D_{i \frac{m_f^2 + \mathbf{p}_\perp^2}{2|q_i^{(\text{fund.})} \bar{E}_0|} - 1} (e^{-i\pi/4} \sqrt{\frac{2}{|q_i^{(\text{fund.})} \bar{E}_0|}} (p_z + q_i^{(\text{fund.})} \bar{E}_0 t)) \Big], \quad (4.82)$$

$$\tilde{\beta}_{(\psi)f,i,\mathbf{p},s}(t) = \exp \left[ +i \int_{-\infty}^t \omega_{\mathbf{p}+q_i^{(\text{fund.})} \bar{E}_0 t} dt \right] \exp \left[ -\pi \frac{m_f^2 + \mathbf{p}_\perp^2}{8|q_i^{(\text{fund.})} \bar{E}_0|} \right] \\ \times \left[ \frac{1}{\sqrt{2}} \sqrt{1 - \frac{p_z + q_i^{(\text{fund.})} \bar{E}_0 t}{\omega_{\mathbf{p}+q_i^{(\text{fund.})} \bar{E}_0 t}} e^{i\pi/8}} D_{i \frac{m_f^2 + \mathbf{p}_\perp^2}{2|q_i^{(\text{fund.})} \bar{E}_0|}} (e^{-i\pi/4} \sqrt{\frac{2}{|q_i^{(\text{fund.})} \bar{E}_0|}} (p_z + q_i^{(\text{fund.})} \bar{E}_0 t)) \right. \\ \left. - \frac{1}{\sqrt{2}} \sqrt{1 + \frac{p_z + q_i^{(\text{fund.})} \bar{E}_0 t}{\omega_{\mathbf{p}+q_i^{(\text{fund.})} \bar{E}_0 t}} e^{-i\pi/8}} \sqrt{\frac{m_f^2 + \mathbf{p}_\perp^2}{2|q_i^{(\text{fund.})} \bar{E}_0|}} \right. \\ \left. \times D_{i \frac{m_f^2 + \mathbf{p}_\perp^2}{2|q_i^{(\text{fund.})} \bar{E}_0|} - 1} (e^{-i\pi/4} \sqrt{\frac{2}{|q_i^{(\text{fund.})} \bar{E}_0|}} (p_z + q_i^{(\text{fund.})} \bar{E}_0 t)) \right], \quad (4.83)$$

and

$$\tilde{\alpha}_{(A)A,\sigma,\mathbf{p}}(t) = \frac{-i}{\sqrt{2|\mathbf{p} + q_A^{(\text{ad.})} \bar{E}_0 t|}} \frac{\exp \left[ -\pi \frac{\mathbf{p}_\perp^2}{8|q_A^{(\text{ad.})} \bar{E}_0|} \right]}{(2|q_A^{(\text{ad.})} \bar{E}_0|)^{1/4}} \exp \left[ -i \int_{-\infty}^t |\mathbf{p} + q_A^{(\text{ad.})} \bar{E}_0 t| dt \right] \\ \times \left[ \left( |\mathbf{p} + q_A^{(\text{ad.})} \bar{E}_0 t| - (p_z + q_A^{(\text{ad.})} \bar{E}_0 t) \right) D_{i \frac{\mathbf{p}_\perp^2}{2|q_A^{(\text{ad.})} \bar{E}_0|} - 1/2} (e^{-i\pi/4} \sqrt{\frac{2}{|q_A^{(\text{ad.})} \bar{E}_0|}} (q_A^{(\text{ad.})} \bar{E}_0 t + p_z)) \right. \\ \left. + e^{i\pi/4} \sqrt{2|q_A^{(\text{ad.})} \bar{E}_0|} D_{i \frac{\mathbf{p}_\perp^2}{2|q_A^{(\text{ad.})} \bar{E}_0|} + 1/2} (e^{-i\pi/4} \sqrt{\frac{2}{|q_A^{(\text{ad.})} \bar{E}_0|}} (q_A^{(\text{ad.})} \bar{E}_0 t + p_z)) \right], \quad (4.84)$$

$$\tilde{\beta}_{(A)A,\sigma,\mathbf{p}}(t) = \frac{i}{\sqrt{2|\mathbf{p} + q_A^{(\text{ad.})} \bar{E}_0 t|}} \frac{\exp \left[ -\pi \frac{\mathbf{p}_\perp^2}{8|q_A^{(\text{ad.})} \bar{E}_0|} \right]}{(2|q_A^{(\text{ad.})} \bar{E}_0|)^{1/4}} \exp \left[ +i \int_{-\infty}^t |\mathbf{p} + q_A^{(\text{ad.})} \bar{E}_0 t| dt \right] \\ \times \left[ \left( |\mathbf{p} + q_A^{(\text{ad.})} \bar{E}_0 t| + (p_z + q_A^{(\text{ad.})} \bar{E}_0 t) \right) D_{i \frac{\mathbf{p}_\perp^2}{2|q_A^{(\text{ad.})} \bar{E}_0|} - 1/2} (e^{-i\pi/4} \sqrt{\frac{2}{|q_A^{(\text{ad.})} \bar{E}_0|}} (q_A^{(\text{ad.})} \bar{E}_0 t + p_z)) \right. \\ \left. - e^{i\pi/4} \sqrt{2|q_A^{(\text{ad.})} \bar{E}_0|} D_{i \frac{\mathbf{p}_\perp^2}{2|q_A^{(\text{ad.})} \bar{E}_0|} + 1/2} (e^{-i\pi/4} \sqrt{\frac{2}{|q_A^{(\text{ad.})} \bar{E}_0|}} (q_A^{(\text{ad.})} \bar{E}_0 t + p_z)) \right]. \quad (4.85)$$

**analytic formula at  $t \rightarrow \infty$** 

In the limit of  $t \rightarrow \infty$  (or the infinite kinetic momentum limit  $P_z = p_z + q\bar{E}_0 t \rightarrow \text{sgn}(q\bar{E}_0) \times \infty$ ), one reproduces the well-known Schwinger formula for a constant electric field (see Eqs. (1.17) and (1.18)) as

$$\frac{d^6 N_{(-)}(f, i, \mathbf{p})}{d\mathbf{p}^3 d\mathbf{x}^3} \xrightarrow{t \rightarrow \infty} \frac{1}{(2\pi)^3} \exp \left[ -\pi \frac{m_f^2 + \mathbf{p}_\perp^2}{|q_i^{(\text{fund.})} \bar{E}_0|} \right], \quad (4.86)$$

$$\frac{d^6 N_{g\pm}(A, \sigma, \pm \mathbf{p})}{d\mathbf{p}^3 d\mathbf{x}^3} \xrightarrow{t \rightarrow \infty} \frac{1}{(2\pi)^3} \exp \left[ -\pi \frac{\mathbf{p}_\perp^2}{|q_A^{(\text{ad.})} \bar{E}_0|} \right], \quad (4.87)$$

where the use is made of the asymptotic formula for the parabolic cylinder function  $D_\nu(z)$  (3.99).

**dynamical evolution**

We directly evaluate the expressions (4.80) and (4.81) in order to understand dynamical properties of the quark and the gluon production from a constant color electric field. Here, we consider  $N_f = 3$  (i.e., three massless quarks) and set  $\theta = 0$  for simplicity.

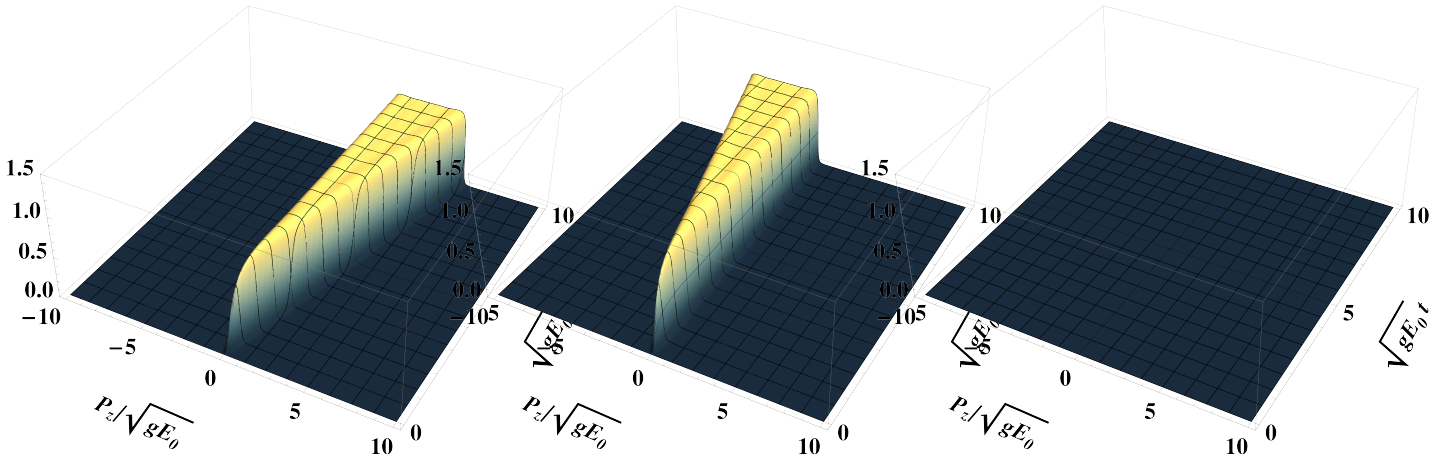


Figure 4.1: The longitudinal kinetic momentum distribution  $d^6 N_q / d\mathbf{p}^3 d\mathbf{x}^3 = |\beta_{(\psi)f,i,\mathbf{p},s}|^2 / (2\pi)^3$  of produced massless ( $m_f / \sqrt{g\bar{E}_0} = 0$ ) quarks at a fixed transverse momentum  $|\mathbf{p}_\perp| / \sqrt{|g\bar{E}_0|} = 0.1$ . Different panels differentiate values of the color charge  $q_i^{(\text{fund.})}$  ( $i = 1, \dots, N_c$ ) of quarks with color  $i$ . We set the color angle  $\theta = 0$ , and the corresponding quark charge  $q_i^{(\text{fund.})}$  read  $q_1^{(\text{fund.})} = q_1^{(\text{fund.})} = 1/2$  (left),  $q_2^{(\text{fund.})} = -1/2$  (middle), and  $q_3^{(\text{fund.})} = 0$  (right).

Results are plotted in Figs. 4.1, 4.2, 4.3, and 4.4: Figures 4.1 and 4.2 (4.3 and 4.4) show the longitudinal (transverse) momentum distribution  $d^6 N / d\mathbf{p}^3 d\mathbf{x}^3$  of produced quarks and gluons, respectively, at a fixed transverse (longitudinal) momentum  $|\mathbf{p}_\perp| / \sqrt{|g\bar{E}_0|} = 0.1$  ( $P_z = p_z - q\bar{A} = 1.5 \times \sqrt{g\bar{E}_0}$ , where  $q = q_i^{(\text{fund.})}$  or  $q_A^{(\text{ad.})}$ ). The three panels in each figure differentiate values

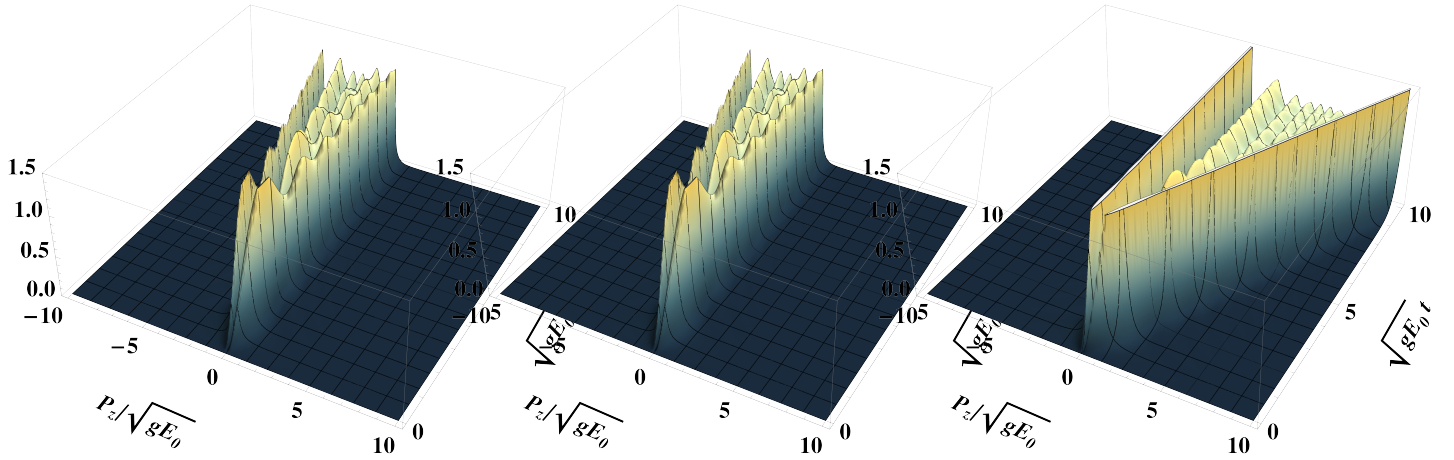


Figure 4.2: The longitudinal kinetic momentum distribution  $d^6 N_{g^+}/d\mathbf{p}^3 d\mathbf{x}^3 = |\beta_{(A)A,\sigma,\mathbf{p}}|^2/(2\pi)^3$  of produced gluons at a fixed transverse momentum  $|\mathbf{p}_{\perp}|/\sqrt{|gE_0|} = 0.1$ . Different panels differentiate values of the color charge  $q_A^{(\text{ad.})}$  ( $A = 1, \dots, N_c(N_c - 1)/2$ ) of gluons with color  $A$ . We set the color angle  $\theta = 0$ , and the corresponding gluon charge  $q_A^{(\text{ad.})}$  read  $q_1^{(\text{ad.})} = -1/2$  (left),  $q_2^{(\text{ad.})} = -1/2$  (middle), and  $q_3^{(\text{ad.})} = 1$  (right).

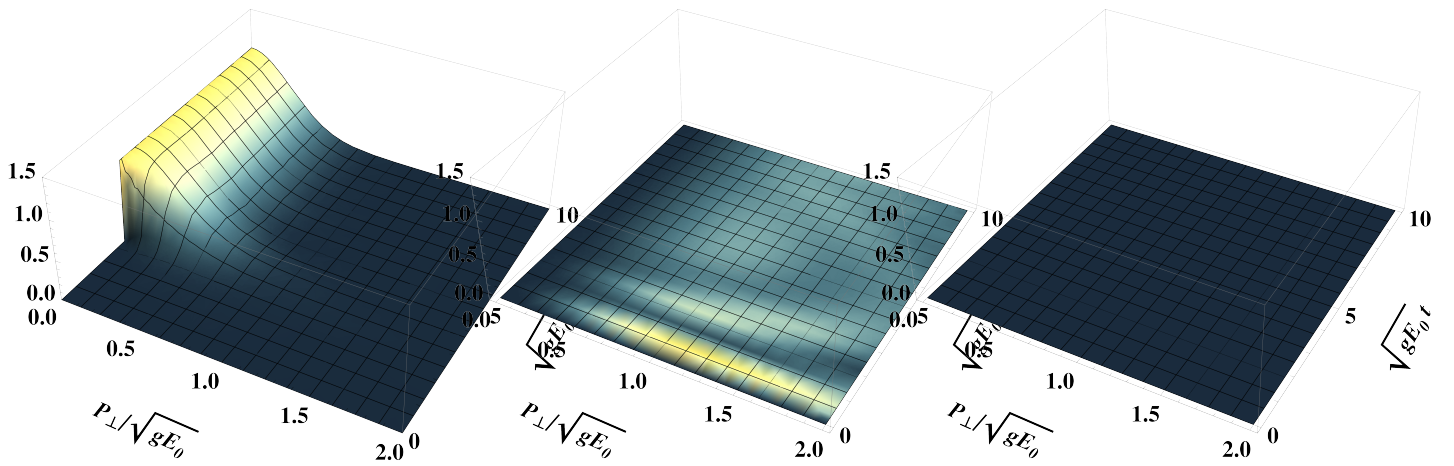


Figure 4.3: The transverse momentum distribution  $d^6 N_q/d\mathbf{p}^3 d\mathbf{x}^3 = |\beta_{(\psi)f,i,\mathbf{p},s}|^2/(2\pi)^3$  of produced massless ( $m_f/\sqrt{gE_0} = 0$ ) quarks at a fixed longitudinal kinetic momentum  $P_z = p_z - q_i^{(\text{fund.})}\bar{A} = 1.5 \times \sqrt{gE_0}$ . Different panels differentiate values of the color charge  $q_i^{(\text{fund.})}$  ( $i = 1, \dots, N_c$ ) of quarks with color  $i$ . We set the color angle  $\theta = 0$ , and the corresponding quark charge  $q_i^{(\text{fund.})}$  read  $q_1^{(\text{fund.})} = 1/2$  (left),  $q_2^{(\text{fund.})} = -1/2$  (middle), and  $q_3^{(\text{fund.})} = 0$  (right).

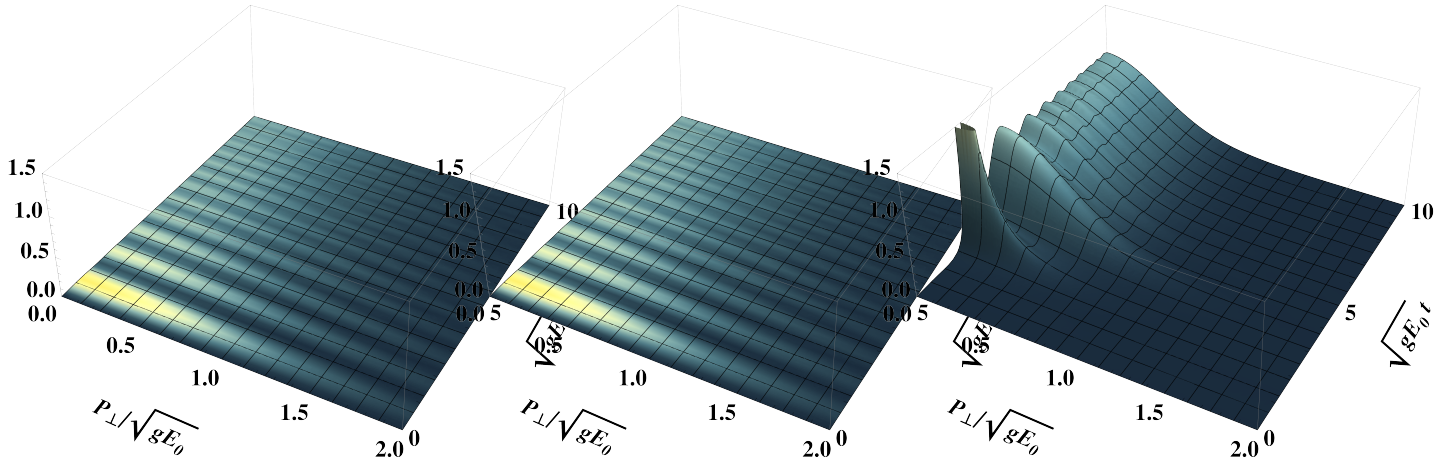


Figure 4.4: The transverse momentum distribution  $d^6 N_{g_{\pm}}/d\mathbf{p}^3 d\mathbf{x}^3 = |\beta_{(\mathcal{A})A,\sigma,p}|^2/(2\pi)^3$  of produced gluons at a fixed kinetic longitudinal momentum  $P_z = p_z - q_A^{(\text{ad.})}\bar{A} = 1.5 \times \sqrt{g\bar{E}_0}$ . Different panels differentiate values of the color charge  $q_A^{(\text{ad.})}$  ( $A = 1, \dots, N_c(N_c - 1)/2$ ) of gluons with color  $A$ . We set the color angle  $\theta = 0$ , and the corresponding gluon charge  $q_A^{(\text{ad.})}$  read  $q_A^{(\text{ad.})} = q_1^{(\text{ad.})} = -1/2$  (left),  $q_2^{(\text{ad.})} = -1/2$  (middle), and  $q_3^{(\text{ad.})} = 1$  (right).

of the color charge of quarks  $q_{i=1,\dots,N_c}^{(\text{fund.})}$  (4.22) and of gluons  $q_{A=1,\dots,N_c(N_c-1)/2}^{(\text{ad.})}$  (4.20). With our particular choice  $\theta = 0$ , the color charges  $q_i^{(\text{fund.})}, q_A^{(\text{ad.})}$  read

$$q_i^{(\text{fund.})} = \begin{pmatrix} 1/2 \\ -1/2 \\ 0 \end{pmatrix}_i, \quad q_A^{(\text{ad.})} = \begin{pmatrix} -1/2 \\ -1/2 \\ 1 \end{pmatrix}_A. \quad (4.88)$$

We remark that the momentum distribution of a particular colored particle is, however, not a physical observable because it is not color singlet; one has to sum up all the color degrees of freedom to get a physically meaningful (gauge-invariant) observable. Nevertheless, the momentum distribution is very useful in understanding that the basics of quark and gluon production in QCD is the same as the previous two studies (see Section 2.4.1 and 3.2.1). Indeed, one immediately notices from the figures that the momentum distribution of created particles strongly depends on the color charges  $q_i^{(\text{fund.})}, q_A^{(\text{ad.})}$ . This means that the value of the color angle  $\theta$ , on which the color charges  $q_i^{(\text{fund.})}, q_A^{(\text{ad.})}$  are uniquely determined, strongly affects the momentum distribution. However, the distributions for *each* color charge is consistent with the Schwinger formula for a constant electric field. That is, quarks and gluons are constantly created at around  $\mathbf{P} = \mathbf{0}$ , and, after they are created, they are accelerated by the electric field in the longitudinal direction as  $d\mathbf{P}/dt = q\bar{\mathbf{E}}_0$ . The transverse distribution, on the other hand, is nicely reproduced by the asymptotic formulas (4.86) and (4.87). Thus, one understands

$$\frac{d^6 N_{g_{\pm}}}{d\mathbf{p}^3 d\mathbf{x}^3} \sim \frac{1}{(2\pi)^3} \exp \left[ -\pi \frac{\mathbf{p}_{\perp}^2}{|q_A^{(\text{ad.})}\bar{\mathbf{E}}(t)|} \right] \theta(\mp p_z(p_z \mp q_A^{(\text{ad.})}\bar{A}(t))),$$

$$\frac{d^6 N_{(-)}^{(q)}}{d\mathbf{p}^3 d\mathbf{x}^3} \sim \frac{1}{(2\pi)^3} \exp \left[ -\pi \frac{m_f^2 + \mathbf{p}_\perp^2}{|q_i^{(\text{fund.})} \bar{E}(t)|} \right] \theta(\mp p_z (p_z \mp q_i^{(\text{fund.})} \bar{A}(t))), \quad (4.89)$$

which are the same as what we found in Section 2.4.1 and 3.2.1.

## 4.2.2 total number of quarks and gluons

### analytical estimate at $t \rightarrow \infty$

One may integrate the asymptotic formulas (4.86) and (4.87) over the momentum space  $\mathbf{p}$  to obtain an analytical estimate for the total number of quarks and gluons produced at  $t \rightarrow \infty$  as

$$\begin{aligned} \frac{d^3 N_{(-)}^{(q)}}{d\mathbf{x}^3} &\xrightarrow{t \rightarrow \infty} \frac{1}{(2\pi)^3} \sum_f \sum_i \sum_s |q_i^{(\text{fund.})} \bar{E}_0|^2 T \exp \left[ -\pi \frac{m_f^2}{|q_i^{(\text{fund.})} \bar{E}_0|} \right] \\ &= \frac{N_s}{(2\pi)^3} \sum_f \sum_i |q_i^{(\text{fund.})} \bar{E}_0|^2 T \exp \left[ -\pi \frac{m_f^2}{|q_i^{(\text{fund.})} \bar{E}_0|} \right], \end{aligned} \quad (4.90)$$

$$\begin{aligned} \frac{d^3 N_{g\pm}}{d\mathbf{x}^3} &\xrightarrow{t \rightarrow \infty} \frac{1}{(2\pi)^3} \sum_A \sum_{\sigma=1,2} |q_A^{(\text{ad.})} \bar{E}_0|^2 T \\ &= \frac{N_\sigma}{(2\pi)^3} \sum_A |q_A^{(\text{ad.})} \bar{E}_0|^2 T, \end{aligned} \quad (4.91)$$

where the use is made of the relation  $\int dp_z \sim |q \bar{E}_0| T$  with  $q = q_i^{(\text{fund.})}, q_A^{(\text{ad.})}$ . We also used the fact that the quark and the gluon production is independent of the spin  $s$  and the physical polarization  $\sigma = 1, 2$ , respectively, because these two degrees of freedom do not couple to the electric field, so that the summation over  $s, \sigma$  trivially gives the factor of  $N_s = 2$  and  $N_\sigma = 2$ . Unfortunately, one cannot take the flavor  $f$  summation analytically, but it may be good to approximate it as

$$\left. \frac{d^3 N_{(-)}^{(q)}}{d\mathbf{x}^3} \right|_{t \rightarrow \infty} \sim \frac{N_s N_{\text{Iq}}}{(2\pi)^3} \sum_i |q_i^{(\text{fund.})} \bar{E}_0|^2 T, \quad (4.92)$$

where we neglected contributions from “heavy” quarks satisfying  $m_f^2 \gtrsim \sqrt{|g \bar{E}_0|}$  and only those from “light” quarks satisfying  $m_f^2 \lesssim \sqrt{|g \bar{E}_0|}$  are counted, which gives the factor of  $N_{\text{Iq}}$  representing the number of “light” quarks. Now, with the help of the color summation formula (4.23), one can easily take the color summation over  $i, A$  to find

$$\left. \frac{d^3 N_{(-)}^{(q)}}{d\mathbf{x}^3} \right|_{t \rightarrow \infty} \sim \frac{N_s N_{\text{Iq}}}{16\pi^3} |g \bar{E}_0|^2 T = \frac{3}{8\pi^3} |g \bar{E}_0|^2 T, \quad (4.93)$$

$$\left. \frac{d^3 N_{g\pm}}{d\mathbf{x}^3} \right|_{t \rightarrow \infty} = \frac{N_\sigma N_c}{16\pi^3} |g \bar{E}_0|^2 T = \frac{3}{8\pi^3} |g \bar{E}_0|^2 T. \quad (4.94)$$

Here, we set  $N_{\text{q}} = 3$ , i.e., we regard the strange quark  $m_s \sim 100$  MeV is sufficiently “light” because the typical color field strength in actual physical situations is  $g\bar{E}_0 \sim \mathcal{O}(1 \text{ GeV})$  (see Fig. 4.7 for the justification of this treatment).

Equations (4.93) and (4.94) tell us that the total number of quarks and gluons produced at  $t \rightarrow \infty$  is independent of the color angle  $\theta$  because of the color summation  $i, A$ . It is also interesting to point out that quarks and gluons are equally produced by the classical field as  $N_{(-)} / N_{\text{g}\pm} = 1$  at  $t \rightarrow \infty$  if one neglects backreaction. This is because the non-perturbative Schwinger mechanism for a constant electric field is independent of statistics of charged particles. We shall see, however, that the situation changes when one considers intermediate particle spectra (see Fig. 4.6) and/or backreaction (see Fig. 4.13), where quantum statistics of particles play some important roles.

### dynamical evolution

Let us discuss the total number of produced quarks and gluons,  $d^3 N_{(-)} / d\mathbf{x}^3 = \sum_{f,i,s} \int d^3 \mathbf{p} d^6 N_{(-)} / d\mathbf{p}^3 d\mathbf{x}^3$  and  $d^3 N_{\text{g}\pm} / d\mathbf{x}^3 = \sum_{A,\sigma} \int d^3 \mathbf{p} d^6 N_{\text{g}\pm} / d\mathbf{p}^3 d\mathbf{x}^3$ , by numerically integrating the Bogoliubov coefficients squared  $|\beta|^2$ . The results are plotted in Figs. 4.5 - 4.7.

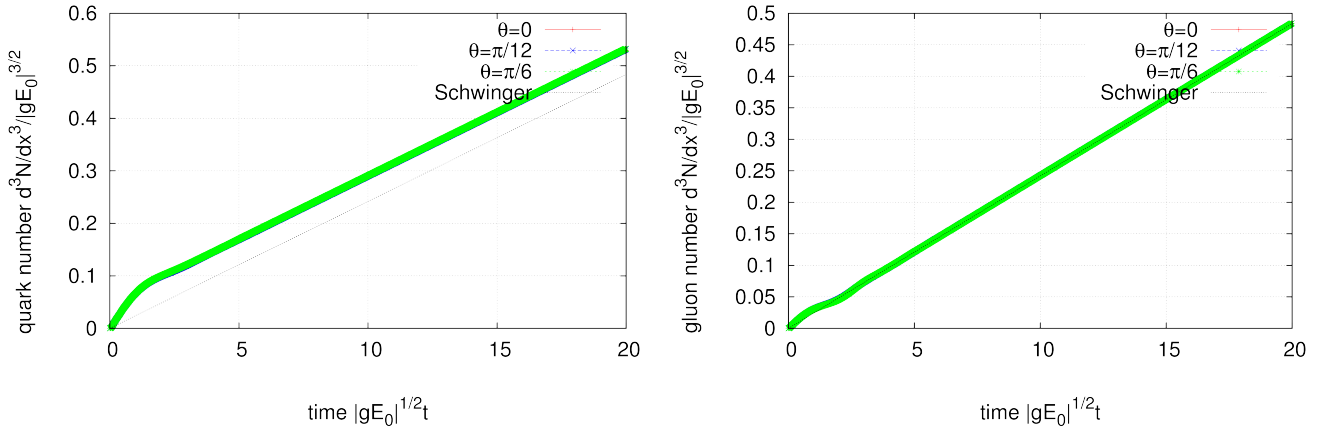


Figure 4.5: Total number of produced quarks  $d^3 N / d\mathbf{x}^3 = \sum_{f,i,s,\text{q}\bar{\text{q}}} \int d^3 \mathbf{p} d^6 N_{(-)} / d\mathbf{p}^3 d\mathbf{x}^3$  (left) and gluons  $d^3 N / d\mathbf{x}^3 = \sum_{A,\sigma,\text{g}\pm} \int d^3 \mathbf{p} d^6 N_{\text{g}\pm} / d\mathbf{p}^3 d\mathbf{x}^3$  (right). The different color corresponds to different color angles  $\theta = 0$  (red),  $\pi/12$  (blue), and  $\pi/6$  (green). The dashed lines are the expectation from the estimates (4.93) and (4.94).

The total number of quarks and gluons produced for several values of the color angle  $\theta$  is plotted in Fig. 4.5. Here, we consider a massless  $N_f = 3$  flavor case (the quark mass  $m_f$ - and the number of flavor  $N_f$ -dependence in quark production will be discussed in Fig. 4.7). By noting the definition of the color charges (4.20) and (4.22), it is sufficient to restrict our attention to  $0 \leq \theta \leq \pi/6$  in investigating the color angle  $\theta$ -dependence. The figures show that the color angle  $\theta$ -dependence in quark and gluon production is negligible. This is because the color angle

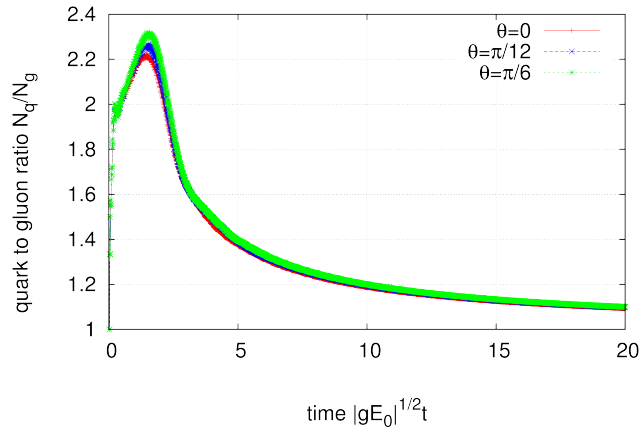


Figure 4.6: A ratio  $R_{q-g}$  of total quark number to gluon number  $R = (N_q + N_{\bar{q}})/(N_{g^+} + N_{g^-})$  for different values of the color angle  $\theta = 0$  (red),  $\pi/12$  (blue), and  $\pi/6$  (green).

$\theta$ -dependence is a higher order effect  $\propto |q_i^{(\text{fund.})}|^n, |q_A^{(\text{ad.})}|^n$  ( $n \leq 3$ ) in terms of the color charges  $q_i^{(\text{fund.})}, q_A^{(\text{ad.})}$ . Indeed, the leading order contribution to quark and gluon production always begin with  $|q_i^{(\text{fund.})}|^2, |q_A^{(\text{ad.})}|^2$  in both the perturbative particle production mechanism which dominates at early times (see Eqs. (2.76) and Eq. (3.104)) and the non-perturbative particle production mechanism which dominates for later times (see Eqs. (4.93) and (4.94)). Because of the color summation formula (4.23), terms proportional to  $|q_i^{(\text{fund.})}|^2, |q_A^{(\text{ad.})}|^2$  are always  $\theta$ -independent after the color degrees of freedom  $i, A$  are summed up. We also find that both quark and gluon number are consistent with the estimates (4.93) and (4.94), although the agreement is better in gluon production. This is because of the perturbative enhancement of particle production at early times as was discussed in Section 3.2.2. That is, the perturbative enhancement of quark production at early times is greater than that of gluon production, which results in a greater excess from the naive estimate (4.93) in quark production. This aspect is more clearly visible in Fig. 4.6, where a ratio  $R_{q-g}$  of the total quark number to the total gluon number is plotted. From the figure, one understands that quarks are produced about two times more than gluons at early times because of the perturbative particle production mechanism. Indeed, one can understand the number “two” within the lowest order perturbation theory: By extending the QED calculation (2.77) and the Yang-Mills one (3.104) to the case of QCD, one easily finds within the lowest order perturbation theory that

$$\begin{aligned}
\frac{d^3 N_{(\bar{q})}}{d\mathbf{x}^3} &= \frac{1}{16\pi^2} \sum_f \sum_i \sum_s \int_{2m_f}^{\infty} d\omega \sqrt{1 - \frac{4m_f^2}{\omega^2}} \frac{1}{3} \left( 2 + \frac{4m_f^2}{\omega^2} \right) |q_i^{(\text{fund.})} \tilde{E}(\omega)|^2 \\
&\xrightarrow{m_f \rightarrow 0} \frac{N_s N_{lq}}{48\pi^2} \int_0^{\infty} |g\tilde{E}(\omega)|^2 \\
&= \frac{1}{8\pi^2} \int_0^{\infty} d\omega |g\tilde{E}(\omega)|^2, \tag{4.95}
\end{aligned}$$

$$\begin{aligned}
\frac{d^3 N_{g\pm}}{d\mathbf{x}^3} &= \frac{1}{48\pi^2} \sum_A \sum_{\sigma=1,2} \int_0^\infty d\omega |q_A^{(\text{ad.})} \tilde{E}(\omega)|^2 \\
&= \frac{N_c N_\sigma}{96\pi^2} \int_0^\infty d\omega |g \tilde{E}(\omega)|^2 \\
&= \frac{1}{16\pi^2} \int_0^\infty d\omega |g \tilde{E}(\omega)|^2,
\end{aligned} \tag{4.96}$$

from which one can perturbatively evaluate  $R$  as

$$R_{q-g} \equiv \frac{N_q + N_{\bar{q}}}{N_{g+} + N_{g-}} \sim 2. \tag{4.97}$$

The lowest order calculation should be valid for  $t \rightarrow 0$  limit. The ratio takes values larger than two, which slightly depends on the color angle  $\theta$ , at early times  $0 \lesssim t \lesssim 2$  because of higher order perturbative contributions  $\propto |q_i^{(\text{fund.})}|^n, |q_A^{(\text{ad.})}|^n$  ( $n \geq 3$ ).

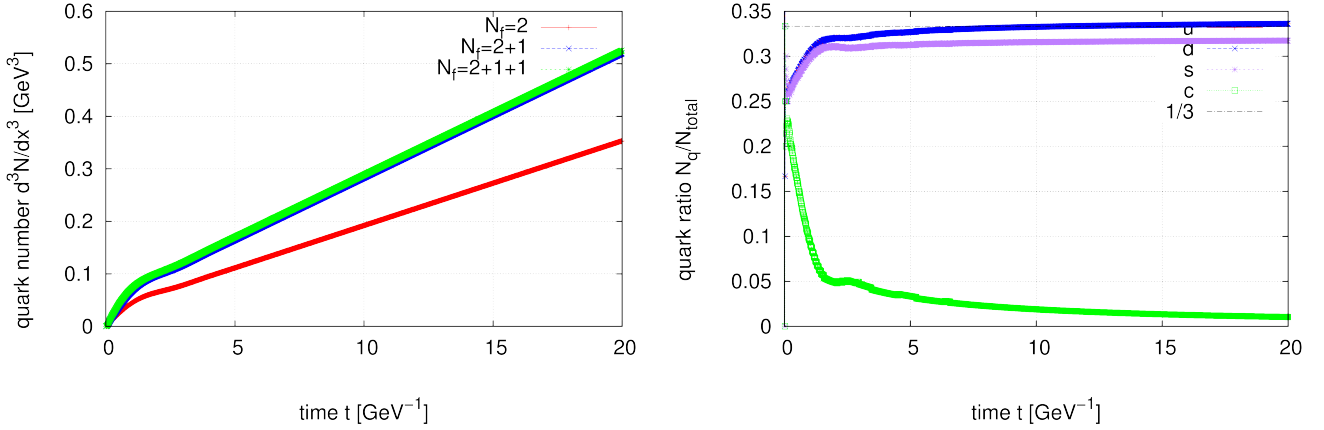


Figure 4.7: [Left] The number of flavor  $N_f$ -dependence in the total number of quarks produced  $d^3(N_q + N_{\bar{q}})/d\mathbf{x}^3$  for  $N_f = 2$  (up, down) in red,  $2 + 1$  (up, down, strange) in blue, and  $2 + 1 + 1$  (up, down, strange, charm) in green. [Right] A suppression factor of charm and strange quark production in  $N_f = 2 + 1 + 1$  case  $R_q = N_q/(N_u + N_d + N_s + N_c)$ . In both panels, parameters are set as  $g\bar{E}_0 = 1 \text{ GeV}^2$ ;  $\theta = 0$ ; and  $m_u = m_d = 0 \text{ GeV}$ ,  $m_s = 0.1 \text{ GeV}$ ,  $m_c = 1.2 \text{ GeV}$ .

The number of flavor  $N_f$ - and the quark mass  $m_f$ -dependence in quark production are investigated in Fig. 4.7. Here, we set  $g\bar{E}_0 = 1 \text{ GeV}^2$ , which is a typical value of the QCD string tension and/or the color electromagnetic field strength produced in the early stage dynamics of heavy ion collisions at the RHIC energy scale. The mass of up, down, strange, and charm quarks are given by  $m_u = m_d = 0 \text{ GeV}$ ,  $m_s = 0.1 \text{ GeV}$ , and  $m_c = 1.2 \text{ GeV}$ , respectively. We also set the color angle  $\theta = 0$  for simplicity; one can explicitly check that the following results depend on the color angle  $\theta$  very slightly as in Figs. 4.4 - 4.6.

In the left panel of Fig. 4.7, the total number of produced quarks is plotted with various values of  $N_f = 2$  (up, down),  $2 + 1$  (up, down, strange), and  $2 + 1 + 1$  (up, down, strange,

charm). We immediately notice that the change of the quark multiplicity from  $N_f = 2$  to  $N_f = 2 + 1$  is significant, while that from  $N_f = 2 + 1$  to  $N_f = 2 + 1 + 1$  is negligible. This results strongly indicate that the inclusion of strange (charm) degree of freedom is inevitable (may be negligible) in understanding actual physical phenomena involving strong color electromagnetic fields for the typical field strength of the order of  $g\bar{E}_0 \sim 1 \text{ GeV}^2$ .

In the right panel of Fig. 4.7, we plotted a ratio of the multiplicity of massive charm and strange quarks to the total quark multiplicity for  $N_f = 2 + 1 + 1$  case, i.e.,  $R_q = N_q / (N_u + N_d + N_s + N_c)$ . From this panel, one understands that the strange quark production is comparable to the production of massless up and down quarks during the whole time-evolution because the strange quark mass is sufficiently “light” compared to the strength of the electric field we are considering as  $m_s^2 \ll |g\bar{E}_0|$ . On the other hand, the charm quark production that it is comparable to the production of the “light” quarks for smaller values of  $t \lesssim 1 \text{ GeV}^{-1}$  because of the perturbative enhancement of the particle production discussed in Section 2.3. Because of this, the ratio takes about 1/4 for all species of quarks at the very beginning of the time-evolution. Whereas, the charm quark production is negligible for larger values of  $t \gtrsim 1 \text{ GeV}^{-1}$  because non-perturbative particle production mechanism is strongly suppressed for the heavy quark production. This is the reason why the ratio for charm quarks decreases to zero, while that for up, down, and strange quarks takes values at around 1/3. Notice that, from the non-perturbative Schwinger formula for a constant electric field (i.e., the estimate (4.90)), one naively expects that the ratio for charm quarks should be exponentially suppressed and hence very tiny as

$$R_q \sim \frac{\sum_i |q_i^{(\text{fund.})}| \exp \left[ -\pi \frac{m_c^2}{|q_i^{(\text{fund.})} \bar{E}_0|} \right]}{\sum_i \sum_f |q_i^{(\text{fund.})}| \exp \left[ -\pi \frac{m_f^2}{|q_i^{(\text{fund.})} \bar{E}_0|} \right]} \sim \frac{\sum_i |q_i^{(\text{fund.})}| \exp \left[ -\pi \frac{m_c^2}{|q_i^{(\text{fund.})} \bar{E}_0|} \right]}{\frac{3}{2} + \sum_i |q_i^{(\text{fund.})}| \exp \left[ -\pi \frac{m_c^2}{|q_i^{(\text{fund.})} \bar{E}_0|} \right]} \sim 0.00004 \quad (4.98)$$

for  $\theta = 0$ . Our result is much larger than this value because the heavy charm quark mass requires a long time for the non-perturbative particle production mechanism to dominate as was discussed in Fig. 2.10.

### 4.3 Dynamical evolution with backreaction

We discuss the dynamical evolution of the system with backreaction by numerically solving the equations of motion (4.32)-(4.37) and computing the quark and the gluon distribution functions, the decay of the color electric field, the total number of quarks and gluons produced, the energy density, and the pressure of the system.

### 4.3.1 setup

We consider the case where there is a spatially homogeneous classical color electric field at an initial time  $t = t_0 = 0$  given by

$$\bar{A}(t_0) = 0, \quad \bar{E}(t_0) = \bar{E}_0, \quad \frac{d\bar{E}(t_0)}{dt} = 0, \quad (4.99)$$

and that there are no classical sources applied on the system  $\bar{J}^\mu = 0$  for  $t > t_0 = 0$ .

Throughout this section, we consider  $N_f = 2+1+1$  case. We set parameters as  $g\bar{E}_0 = 1$  GeV<sup>2</sup> for the initial electric field strength;  $m_u = m_d = 0$  GeV,  $m_s = 0.1$  GeV,  $m_c = 1.2$  GeV for quark masses;  $g = 1$  for the strong coupling constant; and  $\theta = 0$  for the color angle. We note that one can explicitly demonstrate that our results presented below is insensitive to values of the color angle  $\theta$  except for the momentum distributions discussed in Section 4.3.2.

### 4.3.2 quark and gluon distribution

Figures 4.8 and 4.9 (4.10 and 4.11) display the longitudinal (transverse) momentum distribution  $d^6N/d\mathbf{p}^3d\mathbf{x}^3$  of produced quarks and gluons, respectively, at a fixed transverse (longitudinal) momentum  $|\mathbf{p}_\perp| = 0.044$  GeV ( $P_z = p_z - q\bar{A} = 1.5$  GeV, where  $q = q_i^{(\text{fund.})}$  or  $q_A^{(\text{ad.})}$ ). The three panels in each figure correspond to different values of the color charge of quarks  $q_i^{(\text{fund.})}$  and gluons  $q_A^{(\text{ad.})}$ . For our particular parameter choice  $\theta = 0$ , they are given by  $q_1^{(\text{fund.})} = 1/2$ ,  $q_2^{(\text{fund.})} = -1/2$ ,  $q_3^{(\text{fund.})} = 0$  and  $q_1^{(\text{ad.})} = -1/2$ ,  $q_2^{(\text{ad.})} = -1/2$ ,  $q_3^{(\text{ad.})} = 1$ .

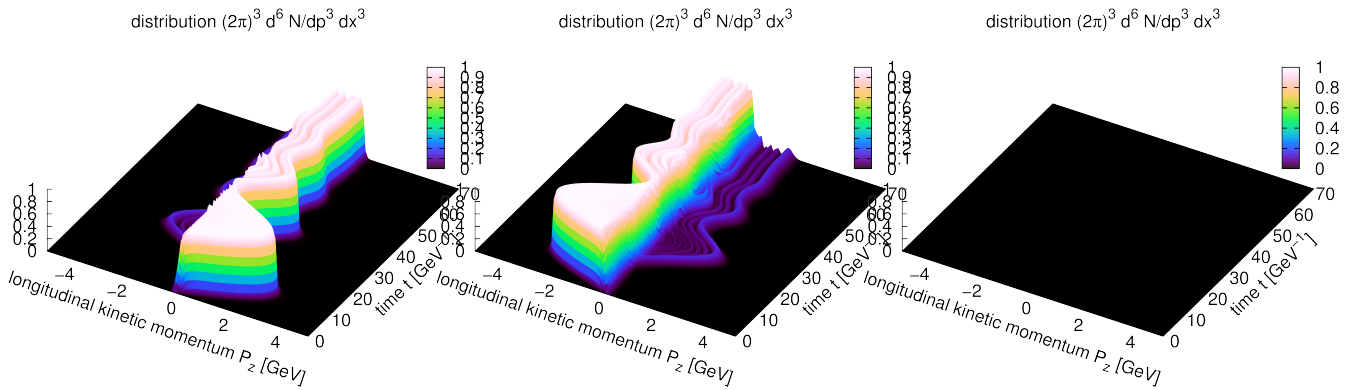


Figure 4.8: The kinetic longitudinal momentum distribution  $d^6N_q/d\mathbf{p}^3d\mathbf{x}^3 = |\beta_{(\psi)f,i,\mathbf{p},s}|^2/(2\pi)^3$  of produced massless quarks (up or down) at a fixed transverse momentum  $|\mathbf{p}_\perp| = 0.044$  GeV. Different panels correspond to different values of the color charge  $q_i^{(\text{fund.})}$  ( $i = 1, \dots, N_c$ ) of quarks with color  $i$ . We set the color angle  $\theta = 0$ , and the corresponding quark charge  $q_i^{(\text{fund.})}$  read  $q_1^{(\text{fund.})} = q_1^{(\text{fund.})} = 1/2$  (left),  $q_2^{(\text{fund.})} = -1/2$  (middle), and  $q_3^{(\text{fund.})} = 0$  (right).

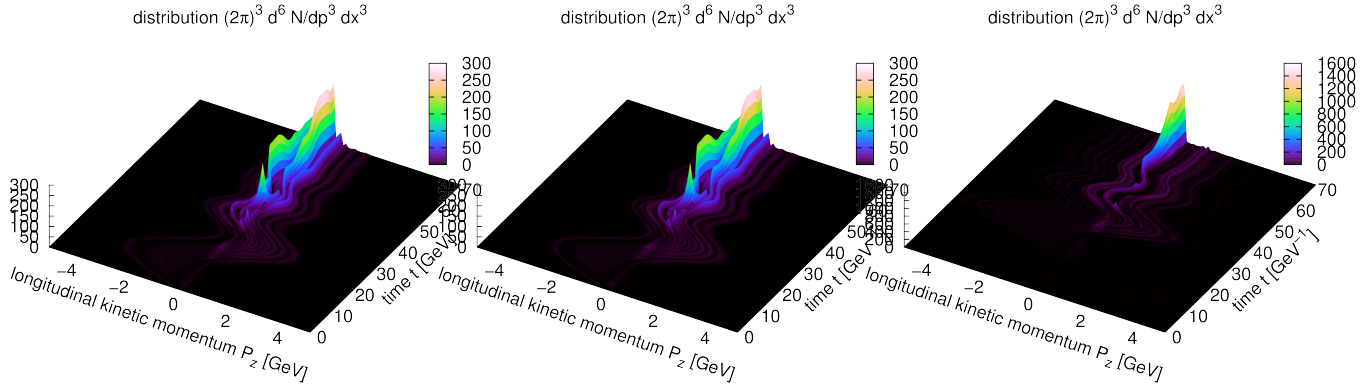


Figure 4.9: The kinetic longitudinal momentum distribution  $d^6 N_{g^+}/d\mathbf{p}^3 d\mathbf{x}^3 = |\beta_{(\mathcal{A})A,\sigma,\mathbf{p}}|^2/(2\pi)^3$  of produced gluons at a fixed transverse momentum  $|\mathbf{p}_\perp| = 0.044$  GeV. Different panels correspond to different values of the color charge  $q_A^{(\text{ad.})}$  ( $i = 1, \dots, N_c(N_c - 1)/2$ ) of gluons with color  $A$ . We set the color angle  $\theta = 0$ , and the corresponding gluon charge  $q_A^{(\text{ad.})}$  read  $q_1^{(\text{ad.})} = q_A^{(\text{ad.})} = -1/2$  (left),  $q_2^{(\text{ad.})} = -1/2$  (middle), and  $q_3^{(\text{ad.})} = 1$  (right).

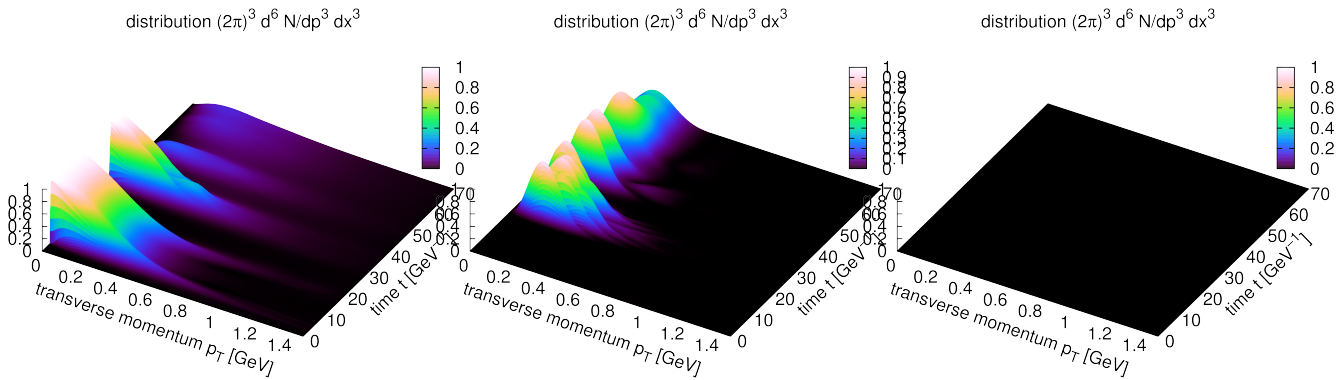


Figure 4.10: The transverse momentum distribution  $d^6 N_q/d\mathbf{p}^3 d\mathbf{x}^3 = |\beta_{(\psi)f,i,\mathbf{p},s}|^2/(2\pi)^3$  of produced massless quarks (up or down) at a fixed longitudinal kinetic momentum  $P_z = p_z - q_i^{(\text{fund.})}\bar{A} = 1.5$  GeV. Different panels correspond to different values of the color charge  $q_i^{(\text{fund.})}$  ( $i = 1, \dots, N_c$ ) of quarks with color  $i$ . We set the color angle  $\theta = 0$ , and the corresponding quark charge  $q_i^{(\text{fund.})}$  read  $q_1^{(\text{fund.})} = q_1^{(\text{fund.})} = 1/2$  (left),  $q_2^{(\text{fund.})} = -1/2$  (middle), and  $q_3^{(\text{fund.})} = 0$  (right).

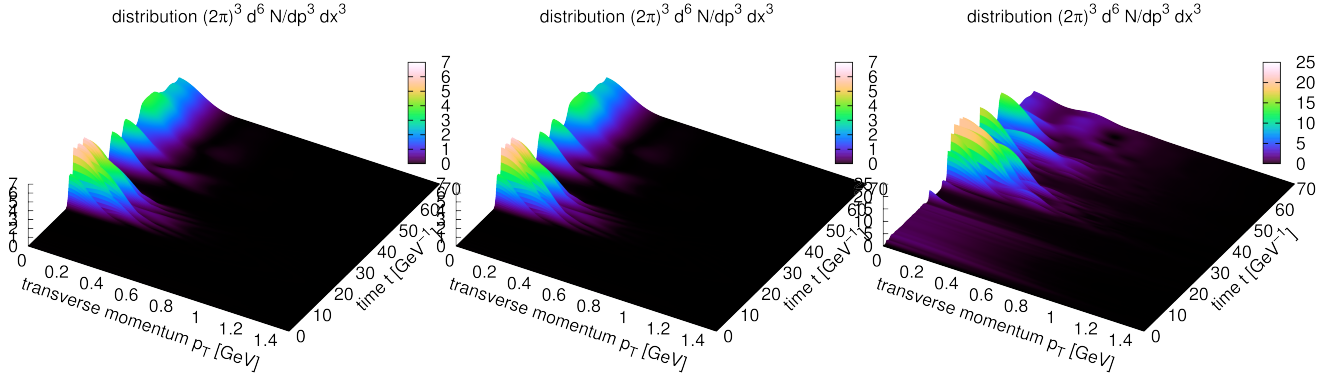


Figure 4.11: The transverse momentum distribution  $d^6 N_{g^+}/d\mathbf{p}^3 d\mathbf{x}^3 = |\beta_{(A)A,\sigma,\mathbf{p}}|^2/(2\pi)^3$  of produced gluons at a fixed longitudinal kinetic momentum  $P_z = p_z - q_A^{(\text{ad.})}\bar{A} = 1.5$  GeV. Different panels correspond to different values of the color charge  $q_A^{(\text{ad.})}$  ( $i = 1, \dots, N_c(N_c - 1)/2$ ) of gluons with color  $A$ . We set the color angle  $\theta = 0$ , and the corresponding gluon charge  $q_A^{(\text{ad.})}$  read  $q_1^{(\text{ad.})} = q_A^{(\text{ad.})} = -1/2$  (left),  $q_2^{(\text{ad.})} = -1/2$  (middle), and  $q_3^{(\text{ad.})} = 1$  (right).

The momentum distributions heavily depend on values of the color charges, or the color angle  $\theta$ , as was discussed in Section 4.2 without the backreaction. The shape of the momentum distributions is, however, very different from what we found without the backreaction (see Figs. 4.1 - 4.4): The classical plasma oscillation and the quantum interferences (i.e., the Bose enhancement for gluons, the Pauli blocking for quarks, and the strong distortion of the spectra) occur as were discussed in QED (see Section 2.5.2) and the Yang-Mills theory (see Section 3.3.2). As there are larger number of charged particle degrees of freedom in QCD ( $N_c \times N_s \times N_{\text{q}} \times N_{\text{q}\bar{\text{q}}} = 36$  light quarks and  $N_c(N_c - 1) \times N_\sigma = 12$  charged gluons) than in QED ( $N_e \pm N_s = 4$  electrons) and in the  $SU_c(N_c = 2)$  Yang-Mills theory ( $N_c(N_c - 1) \times N_\sigma = 2$  charged gluons), the time-scale of the plasma oscillation  $t_{\text{osc}}$  becomes faster. One can estimate the time scale  $t_{\text{osc}}$  in an analogous manner in QED (see Section 2.5.2). By assuming that the quantum interferences are negligible, one finds

$$\sqrt{|g\bar{E}_0|}t_{\text{osc}} \sim \frac{\pi^2}{g} \sqrt{\frac{2\pi g^3}{N_s N_{\text{q}\bar{\text{q}}} N_{\text{q}} \sum_i |q_i^{(\text{fund.})}|^3 + N_\sigma N_{g^\pm} \sum_A |q_A^{(\text{ad.})}|^3}} \sim 9.0 \times g^{-1}, \quad (4.100)$$

which is in agreement with the figures. We note that the charge summations  $\sum_i |q_i^{(\text{fund.})}|^3$ ,  $\sum_A |q_A^{(\text{ad.})}|^3$  do depend on the value of the color angle  $\theta$ , however, one can numerically check that the  $\theta$ -dependence is so tiny that one can safely approximate these summations as  $\sum_i |q_i^{(\text{fund.})}|^3 \sim 0.2 \times g^3$  and  $\sum_A |q_A^{(\text{ad.})}|^3 \sim 1.3 \times g^3$ .

### 4.3.3 decay of color electric field

Figure 4.12 displays the time-evolution of the electric field strength (left) together with the total color current  $\langle : j^z : \rangle \equiv \sum_{\alpha} w_{\alpha} \langle : j_{\alpha}^z : \rangle$  (right). We observe that the electric field decays faster than that in previous two studies (see Section 2.5.3 for QED and Section 3.3.3 for the Yang-Mills theory). This is because the number of charged particles are larger than in the previous two studies. In particular, increase of gluon degrees of freedom is essential: Gluon production is huge because of the Bose enhancement, while quark production is strongly suppressed by the Pauli blocking (see Fig. 4.13 also). Also, it is important that gluon distribution is more severely distorted by the quantum interferences than those for quarks, which further drives the classical field to decohere. Because of these two reasons, gluons create larger color current than that for quarks as in the right panel of Fig. 4.12, and strongly diminish the classical field strength.

Intuitively speaking, our result indicates that the QCD string (with a typical string tension  $\sim 1 \text{ GeV}^2$ ) that binds quarks completely breaks down by producing huge number of quarks and gluons with a relatively short time scale  $\sim 10 \text{ fm}/c$  when they are instantaneously extended macroscopically.

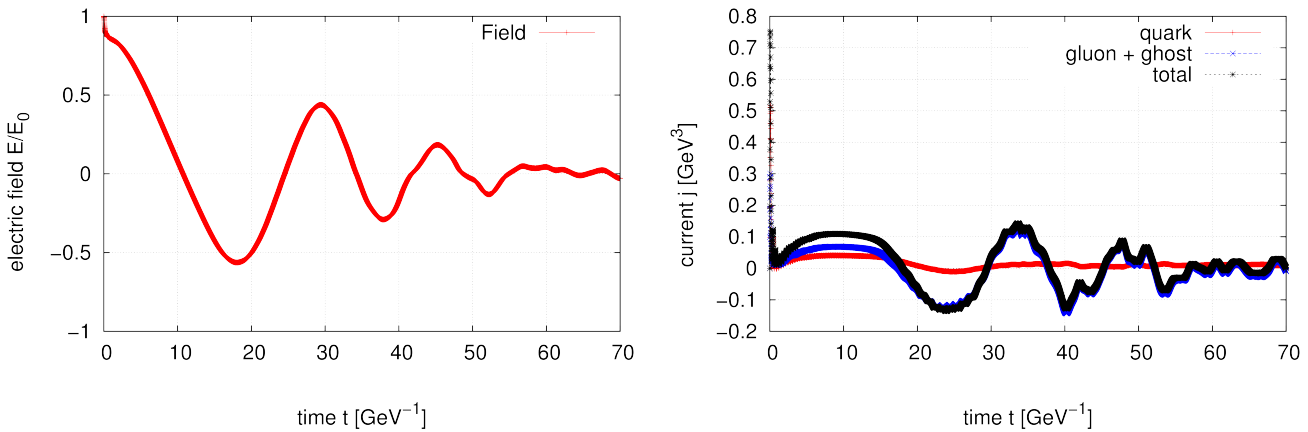


Figure 4.12: [Left] The time-evolution of the electric field strength  $\bar{E}(t)$  [Right] The time-evolution of the color current  $\langle : \hat{j}^z : \rangle$ : The quark contribution (red), the gluon and ghost contribution (blue), and the sum of them (black).

### 4.3.4 total number of quarks and gluons

In Fig. 4.13, the total number of produced quarks  $\sum_{f,i,s,q\bar{q}} \int d^3\mathbf{p} d^6 N_{(-)} / d\mathbf{p}^3 d\mathbf{x}^3$  and gluons  $\sum_{\sigma,A,g_{\pm}} \int d^3\mathbf{p} d^6 N_{g_{\pm}} / d\mathbf{p}^3 d\mathbf{x}^3$  together with their ratio  $R_{q-g} \equiv [\sum_{f,i,s,q\bar{q}} \int d^3\mathbf{p} d^6 N_{(-)} / d\mathbf{p}^3 d\mathbf{x}^3] / [\sum_{\sigma,A,g_{\pm}} \int d^3\mathbf{p} d^6 N_{g_{\pm}} / d\mathbf{p}^3 d\mathbf{x}^3]$  are plotted.

One immediately notices from Fig. 4.13 that gluons are produced much more abundantly than quarks. This is because of the Bose enhancement and the Pauli blocking discussed before.

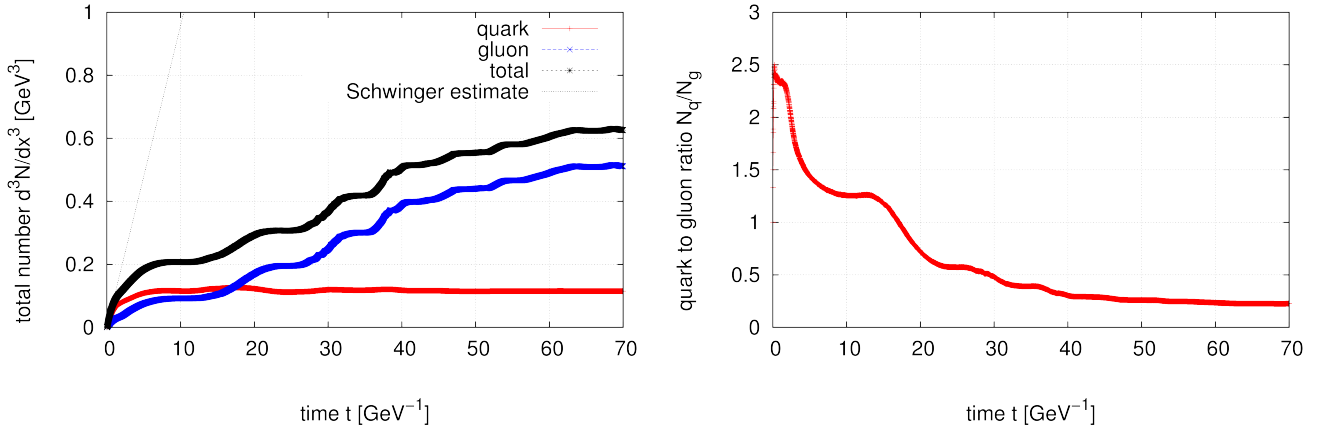


Figure 4.13: [Left] Total number of produced quarks  $\sum_{f,i,s,q\bar{q}} \int d^3\mathbf{p}d^6 N_{(-)} / d\mathbf{p}^3 d\mathbf{x}^3$  (red) and gluons  $\sum_{\sigma,A,g_{\pm}} \int d^3\mathbf{p}d^6 N_{g_{\pm}} / d\mathbf{p}^3 d\mathbf{x}^3$  (blue), and the sum of them (black). The dashed line is an expectation from the Schwinger mechanism without the backreaction, i.e., the sum of Eqs. (4.93) and (4.94). [Right] A ratio of the total of quarks to the total number of gluons  $R_{q-g} \equiv [\sum_{f,i,s,q\bar{q}} \int d^3\mathbf{p}d^6 N_{(-)} / d\mathbf{p}^3 d\mathbf{x}^3] / [\sum_{\sigma,A,g_{\pm}} \int d^3\mathbf{p}d^6 N_{g_{\pm}} / d\mathbf{p}^3 d\mathbf{x}^3]$ .

The ratio of the total quark number to the total gluon number  $R_{q-g}$  is investigated in the right panel of Fig. 4.13. As was expected from the perturbative calculation without the backreaction (4.97), the ratio  $R_{q-g}$  takes values about two around  $t \rightarrow 0$ . On the other hand, the ratio becomes smaller than unity as time goes in contrast to the naive expectation from the Schwinger mechanism for a constant electric field, see Eqs. (4.93) and (4.94), because of the backreaction effects.

In Fig. 4.14, quark production is investigated in more detail. We find that strange quarks are as abundantly produced as the massless up and down quarks for all values of  $t$ . On the other hand, charm production depends on the time scale: For small values of  $t$ , charm production is comparable to the other three “light” quarks (i.e., up, down, and strange quarks) because of the perturbative enhancement as was so without the backreaction (see Section 4.7). Whereas, charm production is strongly suppressed for larger value of  $t$  because of the mass effect. It is interesting to point out that the ratio of charm quark production to the total quark production  $R_q$  asymptotes a constant value which is much larger than the value that the Schwinger formula for a constant electric field gives (4.98). This is because the electric field quickly dies away and the ratio stops decreasing before reaching the value of the Schwinger formula gives.

### 4.3.5 energy density

The time-evolution of the energy density of the system is investigated in Figs. 4.15 and 4.16.

From Fig. 4.15, we find that the total energy of the system is always dominated by the gauge

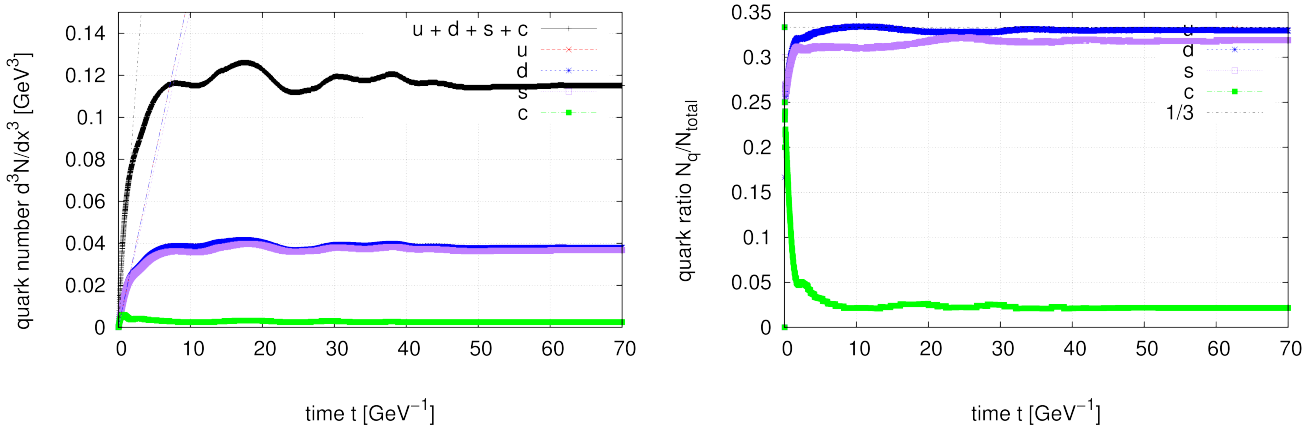


Figure 4.14: [Left] Total number of quarks  $\sum_{f,i,s,q\bar{q}} \int d^3\mathbf{p} d^6 N_{(-)} / d\mathbf{p}^3 d\mathbf{x}^3$  (black), and the contributions from up (red), down (blue), strange (purple), and charm (green). The dashed line are the expectation from the Schwinger formula without the backreaction (4.93). [Right] A suppression factor of charm and strange in quark production  $R_q \equiv N_q / (N_u + N_d + N_s + N_c)$ .

field (the sum of the classical field and the quantum gluons and ghosts), which implies that the dominant degrees of freedom of the system are not (quantum) quarks but (classical and/or quantum) gluons. The ratio of the quark energy to the gauge field energy takes maximum at early times because quark production is larger than gluon production at early times because of the perturbative enhancement (see Fig. 4.13). At later times, the ratio takes values about 0.35, which is roughly consistent with the number ratio  $N_{q-g} \sim 0.23$  displayed in Fig. 4.13. The difference is because gluons are free from the Pauli principle and a large amount of soft gluons is produced.

Details of the total gauge field energy (the left panel) and the quark energy (the right panel) are shown in Fig. 4.16. From the left panel, one understands that the initial classical field energy is quickly converted into quantum gluons, and eventually the system is completely dominated by quantum gluons. The right panel shows that the quark energy is dominated by the three “light” quarks (i.e., up, down, and strange quarks), and the charm contribution is rather negligible in our energy scale  $\sqrt{|g\bar{E}_0|} = 1$  GeV. This is consistent with what we found in the quark production (see Fig. 4.14). We note that there is no peak structure in the charm quark energy. This is because the charm quark mass is so heavy that the energy supply due to the acceleration by the electric field after the production is negligible.

### 4.3.6 pressure

Finally, we investigate the transverse (longitudinal) pressure  $\langle : \hat{P}_\perp : \rangle$  ( $\langle : \hat{P}_z : \rangle$ ) of the system. The results are plotted in Figs. 4.17 and 4.18 (4.19 and 4.20). Also, the degree of an anisotropy of the system is measured by the ratios,  $\langle : \hat{P}_\perp : \rangle / \langle : \hat{\epsilon} : \rangle$  and  $\langle : \hat{P}_z : \rangle / \langle : \hat{\epsilon} : \rangle$ , which are plotted

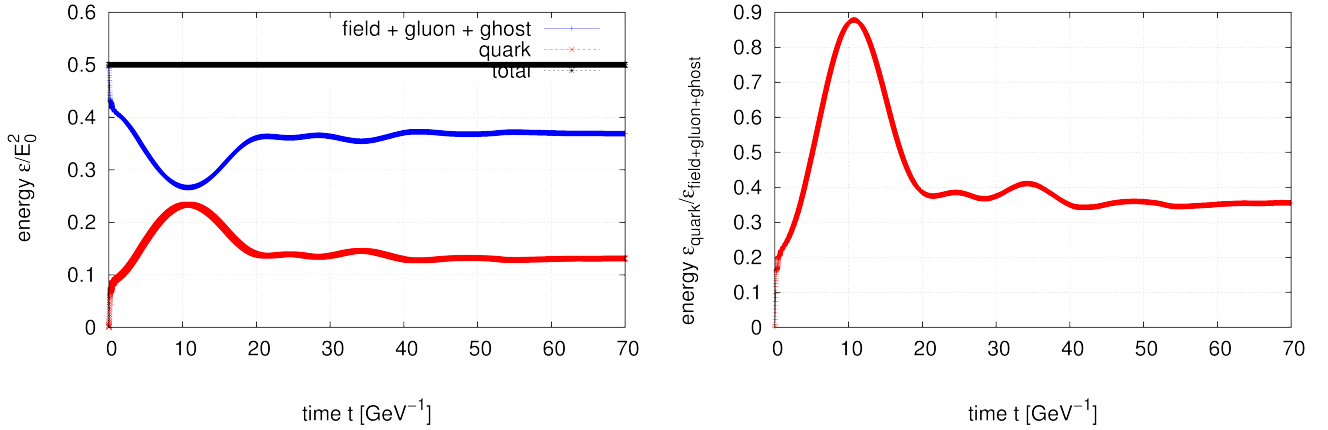


Figure 4.15: [Left] The energy balance between the total gauge field, i.e., the sum of classical field, quantum gluons, and ghosts (blue), and produced quarks (red). The total energy of the system represented by the black line is strictly conserved during the whole time-evolution. [Right] The ratio of the produced quark energy to the total gauge field energy.

in Fig. 4.21. The results are basically the same as what we found in the previous two studies (see Section 2.5.6 for QED and Section 3.3.6 for the Yang-Mills theory).

For the transverse pressure of the system displayed in Figs. 4.17 and 4.18, we find that the transverse pressure of the system is again dominated by the total gauge field (i.e., the sum of the classical field and the quantum gluons and ghosts). Through the decoherence of the classical field into quantum gluons and quarks, the total transverse pressure of the system dies away. This is because quantum particles have only soft transverse momenta, since they are created with almost zero momentum  $\mathbf{P} \sim \mathbf{0}$  and the transverse momentum is conserved during the time-evolution. The quark pressure is dominated by the three “light” quarks, and the contribution from charm quarks is negligible because their production is strongly suppressed as was explained in Fig. 4.13.

The longitudinal pressure of the system is displayed in Figs. 4.19 and 4.20. The longitudinal pressure is again dominated by the total gauge field. The contributions from quantum particles are, in contrast to the transverse pressure, sizable because the longitudinal electric field supplies sizable longitudinal momenta after quantum particles are created. The quark pressure is again dominated by the three “light” quarks, and the charm contribution is negligible. Notice that there is no peak structure in the charm quark pressure. This is because the charm quark mass is so heavy that the longitudinal acceleration by the electric field after the production is negligible. An important point here, as for the previous two studies (see Section 2.5.6 for QED and Section 3.3.6 for the Yang-Mills theory), is that the total longitudinal pressure of the system eventually becomes positive because of the decay of the classical field triggered by the quantum interaction of cubic order among gluons and quarks.

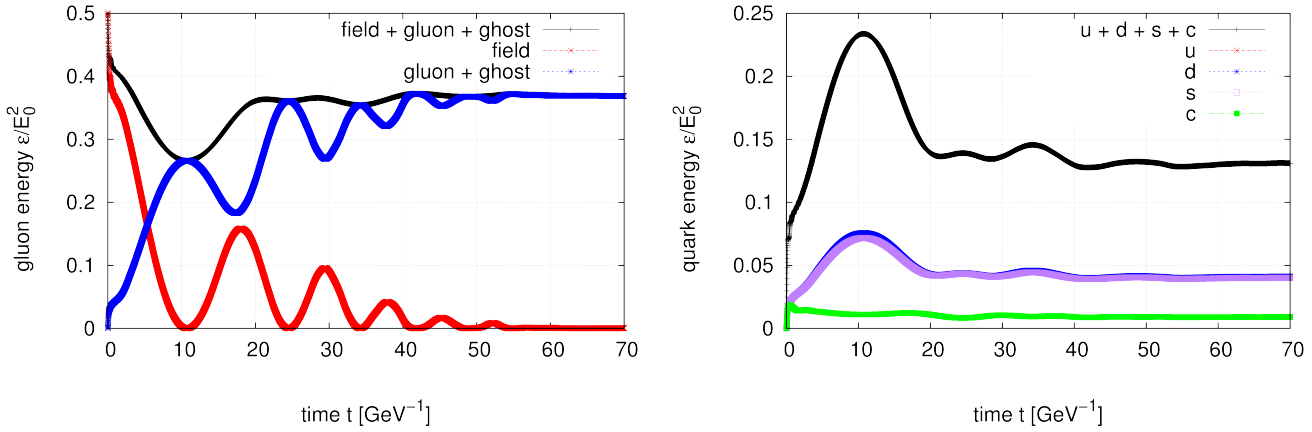


Figure 4.16: [Left] The energy balance of the total gauge field energy (black) in terms of the classical field (red) and the quantum gluons and ghosts (blue). [Right] The total quark energy (black) together with the contributions from up (red), down (blue), strange (purple), and charm (green) quarks.

The isotropization of the system is investigated in Fig. 4.21. We find that the system never gets isotropitized, although the degree of anisotropy gets relaxed. This may be because of our theoretical treatment, where the mean field and massless approximations were adopted and collisional effects among created particles are neglected.

## 4.4 Brief summary

We briefly summarize the main results of this chapter:

- We formulated the Schwinger mechanism in  $SU_f(N_f) \otimes SU_c(N_c = 3)$  QCD including backreaction by adopting the mean field approximation and the massless approximation in Section 4.1.
- By neglecting backreaction, we analytically traced the time-evolution of quark and gluon distribution functions under a constant color electric field in Section 4.2. We showed that quark and gluon production is consistent with what one naively estimates with the Schwinger formula. Various dependences, such as the color angle  $\theta$ -, the number of flavor  $N_f$ -, and the quark mass  $m_f$ -dependences, are examined in detail.
- The backreaction problem was extensively studied in Section 4.3. We revealed that the classical plasma oscillation and the quantum interferences (the Bose enhancement for gluons, the Pauli blocking for quarks, and strong distortion of quark and gluon spectra) occur.

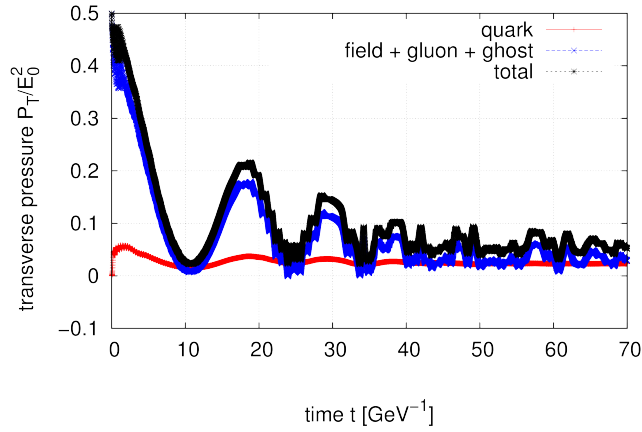


Figure 4.17: The total transverse pressure of the system (black) together with contributions from the total gauge field, i.e., the sum of classical field, quantum gluons, and ghosts (blue), and produced quarks (red).

- As a result of the quantum interferences, the particle production mechanism is dramatically modified. In particular, gluon production is greatly enhanced and they quickly screen the original classical field. The system is eventually dominated by gluons, and quarks are only secondary (see Figs. 4.13 and 4.15).
- Quark mass  $m_f$ -dependences are also investigated including backreaction, and found that the strange (charm) quark production is comparable (negligible) to the massless up and down quark production. It is interesting, however, that the charm quark production is much larger than the value the Schwinger formula for a constant electric field gives (see Fig. 4.14).
- Our formalism does not describe isotropization (or, thermalization) of the system (see Fig. 4.21). This is because of our mean field treatment and the massless approximation, by which we neglect scatterings and collision among quarks and gluons.

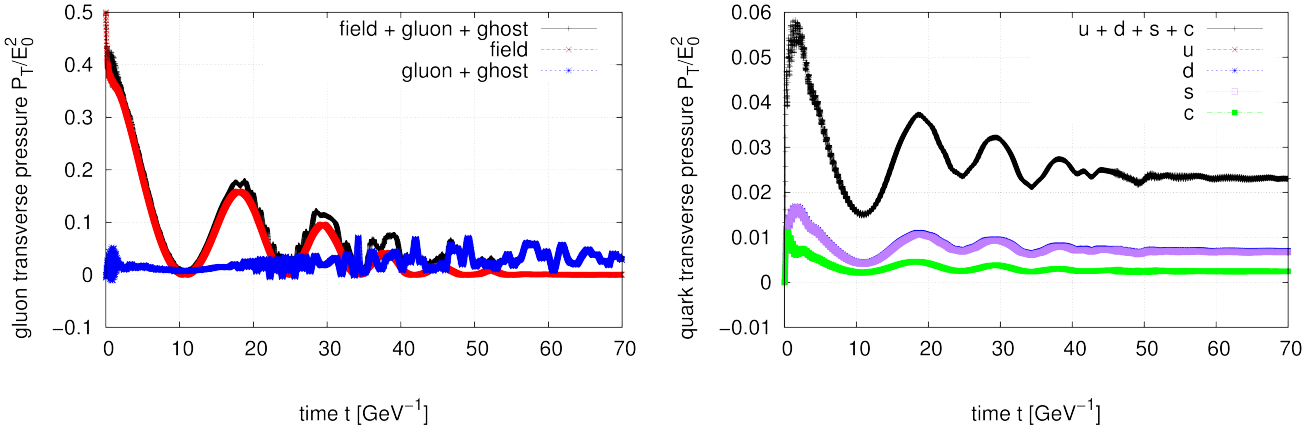


Figure 4.18: [Left] The total transverse pressure of the total gauge field (black) together with contributions from the classical field (red) and the quantum gluons and ghosts (blue). [Right] The total transverse pressure of produced quarks (black) together with the contributions from up (red), down (blue), strange (purple), and charm (green) quarks.

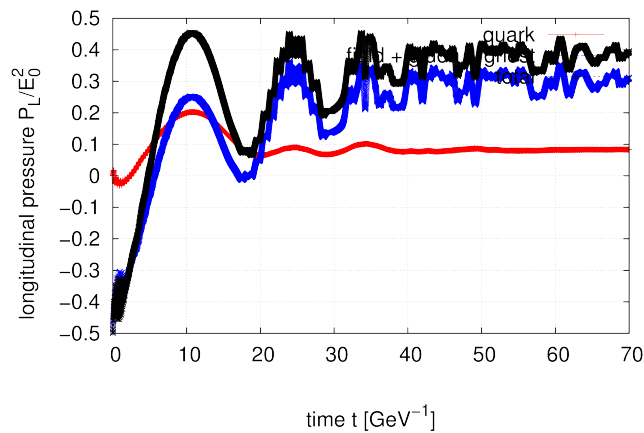


Figure 4.19: The total longitudinal pressure of the system (black) together with contributions from the total gauge field, i.e., the sum of classical field, quantum gluons, and ghosts (blue), and produced quarks (red).

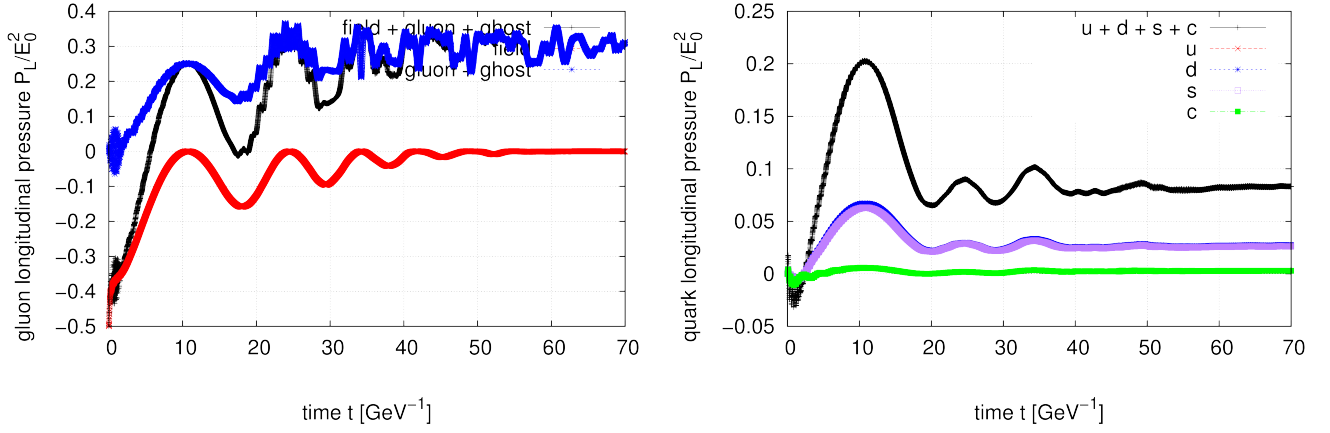


Figure 4.20: [Left] The total longitudinal pressure of the total gauge field (black) together with contributions from the classical field (red) and the quantum gluons and ghosts (blue). [Right] The total longitudinal pressure of produced quarks (black) together with the contributions from up (red), down (blue), strange (purple), and charm (green) quarks.

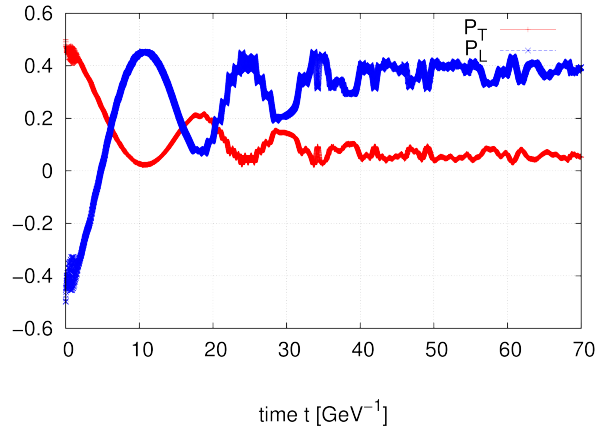


Figure 4.21: Isotropization of the system. The total transverse and longitudinal pressure scaled by the total energy,  $\langle : \hat{P}_\perp : \rangle / \langle : \hat{\epsilon} : \rangle$  and  $\langle : \hat{P}_z : \rangle / \langle : \hat{\epsilon} : \rangle$ , are plotted in red and blue line, respectively.



## Chapter 5

# Particle Production in Ultra-relativistic Heavy Ion Collisions

One of the most important applications of the Schwinger mechanism can be found in the pre-equilibrium stage dynamics of heavy ion collisions. Indeed, the pre-equilibrium stage dynamics is one of the biggest missing pieces in our current understanding of spacetime evolution of ultra-relativistic heavy ion collisions. We apply the QCD formalism developed so far to this issue by modeling the initial strong color electromagnetic flux tubes existing just after a collision of nuclei with a spatially uniform, boost-invariantly expanding electric field<sup>1</sup>.

For this purpose, we first explain how we can extend the previous formulation of Schwinger mechanism in QCD (within the mean field and massless approximation) for non-expanding electric fields to a boost-invariantly expanding one; this will be explained in Section 5.1. In Section 5.2, by neglecting backreaction from quark, gluon, and ghost fluctuations, we analytically show how the Schwinger mechanism for an expanding electric field differs/resembles to the one for the non-expanding electric field previously studied in Section 4. In Section 5.3, we consider the backreaction, and discuss some phenomenological consequences of our formalism to the pre-equilibrium stage dynamics of heavy ion collisions.

We use Latin (Greek) indices  $m, n, \dots$  ( $\mu, \nu, \dots$ ) for the Cartesian ( $\tau$ - $\eta$ ) coordinates throughout this chapter.

A part of Section 5.1 and 5.2 is based on my own work [137].

### 5.1 Schwinger mechanism in $\tau$ - $\eta$ coordinates

This section is organized as follows: In Section 5.1.1, we first introduce the  $\tau$ - $\eta$  coordinates, which are very useful in treating boost-invariant dynamics. After briefly addressing certain as-

---

<sup>1</sup>In reality, the initial strong color electromagnetic flux tubes existing just after a collision of nuclei are spatially inhomogeneous with typical transverse correlation length  $\sim 1/Q_s \sim 0.1$  fm, and have magnetic components in addition to the electric ones as were reviewed in Section 1.2. Inclusion of these properties are important to discuss the pre-equilibrium stage dynamics more realistically, however, we leave these topics for a future work.

assumptions needed to formulate the Schwinger mechanism in QCD for an expanding electric field in a theoretically sound way in Section 5.1.2, we employ the canonical quantization procedure in the  $\tau$ - $\eta$  coordinates to define particle picture for a boost-invariant system in Section 5.1.3. In Section 5.1.4, we explain how one can compute particle spectra produced from a boost-invariant electric field by using the particle picture by following Refs. [137, 159].

### 5.1.1 $\tau$ - $\eta$ coordinates

In dealing with boost-invariant dynamics, it is very convenient to use the  $\tau$ - $\eta$  coordinates  $x^\mu = (\tau, x, y, \eta)$ , instead of the usual Cartesian coordinates  $\xi^m = (t, x, y, z)$ . The  $\tau$ - $\eta$  coordinates are defined by the following change of variables

$$\tau = \sqrt{t^2 - z^2}, \quad \eta = \frac{1}{2} \ln \frac{t+z}{t-z}. \quad (5.1)$$

The line element  $ds^2$  is then expressed as

$$ds^2 = \eta_{mn} d\xi^m d\xi^n = g_{\mu\nu} dx^\mu dx^\nu, \quad (5.2)$$

where

$$\eta_{mn} = \text{diag}(1, -1, -1, -1), \quad (5.3)$$

$$g_{\mu\nu} = \text{diag}(1, -1, -1, -\tau^2) \quad (5.4)$$

are the metric of the Cartesian coordinates and the  $\tau$ - $\eta$  coordinates, respectively.

For later discussions, it is convenient to introduce a *viervein* matrix  $e^m{}_\mu$  [160], which relates the Cartesian coordinates  $\xi^m$  and the  $\tau$ - $\eta$  coordinates  $x^\mu$  as

$$d\xi^m = e^m{}_\mu dx^\mu \quad (5.5)$$

with

$$e^m{}_\mu \equiv \frac{d\xi^m}{dx^\mu} = \begin{pmatrix} \cosh \eta & 0 & 0 & \tau \sinh \eta \\ 0 & 1 & 0 & 0 \\ 0 & 0 & 1 & 0 \\ \sinh \eta & 0 & 0 & \tau \cosh \eta \end{pmatrix}. \quad (5.6)$$

The inverse matrix of  $e^m{}_\mu$ , which we write  $e^\mu{}_m$ , is

$$e^\mu{}_m \equiv \frac{dx^\mu}{d\xi^m} = \begin{pmatrix} \cosh \eta & 0 & 0 & -\sinh \eta \\ 0 & 1 & 0 & 0 \\ 0 & 0 & 1 & 0 \\ -\frac{\sinh \eta}{\tau} & 0 & 0 & \frac{\cosh \eta}{\tau} \end{pmatrix} = \eta_{mn} g^{\mu\nu} e^n{}_\nu. \quad (5.7)$$

With the viervein matrix introduced above, one can define a vector  $V^\mu$  in the  $\tau$ - $\eta$  coordinates for a corresponding vector  $V^m$  in the Cartesian coordinates as

$$V_\mu \equiv e^m{}_\mu V_m, \quad (5.8)$$

$$V^\mu \equiv e^\mu{}_m V^m = g^{\mu\nu} V_\nu. \quad (5.9)$$

One can also generalize these definitions (5.8) and (5.9) to general tensors  $T^{\mu\dots\nu\dots}$  as

$$T^{\mu\dots\nu\dots} = e^\mu{}_m \dots e^n{}_\nu \dots T^{m\dots n\dots}. \quad (5.10)$$

As derivatives acting on tensors  $\partial_\mu T^{\nu\dots\rho\dots}$  are not covariant under a coordinate transformation, it is convenient to introduce a covariant derivative  $\nabla_\mu$  for curvilinear coordinates by

$$\nabla_\mu T^{\nu\dots\rho\dots} = \partial_\mu T^{\nu\dots\rho\dots} + \Gamma^\nu{}_{\mu\lambda} T^{\lambda\dots\rho\dots} + \dots - \Gamma^\lambda{}_{\mu\rho} T^{\nu\dots\lambda\dots} - \dots, \quad (5.11)$$

where  $\Gamma^\mu{}_{\nu\rho}$  is the Christoffel symbol denoted by

$$\Gamma^\mu{}_{\nu\lambda} \equiv \frac{1}{2} g^{\mu\rho} (\partial_\nu g_{\lambda\rho} + \partial_\lambda g_{\rho\nu} - \partial_\rho g_{\nu\lambda}), \quad (5.12)$$

whose non-zero elements in the  $\tau$ - $\eta$  coordinates are

$$\Gamma^\eta{}_{\eta\tau} = \Gamma^\tau{}_{\tau\eta} = 1/\tau, \quad \Gamma^\tau{}_{\eta\eta} = \tau. \quad (5.13)$$

One can easily check that the covariant derivative defined above surely preserves the covariance under an arbitrary coordinate transformation. We note that the covariant derivative commutes with the metric  $g^{\mu\nu}$  and the viervein matrix  $e^\mu{}_m$  because  $0 = \nabla_\lambda g^{\mu\nu} = \nabla_\lambda e^\mu{}_m$ .

### equations of motion

One can easily obtain equations of motion in the  $\tau$ - $\eta$  coordinates  $x^\mu$  from those in the Cartesian coordinates  $\xi^m$  by the following replacements<sup>2</sup>:

$$\begin{aligned} \eta^{mn} &\rightarrow g^{\mu\nu}, \\ T^{mn\dots} &\rightarrow T^{\mu\nu\dots}, \\ \partial_m &\rightarrow \nabla_\mu, \end{aligned} \quad (5.14)$$

where  $T^{mn\dots}$  is an arbitrary tensor.

Now, let us assume the Abelian dominance and apply the mean field and massless approximations as in Section 4.1. For this case, the corresponding equations of motion of QCD in the

<sup>2</sup>In general curved spacetime coordinates, there exists an additional term coming from spin connections  $\Gamma_\mu$  in the fermion covariant derivative, which is zero in the  $\tau$ - $\eta$  coordinates.

Cartesian coordinates are given by Eqs. (4.32)-(4.37). From the replacement rule (5.14), we find the equations of motion of QCD in the  $\tau$ - $\eta$  coordinates as

$$\sum_{\alpha} w_{\alpha} \langle : \hat{j}_{\alpha,\mu} : \rangle + \bar{J}_{\mu} = \nabla^{\nu} \nabla_{\nu} \bar{A}_{\mu}, \quad (5.15)$$

$$0 = [i\hat{\not{D}} - q_i^{(\text{fund.})} \bar{A} - m_f] \hat{\psi}_{f,i}, \quad (5.16)$$

$$0 = \nabla^{\nu} \nabla_{\nu} \hat{a}_{\alpha,\mu}, \quad (5.17)$$

$$0 = \bar{\nabla}_A^{\nu} \bar{\nabla}_{A,\nu} \hat{A}_{A,\mu}, \quad (5.18)$$

$$0 = \nabla^{\nu} \nabla_{\nu} \hat{C}_{\alpha}, \quad (5.19)$$

$$0 = \bar{\nabla}_A^{\mu} \bar{\nabla}_{A,\mu} \hat{C}_A, \quad (5.20)$$

where

$$\bar{\nabla}_{A,\mu} \equiv \nabla_{\mu} + iq_A^{(\text{ad.})} \bar{A}_{\mu} \quad (5.21)$$

is the covariant derivative with respect to the classical gauge field  $\bar{A}_{\mu}$ . The color current (in the Abelian  $H_{\alpha}$ -directions)  $\langle : j_{\alpha,\mu} : \rangle$  can also be obtained from  $\langle : j_{\alpha,m} : \rangle$  (4.27) by the replacement rule (5.14), and its explicit expression will be given in Eq. (5.29). We again regulate the vacuum divergence by the normal ordering procedure  $\langle \hat{\bullet} \rangle \rightarrow \langle : \hat{\bullet} : \rangle$  in terms of intermediate operators at “time”  $\tau$  (see Section 5.1.3), not by that at time  $t$ , because the proper “time” variable is  $\tau$  in a boost-invariantly expanding system.

In solving the gluon field equations (5.17) and (5.18), it is convenient to expand the gluon fields  $\hat{a}_{\alpha,\mu}, \hat{A}_{A,\mu}$  by a polarization vector  $\epsilon_{\sigma,\mu}(x)$  ( $\sigma = 0, 1, 2, 3$ ), which can depend on spacetime in general, as

$$\begin{pmatrix} \hat{a}_{\alpha,\mu} \\ \hat{A}_{A,\mu} \end{pmatrix} \equiv \sum_{\sigma} \epsilon_{\sigma,\mu} \begin{pmatrix} \hat{a}_{\alpha,\sigma} \\ \hat{A}_{A,\sigma} \end{pmatrix}. \quad (5.22)$$

Here, we construct the polarization vector  $\epsilon_{\sigma,\mu}$  by contracting an arbitrary constant four vector  $\tilde{\epsilon}_{\sigma,m}$  by the viervein matrix  $e^m_{\mu}$  as

$$\epsilon_{\sigma,\mu} \equiv e^m_{\mu} \tilde{\epsilon}_{\sigma,m}. \quad (5.23)$$

The important property of the above defined polarization vector  $\epsilon_{\sigma,\mu}(x)$  is that whose covariant derivative is vanishing as

$$\nabla_{\mu} \epsilon_{\sigma,\nu} = 0. \quad (5.24)$$

For later purposes, it is convenient to normalize the constant vector  $\tilde{\epsilon}_{\sigma,m}$  in the same manner as was so for the non-expanding polarization vector  $\epsilon_{\sigma,m}$  (3.42) as

$$\eta^{mn} \tilde{\epsilon}_{\sigma,m}^* \tilde{\epsilon}_{\sigma',n} = -\xi_{\sigma\sigma'}, \quad \sum_{\sigma\sigma'} \xi_{\sigma\sigma'} \tilde{\epsilon}_{\sigma,m}^* \tilde{\epsilon}_{\sigma',n} = -\eta_{mn}. \quad (5.25)$$

This normalization condition for  $\tilde{\epsilon}_{\sigma,m}$  is equivalent to normalizing  $\epsilon_{\sigma,\mu}$  as

$$g^{\mu\nu} \epsilon_{\sigma,\mu}^* \epsilon_{\sigma',\nu} = -\xi_{\sigma\sigma'}, \quad \sum_{\sigma\sigma'} \xi_{\sigma\sigma'} \epsilon_{\sigma,\mu}^* \epsilon_{\sigma',\nu} = -g_{\mu\nu}. \quad (5.26)$$

Now, by noting the relation (5.24) and the fact that  $\hat{a}_{\alpha,\sigma}, \hat{\mathcal{A}}_{A,\sigma}$  are scalar functions, we find that  $\hat{a}_{\alpha,\sigma}, \hat{C}_\alpha$  and  $\hat{\mathcal{A}}_{A,\sigma}, \hat{C}_A$  obey the same differential equation, respectively, as

$$0 = \nabla^\nu \nabla_\nu \begin{pmatrix} \hat{a}_{\alpha,\sigma} \\ \hat{C}_\alpha \end{pmatrix} = \left[ \partial_\tau^2 + \frac{\partial_\tau}{\tau} - \mathbf{d}_\perp^2 - \frac{\partial_\eta^2}{\tau^2} \right] \begin{pmatrix} \hat{a}_{\alpha,\sigma} \\ \hat{C}_\alpha \end{pmatrix}, \quad (5.27)$$

$$0 = \bar{\nabla}^\nu \bar{\nabla}_\nu \begin{pmatrix} \hat{\mathcal{A}}_{A,\sigma} \\ \hat{C}_A \end{pmatrix} = \left[ \bar{D}_\tau^2 + \frac{\bar{D}_\tau}{\tau} - \bar{\mathbf{D}}_\perp^2 - \frac{\bar{D}_\eta^2}{\tau^2} \right] \begin{pmatrix} \hat{\mathcal{A}}_{A,\sigma} \\ \hat{C}_A \end{pmatrix}. \quad (5.28)$$

### conservation law

Because of the symmetries in the (approximated) QCD Lagrangian, the color current  $\langle : j_{\alpha,\mu} : \rangle$  and the symmetric energy-momentum tensor  $\langle : T^{\mu\nu} : \rangle$  are conserved in the  $\tau$ - $\eta$  coordinates as well.

#### color current $\hat{j}_{\alpha,\mu}$

One can explicitly express the vacuum expectation value of the color current  $\langle : j_{\alpha,\mu} : \rangle$  in the  $\tau$ - $\eta$  coordinates as

$$\begin{aligned} \langle : \hat{j}_\alpha^\mu : \rangle &= g \sum_f \sum_i (H_\alpha)_{ii} \langle : \hat{\psi}_{f,i} \gamma^\mu \hat{\psi}_{f,i} : \rangle \\ &\quad ig \sum_A v_{\alpha,A} \left\langle : \hat{\mathcal{A}}_{A,\nu}^\dagger \left( \bar{\nabla}_A^\mu \hat{\mathcal{A}}_A^\nu \right) - \left( \bar{\nabla}_A^\mu \hat{\mathcal{A}}_A^\nu \right)^\dagger \hat{\mathcal{A}}_{A,\nu} : \right\rangle \\ &\quad - g \sum_A v_{\alpha,A} \left\langle : \hat{\mathcal{C}}_A^\dagger \left( \bar{\nabla}_{A,\mu} \hat{\mathcal{C}}_A \right) + \left( \bar{\nabla}_{A,\mu} \hat{\mathcal{C}}_A \right)^\dagger \hat{\mathcal{C}}_A - \left( \bar{\nabla}_{A,\mu} \hat{\mathcal{C}}_A \right)^\dagger \hat{\mathcal{C}}_A - \hat{\mathcal{C}}_A^\dagger \left( \bar{\nabla}_{A,\mu} \hat{\mathcal{C}}_A \right) : \right\rangle. \end{aligned} \quad (5.29)$$

The color current  $\langle : j_{\alpha,\mu} : \rangle$  is conserved as

$$\begin{aligned} 0 &= \nabla^\mu \langle : j_{\alpha,\mu} : \rangle \\ &= \frac{1}{\tau} \partial^\mu [\tau \langle : j_{\alpha,\mu} : \rangle]. \end{aligned} \quad (5.30)$$

Notice that, in the first line, the divergence is taken not by the simple derivative  $\partial_\mu$  as in the Cartesian coordinates (4.28) but by the covariant one  $\nabla_\mu$  in the  $\tau$ - $\eta$  coordinates. The factor  $\tau$  in the bracket of the second line physically means that the current density decreases as  $\propto 1/\tau$  because the system volume increases as  $\propto \tau$  due to the longitudinal expansion.

#### symmetric energy-momentum tensor $\hat{T}^{\mu\nu}$

The explicit expressions for the vacuum expectation value of the symmetric energy-momentum

tensor  $\langle : \hat{T}^{\mu\nu} : \rangle$  in the  $\tau$ - $\eta$  coordinates read

$$\begin{aligned}
\langle : \hat{T}_{\mu\nu} : \rangle = & g^{\mu\nu} \left[ \frac{1}{4} \bar{F}^{\rho\sigma} \bar{F}_{\rho\sigma} - \frac{1}{2} (\nabla_\lambda \bar{A}^\lambda)^2 - \bar{A}^\rho \nabla_\rho \nabla_\sigma \bar{A}^\sigma \right] - [\bar{F}^\mu{}_\lambda \bar{F}^{\nu\lambda} - \bar{A}^\mu \nabla^\nu \nabla_\lambda \bar{A}^\lambda - \bar{A}^\nu \nabla^\mu \nabla_\lambda \bar{A}^\lambda] \\
& + g^{\mu\nu} \sum_\alpha \text{Re} \left\langle : \frac{1}{4} \hat{f}_\alpha^{\rho\sigma} \hat{f}_{\alpha,\rho\sigma} - \frac{1}{2} (\nabla_\lambda \hat{a}_\alpha^\lambda)^2 - \hat{a}_\alpha^\rho \nabla_\rho \nabla_\sigma \hat{a}_\alpha^\sigma : \right\rangle \\
& \quad - \sum_\alpha \text{Re} \left\langle : \hat{f}_{\alpha,\lambda}{}^\mu \hat{f}_\alpha{}^{\lambda\nu} - \hat{a}_\alpha{}^\mu \nabla^\nu \nabla_\lambda \hat{a}_\alpha{}^\lambda - \hat{a}_\alpha{}^\nu \nabla^\mu \nabla_\lambda \hat{a}_\alpha{}^\lambda : \right\rangle \\
& + 2 \times \left( g^{\mu\nu} \sum_A \text{Re} \left\langle : \frac{1}{4} \hat{\mathcal{F}}_{A,\rho\sigma}^\dagger \hat{\mathcal{F}}_A{}^{\rho\sigma} - \frac{1}{2} \left| \bar{\nabla}_{A,\lambda} \hat{\mathcal{A}}_A{}^\lambda \right|^2 - \hat{\mathcal{A}}_A{}^{\rho\dagger} (\bar{\nabla}_{A,\rho} \bar{\nabla}_{A,\sigma} \hat{\mathcal{A}}_A{}^\sigma) : \right\rangle \right. \\
& \quad \left. - \sum_A \text{Re} \left\langle : \hat{\mathcal{F}}_{A,\lambda}{}^{\mu\dagger} \hat{\mathcal{F}}_A{}^{\lambda\nu} - \hat{\mathcal{A}}_A{}^{\mu\dagger} (\bar{\nabla}_A{}^\nu \bar{\nabla}_{A,\lambda} \hat{\mathcal{A}}_A{}^\lambda) - \hat{\mathcal{A}}_A{}^{\nu\dagger} (\bar{\nabla}_A{}^\mu \bar{\nabla}_{A,\lambda} \hat{\mathcal{A}}_A{}^\lambda) : \right\rangle \right) \\
& + \sum_\alpha \text{Re} \left\langle : i \times \left[ g^{\mu\nu} (\nabla_\lambda \hat{C}_\alpha) (\nabla^\lambda \hat{C}_\alpha) - (\nabla^\mu \hat{C}_\alpha) (\nabla^\nu \hat{C}_\alpha) - (\nabla^\nu \hat{C}_\alpha) (\nabla^\mu \hat{C}_\alpha) \right] : \right\rangle \\
& + 2 \times \sum_A \text{Re} \left\langle : i \left[ g^{\mu\nu} (\bar{\nabla}_{A,\lambda} \hat{\mathcal{C}}_A)^\dagger (\bar{\nabla}_A{}^\lambda \hat{\mathcal{C}}_A) - (\bar{\nabla}_A{}^\mu \hat{\mathcal{C}}_A)^\dagger (\bar{\nabla}_A{}^\nu \hat{\mathcal{C}}_A) - (\bar{\nabla}_A{}^\nu \hat{\mathcal{C}}_A)^\dagger (\bar{\nabla}_A{}^\mu \hat{\mathcal{C}}_A) \right] : \right\rangle,
\end{aligned} \tag{5.31}$$

where  $\bar{F}_{\mu\nu}$ ,  $\hat{f}_{\alpha,\mu\nu}$ , and  $\hat{\mathcal{F}}_{A,\mu\nu}$  are (a part of) an Abelian and a non-Abelian component of the total field strength tensor  $\hat{F}_{\mu\nu} \equiv \nabla_\mu \hat{A}_\nu - \nabla_\nu \hat{A}_\mu + ig[\hat{A}_\mu, \hat{A}_\nu] = \partial_\mu \hat{A}_\nu - \partial_\nu \hat{A}_\mu + ig[\hat{A}_\mu, \hat{A}_\nu]$  as was introduced in Eq. (4.24). In  $\tau$ - $\eta$  coordinates, they read

$$\begin{aligned}
\bar{F}_{\mu\nu} & \equiv \nabla_\mu \bar{A}_\nu - \nabla_\nu \bar{A}_\mu \\
& = \partial_\mu \bar{A}_\nu - \partial_\nu \bar{A}_\mu, \\
\hat{f}_{\alpha,\mu\nu} & \equiv \nabla_\mu \hat{a}_{\alpha,\nu} - \nabla_\nu \hat{a}_{\alpha,\mu} \\
& = \partial_\mu \hat{a}_{\alpha,\nu} - \partial_\nu \hat{a}_{\alpha,\mu}, \\
\hat{\mathcal{F}}_{A,\mu\nu} & \equiv \bar{\nabla}_{A,\mu} \hat{\mathcal{A}}_{A,\nu} - \bar{\nabla}_{A,\nu} \hat{\mathcal{A}}_{A,\mu} \\
& = \bar{D}_{A,\mu} \hat{\mathcal{A}}_{A,\nu} - \bar{D}_{A,\nu} \hat{\mathcal{A}}_{A,\mu},
\end{aligned} \tag{5.32}$$

where the connection contributions cancel out.

The conservation law for the symmetric energy-momentum tensor  $\langle : \hat{T}^{\mu\nu} : \rangle$  becomes

$$\nabla_\mu \langle : \hat{T}^{\mu\nu} : \rangle = \bar{J}_\mu \bar{F}^{\mu\nu} + \bar{A}^\nu \nabla_\mu \bar{J}^\mu. \tag{5.33}$$

As was the conservation law for the color current (5.30), the covariant divergence gives the correct energy conservation law in the  $\tau$ - $\eta$  coordinates.

The energy density and the transverse/longitudinal pressure in the  $\tau$ - $\eta$  coordinates can be

obtained by the diagonal components of the symmetric energy-momentum tensor as

$$\begin{aligned}\langle : \hat{\epsilon} : \rangle &\equiv \langle : \hat{T}_{\tau\tau} : \rangle, \\ \langle : \hat{P}_{\perp} : \rangle &\equiv \frac{\langle : \hat{T}_{xx} + \hat{T}_{yy} : \rangle}{2}, \\ \langle : \hat{P}_z : \rangle &\equiv \frac{1}{\tau^2} \langle : \hat{T}_{\eta\eta} : \rangle.\end{aligned}\tag{5.34}$$

### 5.1.2 assumptions on the system

So far, we assumed the Abelian dominance and adopted the mean field and massless approximations to get the equations of motion (5.15)-(5.20). We make some more assumptions to proceed further as were done in formulating the Schwinger mechanism in a non-expanding system within QED (Section 2.1.2); the Yang-Mills theory (Section 3.1.2); and QCD (Section 4.1.2):

- (i) (Homogeneity in space)

We restrict our attention to the case, where only a boost-invariant and spatially uniform classical electric field is present, i.e., the electric field does not depend on the spatial variables  $x, y, \eta$  and depends only on  $\tau$ . Suppose that we define the  $z$ -axis by the direction of the electric field. Then, we can express the classical gauge field  $\bar{A}_{\mu}$  in the following form without loss of generality by fixing the residual gauge freedom as

$$\bar{A}_{\tau}(x) = \bar{A}_x(x) = \bar{A}_y(x) = 0, \quad \bar{A}_{\eta}(x) = - \int^{\tau} d\tau' \tau' \bar{E}(\tau').\tag{5.35}$$

In terms of the classical source  $\bar{J}^{\mu}$ , this assumption is equivalent to assuming that the source is independent of  $x, y, \eta$  and has a current component in the  $\eta$ -direction only  $J^{\mu}(x) = \delta^{\mu\eta} J(\tau)$ .

- (ii) (Vacuum initial condition)

We assume that the initial state is given by a vacuum  $|\text{state}; \text{in}\rangle = |\text{vac}; \text{in}\rangle$ , i.e., there are no particles initially.

- (iii) (Adiabatic hypothesis)

We assume that the classical field exists only in the forward light cone region  $t > |z|$  by appropriately switching on and off the classical current  $\bar{J}^{\mu}$ , and that the classical gauge field *smoothly* approaches a pure gauge field (i.e., no interaction with the classical gauge field) at the boundary  $t \rightarrow 0$ .

The second assumption is completely the same as the ‘‘assumption (ii)’’ in the non-expanding studies (see Section 2.1.2, 3.1.2, and 4.1.2). The remaining two assumptions are essentially the same as those in the non-expanding studies.

The first assumption is required so as to surely regulate the unwanted vacuum divergences via the normal ordering procedure as was addressed in Section 2.1.2. This assumption is also useful because it largely simplifies the backreaction equation (5.15) as

$$0 = \sum_{\alpha} w_{\alpha} \langle : \hat{j}_{\alpha, \tau} : \rangle = \sum_{\alpha} w_{\alpha} \langle : \hat{j}_{\alpha, x} : \rangle = \sum_{\alpha} w_{\alpha} \langle : \hat{j}_{\alpha, y} : \rangle, \quad (5.36)$$

$$-\frac{1}{\tau} \frac{d\bar{E}}{d\tau} = \sum_{\alpha} w_{\alpha} \langle : \hat{j}_{\alpha}{}^{\eta} : \rangle + \bar{J}^{\eta}. \quad (5.37)$$

Also, the energy conservation law (5.33) gets simplified as

$$\partial_{\tau}(\tau \langle : \hat{\epsilon} : \rangle) + \langle : \hat{P}_z : \rangle = -\tau^2 \bar{E} \bar{J}^{\eta}. \quad (5.38)$$

As was noted in the footnote 1, this assumption is a somewhat strong simplification because the color electromagnetic flux tubes existing just after a collision have inhomogeneous spatial structure in the transverse plane, which might modify our phenomenological results presented below; we leave this improvement for a future work.

The second assumption is required so as to be consistent with the assumption (i) and the resulting backreaction equation (5.36) as for the non-expanding studies (see Section 2.1.2). In ultra-relativistic heavy ion collisions, an initial state is actually given by a vacuum state.

The third assumption is useful in uniquely defining a particle picture at time  $\tau \rightarrow 0$  in the canonical quantization procedure as was explained in detail in Section 2.1. This assumption is also reasonable in ultra-relativistic heavy ion collisions because projectile nuclei are running on the light-cone  $\tau = 0$  and the classical gauge field created from the nuclei is smoothly connected between  $\tau = 0^+$  (color electromagnetic field present) and  $0^-$  (only pure gauge fields present).

### 5.1.3 canonical quantization

Now, we canonically quantize the (charged) fluctuations  $\hat{\psi}_{f,i}, \hat{\mathcal{A}}_{A,\sigma}, \hat{\mathcal{C}}_A$  in the  $\tau$ - $\eta$  coordinates. Here, we do not consider the fluctuations  $\hat{a}_{\alpha,\sigma}, \hat{C}_{\alpha}$  for simplicity because they do not couple to the classical field so that no particle production occur for these fluctuations.

The canonical quantization in the  $\tau$ - $\eta$  coordinates is recently developed by Tanji [159] within scalar QED, and later extended to the QCD problem, i.e., quark and gluon production by the author [137] (although both studies neglect backreaction effects). The canonical quantization procedure is basically done in the same way as was done in the non-expanding case (see Section 4.1.4), however, there are some differences because of the expansion:

- Now that the system expands in the longitudinal direction, the longitudinal momentum label  $p_z$  is no longer a good quantum number. Instead of  $p_z$ , one has to use  $p_{\eta}$ , which is a Fourier conjugate to the spacetime rapidity  $\eta$ , in labeling the momentum space in a boost-invariant way.

- The time variable that manifestly treats the boost-invariance of the system is not  $t$ , but  $\tau$ , so that one should quantize fluctuations on an equal  $\tau$ -surface, not on an equal  $t$ -surface.
- The Poincare invariance is obviously broken in the  $\tau$ - $\eta$  coordinates so that a correct definition of the positive/negative frequency mode function becomes unclear.

### quarks

Let us begin with quantizing the quark fluctuation  $\hat{\psi}_{f,i}$  in the  $\tau$ - $\eta$  coordinates. By noting the homogeneity in space (the assumption (i) in Section 5.1.2), we Fourier expand the fluctuation  $\hat{\psi}_{f,i}$  to write

$$\hat{\psi}_{f,i}(x) = \sum_s \int d^2\mathbf{p}_\perp dp_\eta \left[ +\psi_{f,i,\mathbf{p}_\perp,p_\eta,s}^{(\tau)}(\tau) \hat{a}_{f,i,\mathbf{p}_\perp,p_\eta,s}(\tau) + -\psi_{f,i,\mathbf{p}_\perp,p_\eta,s}^{(\tau)}(\tau) \hat{b}_{f,i,-\mathbf{p}_\perp,-p_\eta,s}^\dagger(\tau) \right] \frac{e^{i\mathbf{p}_\perp \cdot \mathbf{x}_\perp} e^{ip_\eta \eta}}{(2\pi)^{3/2}}. \quad (5.39)$$

As was noted in the beginning of this section, here we label the momentum space by  $p_\eta$  conjugate to the spacetime rapidity  $\eta$ , not by  $p_z$  conjugate to  $z$ , so as to treat the boost-invariance of the system manifestly. The physical meaning of the boost-invariant momentum  $p_\eta$  is the longitudinal  $p_z$ -momentum observed in a frame moving with velocity  $v = z/t$  (the *co-moving* frame): The change of variable (5.1) tells us that the boost-invariant momentum  $p_\eta$  is related to the momenta  $p_m$  in the Cartesian coordinates (or in the center-of-mass frame) as  $p_\eta = e^m_\eta p_m = zp_t + tp_z$ . Now, we consider to boost this relation with the velocity  $v = z/t$  ( $\eta = \tanh^{-1}(z/t)$ ), by which  $t, z$  transform as  $t \rightarrow \tau, z \rightarrow 0$ . Since  $p_\eta$  is a boost-invariant quantity, one obtains  $p_\eta/\tau = p'_z$ , where  $p'_z$  is the longitudinal momentum observed in the co-moving frame.

$\pm\psi_{f,i,\mathbf{p}_\perp,p_\eta,s}^{(\tau)}$  are intermediate mode functions at an intermediate time  $\tau$ . We only consider to quantize the fluctuation at an intermediate time  $0 < \tau < \infty$ , where interactions with the classical gauge field are still present. The identification of the *correct* intermediate positive/negative frequency mode functions  $\pm\psi_{f,i,\mathbf{p}_\perp,p_\eta,s}^{(\tau)}$  can be done in an analogous manner to the non-expanding study (see Section 2.1.4). That is, we define the positive/negative frequency mode functions at an intermediate time by *plane waves*  $\pm\psi_{f,i,\mathbf{p}_\perp,p_\eta,s}^{(\tau)} \sim \pm\psi_{f,i,\mathbf{p}_\perp,p_\eta,s}^{(\text{plane})}$  by assuming that the classical gauge field is sufficiently adiabatic in time  $\tau$ . The difference is that the plane wave solutions in the  $\tau$ - $\eta$  coordinates are not given by the simple exponential waves  $\propto e^{\pm i\omega_{\mathbf{p}} t}$ , which was the case for the non-expanding problems, because they do not satisfy the equation of motion (5.15) in our expanding problem as was noted in the beginning of this section. In view of this circumstance, before quantizing the fluctuation, let us first explain what are the correct plane wave solutions in the  $\tau$ - $\eta$  coordinates by explicitly solving the equation of motion (5.15) without the classical gauge field  $\bar{A}_\mu = 0$ .

### plane wave solutions

From the equation of motion (5.15) together with the spatial homogeneity (assumption (i) in Section 5.1.2), one obtains the differential equation for Fourier modes  $\pm\psi_{f,i,\mathbf{p}_\perp,p_\eta,s}(\tau) \exp[i\mathbf{p}_\perp \cdot$

$\mathbf{x}_\perp + ip_\eta\eta]/(2\pi)^{3/2}$  as

$$0 = \left[ i\gamma^\tau \partial_\tau - \boldsymbol{\gamma}_\perp \cdot \mathbf{p}_\perp - \gamma^\eta (p_\eta + q_i^{(\text{fund.})} \bar{A}_\eta) - m_f \right] \pm \psi_{f,i,\mathbf{p}_\perp,p_\eta,s}. \quad (5.40)$$

In solving the mode equation (5.40), we first note that the gamma matrices  $\gamma^\tau, \gamma^\eta$  are  $\eta$ -dependent. In order to remove this complexity, it is convenient to transform  $\pm \psi_{f,i,\mathbf{p}_\perp,p_\eta,s}$  by a boost operator  $S$  as

$$\pm \psi_{f,i,\mathbf{p}_\perp,p_\eta,s} \equiv S \pm \tilde{\psi}_{f,i,\mathbf{p}_\perp,p_\eta,s}, \quad (5.41)$$

where

$$S \equiv \exp \left[ \frac{\eta}{2} \gamma^t \gamma^z \right]. \quad (5.42)$$

By noting that the gamma matrices  $\gamma^\tau, \gamma^\eta$  are transformed by the boost operator  $S$  as

$$\begin{pmatrix} \gamma^\tau \\ \gamma^\eta \end{pmatrix} = S \begin{pmatrix} \gamma^t \\ \gamma^z \end{pmatrix} S^{-1}, \quad (5.43)$$

one obtains a differential equation for  $\pm \tilde{\psi}_{f,i,\mathbf{p}_\perp,p_\eta,s}$  as

$$0 = \left[ i\gamma^t \partial_\tau - \boldsymbol{\gamma}_\perp \cdot \mathbf{p}_\perp - \gamma^z \frac{1}{\tau} \left( p_\eta + q_i^{(\text{fund.})} \bar{A}_\eta(\tau) - \frac{i}{2} \gamma^t \gamma^z \right) - m_f \right] \pm \tilde{\psi}_{f,i,\mathbf{p}_\perp,p_\eta,s}. \quad (5.44)$$

This equation (5.44) can be solved in the same manner as what we did in solving the non-expanding mode equation (see Appendix A). That is, we decompose  $\pm \tilde{\psi}_{f,i,\mathbf{p}_\perp,p_\eta,s}$  by eigen-spinors of a projection operator  $P^\pm \equiv (1 \pm \gamma^t \gamma^z)/2$  as

$$\begin{aligned} +\tilde{\psi}_{f,i,\mathbf{p}_\perp,p_\eta,s} &= A_{f,i,\mathbf{p}_\perp,p_\eta,s} U_{f,i,\mathbf{p}_\perp,p_\eta,s} + B_{f,i,\mathbf{p}_\perp,p_\eta,s} V_{f,i,\mathbf{p}_\perp,p_\eta,s}, \\ -\tilde{\psi}_{f,i,\mathbf{p}_\perp,p_\eta,s} &= B_{f,i,\mathbf{p}_\perp,p_\eta,s}^* U_{f,i,\mathbf{p}_\perp,p_\eta,s} - A_{f,i,\mathbf{p}_\perp,p_\eta,s}^* V_{f,i,\mathbf{p}_\perp,p_\eta,s}, \end{aligned} \quad (5.45)$$

where  $U_{f,i,\mathbf{p}_\perp,p_\eta,s}, V_{f,i,\mathbf{p}_\perp,p_\eta,s}$  satisfy

$$P^+ U_{f,i,\mathbf{p}_\perp,p_\eta,s} = U_{f,i,\mathbf{p}_\perp,p_\eta,s}, \quad P^- V_{f,i,\mathbf{p}_\perp,p_\eta,s} = V_{f,i,\mathbf{p}_\perp,p_\eta,s}, \quad (5.46)$$

and

$$\delta_{ss'} = U_{f,i,\mathbf{p}_\perp,p_\eta,s}^\dagger U_{f,i,\mathbf{p}_\perp,p_\eta,s'} = V_{f,i,\mathbf{p}_\perp,p_\eta,s}^\dagger V_{f,i,\mathbf{p}_\perp,p_\eta,s'}, \quad 0 = V_{f,i,\mathbf{p}_\perp,p_\eta,s}^\dagger U_{f,i,\mathbf{p}_\perp,p_\eta,s'}. \quad (5.47)$$

We also normalize the scalar functions  $A_{f,i,\mathbf{p}_\perp,p_\eta,s}, B_{f,i,\mathbf{p}_\perp,p_\eta,s}$  by

$$\frac{1}{\tau} = |A_{f,i,\mathbf{p}_\perp,p_\eta,s}|^2 + |B_{f,i,\mathbf{p}_\perp,p_\eta,s}|^2 \quad (5.48)$$

so as to properly normalize the mode function  $\pm \psi_{f,i,\mathbf{p}_\perp,p_\eta,s}$  as

$$\frac{1}{\tau} \delta_{ss'} = [\pm \psi_{f,i,\mathbf{p}_\perp,p_\eta,s} | \pm \psi_{f,i,\mathbf{p}_\perp,p_\eta,s'}]_{\text{F}}, \quad 0 = [\pm \psi_{f,i,\mathbf{p}_\perp,p_\eta,s} | \mp \psi_{f,i,\mathbf{p}_\perp,p_\eta,s'}]_{\text{F}}, \quad (5.49)$$

where the conserved inner product for fermions in the  $\tau$ - $\eta$  coordinates,  $[\psi_1|\psi_2]_F$ , is denoted by

$$[\psi_1|\psi_2]_F \equiv \bar{\psi}_1 \gamma^\tau \psi_2 = \tilde{\psi}_1^\dagger \tilde{\psi}_2. \quad (5.50)$$

Here,  $\bar{\psi} \equiv \psi^\dagger \gamma^t$  as usual. The factor  $1/\tau$  in Eq. (5.49) comes from the Jacobian of the  $\tau$ - $\eta$  coordinates  $\sqrt{|\mathbf{g}|} = \tau$ . The scalar functions  $A_{f,i,\mathbf{p}_\perp,p_\eta,s}$ ,  $B_{f,i,\mathbf{p}_\perp,p_\eta,s}$  and the spinors  $U_{f,i,\mathbf{p}_\perp,p_\eta,s}$ ,  $V_{f,i,\mathbf{p}_\perp,p_\eta,s}$  introduced above are not independent of each other. By substituting Eq. (5.45) into the mode equation (5.44), one obtains the following relations

$$i \frac{d}{d\tau} \begin{pmatrix} A_{f,i,\mathbf{p}_\perp,p_\eta,s} \\ B_{f,i,\mathbf{p}_\perp,p_\eta,s} \end{pmatrix} = \begin{pmatrix} \frac{p_\eta + q_i^{(\text{fund.})} \bar{A}_\eta(\tau) - i/2}{\tau} & \frac{\sqrt{m_f^2 + \mathbf{p}_\perp^2}}{\tau} \\ \frac{\sqrt{m_f^2 + \mathbf{p}_\perp^2}}{\tau} & -\frac{p_\eta + q_i^{(\text{fund.})} \bar{A}_\eta(\tau) + i/2}{\tau} \end{pmatrix} \begin{pmatrix} A_{f,i,\mathbf{p}_\perp,p_\eta,s} \\ B_{f,i,\mathbf{p}_\perp,p_\eta,s} \end{pmatrix}, \quad (5.51)$$

and

$$V_{f,i,\mathbf{p}_\perp,p_\eta,s} = \gamma^t \frac{\boldsymbol{\gamma}_\perp \cdot \mathbf{p}_\perp + m_f}{\sqrt{m_f^2 + \mathbf{p}_\perp^2}} U_{f,i,\mathbf{p}_\perp,p_\eta,s}. \quad (5.52)$$

We note that Eqs. (5.51) and (5.52) can be applicable to classical fields  $\bar{A}_\eta(\tau)$  with arbitrary time  $\tau$ -dependence because we have not specified the time  $\tau$ -dependence of  $\bar{A}_\eta$  in the above derivation so far.

For now, let us set  $\bar{A}_\eta = 0$  in order to find out plane wave solutions  $\pm \psi_{f,i,\mathbf{p}_\perp,p_\eta,s}^{(\text{plane})}$  of the mode equation (5.40), or Eq. (5.51) for the scalar functions  $A_{f,i,\mathbf{p}_\perp,p_\eta,s}^{(\text{plane})}$ ,  $B_{f,i,\mathbf{p}_\perp,p_\eta,s}^{(\text{plane})}$ . By squaring the both hand sides of Eq. (5.51) to find that  $A_{f,i,\mathbf{p}_\perp,p_\eta,s}^{(\text{plane})}$  obeys the Bessel differential equation:

$$0 = \left[ \frac{d^2}{d\tau^2} + \frac{1}{\tau} \frac{d}{d\tau} - \left( \frac{ip_\eta + 1/2}{\tau} \right)^2 + \mathbf{p}_\perp^2 + m_f^2 \right] A_{f,i,\mathbf{p}_\perp,p_\eta,s}^{(\text{plane})}. \quad (5.53)$$

The general solution of Eq. (5.53) is given by the linear combination of the Hankel function of the  $n$ -th kind ( $n = 1, 2$ )  $H_\nu^{(n)}(z)$  as

$$A_{f,i,\mathbf{p}_\perp,p_\eta,s}^{(\text{plane})} = c_1 \times H_{ip_\eta+1/2}^{(2)}(\sqrt{m_f^2 + \mathbf{p}_\perp^2} \tau) + c_2 \times H_{-ip_\eta-1/2}^{(1)}(\sqrt{m_f^2 + \mathbf{p}_\perp^2} \tau). \quad (5.54)$$

By substituting this expression (5.54) back into Eq. (5.51), one obtains the corresponding solution for  $B_{f,i,\mathbf{p}_\perp,p_\eta,s}^{(\text{plane})}$  as

$$B_{f,i,\mathbf{p}_\perp,p_\eta,s}^{(\text{plane})} = c_1 \times i H_{ip_\eta-1/2}^{(2)}(\sqrt{m_f^2 + \mathbf{p}_\perp^2} \tau) - c_2 \times i H_{-ip_\eta+1/2}^{(1)}(\sqrt{m_f^2 + \mathbf{p}_\perp^2} \tau), \quad (5.55)$$

where the use is made of an identity [162]

$$H_{\nu \mp 1}^{(n)}(z) = \left[ \frac{\nu}{z} \pm \frac{d}{dz} \right] H_\nu^{(n)}(z). \quad (5.56)$$

Now, we wish to identify positive/negative frequency mode out from the general solutions (5.54) and (5.55). As was noted in the beginning of this section, this identification is non-trivial because the Poincare invariance is broken due to the expansion so that one cannot regard  $e^{\mp i\omega_{\mathbf{p}}t}$  as positive/negative frequency modes. The correct identification can be done in the following way [159, 161]: Now, the  $\tau$ - $\eta$  coordinates are essentially flat because the Ricci curvature is always vanishing and are simply related to the Cartesian coordinates with the change of variables introduced in Eq. (5.1). The change of variables must not mix up the positive and the negative frequency modes since any change of variables is just a matter of how we compute physical observables and it must not affect the results; otherwise we would have non-vanishing particle production from free fields in the  $\tau$ - $\eta$  coordinates, which is obviously unphysical<sup>3</sup>. By noting this, it is natural to require that the correct plane wave solutions with positive (negative) frequency in the  $\tau$ - $\eta$  coordinates  $+\psi_{f,i,\mathbf{p}_\perp,p_\eta,s}^{(\text{plane})}$  ( $-\psi_{f,i,\mathbf{p}_\perp,p_\eta,s}^{(\text{plane})}$ ) must be a superposition of that in the Cartesian coordinates  $+\psi_{f,i,\mathbf{p}_\perp,p_z,s}^{(\text{plane})}$  ( $-\psi_{f,i,\mathbf{p}_\perp,p_z,s}^{(\text{plane})}$ ) (see Appendix A.1 for details of  $\pm\psi_{f,i,\mathbf{p}_\perp,p_z,s}^{(\text{plane})}$ ) as

$$\begin{aligned} & \pm\psi_{f,i,\mathbf{p}_\perp,p_\eta,s}^{(\text{plane})}(\tau) \frac{e^{i\mathbf{p}_\perp \cdot \mathbf{x}_\perp} e^{ip_\eta \eta}}{(2\pi)^{3/2}} \\ &= \sum_{f'} \sum_{i'} \sum_{s'} \int d^2\mathbf{p}'_\perp dp'_z \pm w_{f,i,\mathbf{p}_\perp,p_\eta,s;f',i',\mathbf{p}'_\perp,p'_z,s'} \pm \psi_{f',i',\mathbf{p}'_\perp,p'_z,s'}^{(\text{plane})}(t) \frac{e^{i\mathbf{p}'_\perp \cdot \mathbf{x}_\perp} e^{ip'_z z}}{(2\pi)^{3/2}}. \end{aligned} \quad (5.57)$$

The requirement (5.57) together with the normalization condition (5.48) uniquely determines the coefficients  $c_1, c_2$  to obtain the correct plane wave solutions with positive/negative frequency in the  $\tau$ - $\eta$  coordinates. By appropriately choosing the spinor decomposition of  $\pm\psi_{f,i,\mathbf{p}_\perp,p_\eta,s}$  and  $\pm\psi_{f,i,\mathbf{p}_\perp,p_z,s}$  (i.e., we choose  $U_{f,i,\mathbf{p}_\perp,p_\eta,s} = U_{f,i,\mathbf{p}_\perp,p_z,s}$ ) and by using integral representations of the Hankel functions [162]

$$H_\nu^{(1)}(z) = \frac{e^{-i\pi\nu/2}}{i\pi} \int_{-\infty}^{\infty} dt e^{iz \cosh t - \nu t}, \quad H_\nu^{(2)}(z) = -\frac{e^{i\pi\nu/2}}{i\pi} \int_{-\infty}^{\infty} dt e^{-iz \cosh t - \nu t}, \quad (5.58)$$

one obtains

$$\pm\psi_{f,i,\mathbf{p}_\perp,p_\eta,s}^{(\text{plane})} \frac{e^{ip_\eta \eta}}{\sqrt{2\pi}} = \int dp_z \frac{e^{\pm ip_\eta y_{\mathbf{p}}}}{\sqrt{2\pi\omega_{\mathbf{p}}}} \pm\psi_{f,i,\mathbf{p}_\perp,p_z,s}^{(\text{plane})} \frac{e^{ip_z z}}{\sqrt{2\pi}}, \quad (5.59)$$

or more explicitly,

$$\begin{pmatrix} A_{f,i,\mathbf{p}_\perp,p_\eta,s}^{(\text{plane})} \\ B_{f,i,\mathbf{p}_\perp,p_\eta,s}^{(\text{plane})} \end{pmatrix} = \frac{\sqrt{\pi} \sqrt{m_f^2 + \mathbf{p}_\perp^2}}{2} e^{\pi p_\eta/2} \begin{pmatrix} e^{-i\pi/4} H_{ip_\eta+1/2}^{(2)}(\sqrt{m_f^2 + \mathbf{p}_\perp^2} \tau) \\ e^{+i\pi/4} H_{ip_\eta-1/2}^{(2)}(\sqrt{m_f^2 + \mathbf{p}_\perp^2} \tau) \end{pmatrix} \quad (5.60)$$

<sup>3</sup>We remark that these arguments are valid only if coordinates are essentially flat, where the Ricci curvature vanishes. For general curved spacetime coordinates, where the Ricci curvature is non-vanishing, these arguments do not hold. Indeed, the non-zero curvature can interact with quantum fluctuations, which results in a mixing of the positive and the negative frequency mode functions, i.e., particle production.

Here, we introduced the momentum rapidity  $y_{\mathbf{p}}$  as

$$y_{\mathbf{p}} \equiv \frac{1}{2} \ln \frac{\omega_{\mathbf{p}} + p_z}{\omega_{\mathbf{p}} - p_z}. \quad (5.61)$$

Notice that the weight factor  $\pm w_{f,i,\mathbf{p}_{\perp},p_{\eta},s;f',i',\mathbf{p}'_{\perp},p'_{\eta},s'}$  is diagonal with respect to the labels  $i, f, \mathbf{p}_{\perp}, s$  because the longitudinal expansion does modify the longitudinal motion  $p_{\eta}, p_z$  only and does not affect the other degrees of freedom.

### canonical quantization at intermediate times

Now, we canonically quantize the fluctuation at an intermediate time  $0 < \tau < \infty$  by defining the intermediate mode function  $\pm \psi_{f,i,\mathbf{p}_{\perp},p_{\eta},s}^{(\tau)}$  by the plane waves  $\pm \psi_{f,i,\mathbf{p}_{\perp},p_{\eta},s}^{(\text{plane})}$  (5.60) as

$$\pm \psi_{f,i,\mathbf{p}_{\perp},p_{\eta},s}^{(\tau)} \equiv \pm \psi_{f,i,\mathbf{p}_{\perp},p_{\eta}+q_i^{(\text{fund.})}\bar{A}_{\eta}(\tau),s}^{(\text{plane})}. \quad (5.62)$$

Since we are working in the  $\tau$ - $\eta$  coordinates, we impose canonical commutation relations on an equal  $\tau$ -surface, instead of on an equal  $t$ -surface as in the Cartesian coordinates:

$$\{\hat{\psi}_{f,i}(\tau, \mathbf{x}_{\perp}, \eta), \hat{\pi}_{f',i'}(\tau, \mathbf{x}'_{\perp}, \eta')\} = i\delta_{ii'}\delta_{ff'}\delta^2(\mathbf{x}_{\perp} - \mathbf{x}'_{\perp})\frac{\delta(\eta - \eta')}{\tau}, \quad (5.63)$$

$$\{\hat{\pi}_{f,i}(\tau, \mathbf{x}_{\perp}, \eta), \hat{\psi}_{f',i'}(\tau, \mathbf{x}'_{\perp}, \eta')\} = \{\hat{\psi}_{f,i}(\tau, \mathbf{x}_{\perp}, \eta), \hat{\psi}_{f',i'}(\tau, \mathbf{x}'_{\perp}, \eta')\} = 0, \quad (5.64)$$

where the canonical conjugate field  $\hat{\pi}_{f,i}$  to the quark field  $\hat{\psi}_{f,i}$  is given by  $\hat{\pi}_{f,i} = \delta\hat{\mathcal{L}}_{\text{QCD}}/\delta(\partial_{\tau}\hat{\psi}_{f,i}) = i\hat{\psi}_{f,i}\gamma^{\tau}$ . The factor  $1/\tau$  in Eq. (5.63) comes from the Jacobian  $\sqrt{|\mathbf{g}|} = \tau$  of the  $\tau$ - $\eta$  coordinates. The canonical commutation relations, Eqs. (5.63) and (5.64), are equivalent to requiring that the intermediate operators  $\hat{a}_{f,i,\mathbf{p}_{\perp},p_{\eta},s}, \hat{b}_{f,i,\mathbf{p}_{\perp},p_{\eta},s}$  anti-commute as

$$\{\hat{a}_{f,i,\mathbf{p}_{\perp},p_{\eta},s}, \hat{a}_{f',i',\mathbf{p}'_{\perp},p'_{\eta},s'}^{\dagger}\} = \{\hat{b}_{f,i,\mathbf{p}_{\perp},p_{\eta},s}, \hat{b}_{f',i',\mathbf{p}'_{\perp},p'_{\eta},s'}^{\dagger}\} = \delta_{ii'}\delta_{ff'}\delta_{ss'}\delta^2(\mathbf{p}_{\perp} - \mathbf{p}'_{\perp})\delta(p_{\eta} - p'_{\eta}),$$

$$(\text{others}) = 0. \quad (5.65)$$

Because of the assumption (iii) made in Section 5.1.2, the positive/negative frequency mode functions  $\pm \psi_{f,i,\mathbf{p}_{\perp},p_{\eta},s}^{(\tau)}$  and the annihilation operators  $\hat{a}_{f,i,\mathbf{p}_{\perp},p_{\eta},s}, \hat{b}_{f,i,\mathbf{p}_{\perp},p_{\eta},s}$  at an intermediate time naturally reproduce the correct mode functions  $\pm \psi_{f,i,\mathbf{p}_{\perp},p_{\eta},s}^{(\text{in})}$  and the annihilation operators  $\hat{a}_{f,i,\mathbf{p}_{\perp},p_{\eta},s}^{(\text{in})}, \hat{b}_{f,i,\mathbf{p}_{\perp},p_{\eta},s}^{(\text{in})}$  at  $\tau \rightarrow 0$  as

$$\pm \psi_{f,i,\mathbf{p}_{\perp},p_{\eta},s}^{(\tau)} \xrightarrow{\tau \rightarrow 0} \pm \psi_{f,i,\mathbf{p}_{\perp},p_{\eta},s}^{(\text{in})}, \quad (5.66)$$

and

$$\begin{pmatrix} \hat{a}_{f,i,\mathbf{p}_{\perp},p_{\eta},s}(\tau) \\ \hat{b}_{f,i,\mathbf{p}_{\perp},p_{\eta},s}(\tau) \end{pmatrix} \xrightarrow{\tau \rightarrow 0} \begin{pmatrix} \hat{a}_{f,i,\mathbf{p}_{\perp},p_{\eta},s}^{(\text{in})} \\ \hat{b}_{f,i,\mathbf{p}_{\perp},p_{\eta},s}^{(\text{in})} \end{pmatrix}. \quad (5.67)$$

The Bogoliubov transformation that connects the in-state annihilation operators  $\hat{a}_{f,i,\mathbf{p}_{\perp},p_{\eta},s}^{(\text{in})}, \hat{b}_{f,i,\mathbf{p}_{\perp},p_{\eta},s}^{(\text{in})}$  and those at intermediate times  $\hat{a}_{f,i,\mathbf{p}_{\perp},p_{\eta},s}, \hat{b}_{f,i,\mathbf{p}_{\perp},p_{\eta},s}$  is given by

$$\begin{pmatrix} \hat{a}_{f,i,\mathbf{p}_{\perp},p_{\eta},s}(\tau) \\ \hat{b}_{f,i,-\mathbf{p}_{\perp},-p_{\eta},s}^{\dagger}(\tau) \end{pmatrix} = \begin{pmatrix} \alpha_{(\psi)f,i,\mathbf{p}_{\perp},p_{\eta},s}(\tau) & \beta_{(\psi)f,i,\mathbf{p}_{\perp},p_{\eta},s}(\tau) \\ -\beta_{(\psi)f,i,\mathbf{p}_{\perp},p_{\eta},s}^*(\tau) & \alpha_{(\psi)f,i,\mathbf{p}_{\perp},p_{\eta},s}^*(\tau) \end{pmatrix} \begin{pmatrix} \hat{a}_{f,i,\mathbf{p}_{\perp},p_{\eta},s}^{(\text{in})} \\ \hat{b}_{f,i,-\mathbf{p}_{\perp},-p_{\eta},s}^{(\text{in})\dagger} \end{pmatrix}, \quad (5.68)$$

where

$$\alpha_{(\psi)f,i,\mathbf{p}_\perp,p_\eta,s}(\tau) \equiv \tau [ {}_+\psi_{f,i,\mathbf{p}_\perp,p_\eta,s}^{(\tau)} | {}_+\psi_{f,i,\mathbf{p}_\perp,p_\eta,s}^{(\text{in})} ]_{\text{F}} = \tau [ {}_-\psi_{f,i,\mathbf{p}_\perp,p_\eta,s}^{(\tau)} | {}_-\psi_{f,i,\mathbf{p}_\perp,p_\eta,s}^{(\text{in})} ]_{\text{F}}^*, \quad (5.69)$$

$$\beta_{(\psi)f,i,\mathbf{p}_\perp,p_\eta,s}(\tau) \equiv \tau [ {}_+\psi_{f,i,\mathbf{p}_\perp,p_\eta,s}^{(\tau)} | {}_-\psi_{f,i,\mathbf{p}_\perp,p_\eta,s}^{(\text{in})} ]_{\text{F}} = -\tau [ {}_-\psi_{f,i,\mathbf{p}_\perp,p_\eta,s}^{(\tau)} | {}_+\psi_{f,i,\mathbf{p}_\perp,p_\eta,s}^{(\text{in})} ]_{\text{F}}^*. \quad (5.70)$$

Because of the normalization condition (5.49), the Bogoliubov coefficients satisfy

$$1 = |\alpha_{(\psi)f,i,\mathbf{p}_\perp,p_\eta,s}(\tau)|^2 + |\beta_{(\psi)f,i,\mathbf{p}_\perp,p_\eta,s}(\tau)|^2. \quad (5.71)$$

Because of the plus sign in front of  $|\beta|^2$ ,  $|\beta|^2$  for quarks never exceeds unity, which is a manifestation of the fermion statistics.

## gluons

Next, we consider the canonical quantization of gluons  $\hat{\mathcal{A}}_{A,\sigma}$ . This can be done in the same manner as that in quarks, although there are slight differences due to the boson nature of gluons. We first derive a correct plane wave solution of gluons with positive/negative frequency in the  $\tau$ - $\eta$  coordinates by explicitly solving the equation of motion (5.28). After that, we employ the canonical quantization procedure to obtain annihilation operators at intermediate times by defining the intermediate mode functions by the plane wave solutions.

### plane wave solutions

By noting the spatial homogeneity of the system (assumption (i) in Section 5.1.2), we Fourier expand the gluon fluctuation  $\hat{\mathcal{A}}_{A,\sigma}$  as  $\pm \mathcal{A}_{A,\sigma,\mathbf{p}_\perp,p_\eta}(\tau) \exp[i\mathbf{p}_\perp \cdot \mathbf{x}_\perp + ip_\eta \eta] / (2\pi)^{3/2}$  to solve the equation of motion (5.28). The differential equation for the Fourier modes  $\pm \mathcal{A}_{A,\sigma,\mathbf{p}_\perp,p_\eta}$  read

$$0 = \left[ \frac{d^2}{d\tau^2} + \frac{1}{\tau} \frac{d}{d\tau} + \left( \frac{p_\eta + q_A^{(\text{ad.})} \bar{A}_\eta}{\tau} \right)^2 + \mathbf{p}_\perp^2 \right] \pm \mathcal{A}_{A,\sigma,\mathbf{p}_\perp,p_\eta}. \quad (5.72)$$

For  $\bar{A}_\eta = 0$ , one can easily solve Eq. (5.72) to find that the plane wave solutions  $\pm \mathcal{A}_{A,\sigma,\mathbf{p}_\perp,p_\eta}^{(\text{plane.})}$  for the gluon fluctuation can be written as

$${}_+\mathcal{A}_{A,\sigma,\mathbf{p}_\perp,p_\eta}^{(\text{plane.})} = c_1 H_{ip_\eta}^{(2)}(|\mathbf{p}_\perp|\tau) + c_2 H_{-ip_\eta}^{(1)}(|\mathbf{p}_\perp|\tau), \quad {}_-\mathcal{A}_{A,\sigma,\mathbf{p}_\perp,p_\eta}^{(\text{plane.})} = [{}_+\mathcal{A}_{A,\sigma,\mathbf{p}_\perp,p_\eta}^{(\text{plane.})}]^*. \quad (5.73)$$

As in the quark case, the coefficients  $c_1, c_2$  can be uniquely determined by a normalization condition

$$\sum_{\sigma'} \xi_{\sigma\sigma'} [ \pm \mathcal{A}_{A,\sigma,\mathbf{p}_\perp,p_\eta}^{(\text{plane.})} | \pm \mathcal{A}_{A,\sigma',\mathbf{p}_\perp,p_\eta}^{(\text{plane.})} ]_{\text{B}} = \pm \frac{1}{\tau}, \quad \sum_{\sigma'} \xi_{\sigma\sigma'} [ \pm \mathcal{A}_{A,\sigma,\mathbf{p}_\perp,p_\eta}^{(\text{plane.})} | \mp \mathcal{A}_{A,\sigma',\mathbf{p}_\perp,p_\eta}^{(\text{plane.})} ]_{\text{B}} = 0, \quad (5.74)$$

where the conserved boson inner product in the  $\tau$ - $\eta$  coordinates is defined by

$$[\phi_1 | \phi_2]_{\text{B}} \equiv i \phi_1^* \overleftrightarrow{\partial}_\tau \phi_2, \quad (5.75)$$

and the criterion for the positive/negative frequency mode is expressed as

$$\begin{aligned} & \pm \mathcal{A}_{A,\sigma,\mathbf{p}_\perp,p_\eta}^{(\text{plane.})}(\tau) \frac{e^{i\mathbf{p}_\perp \cdot \mathbf{x}_\perp} e^{ip_\eta \eta}}{(2\pi)^{3/2}} \\ &= \sum_{A'} \sum_{\sigma'} \int d^2 \mathbf{p}'_\perp dp'_z \pm w_{A,\sigma,\mathbf{p}_\perp,p_\eta;A',\sigma',\mathbf{p}'_\perp,p'_z} \pm \mathcal{A}_{A',\sigma',\mathbf{p}'_\perp,p'_z}^{(\text{plane.})}(t) \frac{e^{i\mathbf{p}_\perp \cdot \mathbf{x}_\perp} e^{ip_z z}}{(2\pi)^{3/2}}, \end{aligned} \quad (5.76)$$

where  $\pm \mathcal{A}_{A,\sigma,\mathbf{p}_\perp,p_z}^{(\text{plane.})}$  is the plane wave solutions in the Cartesian coordinates (see Appendix B.1 for details). As a result of these conditions and with the use of the integral representation of the Hankel functions (5.58), one obtains

$$\pm \mathcal{A}_{A,\sigma,\mathbf{p}_\perp,p_\eta}^{(\text{plane.})} \frac{e^{ip_\eta \eta}}{\sqrt{2\pi}} = \int dp_z \frac{e^{\pm ip_\eta y_{\mathbf{p}}}}{\sqrt{2\pi\omega_{\mathbf{p}}}} \pm \mathcal{A}_{A,\sigma,\mathbf{p}_\perp,p_z}^{(\text{plane.})} \frac{e^{ip_z z}}{\sqrt{2\pi}}, \quad (5.77)$$

or more explicitly

$$+\mathcal{A}_{A,\sigma,\mathbf{p}_\perp,p_\eta}^{(\text{plane.})} = \frac{\sqrt{\pi}}{2i} e^{\pi p_\eta/2} H_{ip_\eta}^{(2)}(|\mathbf{p}_\perp|\tau), \quad -\mathcal{A}_{A,\sigma,\mathbf{p}_\perp,p_\eta}^{(\text{plane.})} = [+\mathcal{A}_{A,\sigma,\mathbf{p}_\perp,p_\eta}^{(\text{plane.})}]^* = -\frac{\sqrt{\pi}}{2i} e^{\pi p_\eta/2} H_{-ip_\eta}^{(1)}(|\mathbf{p}_\perp|\tau). \quad (5.78)$$

We note that the weight factor  $\pm w_{A,\sigma,\mathbf{p}_\perp,p_\eta;A',\sigma',\mathbf{p}'_\perp,p'_z}$  coincides with the quark one (5.59). This is reasonable because the change of variables (5.1) is independent of quantum statistics.

#### canonical quantization at intermediate times

By noting the spatial homogeneity of the system (assumption (i) in Section 5.1.2), we Fourier expand the gluon fluctuation  $\hat{\mathcal{A}}_{A,\sigma}$  as

$$\hat{\mathcal{A}}_{A,\sigma} = \int d^2 \mathbf{p}_\perp dp_\eta \left[ +\mathcal{A}_{A,\sigma,\mathbf{p}_\perp,p_\eta}^{(\tau)}(\tau) \mathfrak{c}_{A,\sigma,\mathbf{p}_\perp,p_\eta}(\tau) + -\mathcal{A}_{A,\sigma,\mathbf{p}_\perp,p_\eta}^{(\tau)}(\tau) \mathfrak{d}_{A,\sigma,-\mathbf{p}_\perp,-p_\eta}^\dagger(\tau) \right] \frac{e^{i\mathbf{p}_\perp \cdot \mathbf{x}_\perp} e^{ip_\eta \eta}}{(2\pi)^{3/2}} \quad (5.79)$$

in order to canonically quantize it at intermediate times. Here, we define the intermediate mode functions  $\pm \mathcal{A}_{A,\sigma,\mathbf{p}_\perp,p_\eta}^{(\tau)}$  by the plane wave solutions  $\pm \mathcal{A}_{A,\sigma,\mathbf{p}_\perp,p_\eta}^{(\text{plane.})}$  (5.78). Namely, the intermediate mode functions  $\pm \mathcal{A}_{A,\sigma,\mathbf{p}_\perp,p_\eta}^{(\tau_0)}$  at the instant of an intermediate time  $\tau = \tau_0$  are defined by

$$\begin{aligned} & \pm \mathcal{A}_{A,\sigma,\mathbf{p}_\perp,p_\eta}^{(\tau_0)}(\tau_0) = \pm \mathcal{A}_{A,\sigma,\mathbf{p}_\perp,p_\eta+q_A^{(\text{ad.})}\bar{A}_\eta(\tau_0)}^{(\text{plane.})}(\tau_0), \\ & \frac{d_\pm \mathcal{A}_{A,\sigma,\mathbf{p}_\perp,p_\eta}^{(\tau_0)}(\tau_0)}{d\tau} = \frac{d_\pm \mathcal{A}_{A,\sigma,\mathbf{p}_\perp,p_\eta+q_A^{(\text{ad.})}\bar{A}_\eta(\tau_0)}^{(\text{plane.})}(\tau)}{d\tau} \Bigg|_{\tau=\tau_0} \end{aligned} \quad (5.80)$$

Notice that as the Klein-Gordon equation is a second order differential equation, one needs two connecting conditions to uniquely expand the field operator  $\hat{\mathcal{A}}_{A,\sigma}$ .

Now, we impose canonical commutation relations on an equal  $\tau$ -surface,

$$\begin{aligned} & [\hat{\mathcal{A}}_{A,\mu}(\tau, \mathbf{x}_\perp, \eta), \hat{\pi}_{A',\nu}(\tau, \mathbf{x}'_\perp, \eta')] = ig_{\mu\nu} \delta_{AA'} \delta^2(\mathbf{x}_\perp - \mathbf{x}'_\perp) \frac{\delta(\eta - \eta')}{\tau}, \\ & [\hat{\mathcal{A}}_{A,\mu}(\tau, \mathbf{x}_\perp, \eta), \hat{\mathcal{A}}_{A',\nu}(\tau, \mathbf{x}'_\perp, \eta')] = [\hat{\pi}_{A,\mu}(\tau, \mathbf{x}_\perp, \eta), \hat{\pi}_{A',\nu}(\tau, \mathbf{x}'_\perp, \eta')] = 0, \end{aligned} \quad (5.81)$$

to complete the canonical quantization procedure. Here, the canonical conjugate field  $\hat{\pi}_{A,\mu}$  to the gluon field operator  $\hat{\mathcal{A}}_{A,\mu}$  is  $\hat{\pi}_{A,\mu} \equiv \partial \hat{\mathcal{L}}_{\text{QCD}} / \partial (\nabla_\tau \hat{\mathcal{A}}_A^\mu) = -\nabla_\tau \hat{\mathcal{A}}_{A,\mu}^\dagger$ . From the canonical commutation relation (5.81), one obtains a commutation relation for the intermediate annihilation operators  $\hat{\mathbf{c}}_{A,\sigma,\mathbf{p}_\perp,p_\eta}, \hat{\mathbf{d}}_{A,\sigma,\mathbf{p}_\perp,p_\eta}$  as

$$\begin{aligned} [\hat{\mathbf{c}}_{A,\sigma,\mathbf{p}_\perp,p_\eta}, \hat{\mathbf{c}}_{A',\sigma',\mathbf{p}'_\perp,p'_\eta}^\dagger] &= [\hat{\mathbf{d}}_{A,\sigma,\mathbf{p}_\perp,p_\eta}, \hat{\mathbf{d}}_{A',\sigma',\mathbf{p}'_\perp,p'_\eta}^\dagger] = \delta_{AA'} \xi_{\sigma\sigma'} \delta^2(\mathbf{p}_\perp - \mathbf{p}'_\perp) \delta(p_\eta - p'_\eta), \\ (\text{others}) &= 0. \end{aligned} \quad (5.82)$$

Thanks to the assumption (iii) made in Section 5.1.2, the positive/negative frequency mode functions  $\pm \mathcal{A}_{A,\sigma,\mathbf{p}_\perp,p_\eta}^{(\text{in})}$  and the annihilation operators  $\hat{\mathbf{c}}_{A,\sigma,\mathbf{p}_\perp,p_\eta}^{(\text{in})}, \hat{\mathbf{d}}_{A,\sigma,\mathbf{p}_\perp,p_\eta}^{(\text{in})}$  at the in-state ( $\tau \rightarrow 0$ ) coincides with those at an intermediate time in the limit of  $\tau \rightarrow 0$  as

$$\pm \mathcal{A}_{A,\sigma,\mathbf{p}_\perp,p_\eta}^{(\tau)} \xrightarrow{\tau \rightarrow 0} \pm \mathcal{A}_{A,\sigma,\mathbf{p}_\perp,p_\eta}^{(\text{in})}, \quad (5.83)$$

$$\begin{pmatrix} \hat{\mathbf{c}}_{A,\sigma,\mathbf{p}_\perp,p_\eta}(\tau) \\ \hat{\mathbf{d}}_{A,\sigma,\mathbf{p}_\perp,p_\eta}(\tau) \end{pmatrix} \xrightarrow{\tau \rightarrow 0} \begin{pmatrix} \hat{\mathbf{c}}_{A,\sigma,\mathbf{p}_\perp,p_\eta}^{(\text{in})} \\ \hat{\mathbf{d}}_{A,\sigma,\mathbf{p}_\perp,p_\eta}^{(\text{in})} \end{pmatrix} \quad (5.84)$$

The in-state annihilation operators  $\hat{\mathbf{c}}_{A,\sigma,\mathbf{p}_\perp,p_\eta}^{(\text{in})}, \hat{\mathbf{d}}_{A,\sigma,\mathbf{p}_\perp,p_\eta}^{(\text{in})}$  and those at intermediate times  $\hat{\mathbf{c}}_{A,\sigma,\mathbf{p}_\perp,p_\eta}, \hat{\mathbf{d}}_{A,\sigma,\mathbf{p}_\perp,p_\eta}$  are not independent of each other. Their relationship is given by the following Bogoliubov transformation:

$$\begin{pmatrix} \hat{\mathbf{c}}_{A,\sigma,\mathbf{p}_\perp,p_\eta}(\tau) \\ \hat{\mathbf{d}}_{A,\sigma,-\mathbf{p}_\perp,-p_\eta}^\dagger(\tau) \end{pmatrix} = \begin{pmatrix} \alpha_{(A)A,\sigma,\mathbf{p}_\perp,p_\eta}(\tau) & \beta_{(A)A,\sigma,\mathbf{p}_\perp,p_\eta}(\tau) \\ \beta_{(A)A,\sigma,\mathbf{p}_\perp,p_\eta}^*(\tau) & \alpha_{(A)A,\sigma,\mathbf{p}_\perp,p_\eta}^*(\tau) \end{pmatrix} \begin{pmatrix} \hat{\mathbf{c}}_{A,\sigma,\mathbf{p}_\perp,p_\eta}^{(\text{in})} \\ \hat{\mathbf{d}}_{A,\sigma,-\mathbf{p}_\perp,-p_\eta}^{(\text{in})} \end{pmatrix}, \quad (5.85)$$

where

$$\begin{aligned} \alpha_{(A)A,\sigma,\mathbf{p}_\perp,p_\eta}(\tau) &\equiv \tau [ {}_+ \mathcal{A}_{A,\sigma,\mathbf{p}_\perp,p_\eta}^{(\tau)} | {}_+ \mathcal{A}_{A,\sigma,\mathbf{p}_\perp,p_\eta}^{(\text{in})} ]_{\text{B}} = -\tau [ {}_- \mathcal{A}_{A,\sigma,\mathbf{p}_\perp,p_\eta}^{(\tau)} | {}_- \mathcal{A}_{A,\sigma,\mathbf{p}_\perp,p_\eta}^{(\text{in})} ]_{\text{B}}^* \\ \beta_{(A)A,\sigma,\mathbf{p}_\perp,p_\eta}(\tau) &\equiv \tau [ {}_+ \mathcal{A}_{A,\sigma,\mathbf{p}_\perp,p_\eta}^{(\tau)} | {}_- \mathcal{A}_{A,\sigma,\mathbf{p}_\perp,p_\eta}^{(\text{in})} ]_{\text{B}} = -\tau [ {}_- \mathcal{A}_{A,\sigma,\mathbf{p}_\perp,p_\eta}^{(\tau)} | {}_+ \mathcal{A}_{A,\sigma,\mathbf{p}_\perp,p_\eta}^{(\text{in})} ]_{\text{B}}^* \end{aligned} \quad (5.86)$$

Because of the normalization (5.74), the Bogoliubov coefficients satisfy

$$1 = |\alpha_{(A)A,\sigma,\mathbf{p}_\perp,p_\eta}(\tau)|^2 - |\beta_{(A)A,\sigma,\mathbf{p}_\perp,p_\eta}(\tau)|^2. \quad (5.87)$$

We note the minus sign in front of  $|\beta|^2$ , which is in contrast to the plus sign in the quark case (5.71), and that  $|\beta|^2$  for gluons can exceed unity.

## ghosts

The canonical quantization of ghost fluctuations  $\hat{\mathcal{C}}_A, \hat{\bar{\mathcal{C}}}_A$  can be done in the same way as that of gluons, except for the unusual anti-commutative nature of ghosts.

Since the ghost fluctuations  $\hat{\mathcal{C}}_A, \hat{\bar{\mathcal{C}}}_A$  obey the same Klein-Gordon equation (5.28) as for the gluon fluctuation  $\hat{\mathcal{A}}_{A,\sigma}$ , one can immediately identify the plane wave solution with positive/negative frequency for ghost fluctuation  $\pm \mathcal{C}_{A,\mathbf{p}_\perp,p_\eta}^{(\text{plane})}$  by Eq. (5.78).

Now, we expand the ghost fluctuation by Fourier modes in the  $\tau$ - $\eta$  coordinates as

$$\begin{pmatrix} \hat{\mathcal{C}}_A \\ \hat{\bar{\mathcal{C}}}_A \end{pmatrix} = \int d^2\mathbf{p}_\perp dp_\eta \left[ +\mathcal{C}_{A,\mathbf{p}_\perp,p_\eta}^{(\tau)} \begin{pmatrix} \hat{\mathbf{e}}_{A,\mathbf{p}_\perp,p_\eta}(\tau) \\ \hat{\bar{\mathbf{e}}}_{A,\mathbf{p}_\perp,p_\eta}(\tau) \end{pmatrix} + -\mathcal{C}_{A,\mathbf{p}_\perp,p_\eta}^{(\tau)} \begin{pmatrix} \hat{\mathbf{f}}_{A,-\mathbf{p}_\perp,-p_\eta}(\tau) \\ \hat{\bar{\mathbf{f}}}_{A,-\mathbf{p}_\perp,-p_\eta}(\tau) \end{pmatrix} \right] \frac{e^{i\mathbf{p}_\perp \cdot \mathbf{x}_\perp} e^{ip_\eta \eta}}{(2\pi)^{3/2}}. \quad (5.88)$$

Here, the positive/negative frequency mode functions for intermediate times  $\pm \mathcal{C}_{A,\mathbf{p}_\perp,p_\eta}^{(\tau)}$  are defined by the plane wave solutions as in the previous quark and gluon cases. Namely, at an intermediate time  $\tau = \tau_0$ , we define  $\pm \mathcal{C}_{A,\mathbf{p}_\perp,p_\eta}^{(\tau)}$  as

$$\begin{aligned} \pm \mathcal{C}_{A,\mathbf{p}_\perp,p_\eta}^{(\tau_0)} &= \pm \mathcal{C}_{A,\mathbf{p}_\perp,p_\eta+q_A^{(\text{ad.})}\bar{A}_\eta(\tau_0)}^{(\text{plane})}(\tau_0), \\ \frac{d_\pm \mathcal{C}_{A,\mathbf{p}_\perp,p_\eta}^{(\tau_0)}}{d\tau} &= \left. \frac{d_\pm \mathcal{C}_{A,\mathbf{p}_\perp,p_\eta+q_A^{(\text{ad.})}\bar{A}_\eta(\tau)}^{(\text{plane})}(\tau)}{d\tau} \right|_{\tau=\tau_0} \end{aligned} \quad (5.89)$$

Next, we impose a canonical commutation relation on an equal  $\tau$ -surface for the ghost modes  $\hat{\mathcal{C}}_A, \hat{\bar{\mathcal{C}}}_A$  as

$$\begin{aligned} \left\{ \hat{\mathcal{C}}_A(\tau, \mathbf{x}_\perp, \eta), \hat{\pi}_B(\tau, \mathbf{x}'_\perp, \eta') \right\} &= i\delta_{AB} \delta^2(\mathbf{x} - \mathbf{x}') \frac{\delta(\eta - \eta')}{\tau}, \\ \left\{ \hat{\mathcal{C}}_A(\tau, \mathbf{x}_\perp, \eta), \hat{\mathcal{C}}_B(\tau, \mathbf{x}'_\perp, \eta') \right\} &= \left\{ \hat{\pi}_A(\tau, \mathbf{x}_\perp, \eta), \hat{\pi}_B(\tau, \mathbf{x}'_\perp, \eta') \right\} = 0, \end{aligned} \quad (5.90)$$

where  $\hat{\pi}_A$  is the canonical conjugate field to the ghost field  $\hat{\mathcal{C}}_A$  and is defined as  $\hat{\pi}_A = \partial \hat{\mathcal{L}}_{\text{QCD}} / \partial(\partial_\tau \hat{\mathcal{C}}_A) = -i\partial_\tau \hat{\mathcal{C}}_A^\dagger$  and  $\hat{\pi}_A = \partial \hat{\mathcal{L}}_{\text{QCD}} / \partial(\partial_\tau \hat{\bar{\mathcal{C}}}_A) = i\partial_\tau \hat{\bar{\mathcal{C}}}_A^\dagger$ . The canonical commutation relation (5.90) tells us that the intermediate annihilation operators  $\hat{\mathbf{e}}_{A,\mathbf{p}_\perp,p_\eta}^{(-)}$ ,  $\hat{\mathbf{f}}_{A,\mathbf{p}_\perp,p_\eta}^{(-)}$  anti-commute as

$$i\delta_{AA'} \delta^2(\mathbf{p}_\perp - \mathbf{p}'_\perp) \delta(\eta - \eta') = \left\{ \hat{\mathbf{e}}_{A,\mathbf{p}_\perp,p_\eta}, \hat{\mathbf{e}}_{A',\mathbf{p}'_\perp,p'_\eta}^{\dagger} \right\} = \left\{ \hat{\mathbf{f}}_{A,\mathbf{p}_\perp,p_\eta}, \hat{\mathbf{f}}_{A',\mathbf{p}'_\perp,p'_\eta}^{\dagger} \right\}, \quad (\text{others}) = 0. \quad (5.91)$$

Just as in the non-expanding case,  $\hat{\mathbf{e}}_{A,\mathbf{p}_\perp,p_\eta}^{(-)}$ ,  $\hat{\mathbf{e}}_{A,\mathbf{p}_\perp,p_\eta}^{\dagger}$  and  $\hat{\mathbf{f}}_{A,\mathbf{p}_\perp,p_\eta}^{(-)}$ ,  $\hat{\mathbf{f}}_{A,\mathbf{p}_\perp,p_\eta}^{\dagger}$  anti-commute with each other. Because of this property, unphysical ghost modes are never produced and do not appear in the physical spectrum in our expanding geometry as well.

The positive/negative frequency mode functions at  $\tau \rightarrow 0$ ,  $\pm \mathcal{C}_{A,\mathbf{p}_\perp,p_\eta}^{(\text{in})}$ , and the corresponding annihilation operators  $\hat{\mathbf{e}}_{A,\mathbf{p}_\perp,p_\eta}^{(\text{in})}$ ,  $\hat{\mathbf{f}}_{A,\mathbf{p}_\perp,p_\eta}^{(\text{in})}$  can be obtained by taking the  $\tau \rightarrow 0$  limit of those

at intermediate times. Namely,

$$\pm \mathcal{C}_{A,\mathbf{p}_\perp,p_\eta}^{(\tau)} \xrightarrow{\tau \rightarrow 0} \pm \mathcal{C}_{A,\mathbf{p}_\perp,p_\eta}^{(\text{in})} \quad (5.92)$$

and

$$\begin{pmatrix} \hat{(-)} \\ \hat{\mathbf{e}}_{A,\mathbf{p}_\perp,p_\eta} \\ \hat{(-)} \\ \hat{\mathbf{f}}_{A,\mathbf{p}_\perp,p_\eta} \end{pmatrix} \xrightarrow{\tau \rightarrow 0} \begin{pmatrix} \hat{(-)}^{(\text{in})} \\ \hat{\mathbf{e}}_{A,\mathbf{p}_\perp,p_\eta}^{(\text{in})} \\ \hat{(-)}^{(\text{in})} \\ \hat{\mathbf{f}}_{A,\mathbf{p}_\perp,p_\eta} \end{pmatrix}. \quad (5.93)$$

The in-state annihilation operators  $\hat{\mathbf{e}}_{A,\mathbf{p}_\perp,p_\eta}^{(\text{in})}$ ,  $\hat{\mathbf{f}}_{A,\mathbf{p}_\perp,p_\eta}^{(\text{in})}$  and those at intermediate times  $\hat{\mathbf{e}}_{A,\mathbf{p}_\perp,p_\eta}^{(-)}$ ,  $\hat{\mathbf{f}}_{A,\mathbf{p}_\perp,p_\eta}^{(-)}$  are not independent of each other, and their relationship is given by the following Bogoliubov transformation:

$$\begin{pmatrix} \hat{(-)} \\ \hat{\mathbf{e}}_{A,\mathbf{p}_\perp,p_\eta}(\tau) \\ \hat{(-)}^\dagger \\ \hat{\mathbf{f}}_{A,-\mathbf{p}_\perp,-p_\eta}(\tau) \end{pmatrix} = \begin{pmatrix} \alpha_{(\mathcal{C})A,\mathbf{p}_\perp,p_\eta}(\tau) & \beta_{(\mathcal{C})A,\mathbf{p}_\perp,p_\eta}(\tau) \\ \beta_{(\mathcal{C})A,\mathbf{p}_\perp,p_\eta}^*(\tau) & \alpha_{(\mathcal{C})A,\mathbf{p}_\perp,p_\eta}^*(\tau) \end{pmatrix} \begin{pmatrix} \hat{(-)}^{(\text{in})} \\ \hat{\mathbf{e}}_{A,\mathbf{p}_\perp,p_\eta}^{(\text{in})} \\ \hat{(-)}^{(\text{in})\dagger} \\ \hat{\mathbf{f}}_{A,-\mathbf{p}_\perp,-p_\eta} \end{pmatrix}, \quad (5.94)$$

where

$$\begin{aligned} \alpha_{(\mathcal{C})A,\mathbf{p}_\perp,p_\eta}(\tau) &\equiv \tau [ {}_+\mathcal{C}_{A,\mathbf{p}_\perp,p_\eta}^{(\tau)} | {}_+\mathcal{C}_{A,\mathbf{p}_\perp,p_\eta}^{(\text{in})} ]_{\text{B}} = -\tau [ -\mathcal{C}_{A,\mathbf{p}_\perp,p_\eta}^{(\tau)} | -\mathcal{C}_{A,\mathbf{p}_\perp,p_\eta}^{(\text{in})} ]_{\text{B}}^* \\ \beta_{(\mathcal{C})A,\mathbf{p}_\perp,p_\eta}(\tau) &\equiv \tau [ {}_+\mathcal{C}_{A,\mathbf{p}_\perp,p_\eta}^{(\tau)} | -\mathcal{C}_{A,\mathbf{p}_\perp,p_\eta}^{(\text{in})} ]_{\text{B}} = -\tau [ -\mathcal{C}_{A,\mathbf{p}_\perp,p_\eta}^{(\tau)} | {}_+\mathcal{C}_{A,\mathbf{p}_\perp,p_\eta}^{(\text{in})} ]_{\text{B}}^* \end{aligned} \quad (5.95)$$

The Bogoliubov coefficients are normalized as

$$1 = |\alpha_{(\mathcal{C})A,\mathbf{p}_\perp,p_\eta}(\tau)|^2 - |\beta_{(\mathcal{C})A,\mathbf{p}_\perp,p_\eta}(\tau)|^2. \quad (5.96)$$

### 5.1.4 particle production

#### vacuum

From the annihilation operators introduced in the last subsection, one can construct a vacuum state  $|\text{vac};\tau\rangle$  at an intermediate time  $\tau$ . Since the equations of motion (5.16) and (5.28) are linear with respect to the quantum fluctuations, the annihilation operators of quarks ( $\hat{a}_{f,i,\mathbf{p}_\perp,p_\eta,s}$ ,  $\hat{b}_{f,i,\mathbf{p}_\perp,p_\eta,s}$ ), gluons ( $\hat{\mathbf{c}}_{A,\sigma,\mathbf{p}_\perp,p_\eta}$ ,  $\hat{\mathbf{d}}_{A,\sigma,\mathbf{p}_\perp,p_\eta}$ ), and ghosts ( $\hat{\mathbf{e}}_{A,\mathbf{p}_\perp,p_\eta}$ ,  $\hat{\mathbf{f}}_{A,\mathbf{p}_\perp,p_\eta}$ ,  $\hat{\mathbf{e}}_{A,\mathbf{p}_\perp,p_\eta}^*$ ,  $\hat{\mathbf{f}}_{A,\mathbf{p}_\perp,p_\eta}^*$ ) do not mix up with each other during the whole spacetime evolution. Hence, one can decompose the vacuum state  $|\text{vac};\tau\rangle$  into a product of vacua for each fluctuation as

$$|\text{vac};\tau\rangle = |\text{vac}_{(\psi)};\tau\rangle \otimes |\text{vac}_{(\mathcal{A})};\tau\rangle \otimes |\text{vac}_{(\mathcal{C})};\tau\rangle. \quad (5.97)$$

Each vacuum  $|\text{vac}_{(\bullet)}; \tau\rangle$  is annihilated by the corresponding annihilation operator as

$$\begin{aligned} 0 &= \hat{a}_{f,i,\mathbf{p}_\perp,p_\eta,s} |\text{vac}_{(\psi)}; \tau\rangle = \hat{b}_{f,i,\mathbf{p}_\perp,p_\eta,s} |\text{vac}_{(\psi)}; \tau\rangle, \\ 0 &= \hat{\mathbf{c}}_{A,\sigma,\mathbf{p}_\perp,p_\eta} |\text{vac}_{(\mathcal{A})}; \tau\rangle = \hat{\mathbf{d}}_{A,\sigma,\mathbf{p}_\perp,p_\eta} |\text{vac}_{(\mathcal{A})}; \tau\rangle, \\ 0 &= \hat{\mathbf{e}}_{A,\mathbf{p}_\perp,p_\eta} |\text{vac}_{(\mathcal{C})}; \tau\rangle = \hat{\mathbf{f}}_{A,\mathbf{p}_\perp,p_\eta} |\text{vac}_{(\mathcal{C})}; \tau\rangle = \hat{\hat{\mathbf{e}}}_{A,\mathbf{p}_\perp,p_\eta} |\text{vac}_{(\mathcal{C})}; \tau\rangle = \hat{\hat{\mathbf{f}}}_{A,\mathbf{p}_\perp,p_\eta} |\text{vac}_{(\mathcal{C})}; \tau\rangle \end{aligned} \quad (5.98)$$

for all values of the quantum numbers  $i, A, s, \sigma, \mathbf{p}_\perp, p_\eta$ . From the above introduced intermediate vacuum  $|\text{vac}; \tau\rangle$ , one can naturally construct the in-vacuum  $|\text{vac}; \text{in}\rangle$  by taking the  $\tau \rightarrow 0$  limit of  $|\text{vac}; \tau\rangle$  as

$$|\text{vac}; \text{in}\rangle = \lim_{\tau \rightarrow 0} |\text{vac}; \tau\rangle = \lim_{\tau \rightarrow 0} |\text{vac}_{(\psi)}; \tau\rangle \otimes |\text{vac}_{(\mathcal{A})}; \tau\rangle \otimes |\text{vac}_{(\mathcal{C})}; \tau\rangle. \quad (5.99)$$

### $p_\eta$ -spectrum

The number of produced particles is obtained as an in-vacuum  $|\text{vac}; \text{in}\rangle$  expectation value of the corresponding number operator; namely

$$\begin{aligned} \frac{d^6 N_q(f, i, \mathbf{p}_\perp, p_\eta, s; \tau)}{d\mathbf{p}_\perp^2 dp_\eta d\mathbf{x}_\perp^2 d\eta} &= \frac{1}{V_\tau} \langle \hat{a}_{f,i,\mathbf{p}_\perp,p_\eta,s}^\dagger \hat{a}_{f,i,\mathbf{p}_\perp,p_\eta,s} \rangle = \frac{|\beta_{(\psi)f,i,\mathbf{p}_\perp,p_\eta,s}|^2}{(2\pi)^3}, \\ \frac{d^6 N_{\bar{q}}(f, i, \mathbf{p}_\perp, p_\eta, s; \tau)}{d\mathbf{p}_\perp^2 dp_\eta d\mathbf{x}_\perp^2 d\eta} &= \frac{1}{V_\tau} \langle \hat{b}_{f,i,\mathbf{p}_\perp,p_\eta,s}^\dagger \hat{b}_{f,i,\mathbf{p}_\perp,p_\eta,s} \rangle = \frac{|\beta_{(\psi)f,i,-\mathbf{p}_\perp,-p_\eta,s}|^2}{(2\pi)^3} \end{aligned} \quad (5.100)$$

for quarks and anti-quarks;

$$\begin{aligned} \frac{d^6 N_{g_+}(A, \sigma, \mathbf{p}_\perp, p_\eta; \tau)}{d\mathbf{p}_\perp^2 dp_\eta d\mathbf{x}_\perp^2 d\eta} &= \frac{1}{V_\tau} \langle \hat{\mathbf{c}}_{A,\sigma,\mathbf{p}_\perp,p_\eta}^\dagger \hat{\mathbf{c}}_{A,\sigma,\mathbf{p}_\perp,p_\eta} \rangle = \begin{cases} 0 & (\sigma = 0, 3) \\ \frac{|\beta_{(\mathcal{A})A,\sigma,\mathbf{p}_\perp,p_\eta}|^2}{(2\pi)^3} & (\sigma = 1, 2) \end{cases}, \\ \frac{d^6 N_{g_-}(A, \sigma, \mathbf{p}_\perp, p_\eta; \tau)}{d\mathbf{p}_\perp^2 dp_\eta d\mathbf{x}_\perp^2 d\eta} &= \frac{1}{V_\tau} \langle \hat{\mathbf{d}}_{A,\sigma,\mathbf{p}_\perp,p_\eta}^\dagger \hat{\mathbf{d}}_{A,\sigma,\mathbf{p}_\perp,p_\eta} \rangle = \begin{cases} 0 & (\sigma = 0, 3) \\ \frac{|\beta_{(\mathcal{A})A,\sigma,-\mathbf{p}_\perp,-p_\eta}|^2}{(2\pi)^3} & (\sigma = 1, 2) \end{cases} \end{aligned} \quad (5.101)$$

for charged gluons with the color charge  $q_A^{(\text{ad.})}$  and  $-q_A^{(\text{ad.})}$ , respectively; and

$$\begin{aligned} \frac{d^6 N_{\text{gh}_+}^{(-)}(A, \mathbf{p}_\perp, p_\eta; \tau)}{d\mathbf{p}_\perp^2 dp_\eta d\mathbf{x}_\perp^2 d\eta} &= \frac{1}{V_\tau} \left\langle \begin{pmatrix} \hat{\mathbf{e}}_{A,\mathbf{p}_\perp,p_\eta}^\dagger & \hat{\mathbf{e}}_{A,\mathbf{p}_\perp,p_\eta} \end{pmatrix} \right\rangle = 0, \\ \frac{d^6 N_{\text{gh}_-}^{(-)}(A, \mathbf{p}_\perp, p_\eta; \tau)}{d\mathbf{p}_\perp^2 dp_\eta d\mathbf{x}_\perp^2 d\eta} &= \frac{1}{V_\tau} \left\langle \begin{pmatrix} \hat{\mathbf{f}}_{A,\mathbf{p}_\perp,p_\eta}^\dagger & \hat{\mathbf{f}}_{A,\mathbf{p}_\perp,p_\eta} \end{pmatrix} \right\rangle = 0 \end{aligned} \quad (5.102)$$

for charged ghosts (anti-ghosts) with the color charge  $q_A^{(\text{ad.})}$  and  $-q_A^{(\text{ad.})}$ , respectively. Here,  $V_\tau \equiv \int d^2\mathbf{x}_\perp d\eta$  denotes the system volume on a constant  $\tau$ -surface. The quark density never exceeds unity because of the relation (5.71), which is a manifestation of the Pauli principle. As in the non-expanding case (see Section 3.1.4),  $\sigma = 0, 3$  modes of gluons and ghosts are unphysical and never produced in the expanding geometry as well because of their (anti-)commutation relation (5.82) and (5.90), respectively.

### momentum rapidity $y_{\mathbf{P}}$ -spectrum

So far, we have characterized the ‘‘longitudinal’’ momentum of produced particles by the label  $p_\eta$  because it is a natural quantum number conjugate to the spacetime rapidity  $\eta$  and that manifestly respects the boost invariance of the system. Consequently, what we have obtained for the particle spectra in Eqs. (5.100)-(5.102) are  $p_\eta$ -spectra. However, what we actually observe in experiments is not the  $p_\eta$ -spectra, but  $p_z$ -spectra and/or the (kinetic) momentum rapidity  $y_{\mathbf{P}}$ -spectra.

The  $p_z$ -spectra and the momentum rapidity  $y_{\mathbf{P}}$ -spectra can be obtained from the  $p_\eta$ -spectra in the following way [137, 159]: Let us consider the quark spectrum as an example. The  $p_z$ -spectra and the momentum rapidity  $y_{\mathbf{P}}$ -spectra are obtained as vacuum expectation values of the number operators labeled by  $p_z$ , not by  $p_\eta$ . The number operator labeled by  $p_z$  can be obtained by expanding the fluctuation  $\hat{\psi}_{f,i}$  by  $e^{ip_z z}$ , instead by  $e^{ip_\eta \eta}$ . This can be easily done with the help of the integral transformation (5.59) as

$$\begin{aligned} \hat{\psi}_{f,i} &= \sum_s \int d^2 \mathbf{p}_\perp dp_\eta \left[ +\psi_{f,i,\mathbf{p}_\perp,p_\eta,s}^{(\tau)} \hat{a}_{f,i,\mathbf{p}_\perp,p_\eta,s} + -\psi_{f,i,\mathbf{p}_\perp,p_\eta,s}^{(\tau)} \hat{b}_{f,i,-\mathbf{p}_\perp,-p_\eta,s}^\dagger \right] \frac{e^{i\mathbf{p}_\perp \cdot \mathbf{x}_\perp} e^{ip_\eta \eta}}{(2\pi)^{3/2}} \\ &= \sum_s \int d^2 \mathbf{p}_\perp dp_z \left[ +\psi_{f,i,\mathbf{p}_\perp,p_z,s}^{(t)} \left\{ \int dp_\eta \frac{e^{+i(p_\eta + q_i^{(\text{fund.})} \bar{A}_\eta) y_{\mathbf{P}}}}{\sqrt{2\pi\omega_{\mathbf{P}}}} \hat{a}_{f,i,\mathbf{p}_\perp,p_\eta,s} \right\} \right. \\ &\quad \left. + -\psi_{f,i,\mathbf{p}_\perp,p_z,s}^{(t)} \left\{ \int dp_\eta \frac{e^{-i(p_\eta + q_i^{(\text{fund.})} \bar{A}_\eta) y_{\mathbf{P}}}}{\sqrt{2\pi\omega_{\mathbf{P}}}} \hat{b}_{f,i,-\mathbf{p}_\perp,-p_\eta,s}^\dagger \right\} \right] \frac{e^{i\mathbf{p}_\perp \cdot \mathbf{x}_\perp} e^{ip_z z}}{(2\pi)^{3/2}}, \end{aligned} \quad (5.103)$$

where  $\pm\psi_{f,i,\mathbf{p}_\perp,p_z,s}^{(t)}$  is the intermediate mode function in the Cartesian coordinates under the classical gauge field  $\bar{A}_\eta$  (see Eq. (2.40)).  $\mathbf{P} \equiv \mathbf{p} - q_i^{(\text{fund.})} \bar{\mathbf{A}}$  is the kinetic momentum. From this expansion, we can define annihilation operators labeled by  $p_z$  as

$$\begin{pmatrix} \hat{a}_{f,i,\mathbf{p}_\perp,p_z,s} \\ \hat{b}_{f,i,\mathbf{p}_\perp,p_z,s} \end{pmatrix} \equiv \int dp_\eta \frac{e^{i(p_\eta + q_i^{(\text{fund.})} \bar{A}_\eta) y_{\mathbf{P}}}}{\sqrt{2\pi\omega_{\mathbf{P}}}} \begin{pmatrix} \hat{a}_{f,i,\mathbf{p}_\perp,p_\eta,s} \\ \hat{b}_{f,i,\mathbf{p}_\perp,p_\eta,s} \end{pmatrix}, \quad (5.104)$$

and we find that the quark  $p_z$ -spectrum can be related to the  $p_\eta$ -spectrum as

$$\begin{aligned} \frac{d^3 N_q(f, i, \mathbf{p}_\perp, p_z, s; \tau)}{d\mathbf{p}_\perp^2 dp_z} &\equiv \langle \hat{a}_{f,i,\mathbf{p}_\perp,p_z,s}^\dagger \hat{a}_{f,i,\mathbf{p}_\perp,p_z,s} \rangle \\ &= \int dp_\eta dp'_\eta \frac{e^{i(p_\eta - p'_\eta) y_{\mathbf{P}}}}{2\pi\omega_{\mathbf{P}}} \langle \hat{a}_{f,i,\mathbf{p}_\perp,p'_\eta,s}^\dagger \hat{a}_{f,i,\mathbf{p}_\perp,p_\eta,s} \rangle \\ &= \delta^2(\mathbf{p}_\perp = \mathbf{0}) \times \frac{1}{2\pi\omega_{\mathbf{P}}} \int dp_\eta |\beta_{(\psi)f,i,\mathbf{p}_\perp,p_\eta,s}|^2 \\ &= (2\pi)^2 \delta^2(\mathbf{p}_\perp = \mathbf{0}) \times \frac{1}{\omega_{\mathbf{P}}} \int dp_\eta \frac{d^6 N_q(f, i, \mathbf{p}_\perp, p_\eta, s; \tau)}{d\mathbf{p}_\perp^2 dp_\eta d^2 \mathbf{x}_\perp d\eta}. \end{aligned} \quad (5.105)$$

Thus, by noting  $dy_{\mathbf{P}} = dp_z/\omega_{\mathbf{P}}$ , we finally obtain

$$\omega_{\mathbf{P}} \frac{d^5 N_q(f, i, \mathbf{p}_\perp, p_z, s; \tau)}{d\mathbf{p}_\perp^2 dp_z d^2 \mathbf{x}_\perp} = \frac{d^5 N_q(f, i, \mathbf{p}_\perp, p_z, s; \tau)}{d\mathbf{p}_\perp^2 dy_{\mathbf{P}} d^2 \mathbf{x}_\perp} = \int dp_\eta \frac{d^6 N_q(f, i, \mathbf{p}_\perp, p_\eta, s; \tau)}{d\mathbf{p}_\perp^2 dp_\eta d^2 \mathbf{x}_\perp d\eta}. \quad (5.106)$$

The same arguments hold for the anti-quark spectra, and one can find

$$\omega_{\mathbf{P}} \frac{d^5 N_{\bar{q}}(f, i, \mathbf{p}_{\perp}, p_z, s; \tau)}{d\mathbf{p}_{\perp}^2 dp_z d^2 \mathbf{x}_{\perp}} = \frac{d^5 N_{\bar{q}}(f, i, \mathbf{p}_{\perp}, p_z, s; \tau)}{d\mathbf{p}_{\perp}^2 dy_{\mathbf{P}} d^2 \mathbf{x}_{\perp}} = \int dp_{\eta} \frac{d^6 N_{\bar{q}}(f, i, \mathbf{p}_{\perp}, p_{\eta}, s; \tau)}{d\mathbf{p}_{\perp}^2 dp_{\eta} d^2 \mathbf{x}_{\perp} d\eta}. \quad (5.107)$$

Notice that the momentum rapidity  $y_{\mathbf{P}}$ -spectra do not depend on  $y_{\mathbf{P}}$ . This is a manifestation of the perfect boost-invariance of the system (assumption (i) in Section 5.1.2). Indeed, if the system depends on the spacetime rapidity  $\eta$ , the boost-invariant momentum label  $p_{\eta}$  is no longer a good quantum number and  $\langle \hat{a}_{f,i,\mathbf{p}_{\perp},p'_{\eta},s}^{\dagger} \hat{a}_{f,i,\mathbf{p}_{\perp},p_{\eta},s} \rangle \not\propto \delta(p_{\eta} - p'_{\eta})$  in the third line of Eq. (5.105), which leaves  $y_{\mathbf{P}}$ -dependences in the final result.

One can equally apply the above discussion to gluons and ghosts, and obtains the same results,

$$\omega_{\mathbf{P}} \frac{d^5 N_{g_{\pm}}(A, \sigma, \mathbf{p}_{\perp}, p_z; \tau)}{d\mathbf{p}_{\perp}^2 dp_z d^2 \mathbf{x}_{\perp}} = \frac{d^5 N_{g_{\pm}}(A, \sigma, \mathbf{p}_{\perp}, p_z; \tau)}{d\mathbf{p}_{\perp}^2 dy_{\mathbf{P}} d^2 \mathbf{x}_{\perp}} = \int dp_{\eta} \frac{d^6 N_{g_{\pm}}(A, \sigma, \mathbf{p}_{\perp}, p_{\eta}; \tau)}{d\mathbf{p}_{\perp}^2 dp_{\eta} d^2 \mathbf{x}_{\perp} d\eta}, \quad (5.108)$$

$$\omega_{\mathbf{P}} \frac{d^5 N_{\text{gh}_{\pm}}(A, \mathbf{p}_{\perp}, p_z; \tau)}{d\mathbf{p}_{\perp}^2 dp_z d^2 \mathbf{x}_{\perp}} = \frac{d^5 N_{\text{gh}_{\pm}}(A, \mathbf{p}_{\perp}, p_z; \tau)}{d\mathbf{p}_{\perp}^2 dy_{\mathbf{P}} d^2 \mathbf{x}_{\perp}} = \int dp_{\eta} \frac{d^6 N_{\text{gh}_{\pm}}(A, \mathbf{p}_{\perp}, p_{\eta}; \tau)}{d\mathbf{p}_{\perp}^2 dp_{\eta} d^2 \mathbf{x}_{\perp} d\eta} = 0. \quad (5.109)$$

This is because the weight factor  $w$  that connects the plane wave solutions in the  $\tau$ - $\eta$  coordinates and those in the Cartesian coordinates is independent of quantum statistics (see Eqs. (5.59) and (5.77)).

We note that we have derived the formulas (5.106)-(5.109) in a quantum field theoretical manner by following Ref. [137, 159], but one can also obtain the same formulas within classical mechanics [163, 164], though these two derivations agree with each other only if the system is perfectly boost invariant [137].

## 5.2 Dynamical evolution without backreaction

In this section, we dare neglect backreaction from quark, gluon, and ghost fluctuations by artificially setting  $\langle : \hat{j}_{\alpha,\mu} : \rangle = 0$ . For this case, one can analytically compute quark and gluon spectra for some particular configurations of expanding electric fields. This enables us to better understand effects of the longitudinal expansion to quark and gluon production, and to clarify similarities/differences between the quark and gluon production in non-expanding systems previously studied in Section 4.

To be more specific, we consider a boost-invariantly expanding, homogeneous color electric field described by

$$\mathbf{E} = \bar{E}_0 \theta(\tau) \mathbf{e}_z, \quad (5.110)$$

or, in terms of the classical gauge field  $\bar{A}_{\mu}$ , by

$$\begin{aligned} \bar{A}_{\tau} = \bar{A}_x = \bar{A}_y = 0, \\ \bar{A}_{\eta} = -\frac{\tau^2}{2} \bar{E}_0 \theta(\tau). \end{aligned} \quad (5.111)$$

Under the given gauge background field (5.111), one can analytically solve the equations of motion (5.16) for quarks  $\hat{\psi}_{f,i}$  and (5.28) for gluons  $\hat{\mathcal{A}}_{A,\sigma}$  (see Appendix C), and can find analytical expressions for the  $p_\eta$ -spectra,  $d^6 N_{(q)}/d\mathbf{p}_\perp^2 dp_\eta d\mathbf{x}_\perp^2 d\eta$  for quarks and  $d^6 N_{g\pm}/d\mathbf{p}_\perp^2 dp_\eta d\mathbf{x}_\perp^2 d\eta$  for gluons.

### 5.2.1 $p_\eta$ -spectrum of quarks and gluons

The distribution function labeled by the boost-invariant momentum  $p_\eta$  for quarks  $d^6 N_q/d\mathbf{p}_\perp^2 dp_\eta d\mathbf{x}_\perp^2 d\eta$  and gluons  $d^6 N_{g\pm}/d\mathbf{p}_\perp^2 dp_\eta d\mathbf{x}_\perp^2 d\eta$  are plotted in Figs. 5.1 - 5.4: In Figs. 5.1 and 5.2, the boost-invariant kinetic momentum  $P_\eta = p_\eta + q\bar{A}_\eta$ -dependence at a fixed transverse momentum is displayed. There, we plotted the distribution functions as a function of  $P_\eta/\sqrt{g\bar{E}_0}\tau$  ( $\sqrt{g\bar{E}_0}$  is a dimensional factor to make  $P_\eta/\tau$  dimensionless), not by  $P_\eta$  itself, because the former has a clear physical meaning:  $P_\eta/\sqrt{g\bar{E}_0}\tau$  is a kinetic longitudinal momentum  $P_z/\sqrt{g\bar{E}_0}$  observed in the co-moving frame as was addressed in Section 5.1.3. Figures 5.3 and 5.4 display the transverse momentum  $\mathbf{p}_\perp$ -dependence at a fixed boost-invariant kinetic momentum  $P_\eta/\sqrt{g\bar{E}_0}\tau$ . Different three panels in each figure differentiate the value of the color charges  $q_i^{(\text{fund.})}$  ( $i = 1, \dots, N_c$ ) for quarks and  $q_A^{(\text{ad.})}$  ( $i = 1, \dots, N_c(N_c - 1)/2$ ) for gluons just as in Figs. 4.1 - 4.4 for the non-expanding study. In these figures, we only consider  $N_f = 3$  (i.e., massless three quarks) case and set  $\theta = 0$  for simplicity. Notice that for  $N_f = 3$  case,  $g\bar{E}_0$  is the only dimensionful parameter characterizing the system, so that any dimensionful quantity can be scaled by  $g\bar{E}_0$  to make it dimensionless.

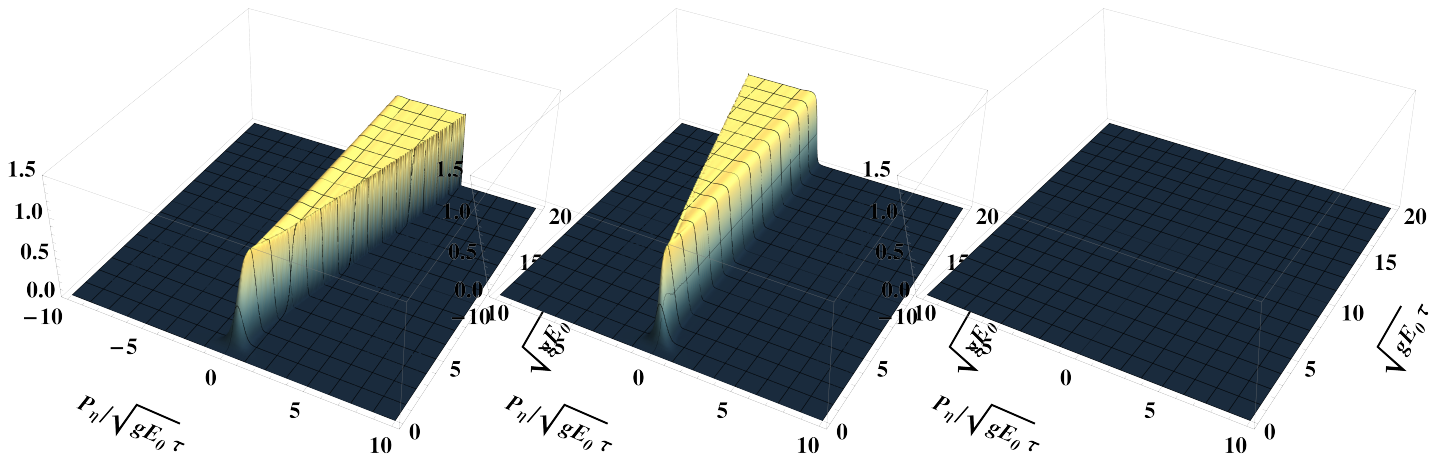


Figure 5.1: The boost-invariant kinetic momentum  $P_\eta = p_\eta + q_i^{(\text{fund.})}\bar{A}_\eta$ -distribution  $d^6 N_q/d\mathbf{p}_\perp^2 dp_\eta d\mathbf{x}_\perp^2 d\eta = |\beta_{(\psi)f,i,p_\perp,p_\eta,s}|^2/(2\pi)^3$  of produced massless quarks (up or down) at a fixed transverse momentum  $|\mathbf{p}_\perp|/\sqrt{|g\bar{E}_0|} = 0.1$ . Different panels differentiate the color charge  $q_i^{(\text{fund.})}$  ( $i = 1, \dots, N_c$ ) of quarks with color  $i$ . We set the color angle  $\theta = 0$ , and the corresponding quark charge  $q_i^{(\text{fund.})}$  read  $q_i^{(\text{fund.})} = q_1^{(\text{fund.})} = 1/2$  (left),  $q_2^{(\text{fund.})} = -1/2$  (middle), and  $q_3^{(\text{fund.})} = 0$  (right).

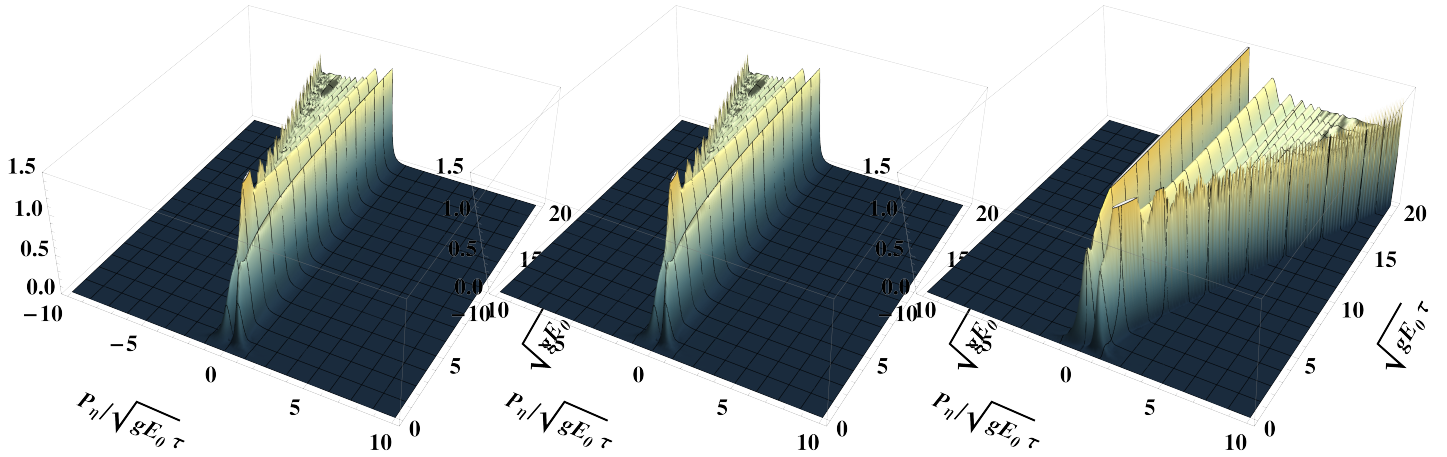


Figure 5.2: The boost-invariant kinetic momentum  $P_\eta = p_\eta + q_A^{(\text{ad.})} \bar{A}_\eta$ -distribution  $d^6 N_{g^+} / d\mathbf{p}^2 dp_\eta d\mathbf{x}_\perp^2 d\eta = |\beta_{(\mathcal{A})A,\sigma,\mathbf{p}_\perp,p_\eta}|^2 / (2\pi)^3$  of produced gluons at a fixed transverse momentum  $|\mathbf{p}_\perp| / \sqrt{|g\bar{E}_0|} = 0.1$ . Different panels differentiate the color charge  $q_A^{(\text{ad.})}$  ( $i = 1, \dots, N_c(N_c - 1)/2$ ) of gluons with color  $A$ . We set the color angle  $\theta = 0$ , and the corresponding gluon charge  $q_A^{(\text{ad.})}$  read  $q_A^{(\text{ad.})} = q_1^{(\text{ad.})} = -1/2$  (left),  $q_2^{(\text{ad.})} = -1/2$  (middle), and  $q_3^{(\text{ad.})} = 1$  (right).

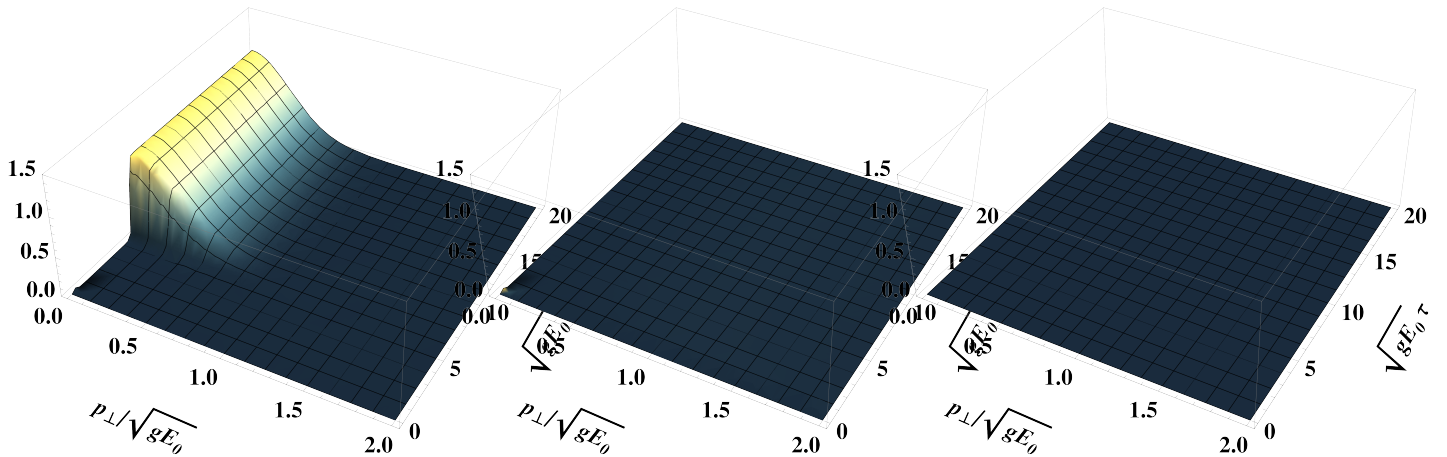


Figure 5.3: The transverse momentum  $\mathbf{p}_\perp$ -distribution  $d^6 N_q / d\mathbf{p}^2 dp_\eta d\mathbf{x}_\perp^2 d\eta = |\beta_{(\psi)f,i,\mathbf{p}_\perp,p_\eta,s}|^2 / (2\pi)^3$  of produced massless quarks (up or down) at a fixed boost-invariant kinetic momentum  $P_\eta = p_\eta + q_i^{(\text{fund.})} \bar{A}_\eta = 1.5 \times \sqrt{|g\bar{E}_0|}$ . Different panels differentiate the color charge  $q_i^{(\text{fund.})}$  ( $i = 1, \dots, N_c$ ) of quarks with color  $i$ . We set the color angle  $\theta = 0$ , and the corresponding quark charge  $q_i^{(\text{fund.})}$  read  $q_i^{(\text{fund.})} = q_1^{(\text{fund.})} = 1/2$  (left),  $q_2^{(\text{fund.})} = -1/2$  (middle), and  $q_3^{(\text{fund.})} = 0$  (right).

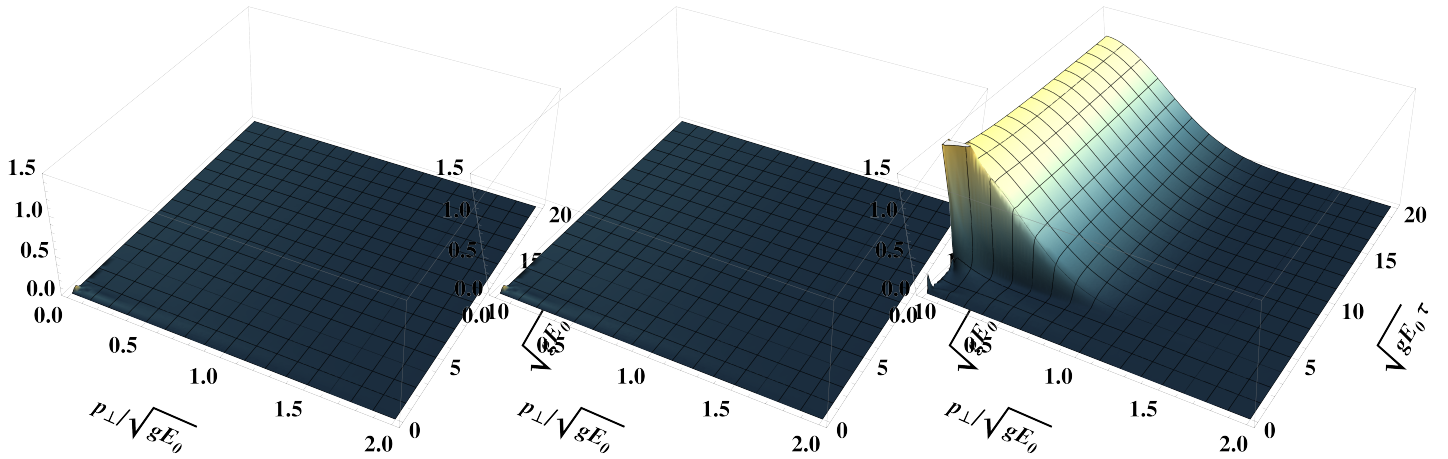


Figure 5.4: The transverse momentum  $\mathbf{p}_\perp$ -distribution  $d^6 N_{g^+} / d\mathbf{p}^2 dp_\eta d\mathbf{x}_\perp^2 d\eta = |\beta_{(A)A,\sigma,\mathbf{p}_\perp,p_\eta}|^2 / (2\pi)^3$  of produced gluons at a fixed boost-invariant kinetic momentum  $P_\eta = p_\eta + q_A^{(\text{ad.})} \bar{A}_\eta = 1.5 \times \sqrt{|g\bar{E}_0|}$ . Different panels differentiate the color charge  $q_A^{(\text{ad.})}$  ( $i = 1, \dots, N_c(N_c - 1)/2$ ) of gluons with color  $A$ . We set the color angle  $\theta = 0$ , and the corresponding gluon charge  $q_A^{(\text{ad.})}$  read  $q_A^{(\text{ad.})} = q_1^{(\text{ad.})} = -1/2$  (left),  $q_2^{(\text{ad.})} = -1/2$  (middle), and  $q_3^{(\text{ad.})} = 1$  (right).

Interestingly, one observes from Figs. 5.1 - 5.4 that the essential features of the quark and gluon production from an expanding electric field are essentially the same as the non-expanding case:

- Quarks and gluons are constantly created at approximately zero momentum in the co-moving frame.
- After created, quarks and gluons are accelerated by the electric field according to the classical equation of motion  $dP_\eta/d\tau = q d\bar{A}_\eta/d\tau = q\bar{E}_0\tau$ , or  $P_z \sim q\bar{E}_0\tau/2$ .
- The transverse distribution is nearly Gaussian and is largely consistent with the Schwinger formula for a non-expanding constant electric field,  $d^6 N / d\mathbf{p}_\perp^2 dp_\eta d^2 \mathbf{x}_\perp d\eta \sim \exp[-\pi(m^2 + \mathbf{p}_\perp^2) / |q\bar{E}_0|] / (2\pi)^3$ .

Intuitively speaking, this coincidence is because the system expands with the speed of light so that effects of the longitudinal boundary may be negligible because of the causality. Collecting above observations, one understands that the distribution function is well approximated as

$$\frac{d^6 N_{g^\pm}}{d\mathbf{p}_\perp^2 dp_\eta d\mathbf{x}_\perp^2 d\eta} \sim \frac{1}{(2\pi)^3} \exp \left[ -\pi \frac{\mathbf{p}_\perp^2}{|q_A^{(\text{ad.})} \bar{E}(\tau)|} \right] \theta(\mp p_\eta (p_\eta \pm q_A^{(\text{ad.})} \bar{A}_\eta(\tau))), \quad (5.112)$$

$$\frac{d^6 N_{q^{(-)}}}{d\mathbf{p}_\perp^2 dp_\eta d\mathbf{x}_\perp^2 d\eta} \sim \frac{1}{(2\pi)^3} \exp \left[ -\pi \frac{m_f^2 + \mathbf{p}_\perp^2}{|q_i^{(\text{fund.})} \bar{E}(\tau)|} \right] \theta(\mp p_\eta (p_\eta \pm q_A^{(\text{fund.})} \bar{A}_\eta(\tau))). \quad (5.113)$$

These expressions are valid when the electric field is sufficiently adiabatic  $\partial_\tau \bar{E} \sim 0$  and quantum interferences among created particles are negligible (see Section 5.3).

## 5.2.2 momentum rapidity $y_{\mathbf{P}}$ -spectrum of quarks and gluons

We integrate the  $p_\eta$ -spectra over  $p_\eta$  to discuss the (kinetic) momentum rapidity  $y_{\mathbf{P}}$ -spectra,  $d^5 N_{(-)} / d^2 \mathbf{p}_\perp dy_{\mathbf{P}} d\mathbf{x}_\perp^2$  for (anti-)quarks and  $d^5 N_{g\pm} / d^2 \mathbf{p}_\perp dy_{\mathbf{P}} d\mathbf{x}_\perp^2$  for gluons. Notice that the momentum rapidity  $y_{\mathbf{P}}$ -spectra are independent of  $y_{\mathbf{P}}$  because of the perfect boost-invariance of the system as was shown in Section 5.1.4. In other words, the  $p_\eta$ -integration integrates out the longitudinal motion in the co-moving frame observed in Figs. 5.1 and 5.2.

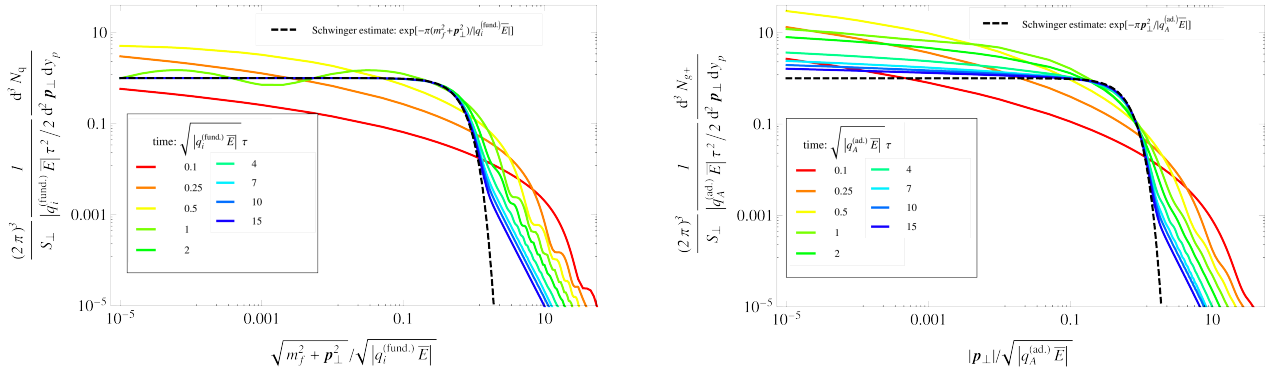


Figure 5.5: The time-evolution of the transverse momentum  $\mathbf{p}_\perp$ -dependence of the momentum rapidity  $y_{\mathbf{P}}$ -spectra. The black dashed lines indicate the estimate from the Schwinger formulas (5.114) and (5.115). [Left] Quark spectra  $d^5 N_{(-)} / d^2 \mathbf{p}_\perp dy_{\mathbf{P}} d\mathbf{x}_\perp^2$ . [Right] Gluon spectra  $d^5 N_{g\pm} / d^2 \mathbf{p}_\perp dy_{\mathbf{P}} d\mathbf{x}_\perp^2$ .

We plotted the transverse momentum  $\mathbf{p}_\perp$ -dependence of the momentum rapidity  $y_{\mathbf{P}}$ -spectra in Fig. 5.5. We observe that, at later times  $\sqrt{|q_i^{(\text{fund.})} \bar{E}_0|} \tau, \sqrt{|q_A^{(\text{ad.})} \bar{E}_0|} \tau \gtrsim 1$ , both spectra approach Gaussian distributions multiplied by a square of the time  $\tau$ . This observation is consistent with what we observed in Figs. 5.1 - 5.4: By integrating Eqs. (5.112) and (5.113), one finds

$$\frac{d^5 N_{(-)}}{d^2 \mathbf{p}_\perp dy_{\mathbf{P}} d^2 \mathbf{x}_\perp^2} \sim \frac{1}{(2\pi)^3} \frac{|q_i^{(\text{fund.})} \bar{E}_0| \tau^2}{2} \exp \left[ -\pi \frac{m_f^2 + \mathbf{p}_\perp^2}{|q_i^{(\text{fund.})} \bar{E}_0|} \right], \quad (5.114)$$

$$\frac{d^5 N_{g\pm}}{d^2 \mathbf{p}_\perp dy_{\mathbf{P}} d^2 \mathbf{x}_\perp^2} \sim \frac{1}{(2\pi)^3} \frac{|q_A^{(\text{ad.})} \bar{E}_0| \tau^2}{2} \exp \left[ -\pi \frac{\mathbf{p}_\perp^2}{|q_A^{(\text{ad.})} \bar{E}_0|} \right], \quad (5.115)$$

which are plotted in the dashed lines as ‘‘Schwinger estimate’’ in Fig. 5.5. The  $\tau^2$ -dependence, which was  $t$  for the non-expanding case, is intuitively because particle production constantly takes place and the spatial volume of the fields increases as  $\propto \tau$  because of the expansion.

On the other hand, at early times  $\sqrt{|q_i^{(\text{fund.})} \bar{E}_0|} \tau, \sqrt{|q_A^{(\text{ad.})} \bar{E}_0|} \tau \lesssim 1$ , the spectra are harder compared to those for later times and do not decay exponentially in  $|\mathbf{p}_\perp|$  because the typical frequency  $\omega \sim 1/\tau$  of the classical field is hard enough to excite hard particles. In other words, a naive application of the Schwinger formula is valid only for large values of  $\tau$ , while one should take care of finite pulse effects for small values of  $\tau$ .

In the low momentum region  $|\mathbf{p}_\perp| \lesssim \sqrt{|q_A^{(\text{fund.})} \bar{E}_0|}, \sqrt{|q_A^{(\text{ad.})} \bar{E}_0|}$ , gluons are more abundant than quarks. This is because the quark production is subjected to the Pauli principle but the gluon production is not. The gluon spectrum shows a weak divergence for  $|\mathbf{p}_\perp| \rightarrow 0$  but the exponent is weaker than minus one and it approaches zero with increasing  $\tau$ .

### 5.2.3 total number of quarks and gluons

We compute the total number of quarks and gluons per unit momentum rapidity  $y_{\mathbf{P}}$  by integrating the momentum rapidity  $y_{\mathbf{P}}$ -spectra over the transverse momentum  $\mathbf{p}_\perp$  and summing up all the quantum numbers as  $d^3 N_q/dy_{\mathbf{P}} d\mathbf{x}_\perp^2 \equiv \sum_{f,i,s,q\bar{q}} \int d^2 \mathbf{p}_\perp^2 d^5 N_{(-)} / d^2 \mathbf{p}_\perp dy_{\mathbf{P}} d\mathbf{x}_\perp^2$  for quarks and  $d^3 N_g/dy_{\mathbf{P}} d\mathbf{x}_\perp^2 \equiv \sum_{A,\sigma,g_\pm} \int d^2 \mathbf{p}_\perp^2 d^5 N_{g_\pm} / d^2 \mathbf{p}_\perp dy_{\mathbf{P}} d\mathbf{x}_\perp^2$  for gluons. The results are plotted in Fig. 5.6, where  $N_f = 3$  (massless three quarks) case is considered for simplicity (for the other values of  $N_f$  and quark mass effects, see Fig. 5.8).

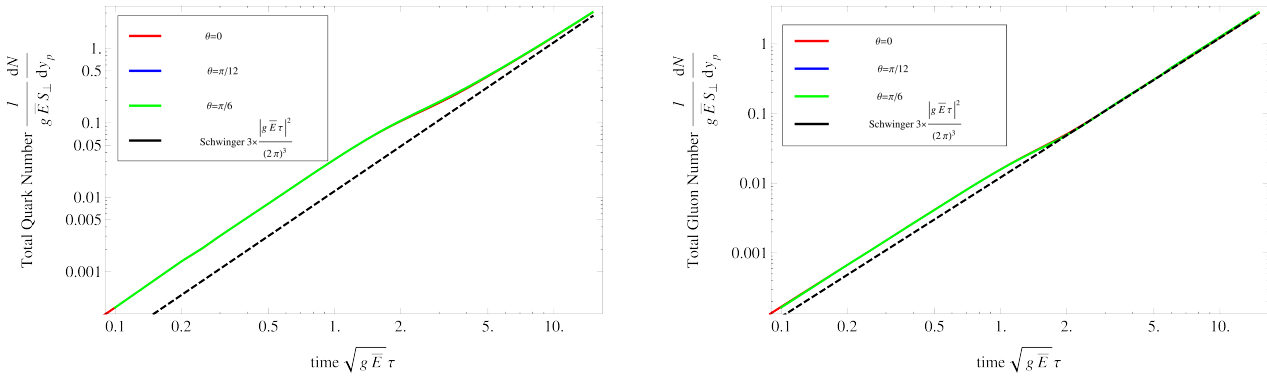


Figure 5.6: Total number of produced quarks  $d^3 N_q/dy_{\mathbf{P}} d\mathbf{x}_\perp^2 \equiv \sum_{f,i,s,q\bar{q}} \int d^2 \mathbf{p}_\perp^2 d^5 N_{(-)} / d^2 \mathbf{p}_\perp dy_{\mathbf{P}} d\mathbf{x}_\perp^2$  for  $N_f = 3$  (left) and gluons  $d^3 N_g/dy_{\mathbf{P}} d\mathbf{x}_\perp^2 \equiv \sum_{A,\sigma,g_\pm} \int d^2 \mathbf{p}_\perp^2 d^5 N_{g_\pm} / d^2 \mathbf{p}_\perp dy_{\mathbf{P}} d\mathbf{x}_\perp^2$  with several values of the color angle  $\theta = 0$  (red),  $\pi/12$  (blue), and  $\pi/6$  (green). The dashed lines are expectations from the Schwinger estimates (5.116) and (5.117).

Different colors in Fig. 5.6 correspond to different values of the color angle  $\theta$ . We immediately observe that the results are insensitive to the values of the color angle  $\theta$ , in contrast to what we observed in the  $p_z$ - and  $p_\eta$ -spectra (see Figs. 5.1 - 5.5). This observation is consistent with what we found in the non-expanding case (see Fig. 4.5).

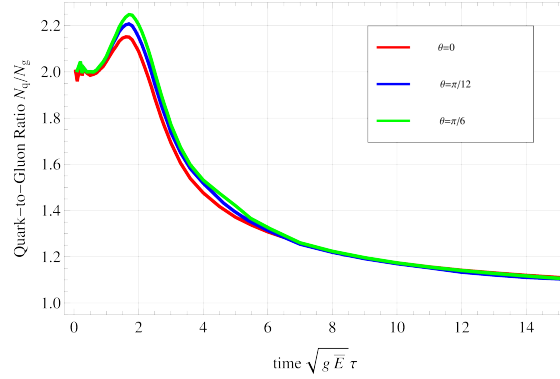


Figure 5.7: The ratio  $R_{q-g}$  of the total number of quarks to that of gluons  $(N_q + N_{\bar{q}})/(N_{g^+} + N_{g^-})$ . Different colors correspond to different values of the color angle  $\theta = 0$  (red),  $\pi/12$  (blue), and  $\pi/6$  (green).

One can naively estimate the total number of quarks and gluons via the Schwinger estimates (5.114) and (5.115) as

$$\frac{d^3 N_q}{dy_{\mathbf{P}} d^2 \mathbf{x}_{\perp}^2} \sim \frac{N_s N_{lq} N_{q\bar{q}} |g\bar{E}_0| \tau^2}{4 (2\pi)^3} \quad (5.116)$$

$$\frac{d^3 N_g}{dy_{\mathbf{P}} d^2 \mathbf{x}_{\perp}^2} \sim \frac{2N_c N_{\sigma} |g\bar{E}_0| \tau^2}{4 (2\pi)^3}, \quad (5.117)$$

which is depicted in the dashed line in Fig. 5.6. When comparing these estimates with the results, one finds that, at later times  $\sqrt{|g\bar{E}_0|} \tau \gtrsim 1$ , quark and gluon production is consistent with what one naively expects from the Schwinger formula for a non-expanding electric field. On the contrary to this, at early times  $\sqrt{|g\bar{E}_0|} \tau \lesssim 1$ , our results give much more abundant particles than what the Schwinger estimates give. This is because the perturbative enhancement of perturbative production, where high frequency components of classical fields can excite larger number of particles.

Interestingly, the perturbative enhancement produces more quarks than gluons. This aspect is more clearly visible in Fig. 5.7, where the ratio  $R_{q-g}$  of the total number of quarks to that of gluons is plotted. We find that the ratio becomes about two at early times, where perturbative particle production mechanism dominates. The ratio decreases as time goes, where non-perturbative particle production begins to dominate, and approaches  $N_s N_{lq} N_{q\bar{q}} / 2N_c N_{\sigma} = 1$  as the Schwinger estimates give. These observations are consistent with what we found in the non-expanding study (see Fig. 4.6).

The quark production is investigated in more detail by examining the number of flavor  $N_f$ - (the quark mass  $m_f$ -) dependence in the left (right) panel of Fig. 5.8. Here, we set  $g\bar{E}_0 = 1 \text{ GeV}^2$ ;  $m_s = 0.1 \text{ GeV}$ ,  $m_c = 1.2 \text{ GeV}$ ; and  $\theta = 0$  as we parametrized in the non-expanding study (see Fig. 4.7). As in the non-expanding study, we again find that there is a significant

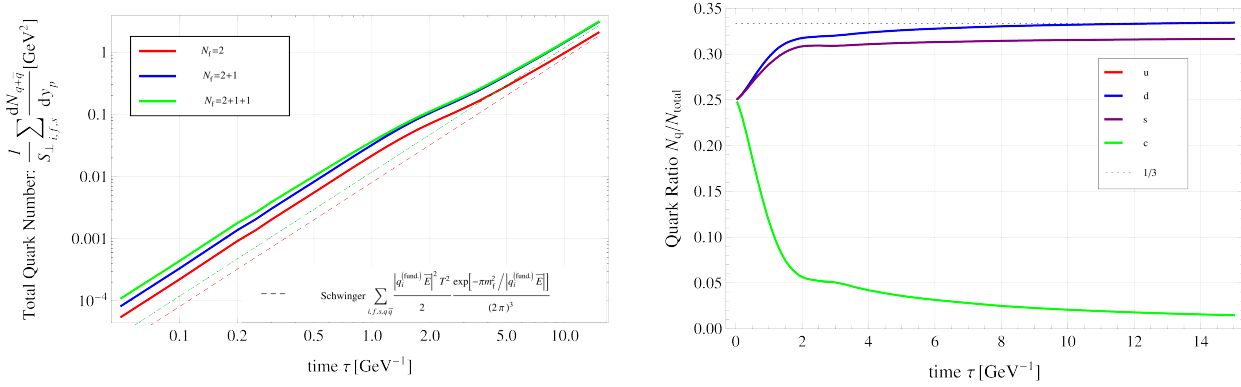


Figure 5.8: [Left] The number of flavor  $N_f$ -dependence in the total number of quarks produced  $d^3(N_q + N_{\bar{q}})/d\mathbf{x}_{\perp}^2 dy_{\mathbf{P}}$  for  $N_f = 2$  (up, down) in red,  $2 + 1$  (up, down, strange) in blue, and  $2 + 1 + 1$  (up, down, strange, charm) in green. [Right] The suppression factor of charm and strange quark production in  $N_f = 2 + 1 + 1$  case  $R_q = N_q/(N_u + N_d + N_s + N_c)$ . In both panels, parameters are set as  $g\bar{E}_0 = 1 \text{ GeV}^2$ ;  $\theta = 0$ ; and  $m_u = m_d = 0 \text{ GeV}$ ,  $m_s = 0.1 \text{ GeV}$ ,  $m_c = 1.2 \text{ GeV}$ .

change from  $N_f = 2$  to  $N_f = 2 + 1$ , i.e., by inclusion of the strange quark, for all values of  $\tau$ . Whereas, the change of the quark multiplicity from  $N_f = 2 + 1$  to  $N_f = 2 + 1 + 1$ , i.e., by inclusion of charm quarks, is negligible (noticeable) at later (early) times  $\tau$  because of the interplay between the perturbative and the non-perturbative particle production mechanism. In particular, the perturbative enhancement of the charm production is significant,  $N_c/(N_u + N_d + N_s + N_c) \gg 0.0004$ , even in our expanding case.

## 5.3 Dynamical evolution with backreaction

Let us discuss the dynamical evolution of the system with the backreaction, and discuss some phenomenological consequences of our formalism to the pre-equilibrium stage dynamics of ultra-relativistic heavy ion collisions. For this purpose, we numerically solve the equations of motion (5.37), (5.16), and (5.28), and compute the time-evolution of the quark and gluon distribution functions, the color electric field strength, and thermodynamic quantities such as the energy density and the pressure of the system.

### 5.3.1 setup

We model the initial color flux tubes existing just after a collision of nuclei (at  $\tau = \tau_0$ ) by a spatially uniform, and boost-invariantly expanding electric field described by

$$\bar{A}_{\mu}(\tau_0) = 0, \quad \bar{E}(\tau_0) = \bar{E}_0, \quad \frac{d\bar{E}(\tau_0)}{d\tau} = 0. \quad (5.118)$$

We also assume that there is no classical current  $\bar{J}^\mu = 0$  in the forward light-cone region  $\tau > 0$  because the projectile nuclei are flying just on the light-cone  $\tau = 0$  in the ultra-relativistic limit.

Our parameter setting is as follows: We set the strong coupling constant  $g$  as  $g = 1$  for simplicity. We also set the initial electric field strength  $\bar{E}_0$  as  $g\bar{E}_0 = 1 \text{ GeV}^2$ , which is the typical value at the RHIC energy scale. As the strange mass scale  $m_s \sim 0.1 \text{ GeV}$  is negligible and the heavy charm ( $m_c \sim 1.2 \text{ GeV}$ ) production heavily suppressed for this value of field strength  $g\bar{E}_0$  (see Figs. 5.3.2 and 5.3.3), we can restrict our attention to  $N_f = 3$  (massless three quarks) case only. The color angle  $\theta$  is set to zero; one can numerically demonstrate that our results presented below (except for momentum distributions in Section 5.3.2 and 5.3.3) are insensitive to the color angle  $\theta$ . Since the  $\tau$ - $\eta$  coordinates have a coordinate singularity at  $\tau = 0$ , we must start our simulation at a finite time  $\tau_0 > 0$ . Here, we choose  $\tau_0 = 0.1 \text{ GeV}^{-1}$  for simplicity; our results presented below is not sensitive to values of  $\tau_0$  as long as  $\tau_0$  is sufficiently small as  $\tau_0 \lesssim 1$ . As it is numerically difficult and heavy to evaluate the Hankel functions with complex orders [165] and due to our limited computer resources, we are reluctant to use relatively small momentum cutoff scales  $\Lambda_\perp = 2 \text{ GeV}$  and  $\Lambda_\eta = 30$ . Because of these relatively small cutoff scales, our results slightly depend on the cutoff scales (in particular  $\Lambda_\perp$ ) for small values of  $\tau$ , where perturbative particle production mechanism creates hard particles, however, the cutoff dependence becomes negligible for larger values of  $\tau$ , where hard particle production is suppressed by the non-perturbative particle production mechanism.

### 5.3.2 $p_\eta$ -spectrum of quarks and gluons

We first examine the  $p_\eta$ -spectrum of produced quarks  $d^6 N_q / d\mathbf{p}^2 dp_\eta d\mathbf{x}_\perp^2 d\eta$  and gluons  $d^6 N_{g+} / d\mathbf{p}^2 dp_\eta d\mathbf{x}_\perp^2 d\eta$ , whose results are shown in Figs. 5.9 - 5.12.

Figures 5.9 - 5.12 tell us that the backreaction significantly affects the spacetime evolution of the system. The basic features of the results are essentially the same as the non-expanding one:

- The classical plasma oscillation occurs in the co-moving frame and the kinetic longitudinal momentum in that frame  $P_z = P_\eta / \tau$  oscillates.
- The Pauli blocking occurs and quark production is heavily suppressed.
- The Bose enhancement occurs for gluon production, which strongly enhances soft gluon production.
- As a result of quantum interferences, the momentum spectra are strongly distorted, and the distortion is stronger for gluon production.

Some differences appear because of the expansion:

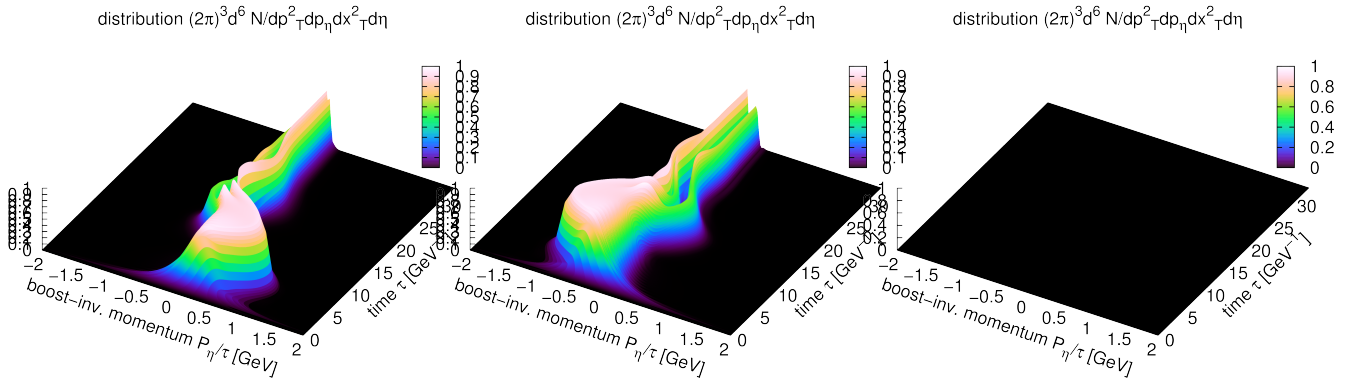


Figure 5.9: The boost-invariant kinetic momentum  $P_\eta = p_\eta + q_i^{(\text{fund.})} \bar{A}_\eta$ -distribution  $d^6 N_q / d\mathbf{p}^2 dp_\eta d\mathbf{x}_\perp^2 d\eta = |\beta_{(\psi)f,i,\mathbf{p}_\perp,p_\eta,s}|^2 / (2\pi)^3$  of produced massless quarks at a fixed transverse momentum  $|\mathbf{p}_\perp| = 0.11$  GeV. Different panels differentiate the color charge  $q_i^{(\text{fund.})}$  ( $i = 1, \dots, N_c$ ) of quarks with color  $i$ . We set the color angle  $\theta = 0$ , and the corresponding quark charge  $q_i^{(\text{fund.})}$  read  $q_1^{(\text{fund.})} = 1/2$  (left),  $q_2^{(\text{fund.})} = -1/2$  (middle), and  $q_3^{(\text{fund.})} = 0$  (right).

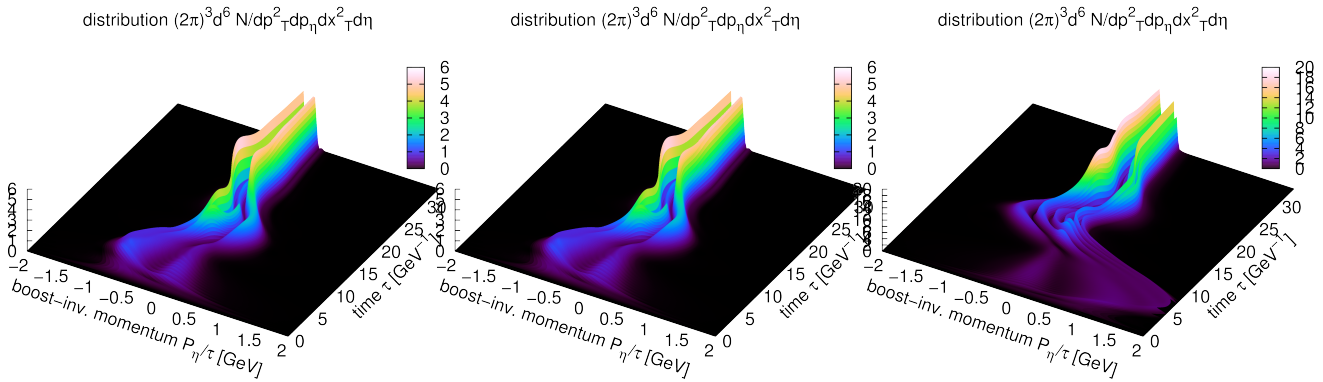


Figure 5.10: The boost-invariant kinetic momentum  $P_\eta = p_\eta + q_A^{(\text{ad.})} \bar{A}_\eta$ -distribution  $d^6 N_{g^+} / d\mathbf{p}^2 dp_\eta d\mathbf{x}_\perp^2 d\eta = |\beta_{(A)A,\sigma,\mathbf{p}_\perp,p_\eta}|^2 / (2\pi)^3$  of produced gluons at a fixed transverse momentum  $|\mathbf{p}_\perp| = 0.11$  GeV. Different panels differentiate the color charge  $q_A^{(\text{ad.})}$  ( $i = 1, \dots, N_c(N_c - 1)/2$ ) of gluons with color  $A$ . We set the color angle  $\theta = 0$ , and the corresponding gluon charge  $q_A^{(\text{ad.})}$  read  $q_1^{(\text{ad.})} = -1/2$  (left),  $q_2^{(\text{ad.})} = -1/2$  (middle), and  $q_3^{(\text{ad.})} = 1$  (right).

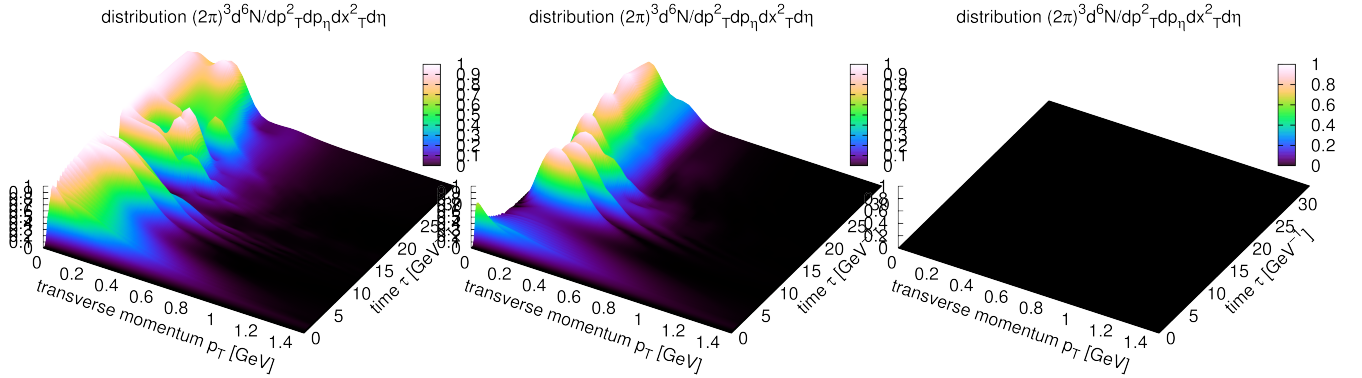


Figure 5.11: The transverse momentum  $\mathbf{p}_\perp$ -distribution  $d^6 N_q / d\mathbf{p}^2 dp_\eta dx_\perp^2 d\eta = |\beta_{(\psi)f,i,\mathbf{p}_\perp,p_\eta,s}|^2 / (2\pi)^3$  of produced massless quarks at a fixed boost-invariant kinetic momentum  $P_\eta = p_\eta + q_i^{(\text{fund.})} \bar{A}_\eta = 0.1$  GeV. Different panels differentiate the color charge  $q_i^{(\text{fund.})}$  ( $i = 1, \dots, N_c$ ) of quarks with color  $i$ . We set the color angle  $\theta = 0$ , and the corresponding quark charge  $q_i^{(\text{fund.})}$  read  $q_1^{(\text{fund.})} = q_1^{(\text{fund.})} = 1/2$  (left),  $q_2^{(\text{fund.})} = -1/2$  (middle), and  $q_3^{(\text{fund.})} = 0$  (right).

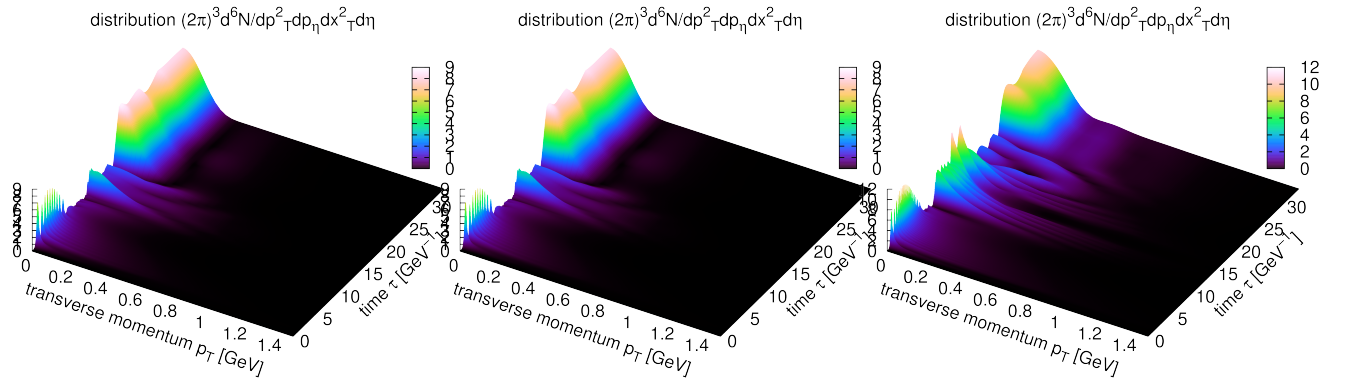


Figure 5.12: The transverse momentum  $\mathbf{p}_\perp$ -distribution  $d^6 N_{g^+} / d\mathbf{p}^2 dp_\eta dx_\perp^2 d\eta = |\beta_{(A)A,\sigma,\mathbf{p}_\perp,p_\eta}|^2 / (2\pi)^3$  of produced gluons at a fixed boost-invariant kinetic momentum  $P_\eta = p_\eta + q_A^{(\text{ad.})} \bar{A}_\eta = 0.1$  GeV. Different panels differentiate the color charge  $q_A^{(\text{ad.})}$  ( $i = 1, \dots, N_c(N_c - 1)/2$ ) of gluons with color  $A$ . We set the color angle  $\theta = 0$ , and the corresponding gluon charge  $q_A^{(\text{ad.})}$  read  $q_1^{(\text{ad.})} = -1/2$  (left),  $q_2^{(\text{ad.})} = -1/2$  (middle), and  $q_3^{(\text{ad.})} = 1$  (right).

- The longitudinal expansion stretches the longitudinal wavelength of created particles (the same as the cosmological red-shift) so that the kinetic longitudinal momentum in the co-moving frame  $P_z = P_\eta/\tau$  decays at later times.
- The longitudinal expansion dilutes the classical electric field so that the field decays faster (see Fig. 5.16). Because of this, the amplitude of the plasma oscillation becomes smaller compared to those for the non-expanding system (see Figs. 4.8 - 4.11).

Let us model the plasma oscillation in our expanding geometry by extending the non-expanding modeling explained in Section 2.5.2. By noting the approximate expressions (5.112) and (5.113) for the  $p_\eta$ -spectra without the backreaction and assuming the electric field is sufficiently adiabatic in time  $\bar{E}(\tau) \sim \bar{E}_0$ , we approximate the  $p_\eta$ -spectra by

$$\frac{d^6 N_{g\pm}}{d\mathbf{p}_\perp^2 dp_\eta d\mathbf{x}_\perp^2 d\eta} \sim \frac{1}{(2\pi)^3} \exp \left[ -\pi \frac{\mathbf{p}_\perp^2}{|q_A^{(\text{ad.})} \bar{E}_0|} \right] \theta(\mp p_\eta (p_\eta \pm q_A^{(\text{ad.})} \bar{A}_\eta(\tau))), \quad (5.119)$$

$$\frac{d^6 N_{\bar{q}}}{d\mathbf{p}_\perp^2 dp_\eta d\mathbf{x}_\perp^2 d\eta} \sim \frac{1}{(2\pi)^3} \exp \left[ -\pi \frac{m_f^2 + \mathbf{p}_\perp^2}{|q_i^{(\text{fund.})} \bar{E}_0|} \right] \theta(\mp p_\eta (p_\eta \pm q_A^{(\text{fund.})} \bar{A}_\eta(\tau))). \quad (5.120)$$

Notice that the above approximations discard the quantum interference effects, which largely modify the spectra from those naively given by the Schwinger estimates. Furthermore, we approximate the current  $\sum_\alpha w_\alpha \langle : \hat{j}_{\alpha,\eta} : \rangle$  by again discarding the quantum interference effects to obtain

$$\begin{aligned} \langle : \hat{j}_{\alpha,\eta} : \rangle &\sim \sum_{q\bar{q}} \sum_i (\mp q_i^{(\text{fund.})}) \sum_f \sum_s \int d^2 \mathbf{p}_\perp dp_\eta \text{sgn}(p_\eta \pm q_i^{(\text{fund.})} \bar{A}_\eta) \frac{d^6 N_{\bar{q}}}{d\mathbf{p}_\perp^2 dp_\eta d\mathbf{x}_\perp^2 d\eta} \\ &\quad + \sum_{g\pm} \sum_A (\mp q_A^{(\text{ad.})}) \sum_\sigma \int d^2 \mathbf{p}_\perp dp_\eta \text{sgn}(p_\eta \pm q_A^{(\text{ad.})} \bar{A}_\eta) \frac{d^6 N_{g\pm}}{d\mathbf{p}_\perp^2 dp_\eta d\mathbf{x}_\perp^2 d\eta} \\ &\sim \frac{1}{8\pi^3} \left[ N_{q\bar{q}} N_s N_{lq} \sum_i |q_i^{(\text{fund.})}|^3 + N_{g\pm} N_\sigma \sum_A |q_A^{(\text{ad.})}|^3 \right] |\bar{E}_0| \bar{A}_\eta(\tau) \\ &\equiv k^2 \bar{A}_\eta(\tau), \end{aligned} \quad (5.121)$$

where

$$k^2 \equiv \frac{1}{8\pi^3} \left[ N_{q\bar{q}} N_s N_{lq} \sum_i |q_i^{(\text{fund.})}|^3 + N_{g\pm} N_\sigma \sum_A |q_A^{(\text{ad.})}|^3 \right] |\bar{E}_0| \sim 3.1 \times 10^{-2} \times g^3 \bar{E}_0. \quad (5.122)$$

Here, we used  $\sum_i |q_i^{(\text{fund.})}|^3 \sim 0.2 \times g^3$  and  $\sum_A |q_A^{(\text{ad.})}|^3 \sim 1.3 \times g^3$  as we did in deriving Eq. (4.100). By substituting this expression into the backreaction equation (5.37), one finds that  $\bar{E}$  satisfies the Bessel differential equation given by

$$0 = \left[ \frac{d^2}{d\tau^2} + \frac{1}{\tau} \frac{d}{d\tau} + k^2 \right] \bar{E}(\tau). \quad (5.123)$$

The solution of Eq. (5.123) is given in terms of the Bessel functions. With the initial condition (5.118), one obtains

$$\bar{E}(\tau) = \bar{E}_0 \frac{J_1(k\tau_0)Y_0(k\tau) - J_0(k\tau)Y_1(k\tau_0)}{J_1(k\tau_0)Y_0(k\tau_0) - J_0(k\tau_0)Y_1(k\tau_0)} \xrightarrow{\tau_0 \rightarrow 0} \bar{E}_0 J_0(k\tau), \quad (5.124)$$

where  $J_n(x)$  and  $Y_n(x)$  are the Bessel function of the first and the second kind, respectively. From Eq. (5.124), one can roughly estimate the time scale of the plasma oscillation as  $\sqrt{|g\bar{E}_0|}\tau_{\text{osc}} \sim 13 \times g^{-1}$  because the first zero point of the Bessel function  $J_0(x)$  is  $x = 2.40$ . Equation (5.124) also tells us that the electric field decays as  $\propto 1/\sqrt{\tau}$  because the Bessel functions decays as  $\propto 1/\sqrt{\tau}$ . This is a result of the longitudinal expansion of the system; for non-expansion systems, what we obtained from the same argument is Eq. (2.98), which says that electric fields never decay due to classical dynamics. As is evident from the derivation, this modeling is, unfortunately, a crude estimate mainly because it completely discards quantum interferences, which dramatically changes the spectra. Nevertheless, it nicely captures the essential features of the plasma oscillation and the effects of the longitudinal expansion because they are purely classical dynamics.

### 5.3.3 momentum rapidity $y_{\mathbf{P}}$ -spectrum of quarks and gluons

Next, we study the kinetic momentum rapidity  $y_{\mathbf{P}}$ -spectrum of produced quarks  $d^5 N_{(-)} / d^2 \mathbf{p}_{\perp} dy_{\mathbf{P}} d\mathbf{x}_{\perp}^2$  and gluons  $d^5 N_{g\pm} / d^2 \mathbf{p}_{\perp} dy_{\mathbf{P}} d\mathbf{x}_{\perp}^2$  by integrating the  $p_{\eta}$ -spectra over  $p_{\eta}$ . The results are plotted in Figs. 5.13 and 5.14.

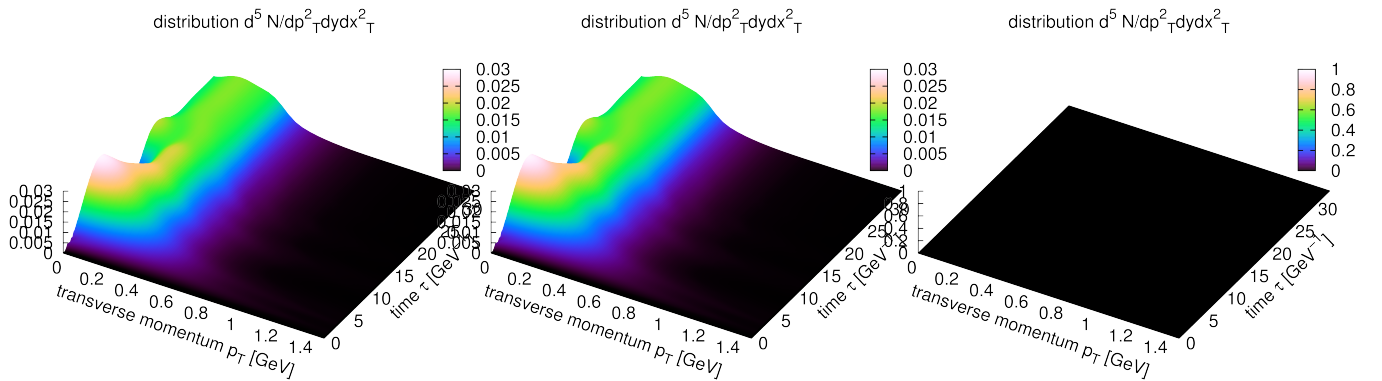


Figure 5.13: The transverse momentum  $\mathbf{p}_{\perp}$ -dependence of the momentum rapidity  $y_{\mathbf{P}}$ -spectra of massless quarks  $d^5 N_{(-)} / d^2 \mathbf{p}_{\perp} dy_{\mathbf{P}} d\mathbf{x}_{\perp}^2$ . Different panels differentiate the color charge  $q_i^{(\text{fund.})}$  ( $i = 1, \dots, N_c$ ) of quarks with color  $i$ . We set the color angle  $\theta = 0$ , and the corresponding quark charge  $q_i^{(\text{fund.})}$  read  $q_1^{(\text{fund.})} = q_1^{(\text{fund.})} = 1/2$  (left),  $q_2^{(\text{fund.})} = -1/2$  (middle), and  $q_3^{(\text{fund.})} = 0$  (right).

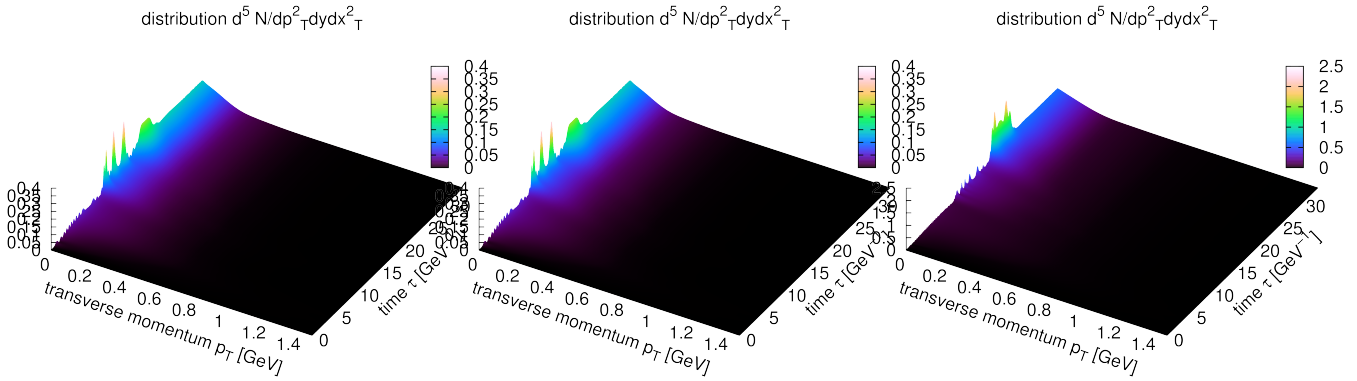


Figure 5.14: The transverse momentum  $\mathbf{p}_\perp$ -dependence of the momentum rapidity  $y_{\mathbf{P}}$ -spectra of gluons  $d^5 N_{g\pm}/d^2 \mathbf{p}_\perp dy_{\mathbf{P}} dx_\perp^2$ . Different panels differentiate the color charge  $q_A^{(\text{ad.})}$  ( $i = 1, \dots, N_c(N_c - 1)/2$ ) of gluons with color  $A$ . We set the color angle  $\theta = 0$ , and the corresponding gluon charge  $q_A^{(\text{ad.})}$  read  $q_A^{(\text{ad.})} = q_1^{(\text{ad.})} = -1/2$  (left),  $q_2^{(\text{ad.})} = -1/2$  (middle), and  $q_3^{(\text{ad.})} = 1$  (right).

From Figs. 5.13 and 5.14, we find that the  $\mathbf{p}_\perp$ -dependence of the quark spectrum is almost Gaussian, while the gluon production favors soft  $\mathbf{p}_\perp$  gluons. This is simply because gluons are not subjected to the Pauli principle and hence soft gluons are produced ceaselessly without any bound. We note that the total number of produced gluons are finite (see Fig. 5.15) because the spectrum only has a weak divergence  $|\mathbf{p}_\perp|^{-\alpha}$  with  $\alpha < 1$  for  $\mathbf{p}_\perp \rightarrow \mathbf{0}$ . We also note that the momentum rapidity  $y_{\mathbf{P}}$ -spectra of both particles are smoothed by the  $p_\eta$ -integral when compared to the  $p_\eta$ -spectra (see Figs. 5.12 and 5.13).

Although the plasma oscillation in the  $p_\eta$ -spectra can be observed only in the co-moving frame and hence is not a direct experimental observable in the center-of-mass frame, the momentum rapidity  $y_{\mathbf{P}}$ -spectra possess some traces of it:

- We can see some dips in the quark  $p_\eta$ -spectrum in the low transverse momentum region. This is because quarks and anti-quarks with soft momenta can annihilate with each other when they overlap at the same phase space. The overlap is possible because of the plasma oscillation.
- The gluon  $p_\eta$ -spectrum shows dramatical increases periodically because of the Bose enhancement followed by the plasma oscillation; in particular, soft gluon production is dramatically enhanced.

### 5.3.4 total number of quarks and gluons

We compute the total number of quarks and gluons produced per unit momentum rapidity  $y_{\mathbf{P}}$  by integrating the momentum rapidity  $y_{\mathbf{P}}$ -spectra over the transverse momentum  $\mathbf{p}_\perp$  and

summing up all the quantum numbers. The results are shown in Fig. 5.15. The left panel shows the total number of produced quarks (red) and gluons (blue), and the right panel shows the ratio  $R_{q-g}$  of the total quark number to the total gluon number  $R_{q-g} \equiv N_q/N_g$ .

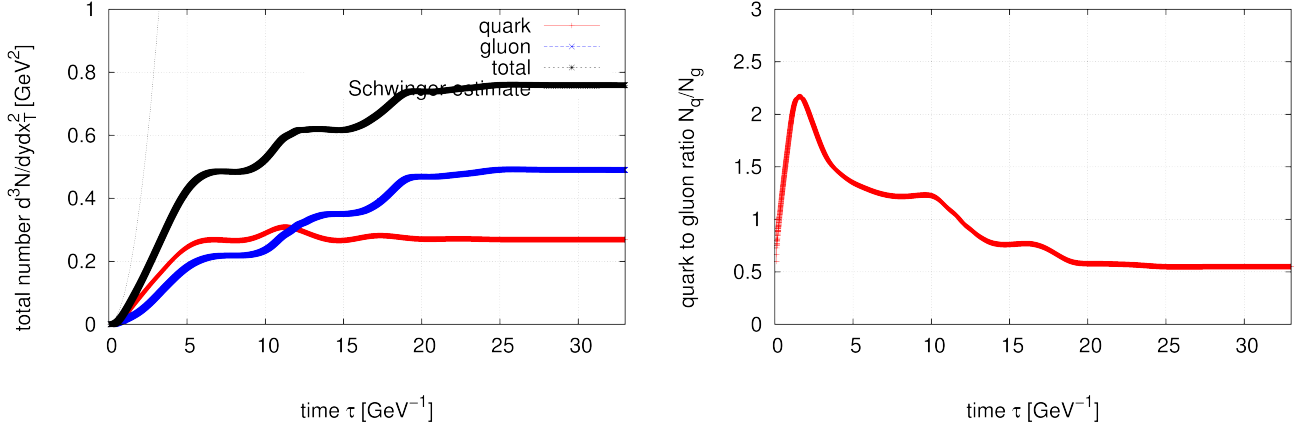


Figure 5.15: [Left] Total number of produced quarks  $\sum_{f,i,s,q\bar{q}} \int d^3\mathbf{p}d^6 N_{(-)} / d\mathbf{p}^3 d\mathbf{x}^3$  (red) and gluons  $\sum_{\sigma,A,g\pm} \int d^3\mathbf{p}d^6 N_{g\pm} / d\mathbf{p}^3 d\mathbf{x}^3$  (blue), and the sum of them (black). The dashed line is an estimate from the Schwinger formula without the backreaction, i.e., the sum of Eqs. (5.116) and (5.117). [Right] The ratio of the total number of quarks to the total number of gluons  $R_{q-g} \equiv [\sum_{f,i,s,q\bar{q}} \int d^3\mathbf{p}d^6 N_{(-)} / d\mathbf{p}^3 d\mathbf{x}^3] / [\sum_{\sigma,A,g\pm} \int d^3\mathbf{p}d^6 N_{g\pm} / d\mathbf{p}^3 d\mathbf{x}^3]$ .

From Fig. 5.15, we first find that the quark production is very fast: The major part of the quark production is completed as early as  $\tau \sim 1$  fm/ $c$ . Within this short time-scale, about 1000 quarks per unit rapidity (for the typical transverse size of heavy ions such as gold  $\sim 7$  fm) are produced and the number is comparable to that of gluons for all values of  $\tau$ . Notice that the value “1000” is also comparable to the experimentally observed hadron yield  $\sim 1000$  charged hadrons per unit rapidity, and thus one might understand that the huge entropy production in the pre-equilibrium stage dynamics of heavy ion collisions could be explained by the Schwinger mechanism (although it is highly non-trivial how to connect the quark and gluon number to the final hadrons because it involves the physics of confinement, and hence one needs a more sophisticated treatment to discuss this issue in detail). Hence, one understands that quarks must have important information about and/or an important role in the pre-equilibrium stage dynamics of ultra-relativistic heavy ion collisions.

We also find that except at the very early times  $\tau \lesssim 1$  fm/ $c$ , where quark production dominates because of the perturbative particle production mechanism, gluons are more abundantly produced than quarks because of the Bose enhancement for gluons and the Pauli blocking for quarks. It is worthwhile to point out that the final ratio  $R_{q-g} \sim 0.5$  is larger than what we found in the non-expanding case ( $R_{q-g} \sim 0.2$ ; see Fig. 4.13). This is because the expansion makes the electric field decay faster (see Fig. 5.16), and the gluon production, which is slower

than the quark production at the early times  $\tau \lesssim 1 \text{ fm}/c$ , becomes ineffective before the ratio grows. If one compares this value  $R_{q-g} \sim 0.5$  with that one naively expects for a chemically equilibrated quark and gluon matter  $R_{q-g} = 9/4$  (where an ideal gas of massless particles with  $N_f = 3$  is assumed), one understands that our result is far away from the chemical equilibrium. This is because our mean field and massless approximation neglects inelastic processes such as  $g \rightarrow q\bar{q}$ ,  $gg \rightarrow g$ ; inclusion of these processes is left to a future work.

### 5.3.5 decay of color electric field

Figure 5.16 shows how the classical electric field decays (left panel) together with the time-evolution of the color current  $\sum_{\alpha} w_{\alpha} \langle : \hat{j}_{\alpha}^{\eta} : \rangle$  (right panel).

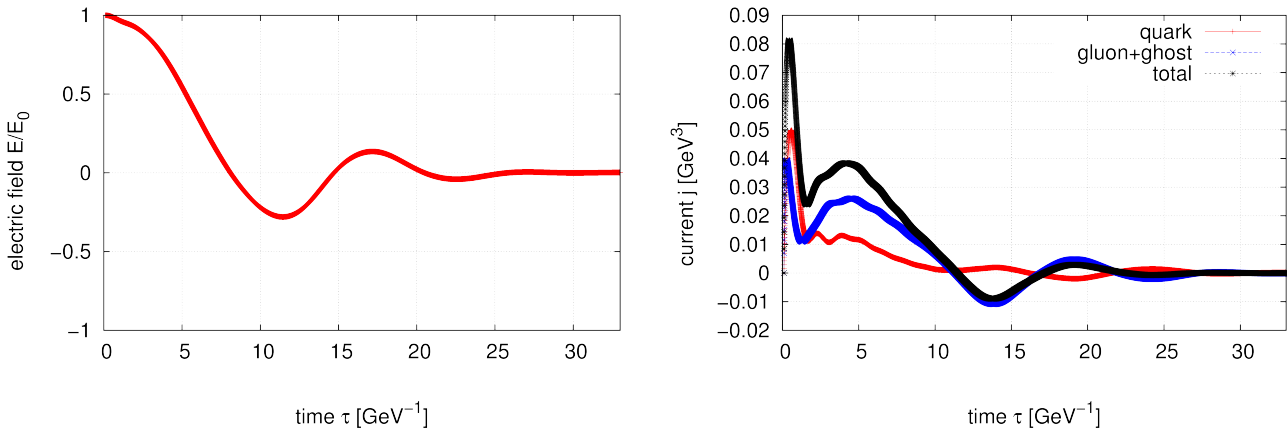


Figure 5.16: [Left] The time-evolution of the electric field strength  $\bar{E}(\tau)$  [Right] The time-evolution of the color current  $\sum_{\alpha} w_{\alpha} \langle : \hat{j}_{\alpha}^{\eta} : \rangle$  in terms of the quark contribution (red), the gluon and ghost contribution (blue), and the sum of them (black).

We again observe the classical plasma oscillating behavior in both the electric field strength and the color current.

An important point here is that not only the particle production, but also the longitudinal expansion dilutes the classical electric field to decay (see Eq. (5.124)). As a result, the electric field decays fast with a typical time-scale  $\tau \sim 3 \text{ fm}/c$ , which is much faster than the value  $t \sim 10 \text{ fm}/c$  for the non-expanding case (see Fig. 4.12).

The typical decay time-scale  $\tau \sim 3 \text{ fm}/c$  is roughly consistent with the speculated QGP formation time  $\tau \sim 1 \text{ fm}/c$ . In this sense, one may say that the Schwinger mechanism supports the early QGP formation scenario. The deviation may be because of our simplification of the initial field configuration. In particular, it may be important to include longitudinal color magnetic field component, which enhances the quark and gluon production as was discussed in Introduction.

### 5.3.6 energy density

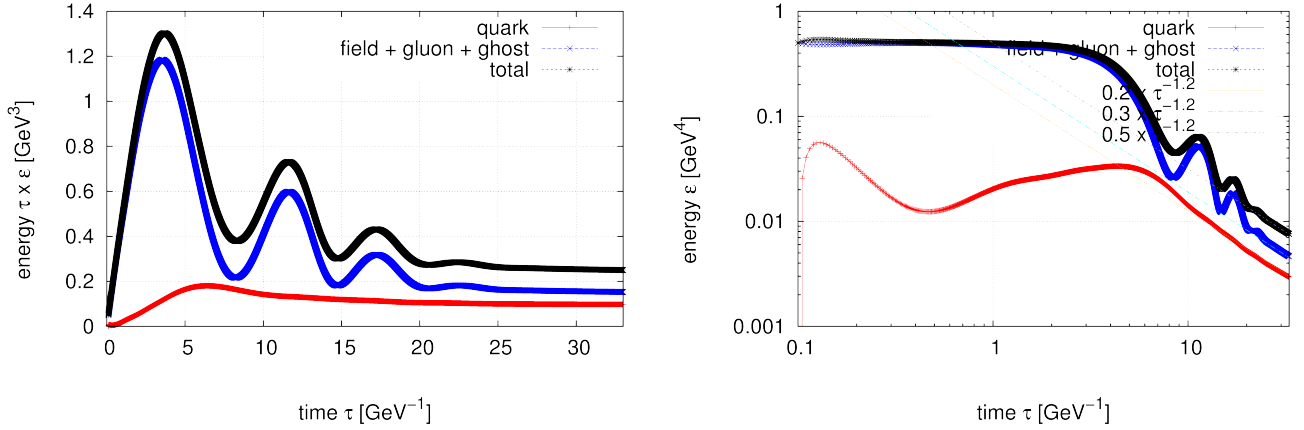


Figure 5.17: [Left] The energy balance between the total gauge field, i.e., the sum of classical field, quantum gluons, and ghosts (blue), and produced quarks (red). The total energy of the system is represented by the black line. [Right] Power-dependence of the late time evolution of the energy density.

The time-evolution of the energy density  $\langle \hat{\epsilon} \rangle$  is plotted in Figs. 5.17 and 5.18. From these figures, one understands that our QCD formalism naturally describes the transition from the *field* regime to the *particle* regime in the pre-equilibrium stage dynamics of heavy ion collisions explained in Section 1.2.2 and reveals the dynamics of the transition quantitatively. Namely, we find:

**field regime** ( $\tau_0 < \tau \lesssim 2 \text{ fm}/c$ )

The system is dominated by the initial classical gauge field, and the quantum particle degrees of freedom (quarks and gluons) are negligible. Hence, the spacetime evolution of the system can solely be determined by the (Abelianized) classical Yang-Mills equation (5.37).

**intermediate regime** ( $2 \text{ fm}/c \lesssim \tau \lesssim 4 \text{ fm}/c$ )

The classical gauge field decays because of the longitudinal expansion and the quark and gluon production via the Schwinger mechanism. A major part of the particle production completes within a few  $\text{fm}/c$  as  $\tau \lesssim 2 \text{ fm}/c$ . At this time-scale, however, the classical field has not decayed completely and the field energy is still comparable to the quantum particle energy. Thus, in this intermediate regime ( $2 \text{ fm}/c \lesssim \tau \lesssim 4 \text{ fm}/c$ ), both classical and quantum degrees of freedom are important in understanding the spacetime evolution of the system. For example, the time-dependence of the total energy density shows an oscillating behavior. This is because of the plasma oscillation, which is a result of the interaction between the quantum particles and the classical field.

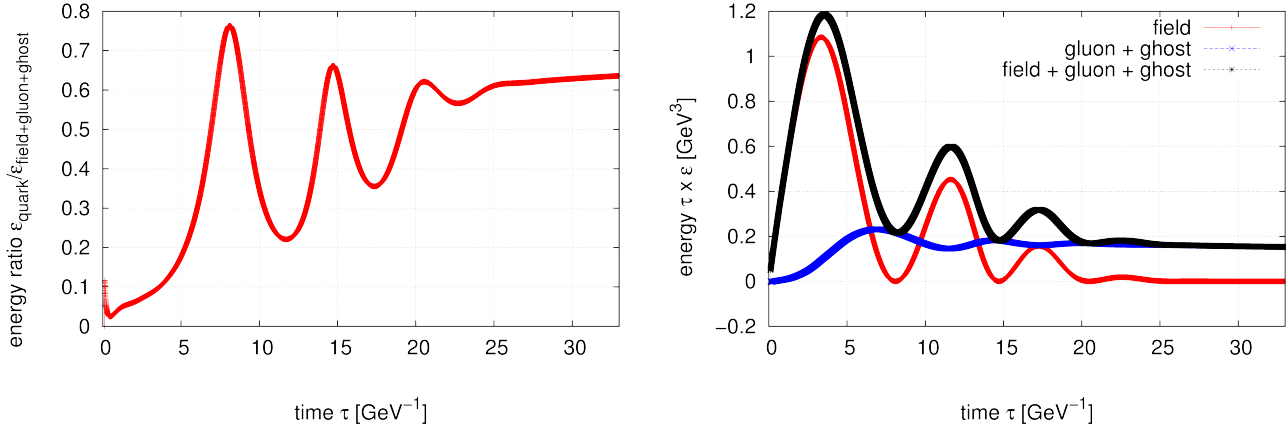


Figure 5.18: [Left] A ratio of the produced quark energy to the total gauge field energy. [Right] The energy balance of the total gauge field energy (black) between the classical field (red) and the quantum gluons and ghosts (blue).

### particle regime ( $4 \text{ fm}/c \lesssim \tau$ )

After the intermediate regime, the classical gauge field completely passed away, and the system is dominated by quantum particle degrees of freedom (quarks and gluons). Hence, the spacetime evolution can solely be determined by the quantum field equations (5.16) and (5.28).

Now, the energy density shows a monotonic behavior in time. This is because the plasma oscillation never takes place after the classical field passed away.

In this particle regime, gluon particles dominate the system as  $\langle : \hat{\epsilon} : \rangle_{\text{q}} / \langle : \hat{\epsilon} : \rangle_{\text{g}} \sim 0.64$  because of the Pauli blocking for quarks and the Bose enhancement for gluons explained previously. Notice that this ratio is larger than what we observed for the non-expanding case,  $\langle : \hat{\epsilon} : \rangle_{\text{q}} / \langle : \hat{\epsilon} : \rangle_{\text{g}} \sim 0.35$  (see Fig. 4.15), in the same reasoning why the number ratio  $N_{\text{q}}/N_{\text{g}}$  becomes larger for the present expanding case (see Section 5.3.4). We also note that the ratio  $\langle : \hat{\epsilon} : \rangle_{\text{q}} / \langle : \hat{\epsilon} : \rangle_{\text{g}} \sim 0.64$  is larger than the number ratio  $N_{\text{q}}/N_{\text{g}} \sim 0.50$  because the gluon production is dominated in the soft momentum region.

We also find that the energy density decays a little bit faster than an inverse of  $\tau$  as  $\langle : \hat{\epsilon} : \rangle \propto \tau^{-1.2}$ , although one naively expects that the energy density might decrease as  $\langle : \hat{\epsilon} : \rangle \propto 1/\tau$  because the system volume increases as  $\propto \tau$ . This is because produced matter composed of quarks and gluons have positive longitudinal pressure that does mechanical work against the expansion, which decreases energy with the expansion.

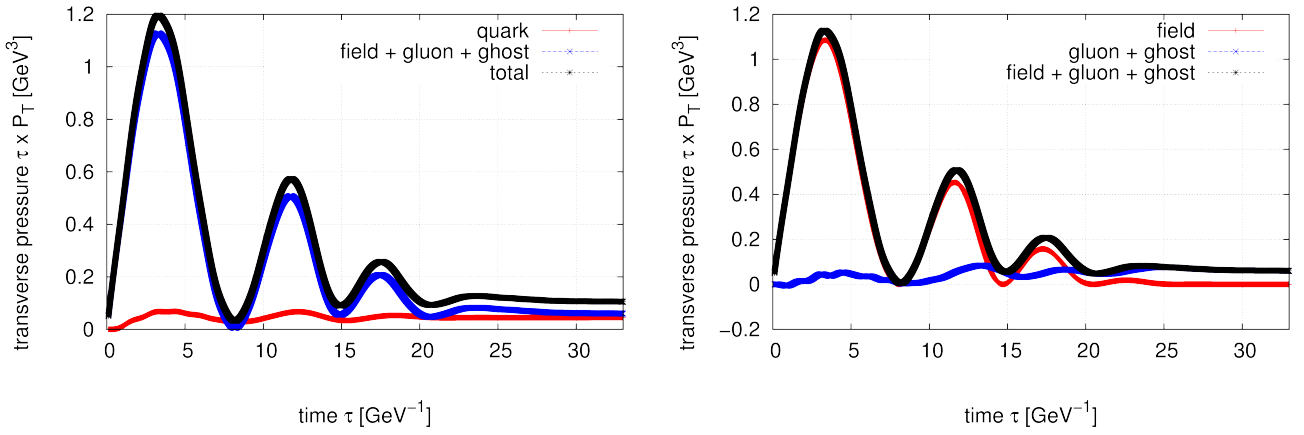


Figure 5.19: [Left] The total transverse pressure of the system (black) together with contributions from the total gauge field, i.e., the sum of classical field, quantum gluons, and ghosts (blue), and produced quarks (red). [Right] The total transverse pressure of the total gauge field (black) together with contributions from the classical field (red) and the quantum gluons and ghosts (blue).

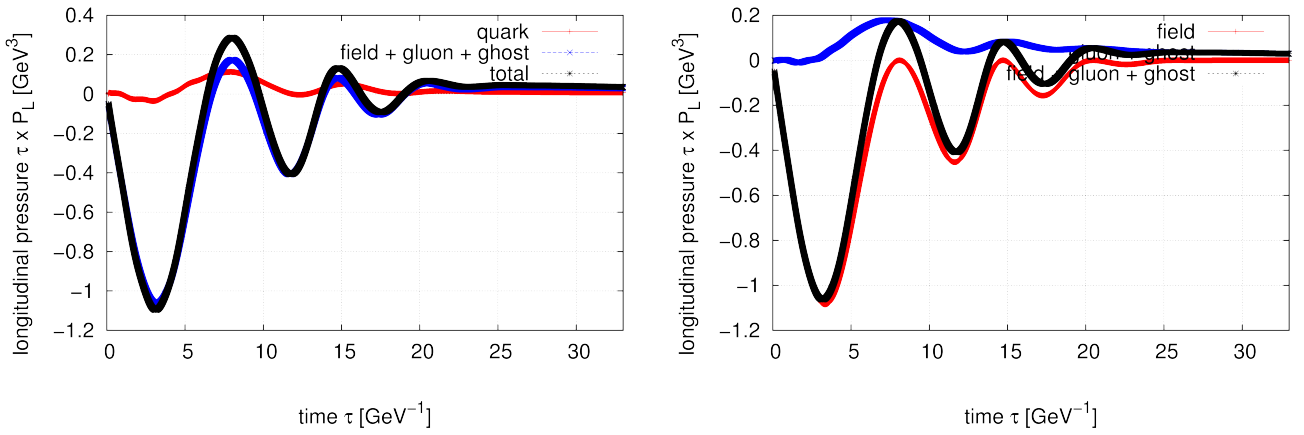


Figure 5.20: [Left] The total longitudinal pressure of the system (black) together with contributions from the total gauge field, i.e., the sum of classical field, quantum gluons, and ghosts (blue), and produced quarks (red). [Right] The total longitudinal pressure of the total gauge field (black) together with contributions from the classical field (red) and the quantum gluons and ghosts (blue).

### 5.3.7 pressure

The time-evolution of the transverse (longitudinal) pressure of the system is shown in Fig. 5.19 (Fig. 5.20). As observed in the energy density (see Figs. 5.17 and 5.18), we again observe the transition from the field regime to the particle regime:

#### field regime ( $\tau_0 < \tau \lesssim 2 \text{ fm}/c$ )

The initial classical gauge field dominates the system, and the quantum particle degrees of freedom (quarks and gluons) are negligible. As a result, the system is highly anisotropic with negative longitudinal pressure  $\langle : \hat{P}_z : \rangle \sim - \langle : \hat{P}_\perp : \rangle \sim -\bar{E}_0^2/2$ .

#### intermediate regime ( $2 \text{ fm}/c \lesssim \tau \lesssim 4 \text{ fm}/c$ )

The classical gauge field decoheres into quarks and gluons. The longitudinal expansion also depletes the strength of the classical field. As a result, the magnitude of the transverse and the longitudinal pressure from the classical field quickly decreases, and that from the produced quarks and gluons begins to increase.

An important point here is that the isotropization of the system takes place during this regime. In particular, the anomalous negative longitudinal pressure, which the system initially has, begins to disappear because the produced particles always have a positive longitudinal pressure and the classical field, which has a negative longitudinal pressure, quickly decays.

We also observe that both the transverse and the longitudinal pressure oscillate in time because of the plasma oscillation due to the interaction between the produced particles and the classical field.

#### particle regime ( $4 \text{ fm}/c \lesssim \tau$ )

Now, the classical gauge field completely passed away and the quantum particle degrees of freedom (quarks and gluons) dominate the system.

In this regime, the longitudinal and the transverse pressure show a monotonic behavior in time because of the absence of the plasma oscillation.

Notice that the longitudinal pressure of the system is smaller than the transverse one  $\langle : \hat{P}_z : \rangle < \langle : \hat{P}_\perp : \rangle$ , which is in contrast to what we found in the non-expanding case  $\langle : \hat{P}_z : \rangle > \langle : \hat{P}_\perp : \rangle$  (see Fig. 4.21). This is because the longitudinal expansion of the system strongly decreases the longitudinal momentum of the produced particles as was explained in Figs. 5.9 and 5.10.

Next, we discuss the isotropization of the system by following the time-evolution of  $\langle : \hat{P}_\perp : \rangle / \langle : \hat{\epsilon} : \rangle$  and  $\langle : \hat{P}_z : \rangle / \langle : \hat{\epsilon} : \rangle$ , whose result is shown in Fig. 5.21. Before discussing the result, it is instructive to see how the quantities,  $\langle : \hat{P}_\perp : \rangle / \langle : \hat{\epsilon} : \rangle$  and  $\langle : \hat{P}_z : \rangle / \langle : \hat{\epsilon} : \rangle$ , are related to the anisotropy

of the system,

$$a \equiv \frac{\langle : \hat{P}_z : \rangle}{\langle : \hat{P}_\perp : \rangle}, \quad (5.125)$$

in our expanding problem. To do this, we first assume that QCD is conformal (which is, in reality, slightly broken by the conformal anomaly [166, 167, 168]). Then, the trace of the symmetric energy-momentum tensor  $\langle : \hat{T}^{\mu\nu} : \rangle$  vanishes, and we find

$$\langle : \hat{\epsilon} : \rangle = 2 \langle : \hat{P}_\perp : \rangle + \langle : \hat{P}_z : \rangle = \left(1 + \frac{2}{a}\right) \langle : \hat{P}_z : \rangle. \quad (5.126)$$

By substituting this relation (5.126) into the energy conservation law (5.38), one obtains

$$0 = \left[ \frac{d}{d\tau} + \frac{1}{\tau} \frac{2+2a}{2+a} \right] \langle : \hat{\epsilon} : \rangle. \quad (5.127)$$

If the system is sufficiently adiabatic in time, or  $\partial_\tau a \sim 0$ , then one can solve Eq. (5.127) to find

$$\langle : \hat{\epsilon} : \rangle \propto \tau^{-\frac{2+2a}{2+a}}, \quad (5.128)$$

and

$$\frac{\langle : \hat{P}_\perp : \rangle}{\langle : \hat{\epsilon} : \rangle} = \frac{1}{2+a}, \quad \frac{\langle : \hat{P}_z : \rangle}{\langle : \hat{\epsilon} : \rangle} = \frac{a}{2+a}. \quad (5.129)$$

From Eqs. (5.128) and (5.129), if the system is completely isotropitized ( $a = 1$ ), one finds

$$\langle : \hat{\epsilon} : \rangle \propto \tau^{-4/3}, \quad \frac{\langle : \hat{P}_\perp : \rangle}{\langle : \hat{\epsilon} : \rangle} = \frac{1}{3}, \quad \frac{\langle : \hat{P}_z : \rangle}{\langle : \hat{\epsilon} : \rangle} = \frac{1}{3}. \quad (5.130)$$

Another interesting value of  $a$  is  $a = 0$ , which corresponds to the situation where the longitudinal pressure vanishes as  $\langle : \hat{P}_z : \rangle = 0$  because of the expansion. This situation is often called the *free-streaming limit*. In this case, one finds

$$\langle : \hat{\epsilon} : \rangle \propto \tau^{-1}, \quad \frac{\langle : \hat{P}_\perp : \rangle}{\langle : \hat{\epsilon} : \rangle} = \frac{1}{2}, \quad \frac{\langle : \hat{P}_z : \rangle}{\langle : \hat{\epsilon} : \rangle} = 0. \quad (5.131)$$

It is known that the classical Yang-Mills evolution favors the free-streaming limit and never isotropitizes [121, 124, 125, 126, 146] as was reviewed in Section 1.2.2 (see Fig. 1.6).

Now, we are ready to discuss Fig. 5.21. One immediately observes that the anisotropy of the system relaxes as time goes because of the decoherence of the classical field into quantum particles. In addition to this, the longitudinal expansion of the system also plays an important role in the isotropization. By noting that the longitudinal pressure of the system is much larger than the transverse one in the non-expanding case (see Fig. 4.21), the longitudinal expansion of the system makes the longitudinal pressure weaker and makes it closer to the value of the transverse pressure. Because of these effects, the system becomes less anisotropic as  $a \sim 0.5$

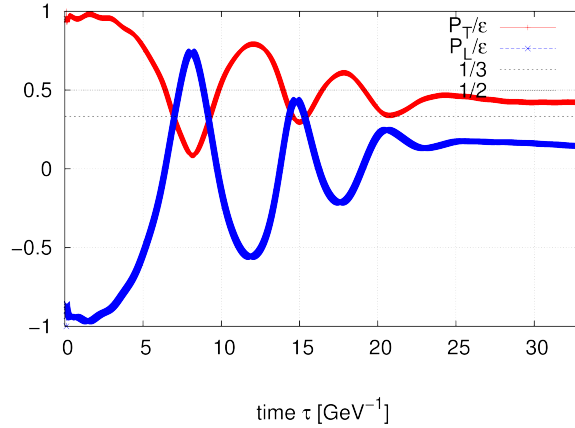


Figure 5.21: Isotropization of the system. The total transverse and longitudinal pressure scaled by the total energy,  $\langle \hat{P}_\perp \rangle / \langle \hat{\epsilon} \rangle$  and  $\langle \hat{P}_z \rangle / \langle \hat{\epsilon} \rangle$ , are plotted in red and blue line, respectively. The horizontal lines 1/2 (dotted) and 1/3 (dashed) correspond to the free-streaming limit (5.131) and the isotropitized limit (5.130), respectively.

within a few fm/c. If we assume that hydrodynamics works even for such a relatively anisotropic regime (for example, Ref. [129] claims that the hydrodynamics still works for  $a \sim 0.2$ ; see Section 1.2.2 also), we may understand that our result implies that the hydrodynamization actually takes place within a few femtoseconds after a collision of nuclei as suggested by experiments. By noting that our mean field and massless approximations neglect collisions and scatterings between produced particles, this consistency implies that the quantum decoherence of the classical field together with the longitudinal expansion are essential in the isotropization in the pre-equilibrium dynamics of ultra-relativistic heavy ion collisions; that is, collisional effects are only secondary, although they should further shorten the time-scale and improve the anisotropy of the system to some extent. This discussion is also consistent with the state-of-art effective kinetic study [129], which states that the typical time-scale of collisional effects is rather long  $\sim 100/Q_s \sim 20$  fm/c and hence may be irrelevant to the fast hydrodynamization.

## 5.4 Brief summary

We briefly summarize the main results of this chapter:

- We formulated the Schwinger mechanism in QCD for an expanding electric field in Section 5.1.
- By neglecting the backreaction, we analytically traced the time-evolution of the quark and gluon distributions in Section 5.2 and find that the quark and gluon production in an expanding geometry is essentially the same as that in a non-expanding geometry, although

there are slight differences in what frame we are observing.

- By modeling the initial color flux tubes just after a collision by a spatially homogeneous, boost-invariantly expanding electric field, we discussed the pre-equilibrium stage dynamics of heavy ion collisions within our QCD formalism including the backreaction (see Section 5.3).
- The classical plasma oscillation occurs in the co-moving frame (see Figs. 5.9 - 5.12), which leaves some traces in the momentum rapidity  $y_{\mathbf{P}}$ -spectra in the center-of-mass frame because of the quantum interferences induced by the plasma oscillation (see Figs. 5.13 and 5.14).
- We quantitatively revealed how the initial classical field degree of freedom decohere into quantum particle degrees of freedom in a unified way. In particular, the classical electric field decays quite fast  $\sim 3 \text{ fm}/c$  (see Fig. 5.17), which does not contradict with the fast QGP formation, because of the decoherence and the longitudinal expansion.
- Huge number of quarks  $\sim 1000$  per unit rapidity are produced very quickly  $\sim 1 \text{ fm}/c$  (see Fig. 5.15). This means that not only gluons but also quarks must have important information about and/or an important role in the pre-equilibrium stage dynamics of ultra-relativistic heavy ion collisions.
- Because of the decoherence and the longitudinal expansion, the system becomes less anisotropic as  $\langle : \hat{P}_z : \rangle / \langle : \hat{P}_\perp : \rangle \sim 0.5$  within a few  $\text{fm}/c$  (see Fig. 5.21), although our mean field and massless approximations do not take into account collisions and scatterings between produced particles.



## Chapter 6

# Summary and Outlook

In this thesis, we extensively studied the Schwinger mechanism in QCD and its applications to the pre-equilibrium stage dynamics of ultra-relativistic heavy ion collisions.

In Section 2, we reviewed the Schwinger mechanism in QED in detail before going into the QCD study. Firstly, we adopted the mean field approximation to formulate the Schwinger mechanism in QED including the backreaction from produced electrons. Next, we applied the formalism to a constant electric field, and saw how one can reproduce the well-known exponential formula for the electron production rate  $\Gamma = \exp[-\pi(m_e^2 + \mathbf{p}_\perp^2)/|eE_0|]/(2\pi)^3$ . We, then, considered a pulsed type electric field to discuss how the time-dependence of the field affects the particle production mechanism (this part is based on my own work [42]). We analytically showed that (i) an interplay between the perturbative and the non-perturbative particle production occurs with changing the field strength  $E_0$  and/or the duration of the field  $\tau$ ; (ii) two dimensionless parameters  $\nu = |eE_0|\tau^2, \gamma = |eE_0|\tau/m_e$  control the interplay; and (ii) the electron production is strongly enhanced in the perturbative regime. After that, we briefly discussed the dynamical evolution of the electron spectrum without the backreaction. In the last half of this section, we discussed the backreaction effects. We found that the electron spectrum is dramatically modified from the one without the backreaction. In particular, we found that (i) the classical plasma oscillation occurs; (ii) the quantum interferences among electrons strongly distort the electron spectrum; (iii) the Pauli principle suppresses the electron production (the Pauli blocking); and (iv) the decoherence of the classical field to electrons relaxes the strong anisotropy of the system.

The following three sections are the main parts of this thesis:

In Section 3, we extended the QED formulation to the case of  $SU_c(N_c = 2)$  Yang-Mills theory without quarks. By adopting the mean field and the massless approximations, we derived a set of linear differential equations, which describes gluon production, backreaction, and partial effects of scatterings. We first applied the formalism to a constant color electric background field, and analytically followed the time-evolution of the gluon distribution function by neglecting the backreaction. We found that the basic features of the gluon production are the same as what we found in the electron production in QED. However, this situation changes

if one treats the backreaction effects: The quantum interferences dramatically enhance the gluon production (the Bose enhancement) and distort the spectrum stronger than electrons. These effects accelerate the decoherence of the classical field.

In Section 4, we extensively studied the Schwinger mechanism in QCD (for a non-expanding electric field) by extending the  $SU_c(N_c = 2)$  Yang-Mills formulation to  $SU_c(N_c = 3) \otimes SU_f(N_f)$  QCD. We first analyzed the formalism without the backreaction, and analytically followed the time-evolution of the quark and gluon distribution functions. Differences and similarities between the quark and the gluon production are discussed; for example, the perturbative enhancement is two times larger for quarks than gluons. Various effects such as the color angle  $\theta$ -, the number of flavor  $N_f$ -, and the quark mass  $m_f$ -effects, are examined in detail. Secondly, we discussed the backreaction effects. Most importantly, we found that the system is eventually dominated by gluons because of the Bose enhancement (the Pauli blocking) for gluon (quark) production, and hence quarks give only secondary contributions. Various effects such as the color angle  $\theta$ -, the number of flavor  $N_f$ -, and the quark mass  $m_f$ -effects, are also investigated with the backreaction. Among them, the quark mass  $m_f$ -dependence is worth mentioning: We found that (i) the strange (charm) quark production is comparable (negligible) to the massless up and down quark production; and (ii) the heavy charm quark production is much larger than what one naively expects from the Schwinger exponential formula for the particle production rate  $\Gamma$ .

In Section 5, we applied our QCD formalism to the pre-equilibrium stage dynamics of ultra-relativistic heavy ion collisions, and discussed some phenomenological consequences. There, we considered a simple toy model: We modeled the initial color flux tubes existing just after a collision of nuclei by a spatially homogeneous and boost-invariantly expanding electric field. In the first part of this chapter, we explained how one can extend the QCD formalism originally developed for a non-expanding electric field to the expanding one. In the second part of this chapter, we analytically traced the time-evolution of the quark and gluon distribution functions without the backreaction (this part is based on my own work [137]). By doing this, we studied effects of the longitudinal expansion in detail, and found that quark and gluon production for an expanding electric field is essentially the same as that for a non-expanding one, although there are slight differences in what frame we are observing (the co-moving frame for the expanding one, and the center-of-mass frame for the non-expanding one). In the last part of this chapter, the backreaction is considered and the phenomenological consequences of our model was investigated in detail. An advantage of our formalism is that it enables us to quantitatively discuss the transition from the field regime to the particle regime in a unified way. We found, in particular, that (i) the classical plasma oscillation takes place in the co-moving frame, which leaves some traces in the momentum rapidity  $y_P$ -spectra observed in the center-of-mass frame because of the quantum interferences; (ii) the classical electric field decays quite fast  $\sim 3 \text{ fm}/c$  because of the decoherence and the longitudinal expansion; (iii) huge number of quarks  $\sim 1000$  per unit rapidity are produced very quickly  $\sim 1 \text{ fm}/c$ ;

and (iv) because of the decoherence and the longitudinal expansion, the system becomes less anisotropic as  $\langle : \hat{P}_z : \rangle / \langle : \hat{P}_\perp : \rangle \sim 0.5$  within a few fm/c, although our mean field and massless approximations do not take into account collisions and scatterings between produced particles.

There are many possible future directions of this work:

The first direction is to improve our formalism to include the higher order quantum corrections such as the effective mass terms  $M$ . The higher order terms are responsible for collisions and scatterings of produced particles, and are important in describing the thermalization; the isotropization; the hydrodynamization; and the chemical equilibration of the system. Inclusion of these terms and evaluating its impacts on the spacetime evolution are also important in justifying our theoretical simplifications (e.g. the mean field and the massless approximations) made in this thesis from a theoretical point of view. Besides, it is discussed vigorously that momentum exchanges due to the scatterings induce spectral cascades (for a recent review covering this topic, see [169]), which result in some interesting behaviors such as a formation of gluonic Bose-Einstein condensates [170, 171, 172, 173].

Another direction is to improve the initial configuration of the classical field: In realistic situations, the classical field has finite extent in the transverse direction and has random fluctuations with a typical transverse correlation length  $\sim Q_s^{-1}$ . Besides, it is known that the classical color field has magnetic components in addition to electric ones in the longitudinal direction [121]. Inclusion of these non-trivial structure in the initial field configuration is important in making a reliable theoretical prediction of various experimental observables and thus in justifying our theoretical framework from an experimental point of view. Also, it is important in constructing a physical initial condition for hydrodynamical simulations (e.g. transverse energy or entropy density and formation time), which was determined by ad hoc ways previously. More or less, these non-trivial structure would modify our results for a homogeneous pure electric field configuration. For instance, as was stated in Introduction, the existence of longitudinal magnetic fields may enhance particle production rate [33, 34, 91, 174, 175]. In addition to this, such field configuration is known to invoke the Nielsen-Olesen type instability [13, 14], although its typical timescale is rather slow. It is interesting to study the particle production under the presence of such instabilities; for non-expanding, static color electromagnetic fields, it was discussed that the instability may dramatically enhance the gluon production [15].

The last direction which we would like to mention is about quark dynamics. As was discussed so far, quarks are abundantly produced at very early times and hence they may have important information about and/or an important role in the pre-equilibrium stage dynamics of ultra-relativistic heavy ion collisions. Since quarks have an U(1) electromagnetic charge, which does not suffer from the strong interactions, one can investigate the quark dynamics by using U(1) electromagnetic probes such as photons [176] and dileptons [177, 178]. Studying the U(1) electromagnetic probes are, hence, very important because it may provide us novel experimental probes for the pre-equilibrium stage dynamics. Another interesting topic involving the quark dynamics is the existence of strong U(1) electromagnetic fields just after a collision of

nuclei [24, 25]. Although such strong U(1) electromagnetic fields die away immediately after a collision within the time less than  $1 \text{ fm}/c$ , they could significantly influence the quark dynamics because the strong U(1) electromagnetic fields are as strong as the pion mass scale and the quark production is fast enough. Thus, one can expect some experimental traces of them, for instance, in U(1) charge dependences in observables. In particular, an U(1) charge dependent directed flow  $v_1^\pm$  in asymmetric heavy ion collisions [179, 180] is recently measured by the STAR collaboration [181]. This should provide important insights in the quark production, or possibly the pre-equilibrium stage dynamics of heavy ion collisions, although theoretical understanding of this observable is still lacking. Another interesting physics that involves the strong U(1) electromagnetic fields is the Chiral Magnetic Effect [182], whose real time dynamics from the microscopic point of view is still incomplete (although there are some primitive works on this topic [183, 184]) and hence is worth to be investigated further by extending our work.

# Acknowledgements

First of all, I would like to express my greatest gratitude to Prof. Hirotugu Fujii for his invaluable comments, fruitful discussions and collaboration throughout my doctoral studies. I am grateful to Prof. Mitsuhiro Kato for giving me chance to study at Komaba. I also thank Prof. Tetsuo Matsui for giving me some interesting tales about physics and showing me his incredible physical insights. I appreciate Prof. Kazunori Itakura for collaboration, stimulating discussions, and encouragements. I thank the members of Komaba particle and nuclear physics group and my colleagues as well for their interests in my work and some helpful conversations.

Lastly but not the least, I am extremely grateful for unstinting supports from my family, without which I could not be here today.



## Appendix A

# Analytic Mode Functions for Fermions in a Box

We consider the Dirac equation under a classical gauge potential  $A^\mu = (0, 0, 0, A(t))$ :

$$0 = [i\gamma^t \partial_t + i\boldsymbol{\gamma}_\perp \cdot \boldsymbol{\partial}_\perp + i\gamma^z (\partial_z - igA) - m]\psi. \quad (\text{A.1})$$

By noting the spacial homogeneity, we Fourier expand  $\psi$  to obtain an equation for positive/negative frequency mode functions  $_\pm\psi_{\mathbf{p},s}$  as

$$0 = [i\gamma^t \partial_t - \boldsymbol{\gamma}_\perp \cdot \mathbf{p}_\perp - \gamma^z (p_z - gA(t)) - m]_\pm\psi_{\mathbf{p},s}. \quad (\text{A.2})$$

In order to solve Eq. (A.2), it is convenient to decompose the mode functions  $_\pm\psi_{\mathbf{p},s}$  as

$$\begin{aligned} +\psi_{\mathbf{p},s} &= A_{\mathbf{p},s} U_{\mathbf{p},s} + B_{\mathbf{p},s} V_{\mathbf{p},s}, \\ -\psi_{\mathbf{p},s} &= B_{\mathbf{p},s}^* U_{\mathbf{p},s} - A_{\mathbf{p},s}^* V_{\mathbf{p},s} \end{aligned} \quad (\text{A.3})$$

where  $U_{\mathbf{p},s}, V_{\mathbf{p},s}$  are eigenvectors of a projection operator  $P^\pm \equiv (1 \pm \gamma^t \gamma^z)/2$  satisfying

$$P^+ U_{\mathbf{p},s} = U_{\mathbf{p},s}, \quad P^- V_{\mathbf{p},s} = V_{\mathbf{p},s}, \quad (\text{A.4})$$

$$\delta_{ss'} = U_{\mathbf{p},s}^\dagger U_{\mathbf{p},s} = V_{\mathbf{p},s}^\dagger V_{\mathbf{p},s}, \quad 0 = V_{\mathbf{p},s}^\dagger U_{\mathbf{p},s}. \quad (\text{A.5})$$

We also normalize the scalar functions  $A_{\mathbf{p},s}, B_{\mathbf{p},s}$  by

$$1 = |A_{\mathbf{p},s}|^2 + |B_{\mathbf{p},s}|^2. \quad (\text{A.6})$$

From these normalization conditions, Eq. (A.5) and (A.6), one immediately obtains an orthonormality relation for  $_\pm\psi_{\mathbf{p},s}$  as

$$\delta_{ss'} = \pm\psi_{\mathbf{p},s}^\dagger \pm\psi_{\mathbf{p},s'}, \quad 0 = \pm\psi_{\mathbf{p},s}^\dagger \mp\psi_{\mathbf{p},s'}. \quad (\text{A.7})$$

The scalar functions  $A_{\mathbf{p},s}$ ,  $B_{\mathbf{p},s}$  and the spinors  $U_{\mathbf{p},s}$ ,  $V_{\mathbf{p},s}$  are not independent with each other. By substituting Eq. (A.3) into the mode equation (A.2), one obtains the following linear relation

$$i \frac{d}{dt} \begin{pmatrix} A_{\mathbf{p},s} \\ B_{\mathbf{p},s} \end{pmatrix} = \begin{pmatrix} p_z - gA(t) & \sqrt{m^2 + \mathbf{p}_\perp^2} \\ \sqrt{m^2 + \mathbf{p}_\perp^2} & -(p_z - gA(t)) \end{pmatrix} \begin{pmatrix} A_{\mathbf{p},s} \\ B_{\mathbf{p},s} \end{pmatrix}, \quad (\text{A.8})$$

and

$$V_{\mathbf{p},s} = \gamma^t \frac{\boldsymbol{\gamma}_\perp \cdot \mathbf{p}_\perp + m}{\sqrt{m^2 + \mathbf{p}_\perp^2}} U_{\mathbf{p},s}. \quad (\text{A.9})$$

## A.1 Plane wave solutions

If the system is free from the classical gauge potential, i.e.,  $A(t) = 0$ , then one can easily diagonalize Eq. (A.8) to obtain a positive frequency solution  $\propto \exp[-i\omega_{\mathbf{p}}t]$  as

$$\begin{pmatrix} A_{\mathbf{p},s} \\ B_{\mathbf{p},s} \end{pmatrix} = \begin{pmatrix} \frac{1}{\sqrt{2}} \sqrt{1 + \frac{p_z}{\omega_{\mathbf{p}}}} \\ \frac{1}{\sqrt{2}} \sqrt{1 - \frac{p_z}{\omega_{\mathbf{p}}}} \end{pmatrix} e^{-i\omega_{\mathbf{p}}t}. \quad (\text{A.10})$$

From Eq. (A.3), one can immediately construct positive/negative frequency mode functions  $\pm\psi_{\mathbf{p},s}$  as

$$+\psi_{\mathbf{p},s} = u_{\mathbf{p},s} e^{-i\omega_{\mathbf{p}}t}, \quad -\psi_{\mathbf{p},s} = v_{-\mathbf{p},s} e^{+i\omega_{\mathbf{p}}t} \quad (\text{A.11})$$

where the free-spinors  $u_{\mathbf{p},s}$ ,  $v_{-\mathbf{p},s}$  are given by

$$u_{\mathbf{p},s} = [A_{\mathbf{p},s} U_{\mathbf{p},s} + B_{\mathbf{p},s} V_{\mathbf{p},s}] e^{+i\omega_{\mathbf{p}}t} = \frac{1}{\sqrt{2}} \left[ \sqrt{1 + \frac{p_z}{\omega_{\mathbf{p}}}} + \sqrt{1 - \frac{p_z}{\omega_{\mathbf{p}}}} \gamma^t \frac{\boldsymbol{\gamma}_\perp \cdot \mathbf{p}_\perp + m}{\sqrt{m^2 + \mathbf{p}_\perp^2}} \right] U_{\mathbf{p},s}, \quad (\text{A.12})$$

$$v_{-\mathbf{p},s} = [B_{\mathbf{p},s}^* U_{\mathbf{p},s} - A_{\mathbf{p},s}^* V_{\mathbf{p},s}] e^{-i\omega_{\mathbf{p}}t} = \frac{1}{\sqrt{2}} \left[ \sqrt{1 - \frac{p_z}{\omega_{\mathbf{p}}}} - \sqrt{1 + \frac{p_z}{\omega_{\mathbf{p}}}} \gamma^t \frac{\boldsymbol{\gamma}_\perp \cdot \mathbf{p}_\perp + m}{\sqrt{m^2 + \mathbf{p}_\perp^2}} \right] U_{\mathbf{p},s}. \quad (\text{A.13})$$

By noting the normalization condition for  $U_{\mathbf{p},s}$ ,  $V_{\mathbf{p},s}$  (Eq. (A.5)), it is easy to see

$$\delta_{ss'} = u_{\mathbf{p},s}^\dagger u_{\mathbf{p},s'} = v_{\mathbf{p},s}^\dagger v_{\mathbf{p},s'}, \quad 0 = v_{-\mathbf{p},s}^\dagger u_{\mathbf{p},s'}. \quad (\text{A.14})$$

## A.2 Under a constant electric field

Under a constant electric field  $A(t) = -E_0 t$  (for now we assume  $gE_0 > 0$  for simplicity), Eq. (A.8) reads

$$i \frac{d}{dt} \begin{pmatrix} A_{\mathbf{p},s} \\ B_{\mathbf{p},s} \end{pmatrix} = \begin{pmatrix} p_z + gE_0 t & \sqrt{m^2 + \mathbf{p}_\perp^2} \\ \sqrt{m^2 + \mathbf{p}_\perp^2} & -(p_z + gE_0 t) \end{pmatrix} \begin{pmatrix} A_{\mathbf{p},s} \\ B_{\mathbf{p},s} \end{pmatrix}. \quad (\text{A.15})$$

By squaring this equation, one obtains a second order differential equation for  $A_{\mathbf{p},s}$ :

$$0 = \left[ \frac{d^2}{dt^2} + (p_z + gE_0t)^2 + \mathbf{p}_\perp^2 + m^2 + igE_0 \right] A_{\mathbf{p},s}. \quad (\text{A.16})$$

Now, we change the variable,

$$\xi \equiv \sqrt{\frac{2}{gE}}(gE_0t + p_z), \quad (\text{A.17})$$

to find that Eq. (A.16) is reduced to a parabolic cylinder differential equation:

$$0 = \left[ \frac{d^2}{d\xi^2} + \frac{\xi^2}{4} + \left( a + \frac{i}{2} \right) \right] A_{\mathbf{p},s} \quad (\text{A.18})$$

with

$$a = \frac{m^2 + \mathbf{p}_\perp^2}{2gE_0}. \quad (\text{A.19})$$

Solutions of Eq. (A.16) are given by the parabolic cylinder function  $D_\nu(z)$  as

$$A_{\mathbf{p},s} = c_1 D_{ia-1}(-e^{-i\pi/4}\xi) + c_2 D_{-ia}(e^{i\pi/4}\xi). \quad (\text{A.20})$$

From Eq. (A.15) and identities [162]

$$\left[ \frac{d}{dz} - \frac{z}{2} \right] D_\nu(z) = -D_{\nu+1}(z), \quad \left[ \frac{d}{dz} + \frac{z}{2} \right] D_\nu(z) = \nu D_{\nu-1}(z), \quad (\text{A.21})$$

one gets

$$\begin{aligned} B_{\mathbf{p},s} &= \frac{1}{\sqrt{a}} \left[ i \frac{d}{d\xi} - \frac{\xi}{2} \right] A_{\mathbf{p},s} \\ &= c_1 \times \frac{e^{i\pi/4}}{\sqrt{a}} D_{ia}(-e^{-i\pi/4}\xi) + c_2 \times \sqrt{a} e^{i\pi/4} D_{-ia-1}(e^{i\pi/4}\xi) \end{aligned} \quad (\text{A.22})$$

The coefficients  $c_1, c_2$  are determined by a boundary condition and the normalization condition (A.6). Now, we require the plane wave boundary condition at the asymptotic times  $t \rightarrow \pm\infty$  (Eq. (2.27) and (2.28)) as in the main text. By using the asymptotic formula for the parabolic cylinder functions  $D_\nu(z)$  [162]

$$D_\nu(z) \xrightarrow{|z| \rightarrow \infty} \begin{cases} z^\nu e^{-z^2/4} & (|\arg z| < 3\pi/4) \\ z^\nu e^{-z^2/4} - \frac{\sqrt{2\pi}}{\Gamma(-\nu)} e^{i\nu\pi} z^{-\nu-1} e^{z^2/4} & (\pi/4 < \arg z < 5\pi/4) \\ z^\nu e^{-z^2/4} - \frac{\sqrt{2\pi}}{\Gamma(-\nu)} e^{-i\nu\pi} z^{-\nu-1} e^{z^2/4} & (-5\pi/4 < \arg z < -\pi/4) \end{cases}, \quad (\text{A.23})$$

one finds that

$$\begin{pmatrix} A_{\mathbf{p},s}^{(\text{in})} \\ B_{\mathbf{p},s}^{(\text{in})} \end{pmatrix} = e^{-\pi a/4} \begin{pmatrix} e^{-i\pi/8} \sqrt{a} D_{ia-1}(-e^{-i\pi/4}\xi) \\ e^{+i\pi/8} D_{ia}(-e^{-i\pi/4}\xi) \end{pmatrix}, \quad (\text{A.24})$$

$$\begin{pmatrix} A_{\mathbf{p},s}^{(\text{out})} \\ B_{\mathbf{p},s}^{(\text{out})} \end{pmatrix} = e^{-\pi a/4} \begin{pmatrix} e^{-i\pi/8} D_{-ia}(e^{i\pi/4}\xi) \\ e^{+i\pi/8} \sqrt{a} D_{-ia-1}(e^{i\pi/4}\xi) \end{pmatrix} \quad (\text{A.25})$$

correspond to the positive frequency solutions at  $t \rightarrow -\infty$  (as = in) and  $t \rightarrow \infty$  (as = out) properly normalized by the condition (A.6).

These two solutions  $A_{\mathbf{p},s}^{(\text{as})}, B_{\mathbf{p},s}^{(\text{as})}$  (as = in, out) are not linearly independent of each other. With the use of an identity [162]

$$D_\nu(z) = \frac{\Gamma(1+\nu)}{\sqrt{2\pi}} [e^{-i\pi\nu/2} D_{-\nu-1}(-iz) + e^{i\pi\nu} D_{-\nu-1}(iz)], \quad (\text{A.26})$$

one obtains the following linear relation:

$$\begin{pmatrix} A_{\mathbf{p},s}^{(\text{in})} \\ B_{\mathbf{p},s}^{(\text{in})*} \end{pmatrix} = \begin{pmatrix} \alpha_{\mathbf{p},s} & -\beta_{\mathbf{p},s}^* \\ \beta_{\mathbf{p},s} & \alpha_{\mathbf{p},s}^* \end{pmatrix} \begin{pmatrix} A_{\mathbf{p},s}^{(\text{out})} \\ B_{\mathbf{p},s}^{(\text{out})*} \end{pmatrix} \quad (\text{A.27})$$

with

$$\alpha_{\mathbf{p},s} = \frac{\sqrt{2\pi a} e^{-\pi a/2}}{\Gamma(1-ia)}, \quad \beta_{\mathbf{p},s} = e^{-\pi a}. \quad (\text{A.28})$$

The linear relation is the same as the Bogoliubov transformation for the mode functions  $\pm\psi_{\mathbf{p},s}^{(\text{as})}$ . Indeed, from Eq. (A.27), one finds

$$\begin{aligned} \begin{pmatrix} +\psi_{\mathbf{p},s}^{(\text{in})} \\ -\psi_{\mathbf{p},s}^{(\text{in})} \end{pmatrix} &= \begin{pmatrix} A_{\mathbf{p},s}^{(\text{in})} & B_{\mathbf{p},s}^{(\text{in})} \\ B_{\mathbf{p},s}^{(\text{in})*} & -A_{\mathbf{p},s}^{(\text{in})*} \end{pmatrix} \begin{pmatrix} U_{\mathbf{p},s} \\ V_{\mathbf{p},s} \end{pmatrix} \\ &= \begin{pmatrix} \alpha_{\mathbf{p},s} & -\beta_{\mathbf{p},s}^* \\ \beta_{\mathbf{p},s} & \alpha_{\mathbf{p},s}^* \end{pmatrix} \begin{pmatrix} A_{\mathbf{p},s}^{(\text{out})} & B_{\mathbf{p},s}^{(\text{out})} \\ B_{\mathbf{p},s}^{(\text{out})*} & -A_{\mathbf{p},s}^{(\text{out})*} \end{pmatrix} \begin{pmatrix} U_{\mathbf{p},s} \\ V_{\mathbf{p},s} \end{pmatrix} \\ &= \begin{pmatrix} \alpha_{\mathbf{p},s} & -\beta_{\mathbf{p},s}^* \\ \beta_{\mathbf{p},s} & \alpha_{\mathbf{p},s}^* \end{pmatrix} \begin{pmatrix} +\psi_{\mathbf{p},s}^{(\text{out})} \\ -\psi_{\mathbf{p},s}^{(\text{out})} \end{pmatrix}. \end{aligned} \quad (\text{A.29})$$

### A.3 Under a Sauter-type electric field

Now, we consider a Sauter-type electric field with height  $E_0$  and width  $\tau$  described by [142]

$$A(t) = -E_0\tau \tanh(t/\tau), \quad \text{or} \quad E = E_0 \text{sech}^2(t/\tau). \quad (\text{A.30})$$

Under this choice of electric field, the differential equation (A.8) for the scalar function  $A_{\mathbf{p},s}, B_{\mathbf{p},s}$  read

$$i \frac{d}{dt} \begin{pmatrix} A_{\mathbf{p},s} \\ B_{\mathbf{p},s} \end{pmatrix} = \begin{pmatrix} p_z + E_0\tau \tanh(t/\tau) & \sqrt{m^2 + \mathbf{p}_\perp^2} \\ \sqrt{m^2 + \mathbf{p}_\perp^2} & -(p_z + E_0\tau \tanh(t/\tau)) \end{pmatrix} \begin{pmatrix} A_{\mathbf{p},s} \\ B_{\mathbf{p},s} \end{pmatrix}. \quad (\text{A.31})$$

By squaring the both hand sides of (A.31) to obtain a second order differential equation for  $A_{\mathbf{p},s}$  as

$$0 = \left[ \frac{d^2}{dt^2} + (p_z + gE_0\tau \tanh(t/\tau))^2 + igE_0 \text{sech}^2(t/\tau) + m^2 + \mathbf{p}_\perp^2 \right] A_{\mathbf{p},s}. \quad (\text{A.32})$$

By changing the variable as

$$u \equiv \frac{1}{2} [1 + \tanh(t/\tau)], \quad (\text{A.33})$$

Eq. (A.32) reads

$$\left[ \frac{4}{\tau^2} u(1-u) \frac{d}{du} \left( u(1-u) \frac{d}{du} \right) + \omega^2(u) + 4igE_0 u(1-u) \right] A_{\mathbf{p},s}, \quad (\text{A.34})$$

where

$$\omega^2(u) \equiv m^2 + \mathbf{p}_\perp^2 + (p_z + gE_0\tau \tanh(t/\tau))^2 \equiv m^2 + \mathbf{p}_\perp^2 + P_z(u)^2. \quad (\text{A.35})$$

In order to solve Eq. (A.34), we furthermore make an ansatz of a form

$$A_{\mathbf{p},s} = u^{-i\tau\omega(0)/2} (1-u)^{i\tau\omega(1)/2} \tilde{A}_{\mathbf{p},s}. \quad (\text{A.36})$$

By substituting this ansatz into Eq. (A.32), one finds that  $\tilde{A}_{\mathbf{p},s}$  satisfy the hypergeometric differential equation of a form

$$0 = \left[ u(1-u) \frac{d^2}{du^2} + \{c - (a+b-1)u\} \frac{d}{du} - ab \right] \tilde{A}_{\mathbf{p},s}, \quad (\text{A.37})$$

where

$$\begin{aligned} a &= -igE_0\tau^2 - \frac{i\tau\omega(0)}{2} + \frac{i\tau\omega(1)}{2}, \\ b &= 1 + igE_0\tau^2 - \frac{i\tau\omega(0)}{2} + \frac{i\tau\omega(1)}{2}, \\ c &= 1 - i\tau\omega(0). \end{aligned} \quad (\text{A.38})$$

Solutions of (A.37) are given by the hypergeometric function  ${}_2F_1(a, b, c; z)$ , and we obtain

$$\begin{aligned} A_{\mathbf{p},s} &= c_1 u^{-i\tau\omega(0)/2} (1-u)^{i\tau\omega(1)/2} {}_2F_1(a, b, c; u) \\ &\quad + c_2 u^{i\tau\omega(0)/2} (1-u)^{-i\tau\omega(1)/2} {}_2F_1(1-a, 1-b, 2-c; u). \end{aligned} \quad (\text{A.39})$$

The coefficients  $c_1, c_2$  are determined by a boundary condition and the normalization condition (A.6). Now, we require the plane wave boundary condition at the asymptotic states  $t \rightarrow \pm\infty$  (Eq. (2.27)) as in the main text. By using [162]

$$\begin{aligned} {}_2F_1(a, b, c; z) &= \frac{\Gamma(x)\Gamma(c-a-b)}{\Gamma(c-a)\Gamma(c-b)} {}_2F_1(a, b, a+b-c+1; 1-z) \\ &\quad + (1-z)^{c-a-b} \frac{\Gamma(c)\Gamma(a+b-c)}{\Gamma(a)\Gamma(b)} {}_2F_1(c-a; c-b, c-a-b+1; 1-z), \end{aligned} \quad (\text{A.40})$$

one can find

$$\begin{aligned} A_{\mathbf{p},s}^{(\text{in})} &= \frac{1}{\sqrt{2}} \sqrt{1 + \frac{P_z(0)}{\omega(0)}} u^{-i\tau\omega(0)/2} (1-u)^{i\tau\omega(1)/2} {}_2F_1(a, b, c; u), \\ B_{\mathbf{p},s}^{(\text{in})} &= \frac{1}{\sqrt{2}} \sqrt{1 - \frac{P_z(0)}{\omega(0)}} u^{-i\tau\omega(0)/2} (1-u)^{i\tau\omega(1)/2} {}_2F_1(1-a^*, 1-b^*, 2-c^*; u), \end{aligned} \quad (\text{A.41})$$

and the out-state solutions  $A_{\mathbf{p},s}^{(\text{out})}$ ,  $B_{\mathbf{p},s}^{(\text{out})}$  are obtained from the in-state solutions  $A_{\mathbf{p},s}^{(\text{in})}$ ,  $B_{\mathbf{p},s}^{(\text{in})}$  by the following linear relation:

$$\begin{pmatrix} A_{\mathbf{p},s}^{(\text{in})} \\ B_{\mathbf{p},s}^{(\text{in})*} \end{pmatrix} = \begin{pmatrix} \alpha_{\mathbf{p},s} & -\beta_{\mathbf{p},s}^* \\ \beta_{\mathbf{p},s} & \alpha_{\mathbf{p},s}^* \end{pmatrix} \begin{pmatrix} A_{\mathbf{p},s}^{(\text{out})} \\ B_{\mathbf{p},s}^{(\text{out})*} \end{pmatrix}, \quad (\text{A.42})$$

where

$$\begin{aligned} \alpha_{\mathbf{p},s} &= \sqrt{\frac{\omega(1)}{\omega(0)}} \sqrt{\frac{\omega(1) - P_z(1)}{\omega(0) - P_z(0)}} \frac{\Gamma(c)\Gamma(c-a-b)}{\Gamma(c-a)\Gamma(c-b)} \\ \beta_{\mathbf{p},s} &= -\sqrt{\frac{\omega(1)}{\omega(0)}} \sqrt{\frac{\omega(1) + P_z(1)}{\omega(0) - P_z(0)}} \frac{\Gamma(c^*)\Gamma(a^* + b^* - c^*)}{\Gamma(a^*)\Gamma(b^*)}. \end{aligned} \quad (\text{A.43})$$

## Appendix B

# Analytic Mode Functions for Bosons in a Box

We consider the Klein-Gordon equation under a classical gauge potential  $A^\mu = (0, 0, 0, A(t))$ :

$$0 = [\partial_t^2 - \boldsymbol{\partial}_\perp^2 - (\partial_z - igA(t))^2 + m^2] \phi. \quad (\text{B.1})$$

As the gauge potential is homogeneous in space, it is useful to Fourier expand  $\phi$  to obtain an equation for positive/negative frequency mode functions  ${}_\pm\phi_{\mathbf{p}}$  as

$$0 = [\partial_t^2 + \mathbf{p}_\perp^2 + (p_z - gA(t))^2 + m^2] {}_\pm\phi_{\mathbf{p}}. \quad (\text{B.2})$$

It is convenient to normalize the mode functions  ${}_\pm\phi_{\mathbf{p}}$  as

$$\pm 1 = i_\pm \phi_{\mathbf{p}}^* \overset{\leftrightarrow}{\partial}_\pm \phi_{\mathbf{p}}, \quad 0 = i_\mp \phi_{\mathbf{p}}^* \overset{\leftrightarrow}{\partial}_\pm \phi_{\mathbf{p}}, \quad (\text{B.3})$$

where  $\overset{\leftrightarrow}{\partial} \equiv \overset{\rightarrow}{\partial} - \overset{\leftarrow}{\partial}$ . The second condition is automatically satisfied when  ${}_{-}\phi_{\mathbf{p}} = [{}_{+}\phi_{\mathbf{p}}]^*$ .

### B.1 Plane wave solutions

One can easily solve Eq. (B.2) when there is no classical field  $A = 0$ . The solutions satisfying the normalization condition (B.3) read

$${}_{+}\phi_{\mathbf{p}} = \frac{1}{\sqrt{2\omega_{\mathbf{p}}}} e^{-i\omega_{\mathbf{p}}t}, \quad {}_{-}\phi_{\mathbf{p}} = [{}_{+}\phi_{\mathbf{p}}]^*, \quad (\text{B.4})$$

where  $\omega_{\mathbf{p}}$  is the on-shell energy  $\omega_{\mathbf{p}} \equiv \sqrt{m^2 + \mathbf{p}^2}$ .

### B.2 Under a constant electric field

For a constant electric field with infinite duration  $\bar{A}(t) = -E_0 t$  (for now, we assume  $gE_0 > 0$  for simplicity), Eq. (B.2) reads

$$0 = [\partial_t^2 + \mathbf{p}_\perp^2 + (p_z + gE_0 t)^2 + m^2] {}_\pm\phi_{\mathbf{p}}. \quad (\text{B.5})$$

By changing the variable

$$\xi \equiv \sqrt{\frac{2}{gE_0}}(gE_0t + p_z), \quad (\text{B.6})$$

Eq. (B.5) is reduced to a parabolic cylinder differential equations as

$$0 = \left[ \frac{d^2}{d\xi^2} + \frac{\xi^2}{4} + a \right]_{\pm} \phi_{\mathbf{p}}, \quad (\text{B.7})$$

where

$$a = \frac{m^2 + \mathbf{p}_{\perp}^2}{2gE_0}. \quad (\text{B.8})$$

Solutions of Eq. (B.7) are given by the parabolic cylinder function  $D_{\nu}(z)$  as

$$+ \phi_{\mathbf{p}} = c_1 D_{ia-1/2}(-e^{-i\pi/4}\xi) + c_2 D_{-ia-1/2}(e^{i\pi/4}\xi), \quad - \phi_{\mathbf{p}} = [+ \phi_{\mathbf{p}}]^*. \quad (\text{B.9})$$

The coefficients  $c_1, c_2$  are determined by a boundary condition and the normalization condition (B.3). Now, we require  $_{\pm} \phi_{\mathbf{p}}^{(\text{in})}$  ( $_{\pm} \phi_{\mathbf{p}}^{(\text{out})}$ ) to be the plane waves (B.4) at asymptotic times  $t \rightarrow -\infty$  ( $t \rightarrow \infty$ ). By noting the asymptotic formula for the parabolic cylinder function  $D_{\nu}(z)$  [162]

$$D_{\nu}(z) \xrightarrow{|z| \rightarrow \infty} \begin{cases} z^{\nu} e^{-z^2/4} & (|\arg z| < 3\pi/4) \\ z^{\nu} e^{-z^2/4} - \frac{\sqrt{2\pi}}{\Gamma(-\nu)} e^{i\nu\pi} z^{-\nu-1} e^{z^2/4} & (\pi/4 < \arg z < 5\pi/4) \\ z^{\nu} e^{-z^2/4} - \frac{\sqrt{2\pi}}{\Gamma(-\nu)} e^{-i\nu\pi} z^{-\nu-1} e^{z^2/4} & (-5\pi/4 < \arg z < -\pi/4) \end{cases}, \quad (\text{B.10})$$

one finds

$$+ \phi_{\mathbf{p}}^{(\text{in})} = \frac{e^{-\pi a/4}}{(2gE_0)^{1/4}} D_{ia-1/2}(-e^{-i\pi/4}\xi), \quad - \phi_{\mathbf{p}}^{(\text{in})} = [+ \phi_{\mathbf{p}}^{(\text{in})}]^*. \quad (\text{B.11})$$

and

$$+ \phi_{\mathbf{p}}^{(\text{out})} = \frac{e^{-\pi a/4}}{(2gE_0)^{1/4}} D_{-ia-1/2}(e^{i\pi/4}\xi), \quad - \phi_{\mathbf{p}}^{(\text{out})} = [+ \phi_{\mathbf{p}}^{(\text{out})}]^*. \quad (\text{B.12})$$

These two solutions  $_{\pm} \phi_{\mathbf{p}}$  (as = in, out) are linearly dependent with each other, and their relationship is given by

$$\begin{pmatrix} + \phi_{\mathbf{p}}^{(\text{in})} \\ - \phi_{\mathbf{p}}^{(\text{in})} \end{pmatrix} = \begin{pmatrix} \alpha_{\mathbf{p},s} & \beta_{\mathbf{p},s}^* \\ \beta_{\mathbf{p},s} & \alpha_{\mathbf{p},s}^* \end{pmatrix} \begin{pmatrix} + \phi_{\mathbf{p}}^{(\text{out})} \\ - \phi_{\mathbf{p}}^{(\text{out})} \end{pmatrix} \quad (\text{B.13})$$

with

$$\alpha_{\mathbf{p}} = -e^{i\pi/4} \frac{\sqrt{2\pi} e^{-\pi a/4}}{\Gamma(1/2 - ia)}, \quad \beta_{\mathbf{p}} = ie^{-\pi a}, \quad (\text{B.14})$$

where the use is made of an identity [162]

$$D_{\nu}(z) = \frac{\Gamma(1+\nu)}{\sqrt{2\pi}} [e^{-i\pi\nu/2} D_{-\nu-1}(-iz) + e^{i\pi\nu} D_{-\nu-1}(iz)]. \quad (\text{B.15})$$

## Appendix C

# Analytic Mode Functions under an Expanding Electric Field

We analytically solve the Dirac equation and the Klein-Gordon equation under a boost-invariantly expanding homogeneous electric field  $\mathbf{E} = E_0\theta(\tau - \tau_0)\mathbf{e}_z$  described by a gauge potential  $A_\mu$  as

$$A_\tau = A_x = A_y = 0, \quad A_\eta = \begin{cases} \frac{E_0\tau_0^2}{2} & (\tau < \tau_0) \\ \frac{E_0\tau^2}{2} & (\tau > \tau_0) \end{cases}. \quad (\text{C.1})$$

### C.1 fermion

The Dirac equation for Fourier modes,

$$\psi(x) \equiv \sum_s \int d^2\mathbf{p}_\perp dp_\eta \psi_{\mathbf{p}_\perp, p_\eta, s}(\tau) \frac{e^{i\mathbf{p}_\perp \cdot \mathbf{x}_\perp} e^{ip_\eta \eta}}{(2\pi)^{3/2}}, \quad (\text{C.2})$$

reads

$$0 = [i\gamma^\tau - \boldsymbol{\gamma}_\perp \cdot \mathbf{p}_\perp - \gamma^\eta(p_\eta + qA_\eta) - m] \psi_{\mathbf{p}_\perp, p_\eta, s}. \quad (\text{C.3})$$

As was explained in the main text (see Section 5.1.3), Eq. (C.3) has two independent solutions  $\pm\psi_{\mathbf{p}_\perp, p_\eta, s}$  of a form:

$$\begin{aligned} +\psi_{\mathbf{p}_\perp, p_\eta, s}(\tau) &= \left[ A_{\mathbf{p}_\perp, p_\eta, s}(\tau) e^{\eta/2} + B_{\mathbf{p}_\perp, p_\eta, s}(\tau) e^{-\eta/2} \gamma^t \frac{\boldsymbol{\gamma}_\perp \cdot \mathbf{p}_\perp + m}{\sqrt{m^2 + \mathbf{p}_\perp^2}} \right] U_{\mathbf{p}_\perp, p_\eta, s}, \\ -\psi_{\mathbf{p}_\perp, p_\eta, s}(\tau) &= \left[ B_{\mathbf{p}_\perp, p_\eta, s}^*(\tau) e^{\eta/2} - A_{\mathbf{p}_\perp, p_\eta, s}^*(\tau) e^{-\eta/2} \gamma^t \frac{\boldsymbol{\gamma}_\perp \cdot \mathbf{p}_\perp + m}{\sqrt{m^2 + \mathbf{p}_\perp^2}} \right] U_{\mathbf{p}_\perp, p_\eta, s} \end{aligned} \quad (\text{C.4})$$

where  $U_{\mathbf{p}_\perp, p_\eta, s}$  is an eigen-spinor of a projection operator  $P^+ \equiv (1 + \gamma^t \gamma^z)/2$  satisfying

$$\begin{aligned} P^+ U_{\mathbf{p}_\perp, p_\eta, s} &= U_{\mathbf{p}_\perp, p_\eta, s}, \\ U_{\mathbf{p}_\perp, p_\eta, s}^\dagger U_{\mathbf{p}_\perp, p_\eta, s'} &= \delta_{ss'}. \end{aligned} \quad (\text{C.5})$$

The differential equation for the scalar functions  $A_{\mathbf{p}_\perp, p_\eta, s}$ ,  $B_{\mathbf{p}_\perp, p_\eta, s}$  read

$$i \frac{d}{d\tau} \begin{pmatrix} A_{\mathbf{p}_\perp, p_\eta, s} \\ B_{\mathbf{p}_\perp, p_\eta, s} \end{pmatrix} = \begin{pmatrix} \frac{p_\eta + qA_\eta(\tau) - i/2}{\tau} & \sqrt{m^2 + \mathbf{p}_\perp^2} \\ \sqrt{m^2 + \mathbf{p}_\perp^2} & -\frac{p_\eta + qA_\eta(\tau) + i/2}{\tau} \end{pmatrix} \begin{pmatrix} A_{\mathbf{p}_\perp, p_\eta, s} \\ B_{\mathbf{p}_\perp, p_\eta, s} \end{pmatrix}, \quad (\text{C.6})$$

or, by squaring the both hand sides, one obtains a second order differential equation for  $A_{\mathbf{p}_\perp, p_\eta, s}$  as

$$0 = \left[ \frac{d^2}{d\tau^2} + \frac{1}{\tau} \frac{d}{d\tau} + \left( \frac{p_\eta + qA_\eta - i/2}{\tau} \right)^2 + iqE(\tau) + m^2 + \mathbf{p}_\perp^2 \right] A_{\mathbf{p}_\perp, p_\eta, s}. \quad (\text{C.7})$$

It is convenient to normalize the scalar functions  $A_{\mathbf{p}_\perp, p_\eta, s}$ ,  $B_{\mathbf{p}_\perp, p_\eta, s}$  as

$$\frac{1}{\tau} = |A_{\mathbf{p}_\perp, p_\eta, s}|^2 + |B_{\mathbf{p}_\perp, p_\eta, s}|^2 \quad (\text{C.8})$$

so as to properly normalize the mode function  $\pm\psi_{\mathbf{p}_\perp, p_\eta, s}$  as

$$\frac{1}{\tau} \delta_{ss'} = [\pm\psi_{\mathbf{p}_\perp, p_\eta, s} | \pm\psi_{\mathbf{p}_\perp, p_\eta, s'}]_{\text{F}}, \quad 0 = [\pm\psi_{\mathbf{p}_\perp, p_\eta, s} | \mp\psi_{\mathbf{p}_\perp, p_\eta, s'}]_{\text{F}}. \quad (\text{C.9})$$

Our strategy to solve the Dirac equation (B.5), or Eq. (C.7) for  $A_{\mathbf{p}_\perp, p_\eta, s}$ , is as follows: We divide the problem into three steps. In the first step, we solve Eq. (C.7) for  $\tau < \tau_0$ , where the gauge field vanishes  $A_\eta = 0$  and the solution is given by the plane wave solutions explained in Section 5.1.3. In the second step, we find out particular solutions of Eq. (C.7) for  $\tau > \tau_0$ . In the third step, we smoothly connect these two solutions obtained in the first and the second step at the boundary  $\tau = \tau_0$  to obtain the solution for all values of  $\tau$ . Note that here we just consider to derive ‘‘in-state’’ mode functions, for which we require  $\pm\psi_{\mathbf{p}_\perp, p_\eta, s}$  to be plane waves with positive/negative frequency at  $\tau \rightarrow 0$ .

(step 1) For  $\tau < \tau_0$ , the solution of Eq. (C.7) is given by the plane wave solutions (5.60), whose derivation was explained in detail in Section 5.1.3:

$$\begin{pmatrix} A_{\mathbf{p}_\perp, p_\eta, s} \\ B_{\mathbf{p}_\perp, p_\eta, s} \end{pmatrix} = \frac{\sqrt{\pi} \sqrt{m^2 + \mathbf{p}_\perp^2}}{2} e^{\pi(p_\eta + qE_0\tau_0^2/2)/2} \times \begin{pmatrix} e^{-i\pi/4} H_{i(p_\eta + qE_0\tau_0^2/2) + 1/2}^{(2)}(\sqrt{m^2 + \mathbf{p}_\perp^2} \tau) \\ e^{+i\pi/4} H_{i(p_\eta + qE_0\tau_0^2/2) - 1/2}^{(2)}(\sqrt{m^2 + \mathbf{p}_\perp^2} \tau) \end{pmatrix} \quad (\text{for } \tau < \tau_0). \quad (\text{C.10})$$

We note that the above scalar functions have a positive frequency in the  $\tau$ - $\eta$  coordinates, so that the resulting mode function  $+\psi_{\mathbf{p}_\perp, p_\eta, s}$  ( $+\psi_{\mathbf{p}_\perp, p_\eta, s}$ ) has a positive (negative) frequency for  $\tau < \tau_0$  and hence satisfies the plane wave boundary condition at  $\tau \rightarrow 0$ .

(step 2) For  $\tau > \tau_0$ , Eq. (C.7) reads

$$0 = \left[ \frac{d^2}{d\tau^2} + \frac{1}{\tau} \frac{d}{d\tau} + \left( \frac{p_\eta + qE_0\tau^2/2 - i/2}{\tau} \right)^2 + iqE_0 + m^2 + \mathbf{p}_\perp^2 \right] A_{\mathbf{p}_\perp, p_\eta, s}. \quad (\text{C.11})$$

By changing the variables as

$$\xi \equiv \sqrt{m^2 + \mathbf{p}_\perp^2} \tau, \quad a \equiv \frac{qE_0}{m^2 + \mathbf{p}_\perp^2}, \quad (\text{C.12})$$

and by making an ansatz of a form,

$$A_{\mathbf{p}_\perp, p_\eta, s} \equiv \xi^{-ip_\eta - 1/2} e^{-ia\xi^2/4} \tilde{A}_{\mathbf{p}_\perp, p_\eta, s}, \quad (\text{C.13})$$

one obtains a hypergeometric differential equation for  $\tilde{A}_{\mathbf{p}_\perp, p_\eta, s}$  as

$$0 = \left[ \xi \frac{d^2}{d\xi^2} + (-ia\xi^2 - 2ip_\eta) \frac{d}{d\xi} + \xi \right] \tilde{A}_{\mathbf{p}_\perp, p_\eta, s}, \quad (\text{C.14})$$

Two independent solutions of Eq. (C.14) are given by the Tricomi hypergeometric function  $U(a, b; z)$  [162], and thus we find

$$\begin{aligned} A_{\mathbf{p}_\perp, p_\eta, s} &= c_1 \times {}_1\chi_{\mathbf{p}_\perp, p_\eta, s} + c_2 \times {}_2\chi_{\mathbf{p}_\perp, p_\eta, s}, \\ B_{\mathbf{p}_\perp, p_\eta, s} &= c_1 \times [{}_2\chi_{\mathbf{p}_\perp, p_\eta, s}]^* - c_2 \times [{}_1\chi_{\mathbf{p}_\perp, p_\eta, s}]^*, \end{aligned} \quad (\text{C.15})$$

where

$$\begin{aligned} {}_1\chi_{\mathbf{p}_\perp, p_\eta, s} &\equiv \frac{1}{\sqrt{\tau}} \exp \left[ -\pi \frac{m^2 + \mathbf{p}_\perp^2}{4|qE_0|} - i \frac{qE_0\tau^2}{4} \right] \\ &\quad \times \left( \sqrt{m^2 + \mathbf{p}_\perp^2} \right)^{-ip_\eta} U \left( i \frac{m^2 + \mathbf{p}_\perp^2}{2qE_0}, \frac{1}{2} - ip_\eta; i \frac{qE_0\tau^2}{2} \right), \\ {}_2\chi_{\mathbf{p}_\perp, p_\eta, s} &\equiv \frac{-i}{2} \frac{1}{\sqrt{\tau}} \exp \left[ -\pi \frac{m^2 + \mathbf{p}_\perp^2}{4|qE_0|} + i \frac{qE_0\tau^2}{4} \right] \\ &\quad \times \left( \sqrt{m^2 + \mathbf{p}_\perp^2} \right)^{1+ip_\eta} U \left( 1 - i \frac{m^2 + \mathbf{p}_\perp^2}{2qE_0}, \frac{3}{2} + ip_\eta; -i \frac{qE_0\tau^2}{2} \right) \end{aligned} \quad (\text{C.16})$$

Here, we normalized the functions  ${}_n\chi_{\mathbf{p}_\perp, p_\eta, s}$  ( $n = 1, 2$ ) as

$$\frac{1}{\tau} = |{}_1\chi_{\mathbf{p}_\perp, p_\eta, s}|^2 + |{}_2\chi_{\mathbf{p}_\perp, p_\eta, s}|^2. \quad (\text{C.17})$$

(step 3) The coefficients  $c_1, c_2$  in Eq. (C.15) can be determined by smoothly connecting the two solutions Eq. (C.10) for  $\tau < \tau_0$  and Eq. (C.15) for  $\tau > \tau_0$ . With the help of the

normalization condition (C.17), one can easily determine the coefficients  $c_1, c_2$  as

$$\begin{aligned}
c_1 &= \tau_0 \times [A_{\mathbf{p}_\perp, p_\eta, s}(\tau_0) [{}_1\chi_{\mathbf{p}_\perp, p_\eta, s}(\tau_0)]^* + B_{\mathbf{p}_\perp, p_\eta, s}(\tau_0) {}_2\chi_{\mathbf{p}_\perp, p_\eta, s}(\tau_0)], \\
&= \frac{\sqrt{\pi} \sqrt{m^2 + \mathbf{p}_\perp^2} \tau_0}{2} e^{\pi(p_\eta + qE_0\tau_0^2/2)/2} \\
&\quad \times \left[ [{}_1\chi_{\mathbf{p}_\perp, p_\eta, s}(\tau_0)]^* e^{-i\pi/4} H_{i(p_\eta + qE_0\tau_0^2/2) + 1/2}^{(2)}(\sqrt{m^2 + \mathbf{p}_\perp^2} \tau_0) \right. \\
&\quad \left. + {}_2\chi_{\mathbf{p}_\perp, p_\eta, s}(\tau_0) e^{+i\pi/4} H_{i(p_\eta + qE_0\tau_0^2/2) - 1/2}^{(2)}(\sqrt{m^2 + \mathbf{p}_\perp^2} \tau_0) \right] \quad (C.18)
\end{aligned}$$

$$\begin{aligned}
c_2 &= \tau_0 \times [A_{\mathbf{p}_\perp, p_\eta, s}(\tau_0) [{}_2\chi_{\mathbf{p}_\perp, p_\eta, s}(\tau_0)]^* - B_{\mathbf{p}_\perp, p_\eta, s}(\tau_0) {}_1\chi_{\mathbf{p}_\perp, p_\eta, s}(\tau_0)], \\
&= \frac{\sqrt{\pi} \sqrt{m^2 + \mathbf{p}_\perp^2} \tau_0}{2} e^{\pi(p_\eta + qE_0\tau_0^2/2)/2} \\
&\quad \times \left[ [{}_2\chi_{\mathbf{p}_\perp, p_\eta, s}(\tau_0)]^* e^{-i\pi/4} H_{i(p_\eta + qE_0\tau_0^2/2) + 1/2}^{(2)}(\sqrt{m^2 + \mathbf{p}_\perp^2} \tau_0) \right. \\
&\quad \left. - {}_1\chi_{\mathbf{p}_\perp, p_\eta, s}(\tau_0) e^{+i\pi/4} H_{i(p_\eta + qE_0\tau_0^2/2) - 1/2}^{(2)}(\sqrt{m^2 + \mathbf{p}_\perp^2} \tau_0) \right], \quad (C.19)
\end{aligned}$$

and hereby one obtains the solution of Eq. (C.7) for all values of  $\tau$ .

## C.2 boson

The Klein-Gordon equation for Fourier modes,

$$\phi(x) \equiv \int d^2\mathbf{p}_\perp dp_\eta(\tau) \frac{e^{i\mathbf{p}_\perp \cdot \mathbf{x}_\perp + ip_\eta \eta}}{(2\pi)^{3/2}} \quad (C.20)$$

reads

$$0 = \left[ \frac{d^2}{d\tau^2} + \frac{1}{\tau} \frac{d}{d\tau} + \left( \frac{p_\eta + qA_\eta}{\tau} \right)^2 + m^2 + \mathbf{p}_\perp^2 \right] \phi_{\mathbf{p}_\perp, p_\eta}. \quad (C.21)$$

There are two independent solutions, which we write  ${}_\pm \phi_{\mathbf{p}_\perp, p_\eta}$ , for this equation (C.21). It is convenient to normalize the modes  ${}_\pm \phi_{\mathbf{p}_\perp, p_\eta}$  as

$${}_\pm \frac{1}{\tau} = [{}_\pm \phi_{\mathbf{p}_\perp, p_\eta} | {}_\pm \phi_{\mathbf{p}_\perp, p_\eta}]_B, \quad 0 = [{}_\pm \phi_{\mathbf{p}_\perp, p_\eta} | {}_\mp \psi_{\mathbf{p}_\perp, p_\eta}]_B. \quad (C.22)$$

Our strategy to solve the Klein-Gordon equation (C.21) is the same as the previous fermion case, i.e., We divide the problem into three steps. We derive particular solutions for  $\tau < \tau_0$  (step 1) and  $\tau > \tau_0$  (step 2), and connect them smoothly at the boundary  $\tau = \tau_0$  to construct the solution for all values of  $\tau$  (step 3). Note that here we just consider ‘‘in-state’’ mode functions, for which we require  ${}_\pm \phi_{\mathbf{p}_\perp, p_\eta}$  to be plane waves with positive/negative frequency at  $\tau \rightarrow 0$ .

(step 1) For  $\tau < \tau_0$ , the solution of Eq. (C.21) is given by the plane wave solutions (5.78), whose derivation was explained in detail in Section 5.1.3, as

$$\begin{aligned} +\phi_{\mathbf{p}_\perp, p_\eta} &= \frac{\sqrt{\pi}}{2i} e^{\pi(p_\eta + qE_0^2\tau_0^2/2)/2} H_{i(p_\eta + qE_0\tau_0^2/2)}^{(2)}(\sqrt{m^2 + \mathbf{p}_\perp^2} \tau) \\ -\phi_{\mathbf{p}_\perp, p_\eta} &= [+\phi_{\mathbf{p}_\perp, p_\eta}]^* = -\frac{\sqrt{\pi}}{2i} e^{\pi(p_\eta + qE_0^2\tau_0^2/2)/2} H_{-i(p_\eta + qE_0\tau_0^2/2)}^{(1)}(\sqrt{m^2 + \mathbf{p}_\perp^2} \tau) \quad (\text{for } \tau < \tau_0). \end{aligned} \quad (\text{C.23})$$

We note that the above mode function  $+\phi_{\mathbf{p}_\perp, p_\eta}$  ( $-\phi_{\mathbf{p}_\perp, p_\eta}$ ) have a correct positive (negative) frequency in the  $\tau$ - $\eta$  coordinates and surely satisfies the plane wave boundary condition at  $\tau \rightarrow 0$ .

(step 2) For  $\tau > \tau_0$ , Eq. (C.21) reads

$$0 = \left[ \frac{d^2}{d\tau^2} + \frac{1}{\tau} \frac{d}{d\tau} + \left( \frac{p_\eta + qE_0\tau^2/2}{\tau} \right)^2 + m^2 + \mathbf{p}_\perp^2 \right] \phi_{\mathbf{p}_\perp, p_\eta}. \quad (\text{C.24})$$

By changing the variables as

$$\xi \equiv \sqrt{m^2 + \mathbf{p}_\perp^2} \tau, \quad a \equiv \frac{qE_0}{m^2 + \mathbf{p}_\perp^2}, \quad (\text{C.25})$$

and by making an ansatz of a form,

$$\phi_{\mathbf{p}_\perp, p_\eta} \equiv \xi^{-ip_\eta} e^{-ia\xi^2/4} \tilde{\phi}_{\mathbf{p}_\perp, p_\eta}, \quad (\text{C.26})$$

one obtains a hypergeometric differential equation for  $\tilde{\phi}_{\mathbf{p}_\perp, p_\eta}$  as

$$0 = \left[ \xi \frac{d^2}{d\xi^2} + (-ia\xi^2 + 1 - 2ip_\eta) \frac{d}{d\xi} (1 - ia)\xi \right] \tilde{\phi}_{\mathbf{p}_\perp, p_\eta}. \quad (\text{C.27})$$

Two independent solutions of Eq. (C.27) are given by the Tricomi hypergeometric function  $U(a, b; z)$  [162], and thus we find

$$\begin{aligned} +\phi_{\mathbf{p}_\perp, p_\eta} &= c_1 \times {}_1\chi_{\mathbf{p}_\perp, p_\eta} + c_2 \times {}_2\chi_{\mathbf{p}_\perp, p_\eta}, \\ -\phi_{\mathbf{p}_\perp, p_\eta} &= [+\phi_{\mathbf{p}_\perp, p_\eta}]^*. \end{aligned} \quad (\text{C.28})$$

where

$$\begin{aligned} {}_1\chi_{\mathbf{p}_\perp, p_\eta} &\equiv \frac{1}{\sqrt{2}} \exp \left[ -\frac{\pi}{2} \left( \frac{m^2 + \mathbf{p}_\perp^2}{2|qE_0|} + p_\eta \right) - i \frac{|qE_0|\tau^2}{4} \right] \\ &\quad \times \left( \frac{|qE_0|\tau^2}{2} \right)^{ip_\eta/2} U \left( \frac{1}{2} + i \frac{m^2 + \mathbf{p}_\perp^2}{2|qE_0|} + ip_\eta, 1 + ip_\eta; i \frac{|qE_0|\tau^2}{2} \right), \\ {}_2\chi_{\mathbf{p}_\perp, p_\eta} &\equiv [{}_1\chi_{\mathbf{p}_\perp, p_\eta}]^* \end{aligned} \quad (\text{C.29})$$

The scalar function  ${}_n\chi_{\mathbf{p}_\perp, p_\eta}$  ( $n = 1, 2$ ) satisfy the following normalization condition

$$\begin{aligned} [{}_1\chi_{\mathbf{p}_\perp, p_\eta} | {}_1\chi_{\mathbf{p}_\perp, p_\eta}]_{\text{B}} &= -[{}_2\chi_{\mathbf{p}_\perp, p_\eta} | {}_2\chi_{\mathbf{p}_\perp, p_\eta}]_{\text{B}} = \frac{1}{\tau}, \\ [{}_1\chi_{\mathbf{p}_\perp, p_\eta} | {}_2\chi_{\mathbf{p}_\perp, p_\eta}]_{\text{B}} &= 0. \end{aligned} \quad (\text{C.30})$$

(step 3) The coefficients  $c_1, c_2$  in Eq. (C.28) can be determined by smoothly connecting the two solutions Eq. (C.23) for  $\tau < \tau_0$  and Eq. (C.28) for  $\tau > \tau_0$ . With the help of the normalization condition (C.30), one can easily determine the coefficients  $c_1, c_2$  as

$$c_1 = \tau_0 \times \left[ 2\chi_{\mathbf{p}_\perp, p_\eta}(\tau_0) \frac{d_+ \phi_{\mathbf{p}_\perp, p_\eta}(\tau_0)}{d\tau} - \frac{d_2 \chi_{\mathbf{p}_\perp, p_\eta}(\tau_0)}{d\tau} + \phi_{\mathbf{p}_\perp, p_\eta}(\tau_0) \right], \quad (\text{C.31})$$

$$c_2 = -\tau_0 \times \left[ 1\chi_{\mathbf{p}_\perp, p_\eta}(\tau_0) \frac{d_+ \phi_{\mathbf{p}_\perp, p_\eta}(\tau_0)}{d\tau} - \frac{d_1 \chi_{\mathbf{p}_\perp, p_\eta}(\tau_0)}{d\tau} + \phi_{\mathbf{p}_\perp, p_\eta}(\tau_0) \right], \quad (\text{C.32})$$

and hereby one obtains the solution of Eq. (C.21) for all values of  $\tau$ .

# References

- [1] P. A. M. Dirac, “*The Quantum Theory of the Electron*,” Proc. R. Soc. Lond. A **117**, 610 (1928).
- [2] P. A. M. Dirac, “*A Theory of Electrons and Protons*,” Proc. R. Soc. Lond. A **126**, 360 (1930).
- [3] O. Klein, “*Die Reflexion von Elektronen an einem Potentialsprung nach der relativistischen Dynamik von Dirac*,” Z. Phys. **53**, 157 (1929).
- [4] F. Sauter, “*Ueber das Verhalten eines Elektrons im homogenen elektrischen Feld nach der relativistischen Theorie Diracs*,” Z. Phys. **69**, 742 (1931).
- [5] W. Heisenberg and H. Euler, “*Folgerungen aus der Diracschen Theorie des Positrons*,” Z. Phys. **98**, 714 (1936).
- [6] J. Schwinger, “*On Gauge Invariance and Vacuum Polarization*,” Phys. Rev. **82**, 664 (1951).
- [7] W. H. Furry, “*A Symmetry Theorem in the Positron Theory*,” Phys. Rev. **51**, 125 (1937).
- [8] A. I. Nikishov, “*Barrier scattering in field theory removal of Klein paradox*,” Nucl. Phys. **B 21**, 346 (1970).
- [9] Thomas D. Cohen and David A. McGady, “*The Schwinger mechanism revisited*,” Phys. Rev. D **78**, 036008 (2008).
- [10] V. Weisskopf, “*Über die Elektrodynamik des Vakuums auf Grund der Quantentheorie des Elektrons*,” Kong. Dans. Vid. Sel. Mat. Fys. Med. **14**, 1 (1936).
- [11] V. S. Vanyashin, and M. V. Terent’ev, “*The Vacuum Polarization of a Charged Vector Field*,” JETP **21**, 375 (1965).
- [12] M. S. Marinov, and V. S. Popov, “*Pair Production in an Electromagnetic Field (Case of Arbitrary Spin)*,” Sov. J. Nucl. Phys. **15**, 702 (1972).
- [13] N. K. Nielsen and P. Olesen, “*An unstable Yang-Mills field mode*,” Nucl. Phys. B **144**, 376 (1978).

- [14] S. J. Chang and N. Weiss, “*Instability of constant Yang-Mills fields,*” Phys. Rev. D **20**, 869 (1979).
- [15] N. Tanji and K. Itakura, “*Schwinger mechanism enhanced by the Nielsen-Olesen instability,*” Phys. Lett. B **713**, 117 (2012).
- [16] V. Yanovsky *et al.*, “*Ultra-high intensity 300 TW laser at 0.1 Hz repetition rate,*” Optics Express **16**, 2109 (2008).
- [17] Gerard A. Mourou, Toshiki Tajima, and Sergei V. Bulanov, “*Optics in the relativistic regime,*” Rev. Mod. Phys. **78**, 309 (2006).
- [18] D. Strickland and G. A. Mourou, “*Compression of amplified chirped optical pulses,*” Opt. Commun. **56**, 219 (1985).
- [19] [www.eli-beams.eu](http://www.eli-beams.eu)
- [20] [www.hiper-laser.org](http://www.hiper-laser.org)
- [21] I. Pomeranchuk and J. Smorodinsky, “*On energy levels in systems with  $Z > 137$ ,*” J. Phys. (USSR) **9**, 97 (1945).
- [22] Ya B. Zeldovich and Valentin. S. Popov, “*Electronic structure of superheavy atoms,*” Sov. Phys. Usp., **14**, 673 (1971).
- [23] B. Müller, J. Rafelski, and W. Greiner, “*Electron shells in overcritical external fields,*” Z. Phys. **257**, 62 (1972).
- [24] A. Bzdak, and V. Skokov, “*Event-by-event fluctuations of magnetic and electric fields in heavy ion collisions,*” Phys. Lett. B **710**, 171 (2012).
- [25] W. T. Deng, and X. G. Huang, “*Event-by-event generation of electromagnetic fields in heavy-ion collisions,*” Phys. Rev. C **85**, 044907 (2012).
- [26] Remo Ruffini, Gregory Vereshchagin, and She-Sheng Xue, “*Electron-positron pairs in physics and astrophysics: from heavy nuclei to black holes,*” Phys. Rept. **487**, 1 (2010).
- [27] Takeshi Kobayashi, and Niayesh Afshordi, “*Schwinger Effect in 4D de Sitter Space and Constraints on Magnetogenesis in the Early Universe,*” JHEP **10**, 166 (2014).
- [28] Markus B. Fröb *et al.*, “*Schwinger effect in de Sitter space,*” JCAP **1404**, 006 (2014).
- [29] Danielle Allor, Thomas D. Cohen, and David A. McGady, “*The Schwinger mechanism and graphene,*” Phys. Rev. D **78**, 096009 (2008).

- [30] V. Kasper, F. Hebenstreit, M. K. Oberthaler, and J. Berges, “*Schwinger pair production with ultracold atoms*,” Phys. Lett. B **760**, 742 (2016).
- [31] N. Szpak, and R. Schützhold, “*Optical lattice quantum simulator for quantum electrodynamics in strong external fields: spontaneous pair creation and the Sauter-Schwinger effect*,” New J. Phys. **14**, 035001 (2012).
- [32] D. Banerjee *et al.*, “*Atomic Quantum Simulation of Dynamical Gauge Fields Coupled to Fermionic Matter: From String Breaking to Evolution after a Quench*,” Phys. Rev. Lett. **109**, 175302 (2012).
- [33] A. I. Nikishov, “*Pair Production by a Constant External Field*,” JETP **30**, 660 (1970)
- [34] Naoto Tanji, “*Dynamical view of pair creation in uniform electric and magnetic fields*,” Ann. Phys. **324**, 1691 (2009).
- [35] S. A. Smolyansky *et al.*, “*Dynamical derivation of a quantum kinetic equation for particle production in the Schwinger mechanism*,” arXiv:hep-ph/9712377.
- [36] S. M. Schmidt, D. Blaschke, G. Ropke, S. A. Smolyansky, A. V. Prozorkevich, and V. D. Toneev, “*A Quantum kinetic equation for particle production in the Schwinger mechanism*,” Int. J. Mod. Phys. E **7**, 709 (1998).
- [37] Gerald V. Dunne, and Christian Schubert, “*Worldline Instantons and Pair Production in Inhomogeneous Fields*,” Phys. Rev. D **72**, 105004 (2005).
- [38] Kenji Fukushima, and Tomoya Hayata, “*Schwinger Mechanism with Stochastic Quantization*,” Phys. Lett. B **735**, 371 (2014).
- [39] E. Brezin and C. Itzykson, “*Pair Production in Vacuum by an Alternating Field*,” Phys. Rev. D **2**, 1191 (1970).
- [40] V. S. Popov, “*Pair production in a variable external field (quasiclassical approximation)*,” JETP **34**, 709 (1972).
- [41] L. V. Keldysh, “*Ionization in the field of a strong electromagnetic wave*,” JETP **20**, 1307 (1965).
- [42] H. Taya, H. Fujii, and K. Itakura, “*Finite pulse effects on  $e^+e^-$  pair creation from strong electric fields*,” Phys. Rev. D **90**, 014039 (2014).
- [43] Ralf Schützhold, Holger Gies, and Gerald Dunne, “*Dynamically Assisted Schwinger Mechanism*,” Phys. Rev. Lett. **101**, 130404 (2008).

- [44] C. Kohlfürst, M. Mitter, G. von Winckel, F. Hebenstreit, and R. Alkofer, “*Optimizing the pulse shape for Schwinger pair production*,” Phys. Rev. D **88**, 045028 (2013).
- [45] F. Hebenstreit, and F. Fillion-Gourdeau, “*Optimization of Schwinger pair production in colliding laser pulses*,” Phys. Lett. B **739**, 189 (2014).
- [46] Malte F. Linder, Christian Schneider, Joachim Sicking, Nikodem Szpak, and Ralf Schützhold, “*Pulse shape dependence in the dynamically assisted Sauter-Schwinger effect*,” Phys. Rev. D **92**, 085009 (2015).
- [47] N. K. Glendenning, and T. Matsui, “*Creation of  $q\bar{q}$  pairs in a chromoelectric flux tube*,” Phys. Rev. D **28**, 2890 (1983).
- [48] K. Kajantie and T. Matsui, “*Decay of strong color electric field and thermalization in ultra-relativistic nucleus-nucleus collisions*,” Phys. Lett. **164B**, 373 (1985).
- [49] G. Gatoff, A. K. Kerman, and T. Matsui, “*Flux-tube model for ultrarelativistic heavy-ion collisions: Electrohydrodynamics of a quark-gluon plasma*,” Phys. Rev. D **36**, 114 (1987).
- [50] N. D. Birrell and P. C. W. Davies, “*Quantum Fields in Curved Space*,” Cambridge University Press (1982).
- [51] Fred Cooper, and Emil Mottola, “*Quantum back reaction in scalar QED as an initial-value problem*,” Phys. Rev. D **40**, 456 (1989).
- [52] Y. Kluger, J. M. Eisenberg, B. Svetitsky, F. Cooper, and E. Mottola, “*Pair production in a strong electric field*,” Phys. Rev. Lett. **67**, 2427 (1991).
- [53] Y. Kluger, J. M. Eisenberg, B. Svetitsky, F. Cooper, and E. Mottola, “*Fermion pair production in a strong electric field*,” Phys. Rev. D **45**, 4659 (1992).
- [54] Y. Kluger, J.M. Eisenberg, and B. Svetitsky, “*Pair production in a strong electric field: an initial value problem in quantum field theory*,” Int. J. Mod. Phys. E **2**, 333 (1993).
- [55] J. C. R. Bloch *et al.*, “*Pair creation: Back reactions and damping*,” Phys. Rev. D **60**, 116011 (1999).
- [56] Jochen Rau, “*Pair production in the quantum Boltzmann equation*,” Phys. Rev. D **50**, 6911 (1994).
- [57] F. Gelis, and N. Tanji, “*Formulation of the Schwinger mechanism in classical statistical field theory*,” Phys. Rev. D **87**, 125035 (2013).
- [58] V. Kasper, F. Hebenstreit, and J. Berges, “*Fermion production from real-time lattice gauge theory in the classical-statistical regime*,” Phys. Rev. D **90**, 025016 (2014).

- [59] F. Hebenstreit, J. Berges, and D. Gelfand, “*Simulating fermion production in 1 + 1 dimensional QED,*” Phys. Rev. D **87**, 105006 (2013).
- [60] A. H. Mueller, and D. T. Son, “*On the equivalence between the Boltzmann equation and classical field theory at large occupation numbers,*” Phys. Lett. B **582**, 279 (2004).
- [61] T. Epelbaum, F. Gelis, and B. Wu “*Nonrenormalizability of the classical statistical approximation,*” Phys. Rev. D **90**, 065029 (2014).
- [62] A. R. Bell, and J. G. Kirk, “*Possibility of Prolific Pair Production with High-Power Laser,*” Phys. Rev. Lett. **101**, 200403 (2008).
- [63] A. M. Fedotov, N. B. Narozhny, G. Mourou, and G. Korn, “*Limitations on the Attainable Intensity of High Power Lasers,*” Phys. Rev. Lett. **105**, 080402 (2010).
- [64] S. S. Bulanov, T. Z. Esirkepov, A. G. R. Thomas, J. R. Koga, and S. V. Bulanov, “*Schwinger Limit Attainability with Extreme Power Lasers,*” Phys. Rev. Lett. **105**, 220407 (2011).
- [65] E. N. Nerush *et al.*, “*Laser field absorption in self-generated electron-positron pair plasma,*” Phys. Rev. Lett. **106**, 109902 (2010).
- [66] N. V. Elkina *et al.*, “*QED cascades induced by circularly polarized laser fields,*” Phys. Rev. ST Accel. Beams **14**, 054401 (2011).
- [67] H. Hirori *et al.*, “*Extraordinary carrier multiplication gated by a picosecond electric field pulse,*” Nature Comm. **2**, 594 (2011).
- [68] John Kogut and Leonard Susskind, “*Hamiltonian formulation of Wilson’s lattice gauge theories,*” Phys. Rev. D **11**, 395 (1975).
- [69] Gunnar S. Bali, “*QCD forces and heavy quark bound states,*” Phys. Rept.. **343**, 1 (2001).
- [70] F. E. Low, “*Model of the bare Pomeron,*” Phys. Rev. D **12**, 163 (1975).
- [71] S. Nussinov, “*Colored-Quark Version of Some Hadronic Puzzles,*” Phys. Rev. Lett. **34**, 1286 (1975).
- [72] A. Casher, H. Neuberger, and S. Nussinov, “*Chromoelectric-flux-tube model of particle production,*” Phys. Rev. D **20**, 179 (1979).
- [73] A. Casher, H. Neuberger, and S. Nussinov, “*Multiparticle production by bubbling flux tubes,*” Phys. Rev. D **21**, 1966 (1980).
- [74] Bo Andersson, “*The Lund Model,*” Camb. Monogr. Part. Phys. Nucl. Phys. Cosmol. **7**, 1 (1998).

- [75] T. Barczyk, “*Color fields around the static quark-antiquark pair,*” Acta Phys. Pol. B **26**, 1347 (1995).
- [76] Richard W. Haymaker, Vandana Singh, Yingcai Peng, and Jacek Wosiek, “*Distribution of the color fields around static quarks: Flux tube profiles,*” Phys. Rev. D **53**, 389 (1996).
- [77] H. Ichie, V. Bornyakov, T. Streuer, and G. Schierholz, “*Flux Tubes of Two- and Three-Quark System in Full QCD,*” Nucl. Phys. A **721**, C899 (2003).
- [78] C. Alexandrou, P. de Forcrand, and O. Jahn, “*The ground state of three quarks,*” Nucl. Phys. B—(Proc. Suppl. ) **119**, 667 (2003).
- [79] Nuno Cardoso, Marco Cardoso, and Pedro Bicudo, “*Color fields computed in  $SU(3)$  lattice QCD for the static tetraquark system,*” Phys. Rev. D **84**, 054508 (2011).
- [80] Nuno Cardoso and Pedro Bicudo, “*Color fields of the static pentaquark system computed in  $SU(3)$  lattice QCD,*” Phys. Rev. D **87**, 034504 (2013).
- [81] Gunnar S. Bali, Hartmut Neff, Thomas Düssel, Thomas Lippert, and Klaus Schilling (SESAM Collaboration), “*Observation of string breaking in QCD,*” Phys. Rev. D **71**, 114513 (2005).
- [82] G. S. Bali, T. Düssel, T. Lippert, H. Neff, Z. Prkacin, and K. Schilling, “*String breaking,*” Nucl. Phys. Proc. Suppl. **153**, 9 (2006).
- [83] J. Ambjorn and R. Hughes, “*Canonical quantisation in non-Abelian background Fields,*” Ann. Phys. **377**, 340 (1983).
- [84] A. Yildiz and P. H. Cox, “*Vacuum behavior in quantum chromodynamics,*” Phys. Rev. D **21**, 1095 (1980).
- [85] I. A. Batalin, S. G. Matinyan and G. K. Savvidi, “*Vacuum polarization by a source-free gauge field,*” Sov. J. Nucl. Phys. **26**, 214 (1977).
- [86] M. Gyulassy and A. Iwazaki, “*Quark and Gluon Pair Production in  $SU(N)$  Covariant Constant Fields,*” Phys. Lett. B **165**, 157 (1985).
- [87] A. Bialas, W. Czyż, A. Dyrek and W. Florkowski, “*Oscillations of quark-gluon plasma generated in strong color fields,*” Nucl. Phys. B **296**, 611 (1988).
- [88] Ulrich Heinz, “*Kinetic Theory for Plasmas with Non-Abelian Interactions,*” Phys. Rev. Lett. **51**, 351 (1983).
- [89] H.-Th. Elze, M. Gyulassy and D. Vasak, “*Transport equations for the QCD quark Wigner operator,*” Nucl. Phys. B **276**, 706 (1986).

- [90] H.-Th. Elze, M. Gyulassy and D. Vasak, “*Transport equations for the QCD gluon Wigner operator,*” Phys. Lett. B **177**, 402 (1986).
- [91] Naoto Tanji, “*Quark pair creation in color electric fields and effects of magnetic fields,*” Ann. Phys. **325**, 2018 (2010).
- [92] J. C. Collins and M. J. Perry, “*Superdense Matter: Neutrons or Asymptotically Free Quarks?,*” Phys. Rev. Lett. **34**, 1353 (1975).
- [93] N. Cabibbo and G. Parisi, “*Exponential Hadronic Spectrum and Quark Liberation,*” Phys. Lett. B **59**, 67 (1975).
- [94] E. V. Shuryak, “*Quark-gluon plasma and hadronic production of leptons, photons and pions,*” Phys. Lett. B **78**, 150 (1978).
- [95] Y. Aoki *et al.*, “*The QCD transition temperature: results with physical masses in the continuum limit II,*” JHEP **06**, 088 (2009).
- [96] A. Bazavov *et al.*, “*Chiral and deconfinement aspects of the QCD transition,*” Phys. Rev. D **85**, 054503 (2012).
- [97] G. Lemaitre, “*Un univers homogene de masse constante et de rayon croissant rendant compte de la vitesse radiale des nebuleuses extragalactiques,*” G. Ann. Soc. Sci. Bruxelles **A47**, 41 (1927).
- [98] R. A. Alpher, H. Bethe, and G. Gamow, “*The Origin of Chemical Elements,*” Phys. Rev. **73**, 803 (1948).
- [99] L. McLerran and R. Venugopalan, “*Computing quark and gluon distribution functions for very large nuclei,*” Phys. Rev. D **49**, 2233 (1994).
- [100] L. McLerran and R. Venugopalan, “*Gluon distribution functions for very large nuclei at small transverse momentum,*” Phys. Rev. D **49**, 3352 (1994).
- [101] L. McLerran and R. Venugopalan, “*Green’s function in the color field of a large nucleus,*” Phys. Rev. D **50**, 2225 (1994).
- [102] Y. V. Kovchegov, “*Non-Abelian Weizsäcker-Williams field and a two-dimensional effective color charge density for a very large nucleus,*” Phys. Rev. D **54**, 5463 (1996).
- [103] F. D. Aaron *et al.*, (H1 and ZEUS Collaboration) “*Combined Measurement and QCD Analysis of the inclusive  $e^\pm p$  Scattering Cross Sections at HERA,*” JHEP **01**, 109 (2010).
- [104] K. Golec-Biernat and M. Wüsthoff, “*Saturation effects in deep inelastic scattering at low  $Q^2$  and its implications on diffraction,*” Phys. Rev. D **59**, 014017 (1999).

- [105] K. Golec-Biernat and M. Wüsthoff, “*Saturation in diffractive deep inelastic scattering*,” Phys. Rev. D **60**, 114023 (1999).
- [106] T. Lappi, “*Wilson line correlator in the MV model: Relating the glasma to deep inelastic scattering*,” Eur. Phys. J. C **55**, 285 (2008).
- [107] A. M. Staśto, K. Golec-Biernat, and J. Kwieciński, “*Geometric Scaling for the Total  $\gamma^*p$  Cross Section in the Low  $x$  Region*,” Phys. Rev. Lett. **86**, 596 (2001).
- [108] A. Freund, K. Rummukainen, H. Weigert, and A. Schafer, “*Geometric Scaling in Inclusive  $eA$  Reactions and Nonlinear Perturbative QCD*,” Phys. Rev. Lett. **90**, 222002 (2003).
- [109] C. Marquet and L. Schoeffel, “*Geometric scaling in diffractive deep inelastic scattering*,” Phys. Lett. B **639**, 471 (2006).
- [110] J. D. Bjorken, “*Highly relativistic nucleus-nucleus collisions: The central rapidity region*,” Phys. Rev. D **27**, 140 (1983).
- [111] D. J. Gross and F. Wilczek, “*Ultraviolet behavior of non-abelian gauge theories*,” Phys. Rev. Lett. **30**, 1343 (1973).
- [112] H. D. Politzer, “*Reliable perturbative results for strong interactions*,” Phys. Rev. Lett. **30**, 1346 (1973).
- [113] B. Alver *et al.*, (PHOBOS Collaboration), “*Charged-particle multiplicity and pseudorapidity distributions measured with the PHOBOS detector in Au+Au, Cu+Cu, d+Au, and p+p collisions at ultrarelativistic energies*,” Phys. Rev. C **83**, 024913 (2011).
- [114] E. Abbas *et al.*, (ALICE Collaboration), “*Centrality dependence of the pseudorapidity density distribution for charged particles in Pb-Pb collisions at  $\sqrt{s_{NN}} = 2.76$  TeV*,” Phys. Lett. B **726**, 610 (2013).
- [115] Hannah Petersen, Jan Steinheimer, Gerhard Burau, Marcus Bleicher, and Horst Stöcker, “*Fully integrated transport approach to heavy ion reactions with an intermediate hydrodynamic stage*,” Phys. Rev. C **78**, 044901 (2008).
- [116] Y. Nara, N. Otuka, A. Ohnishi, K. Niita, and S. Chiba, “*Study of relativistic nuclear collisions at AGS energies from p+Be to Au+Au with hadronic cascade model*,” Phys. Rev. C **61**, 024901 (2000).
- [117] T. Matsui, “*Dynamical evolution of the quark-gluon plasma and phenomenology*,” Nucl. Phys. A **461**, 27c (1987).
- [118] Aleksi Kurkela, “*Initial state of Heavy-Ion Collisions: Isotropization and thermalization*,” Nucl. Phys. A **956**, 136 (2016).

- [119] A. Kovner, L. McLerran, and H. Weigert, “*Gluon Production at High Transverse Momentum in the McLerran-Venugopalan Model of Nuclear Structure Functions*,” Phys. Rev. D **52**, 3809 (1995).
- [120] A. Kovner, L. McLerran, and H. Weigert, “*Gluon Production from Non-Abelian Weizsäcker-Williams Fields in Nucleus-Nucleus Collisions*,” Phys. Rev. D **52**, 6231 (1995).
- [121] T. Lappi and L. McLerran, “*Some Features of the Glasma*,” Nucl. Phys. A **772**, 200 (2006).
- [122] P. Romatschke and R. Venugopalan, “*Collective non-Abelian instabilities in a melting Color Glass Condensate*,” Phys. Rev. Lett. **96**, 062302 (2006).
- [123] P. Romatschke and R. Venugopalan, “*The Unstable Glasma*,” Phys. Rev. D **74**, 045011 (2006).
- [124] Thomas Epelbaum, and Francois Gelis, “*Pressure isotropization in high energy heavy ion collisions*,” Phys. Rev. Lett. **111**, 232301 (2013).
- [125] Juergen Berges, Kirill Boguslavski, Soeren Schlichting, and Raju Venugopalan, “*Universal attractor in a highly occupied non-Abelian plasma*,” Phys. Rev. D **89**, 114007 (2014).
- [126] J.Berges, K.Boguslavski, S.Schlichting, R.Venugopalan, “*Turbulent thermalization process in heavy-ion collisions at ultrarelativistic energies*,” Phys. Rev. D **89**, 074011 (2014).
- [127] Thomas Epelbaum, Francois Gelis, Sangyong Jeon, Guy Moore, and Bin Wu, “*Kinetic theory of a longitudinally expanding system of scalar particles*,” JHEP **09**, 117 (2015).
- [128] Peter Arnold, Guy D. Moore, and Laurence G. Yaffe, “*Effective Kinetic Theory for High Temperature Gauge Theories*,” JHEP **0301**, 030 (2003).
- [129] Aleksi Kurkela, and Yan Zhu, “*Isotropization and hydrodynamization in weakly coupled heavy-ion collisions*,” Phys. Rev. Lett. **115**, 182301 (2015).
- [130] Wojciech Florkowski, and Radoslaw Ryblewski, “*Highly-anisotropic and strongly-dissipative hydrodynamics for early stages of relativistic heavy-ion collisions*,” Phys. RevC. **83**, 034907 (2011).
- [131] Mauricio Martinez, and Michael Strickland, “*Dissipative Dynamics of Highly Anisotropic Systems*,” Nucl. Phys. A **848**, 183 (2010).
- [132] Juergen Berges, Szabolcs Borsanyi, Urko Reinosa, and Julien Serreau, “*Nonperturbative renormalization for 2PI effective action techniques*,” Ann. Phys. **320**, 344 (2005).

- [133] P. M. Chesler, and L. G. Yaffe, “*Horizon formation and far-from-equilibrium isotropization in supersymmetric Yang-Mills plasma,*” Phys. Rev. Lett. **102**, 211601 (2009).
- [134] P. M. Chesler, and L. G. Yaffe, “*Holography and colliding gravitational shock waves in asymptotically AdS<sub>5</sub> spacetime,*” Phys. Rev. Lett. **106**, 021601 (2011).
- [135] D. E. Kharzeev, L. D. McLerran, and H. J. Warringa, “*The effects of topological charge change in heavy ion collisions: “Event by event P and CP violation”,*” Nucl. Phys. A **803**, 227 (2008).
- [136] F. Gelis, K. Kajantie, and T. Lappi, “*Chemical Thermalization in Relativistic Heavy Ion Collisions,*” Phys. Rev. Lett. **96**, 032304 (2006).
- [137] Hidetoshi Taya, “*Quark and Gluon Production from a Boost-invariantly Expanding Color Electric Field,*” arXiv:1609.06189.
- [138] R. Baier, A. H. Mueller, D. Schiff, and D. T. Son, “*Bottom-up thermalization in heavy ion collisions,*” Phys. Lett.B **502**, 51 (2001).
- [139] Jean-Paul Blaizot, Francois Gelis, Jinfeng Liao, Larry McLerran, and Raju Venugopalan, “*Bose-Einstein Condensation and Thermalization of the Quark Gluon Plasma,*” Nucl. Phys. A **873**, 68 (2011).
- [140] H. Fujii and K. Itakura, “*Expanding color flux tubes and instabilities,*” Nucl. Phys. A **809**, 88 (2008).
- [141] Hidekazu Tsukiji, Hideaki Iida, Teiji Kunihiro, Akira Ohnishi, and Toru T. Takahashi, “*Entropy production from chaoticity in Yang-Mills field theory with use of the Husimi function,*” Phys. Rev. D **94**, 091502(R) (2016).
- [142] F. Sauter, “*Zum “Kleinschen Paradoxon”,*” Z. Phys. **73**, 547 (1932).
- [143] Emmy Noether, “*Invariante Variationsprobleme,*” Nachr. d. König. Gesellsch. d. Wiss. zu Göttingen, Math-phys. Klasse, 235 (1918).
- [144] F. J. Belinfante, “*On the current and the density of the electric charge, the energy, the linear momentum and the angular momentum of arbitrary fields,*” Physica **7**, 449 (1940).
- [145] L. Rosenfeld, “*Sur le tenseur d’impulsion-énergie,*” Mem. Acad. Roy. Belg. Sci. **18**, 1 (1940).
- [146] Kenji Fukushima and Francois Gelis, “*The evolving Glasma,*” Nucl. Phys. A **874**, 108 (2012).

- [147] Francois Gelis, and Naoto Tanji, “*Schwinger mechanism revisited*,” Prog. Part. Nucl. Phys. **87**, 1 (2016).
- [148] K. Fukushima, F. Gelis, and T. Lappi, “*Multiparticle correlations in the Schwinger mechanism*,” Nucl. Phys. A **831**, 184 (2009).
- [149] V. V. Skokov and P. Levai, “*Transverse and longitudinal momentum spectra of fermions produced in strong  $SU(2)$  fields*,” Phys. Rev. D **78**, 054004 (2008).
- [150] P. Levai and V. Skokov, “*Nonperturbative enhancement of heavy quark-pair production in a strong  $SU(2)$  color field*,” Phys. Rev. D **82**, 074014 (2010).
- [151] Salman Habib, Yuval Kluger, Emil Mottola, and Juan Pablo Paz, “*Dissipation and Decoherence in Mean Field Theory*,” Phys. Rev. Lett. **76**, 4660 (1996).
- [152] Lewi Tonks and Irving Langmuir, “*Oscillations in Ionized Gases*,” Phys. Rev. **33**, 195 (1929).
- [153] T. Kugo and S. Uehara, “*General procedure of gauge fixing based on BRS invariance principle*,” Nucl. Phys. B **197**, 378 (1982).
- [154] C. Becchi, A. Rouet and R. Stora, “*Renormalization of gauge theories*,” Ann. Phys. **98**, 287 (1976).
- [155] N. Nakanishi, “*Covariant Quantization of the Electromagnetic Field in the Landau Gauge*,” Prog. Theor. Phys. **35**, 1111 (1966).
- [156] B. Lautrup, “*Canonical Quantum Electrodynamics in Covariant Gauges*,” Kong. Dan. Vid. Sel. Mat. Fys. Med. **35**, 11 (1967).
- [157] G. C. Nayak and P. van Nieuwenhuizen, “*Soft-gluon production due to a gluon loop in a constant chromoelectric background field*” Phys. Rev. D **71**, 125001 (2005)
- [158] G. C. Nayak, “*Non-Perturbative Quark-Antiquark Production From a Constant Chromoelectric Field via the Schwinger Mechanism*,” Phys. Rev. D **72**, 125010 (2005)
- [159] Naoto Tanji, “*Pair creation in boost-invariantly expanding electric fields and two-particle correlations*,” Phys. Rev. D **83**, 045011 (2011).
- [160] N. D. Birrell and P. C. W. Davies, “*Quantum Fields in Curved Space*”, Cambridge University Press (1982).
- [161] C. M. Sommerfeld, “*Quantization on Spacetime Hyperboloids*,” Ann. Phys. **84**, 285 (1974).
- [162] The Wolfram Function Site: [functions.wolfram.com](http://functions.wolfram.com)

- [163] F. Cooper, J. M. Eisenberg, Y. Kluger, E. Mottola and B. Svetitsky, “*Particle production in the central rapidity region,*” *Phys. Rev. D* **48**, 190 (1993).
- [164] B. Mihaila, F. Cooper, and J.-F. Dawson, “*Backreaction and particle production in (3+1)-dimensional QED,*” *Phys. Rev.D* **80**, 014010 (2009).
- [165] M. Kodama, “*Algorithm 912: a module for calculating cylindrical functions of complex order and complex argument,*” *ACM Trans. Math. Software* **37**, 47 (2011).
- [166] R. J. Crewther, “*Nonperturbative Evaluation of the Anomalies in Low-Energy Theorems,*” *Phys. Rev. Lett.* **28**, 1421 (1972).
- [167] M. S. Chanowitz and J. Ellis, “*Canonical anomalies and broken scale invariance,*” *Phys. Lett. B* **40**, 397 (1972).
- [168] M. S. Chanowitz and J. Ellis, “*Canonical Trace Anomalies,*” *Phys. Rev. D* **7**, 2490 (1973).
- [169] K. Fukushima, “*Evolution to the Quark-Gluon Plasma,*” arXiv:1603.02340
- [170] J.-P. Blaizot, B. Wu, and L. Yan, “*Quark production, Bose-Einstein condensates and thermalization of the quark-gluon plasma,*” *Nucl. Phys. A* **930**, 139 (2014)
- [171] J.-P. Blaizot, J. Liao, and Y. Mehtar-Tani, “*The subtle interplay of elastic and inelastic collisions in the thermalization of the quark-gluon plasma,*” arXiv:1601.00308
- [172] J.-P. Blaizot, F. Gelis, J. Liao, L. McLerran, and R. Venugopalan, “*Bose-Einstein Condensation and Thermalization of the Quark Gluon Plasma,*” *Nucl. Phys. A* **873**, 68 (2012)
- [173] J.-P. Blaizot, J. Liao, and L. McLerran, “*Gluon Transport Equation in the Small Angle Approximation and the Onset of Bose-Einstein Condensation,*” *Nucl. Phys. A* **920**, 58 (2013)
- [174] Y. Hidaka, T. Iritani, and H. Suganuma, “*Fast Vacuum Decay into Quark Pairs in Strong Color Electric and Magnetic Fields,*” *AIP Conf. Proc.* **1388**, 516 (2011)
- [175] Y. Hidaka, T. Iritani, and H. Suganuma, “*Fast vacuum decay into particle pairs in strong electric and magnetic fields,*” arXiv:1102.0050
- [176] N. Tanji, “*Electromagnetic currents induced by color fields,*” *Phys. Rev. D* **92**, 125012 (2015)
- [177] A. Bialas and J. P. Blaizot, “*Pre-equilibrium emission of lepton pairs from oscillating quark-antiquark plasma,*” *Phys. Rev. D* **32**, 2954 (1985)
- [178] M. Asakawa and T. Matsui, “*Dilepton production from a nonequilibrium quark-gluon plasma in ultrarelativistic nucleus-nucleus collisions,*” *Phys. Rev. D* **43**, 2871 (1991)

- [179] Y. Hirono, M. Hongo, and T. Hirano, “*Estimation of electric conductivity of the quark gluon plasma via asymmetric heavy-ion collisions,*” Phys. Rev. C **90**, 021903 (2014)
- [180] V. Voronyuk, V. D. Toneev, S. A. Voloshin, and W. Cassing, “*Charge-dependent directed flow in asymmetric nuclear collisions,*” Phys. Rev. C **90**, 064903 (2014)
- [181] T. Niida for the STAR Collaboration, “*Charge-dependent anisotropic flow in Cu+Au collisions,*” arXiv:1601.01017
- [182] D. E. Kharzeev, L. D. McLerran, and H. J. Warringa, “*The effects of topological charge change in heavy ion collisions: “Event by event P and CP violation”,*” Nucl. Phys. A **803**, 227 (2008)
- [183] K. Fukushima, D. E. Kharzeev, and H. J. Warringa, “*Real-time dynamics of the Chiral Magnetic Effect,*” Phys. Rev. Lett. **104**, 212001 (2010)
- [184] K. Fukushima, “*What flows in the chiral magnetic effect? – Simulating the particle production with CP-breaking backgrounds,*” Phys. Rev. D **92**, 054009 (2015).